THE DETERMINATION OF TRACE METALS BY CAPILLARY ELECTROPHORESIS

By

Simon Andrew Hardy BSc (Hons).

A thesis submitted to the University of Plymouth in partial fulfilment for the degree of

DOCTOR OF PHILOSOPHY

Department of Environmental Sciences,

Faculty of Science.

In collaboration with

Dionex, UK.

May 2000.

90 0451420 4

UNIVERSITY OF PLYMOUTH
Item No. 900 4514204
Date 22 NOV 2000 S
Class No. T 541.372 HAR
Contl. No. X 70446097
LIBRARY SERVICES

REFERENCE ONLY

LIBRARY STORE

ABSTRACT

THE DETERMINATION OF TRACE METALS BY CAPILLARY ELECTROPHORESIS

By Simon Andrew Hardy BSc (Hons.)

The development of a capillary electrophoresis (CE) method for the determination of inorganic and organo mercury species as their dithizone sulphonate (DzS) complexes using coated capillary columns is described. The complexes were pre-formed before injection and detection was by direct measurement of the visible absorbance of the complexes. Dithizone sulphonate was used in place of cysteine to separate methyl mercury in the final stage of a simplified Westoo extraction procedure. The method was than applied to the analysis of methyl mercury in a crab and several fish meat samples. Good quantitative performance is demonstrated by spiking experiments and analysis of DORM-1 certified reference material. The method was found to be very sensitive and a detection limit of 2 $\mu g\ Kg^{-1}$ could be achieved for a 10g sample of fish flesh.

A CE method for the determination of uranium (VI) as the arsenazo III complex was developed and the effect of interfering metal ions was studied. The calibration was found to be linear from 10 $\mu g\ l^{-1}$ -10 $mg\ l^{-1}$ using gravity injections and a detection limit of less than 1 $\mu g\ l^{-1}$ was achieved with electrokinetic injection.
A study was made of injection techniques and their applicability to the enhancement of sensitivity in synthetic standards and environmental samples.
The effect of capillary surface chemistry on the peak shape of the migrating uranyl-arsenazo III was also studied using fused silica capillaries with two different internal coatings and three polymeric capillaries.

A study was also carried out on the construction and investigation of a post-capillary reactor for the determination of trace metals by UV-Vis absorption after formation of intensely absorbing coloured complexes. The main principle of operation was based on the infusion of the colorimetric reagent into a small 50μm gap between the separation capillary and the reaction capillary. The gap was enclosed by a permeable membrane and the flow of reagent was achieved by the application of a slight pressure to the post-capillary reactor cell. Two reagents were studied, namely, xylenol orange (XO) and 4 (2-pyridylazo) resorcinol (PAR), for the separation and detection of copper (II), cadmium (II), cobalt (II), nickel (II), zinc (II), and manganese (II). Lead (II) was also included in the XO system.

TABLE OF CONTENTS.

LIST OF FIGURES.

CHAPTER 1. INTRODUCTION.

CHAPTER 4. THE DEVELOPMENT OF A POST-CAPILLARY REACTION DETECTION SYSTEM FOR CAPILLARY ELECTROPHORESIS.

LIST OF TABLES

CHAPTER 1. INTRODUCTION.

CHAPTER 2. THE SPECIATION OF MERCURY.

CHAPTER 3. THE DETERMINATION OF URANIUM.

ACKNOWLEDGEMENTS.

I would like to express my deepest gratitude to my supervisor, Dr. Phil Jones for his continuous support, encouragement and patience throughout the period of this study.

Thanks to Alex Adam and Maria Walton of Dionex UK for their sponsorship through the case award scheme.

I would also like to acknowledge the Engineering and Physical Sciences Research Council for their financial support.

Thanks to Nebosja Avdalovic (vice president R&D), and John Riviello, Dionex Corporation for supervision during my visit.

I would also like to thank my wife Catherine for her support throughout the course of my study and apologise to my daughters Philippa and Charlotte for those weekends when I have been working.

I would like to thank my friends at the University of Plymouth, especially Richard Sutton (for broadening my musical out look), Pavel Nesterenko (for his energy and enthusiasm) and all the technicians on the 5th floor, Davy

AUTHOR'S DECLARATION

At no time during the registration for the degree of Doctor of Philosophy has the author been registered for any other university award.

A programme of advanced study was undertaken, which included instruction in capillary electrophoresis theory and instrument operation. The programme also included a three month visit to the Research and Development Department of Dionex in Sunnyvale, CA.

This study was financed by the Engineering and Physical Sciences Research Council (EPSRC) and Dionex, UK.

Relevant scientific seminars and conferences were regularly attended at which work was often presented, external institutions were visited for consultation purposes and papers prepared for publication.

Signed..... 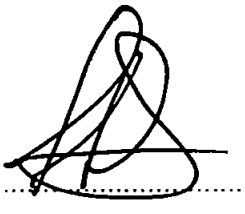 .....

Simon A. Hardy

May 2000

PUBLICATIONS.

Development of a Capillary Electrophoresis Method for the Separation and Determination of Trace Inorganic and Organomercury Species Utilising the Formation of Highly Absorbing Water Soluble Dithizone Sulphonate Complexes. P.Jones and S.A.Hardy, *J. Chromatogr.* A, 765 (1997) 345.

Capillary Electrophoresis Determination of Methylmercury in Fish and Crab Meat after Exraction as the Dithizone Sulphonate Complex. S.A.Hardy and P.Jones, *J. Chromator.* A, 791 (1997) 333.

The Construction and Investigation of a Post-Capillary Reactor for Trace Metal Analysis by Capillary Electrophoresis. S.Hardy, P.Jones, J.M.Riviello and N.Avdalovic, *J. Chromator.* A, 834 (1999) 309.

PRESENTATIONS AND CONFERENCES ATTENDED.

Departmental research lecture, University of Plymouth, UK, November 1995

R and D Topics in Analytical Chemistry, University of Hull, UK, July 1995

IICS '95. Dallas, TX. USA, September 1995.

Departmental research lecture, University of Plymouth, UK, June 1996.

Poster presentation, IICS '96, University of Reading, Reading, UK, September, 1996.

Departmental research lecture, University of Plymouth, UK, May 1997.

Poster presentation, IICS '97, Santa Clara, CA. USA. September, 1997 .

CHAPTER 1. INTRODUCTION.

1.0. Introduction.

The term electrophoresis was first used by Michaelis in 1909 [1] to describe the process of separating ionic species in a conducting background under the influence of an applied electric field. The separation occurs due to differences in the movement of the ions when exposed to the electric field. The passage of current through the support medium is provided by an electrolyte solution, which is also buffered to provide precise pH control. The technique is able to separate an extensive range of solutes with a wide range of molecular size, from small inorganic ions to high molecular weight proteins.

Traditionally these separations were performed in a semisolid gel medium supported on a glass plate. The purpose of the gel is two fold, providing physical support and mechanical stability for the electrolyte solution. Cellulose acetate and paper are also used to provide support for the electrolyte. Gels may also take part in the separation process itself providing a molecular sieve, which impedes the passage of larger molecules [2, 3].

1.1. Electrophoresis in a Capillary.

Capillary electrophoresis (CE) is a group of related analytical techniques employing small-bore capillaries, usually, though not exclusively, made from fused silica, with internal diameters usually between 25-100μm. The technique has to some extent evolved from a merging of conventional electrophoresis and high performance liquid chromatography (HPLC).

The principal reason for performing electrophoresis in a capillary is that gels are no longer required as the capillary walls provide physical support for the electrolyte. Very high separation efficiency and resolution are achievable with rapid analysis times. Heat dissipation is more efficient in narrow bore capillaries allowing the use of higher electric field strengths. Since the speed of the separation is directly proportional to the field strength, analysis times are reduced.

The high efficiency obtainable with CE is due to the flat flow profile generated by electroosmotic flow in comparison with the laminar flow profile produced by an HPLC system. There is no substrate as with an HPLC system, which can contribute to a reduction in the separation efficiency and resolution owing to interactions with the substrate. However, capillary wall interactions may also play an exaggerated role in CE due to the high surface to volume ratio inherent in very narrow bore capillaries.

There are several other advantages of performing electrophoresis in a capillary. Detection can be performed on-line with data acquisition producing an output similar to that of HPLC. Sample injection is easily automated, a necessary step in order to produce reproducible injections. In fact most commercial capillary electrophoresis instruments available today are fully automated. Very small sample volumes are required in CE. This is easily illustrated when considering the entire volume of a capillary with a total length of 65cm and an internal diameter (ID) of 100μm is only 5.1μl. In addition, reagent use is also very low, a factor of importance as the cost of reagent disposal in addition to its consumption is of increasing concern.

In recent years the technique has found considerable favour in the separation of biological macromolecules.

In the separation of small ions the technique has been allied to and compared with ion chromatography (IC). Although there has been considerable interest in the separation of small ions by CE, the technique has yet to be adopted for routine analysis. The main reason for this, in spite of numerous papers describing methods for the separation and determination of small ions, many producing impressive separations, very few have been applied to the determination of real samples. This is principally due to an overall lack of robustness in CE, particularly in respect to the pH and ionic strength of the sample matrix, which are far more critical than in IC. Unfortunately, real samples, particularly those from environmental sources, often contain vastly disparate concentrations of ions and may occur in high ionic strength matrices. Sample extraction

and preparation methods can also result in samples ending up in matrices at extremes of pH or in organic phases that may be unsuitable for injection into a capillary. Ideally for analysis by capillary electrophoresis the samples need to be of very low ionic strength and at moderate pH. Samples containing highly different concentrations of ions may also cause problems with some detection methods due to masking of low concentration peaks by larger high concentration peaks.

1.1. Instrumentation.

Although the theoretical aspects concerning CE have been around for nearly a century, the first direct precursor to CE was developed by Hjertén in 1967 [4] using 3mm ID fused silica capillaries internally coated with methylcellulose. In this system the capillary was rotated about its longitudinal axis to reduce problems with convection currents due to heat production. In 1979 Mikkers *et al.* [5] produced a separation of 16 anions using 0.2mm ID PTFE tubing and a potential gradient detector. The use of smaller ID capillaries improved heat dissipation and allowed the use of higher field strengths without the need to rotate the capillaries. Previously in early capillary electrophoresis work sample injection had proved a significant problem and in 1981 Jorgenson and Lukacs [6] described the first use of electrokinetic injections. This work used 80μm ID borosilicate glass capillaries separating dansyl and fluorescamine derivatives of amine containing compounds detecting by fluorescence.

Commercial instruments have become available since 1988. This is principally due to improvements in the physical engineering aspects allowing reproducible injection, accurate control of voltage or current, highly sensitive detectors and the manufacture of small internal diameter (ID) capillaries with precise and constant internal diameters.

The basic instrumentation for CE, shown in Figure 1.0 is relatively simple, requiring a high voltage power supply connected across the capillary, with a means of introducing the sample into the capillary and a detection system. The power supply is connected across the capillary by

electrodes that are immersed in vials containing an electrolyte. Filling the capillary with the electrolyte and immersing an end in each vial completes the circuit. It is important that the vials are placed at the same level to prevent hydrodynamic flow between them. The detector is normally situated towards one end of the capillary thus allowing the use of greater field strengths.

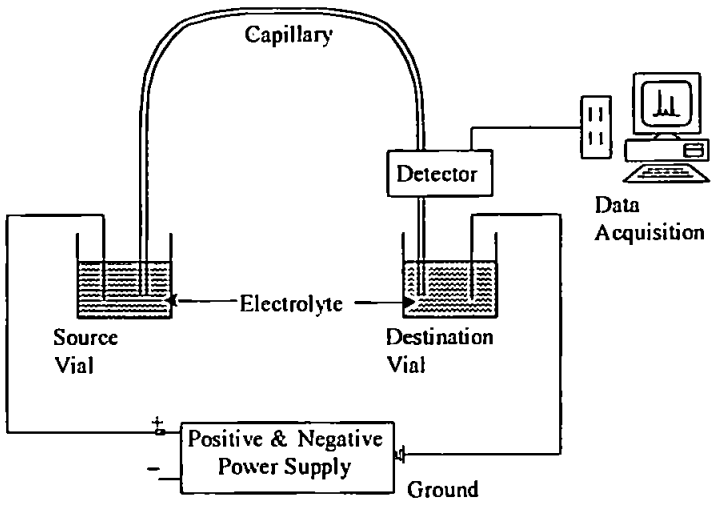

Figure 1.0. Schematic Diagram of a Capillary Electrophoresis System having both Positive and Negative Power Supplies

This is because the voltage is applied across the entire length of the capillary and excess capillary after the detector only serves to decrease the field strength experienced by the solutes in the capillary. Raising the voltage would increase the field strength but excessive voltage can lead to short-circuiting or arcing as the insulation capacity of many materials begins to break down at extreme voltages. Insulation is one of the reasons that commercial instruments are fitted with power supplies producing a maximum of 30,000V.

1.2. The Electroosmotic Process

1.2.1. Conduction in Fluid.

The conductivity in a solution results from the independent migration of ions when an electric field is applied to an ionic solution, where anions migrate towards the anode and cations migrate towards the cathode in equal quantities. Electroneutrality is always maintained as a result of the ionisation of water molecules. The conductivity of a fluid is determined by two factors, the concentration of ionic species and the mobility of those species when exposed to an electric field.

The higher the concentration or the greater the mobility of the ions, the greater the conductivity. Conduction in fluid solution can be described by Ohm's Law, which is given in Equation 1.0.

$$V = IR \qquad \textit{Equation 1.0}$$

Where, V is the Voltage, I is the Current and R is the Resistance.

However, since the strength of the electric field experienced within the capillary is dependent on the total length of the capillary as well as the magnitude of the applied voltage, applied field (E) provides a more appropriate term for CE. Electric field strength can be calculated using Equation 1.1.

$$E = \frac{V}{L_t} \qquad \textit{Equation 1.1}$$

Where L_t is the total length of the capillary in centimetres, and E is expressed in $V\ cm^{-1}$. In capillary electrophoresis, conductivity is provided by the background electrolyte, also termed the buffer, since the electrolyte is usually buffered to provide control of the pH during the separation.

1.2.2. Electrophoretic Mobility and Velocity.

The separation in capillary electrophoresis occurs due to differences in the mobility of specific solutes, under the influence of an applied electric field.

The electrophoretic velocity of an ion is a function of its electrophoretic mobility and the field strength to which it is exposed. In solution, an ion becomes mobile when exposed to an electric field and begins to migrate with a velocity (v_{ep}). Velocity is influenced by the electrophoretic mobility (μ_{ep}) of the solute and the magnitude of the applied electric field

$$v_{ep} = \mu_{ep}\ E \qquad \textit{Equation. 1.2}$$

The velocity of an ion can also be experimentally determined using Equation 1.3.

$$v_{ep} = \frac{L_d}{t_m} \qquad \textit{Equation. 1.3}$$

Where L_d is the length of capillary to detector (cm), t_m is the observed migration time (s) and v_{ep} is expressed in cm s^{-1}.

The electrophoretic mobility (μ_{ep}) of an ion is a fixed property and is independent of the field strength to which it is exposed. The electrophoretic mobility of an ion in solution is determined by its charge to size ratio, being proportional to the charge of the ion and inversely proportional to the frictional forces acting against it. The forces (F) acting on an ion given in Equation 1.4, where q is the ionic charge.

$$F = qE \qquad \textit{Equation 1.4}$$

The frictional forces (F_r) acting against the ion can be expressed by Stokes Law and are given in Equation 1.5.

$$F_r = -6\pi\eta r v_{ep} \qquad \textit{Equation 1.5}$$

Where η is the viscosity of the electrolyte, r is the ionic radius and v_{ep} is the ionic velocity.

During electrophoresis these two forces are in opposition, Equation 1.6.

$$qE = 6\pi\eta r v_{ep} \qquad \textit{Equation 1.6}$$

The electrophoretic mobility (μ_{ep}) of an ion is given in Equation.1.7 and is obtained by substituting Equation 1.6 into Equation 1.2, solving for velocity and rearranging for mobility.

$$\mu_{ep} = \frac{q}{6\pi\eta r} \qquad \textit{Equation 1.7}$$

Where q is the charge of ion and μ_{ep} is expressed in $cm^2\ V^{-1}\ s^{-1}$.

The size of an ion is determined by its mass, physical shape and degree of solvation. The mobility of an ion is not always predictable based on charge and ionic radii alone, even with simple ions such as the alkali metals shown in Table 1.0. In this instance, the reversed order of mobility is due to a greater degree of hydration with the smaller ions.

Table 1.0 Ionic radii and mobilities of the alkaline earth metals.

Metal	Ionic radius (pm)	Hydrated radius (pm)	Mobility ($10^{-7}cm^2 V^{-1} s^{-1}$)
Li	86	340	40.1
Na	112	276	51.9
K	144	232	76.2
Rb	158	228	79.2
Cs	184	228	79.8

Although electrophoretic mobility can be calculated using Equation 1.5 it is far easier and more usually obtained from experimental observation using equation 1.8.

$$\mu_{ep} = \frac{\nu_{ep}}{E} \qquad \textit{Equation 1.8}$$

It important to note that Equation 1.6 defines the observed mobility. In order to calculate the true mobility a correction for electroosmotic flow must also be applied.

Since the mobility of an ion is also dependent on its charge the pH of the electrolyte may also influence the mobility of an ion, Figure 1.1 illustrates this showing the change in mobility for citric and phosphoric acids. An extreme example of the influence of pH on mobility is the analysis of zwitterions, which are cationic at low pH but eventually become anionic as the pH of the electrolyte is increased. Conversely, CE may also be used as a tool for the determination of pI and pK_a values.

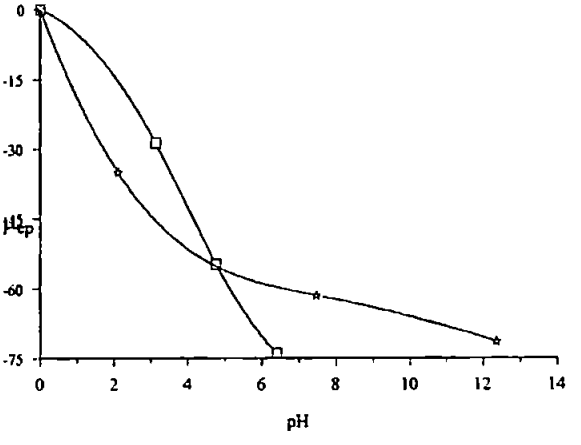

Figure 1.1. Change in mobility with pH. ($\mu_{ep} = 10^{-7}$ cm /V sec)
The data points indicate the three pK_a values of : - boxes; citric acid and stars; phosphoric acid.

1.3. Electroosmotic Flow.

Electroosmotic flow is the bulk flow of solution through the capillary and as such is the fundamental driving mechanism of capillary electrophoresis. Electroosmotic flow is often

considered analogous to the pump in HPLC. Electroosmotic flow enables the separation of cations, neutrals and anions in a single run with the migration order being cations, neutrals then anions. Figure 1.2(a) shows a representation of the injected sample in a matrix such as water. In figure 1.2 (b) a voltage is applied across the capillary causing the sample zone to be drawn towards the cathode by the electroosmotic flow. Cations migrate out of the sample zone and move rapidly towards the detector. Neutral species remain in the sample zone and are swept along by the electroosmotic flow. Since the neutral species have no charge they are not separated from each other. Anions migrate out of the sample zone but their resultant mobility is towards the detector due to the electroosmotic flow. Highly mobile anions will not be detected if their mobility approaches or exceeds that of the electroosmotic flow since their mobility is opposite to that of the flow, preventing them from passing the detector.

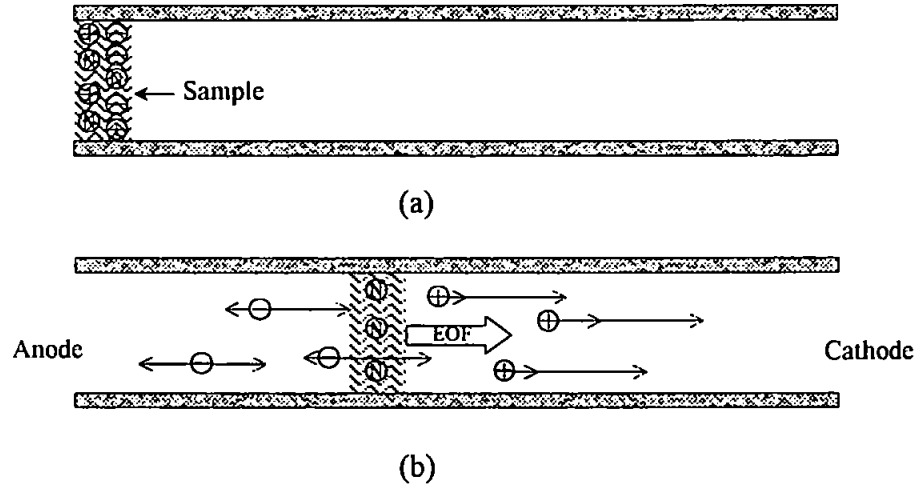

Figure 1.2. The Separation of Cations, Anions and Neutrals with Electroosmotic Flow. (a) Sample Zone at Time of Injection. (b) Migration of Ions under the Influence of an Electric Field. (Black arrows indicate the individual mobility of the ion. Red arrows indicate the actual velocity of the ion due to electroosmosis and electrophoresis).

Electroosmotic flow was first reported by Helmholtz in 1898 whilst studying the effects of an electric field on a glass tube filled with an aqueous salt solution. This flow occurs due to the formation of an electrical double layer on the surface of the tube. When an external electric field is applied across the tube, ions in the double layer are induced to migrate towards the

corresponding electrode. These ions drag water molecules with them giving rise to the bulk flow of fluid, which is referred to as electroosmosis.

Electroosmotic flow was defined by Smoluchowski in 1903 and is given in Equation 1.9.

$$v_{eo} = \frac{\varepsilon\zeta}{4\pi\eta} E \qquad \textit{Equation 1.9}$$

Where v_{eo} is the electroosmotic flow, ε is the Dielectic constant, η is the Viscosity of the Buffer and ζ is the Zeta Potential.

1.3.1. The Electrostatic Double Layer.

When any solid is immersed in an electrolyte solution, an electrostatic double layer is formed at the solid-liquid interface [7]. On immersion in the electrolyte, electrons in the solid are drawn towards the surface, causing the build up of a negative charge. The double layer is created when counter-ions in the electrolyte are attracted towards the surface in an attempt to neutralise the surface charge. When an ionisable surface is immersed in an electrolyte, the effect is more pronounced due to the increased charge of the surface attracting a greater number of compensating counter-ions. The double layer is so called, since in the simple Helmholtz model it was presumed to consist of two parallel layers of opposite charge. The exact structure of the double layer is still contested [7] but is generally depicted using the Gouy-Chapman-Stern-Grahame (GCSG) model, illustrated in Figure 1.3. In the model the double layer is depicted as being composed of an ion bonding layer, also termed the Stern layer, and a diffuse layer, alternatively referred to as the Gouy-Chapman layer. Ions in the Stern layer are strongly attracted to the surface and essentially immobile. This region is further divided into two zones by the Inner Helmholtz Plane (IHP), with counter-ions in the inner zone stripped of their solvation sheathes whilst those in the outer zone remain solvated.

The diffuse layer consists of a region of mobile ions. Close to the surface, the electrolyte has considerable ionic character due to the attraction of counter-ions, but as the distance from the

wall increases the electrolyte becomes electrically neutral as the charged surface becomes shielded.

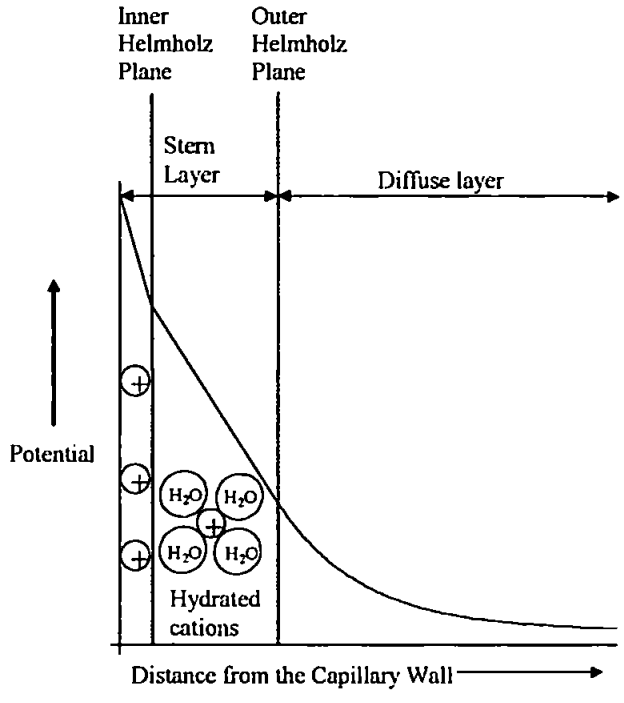

Figure 1.3. Potential distribution in the Gouy-Chapman-Stern-Graham Model of the Electrostatic Double Layer

The Stern and diffuse layers are separated by the Outer Helmholtz Plane (OHP), which is essentially the plane of shear between immobilised and mobile ions.

The charged surface acting on counter-ions in the electrolyte solution induces a potential difference, which decreases with distance from the surface.

In the Stern layer, the potential decrease is linear with the sharpest decrease occurring between the wall and IHP. In the diffuse layer, the potential decrease is exponential. The decrease in potential with distance from the wall is shown in Figure 1.3. The resulting potential at the OHP is termed the zeta potential (ζ) and has an important influence on the generation of electroosmotic flow. The distribution of charge and potential in the Stern layer has a direct influence on the zeta potential. The potential distribution in the Stern layer is dependent on the surface charge, the concentration of counter-ions in the electrolyte and the geometric arrangement of these ions.

The arrangement of the ions in the Stern layer is determined by their size and the short-range interactions between them. Since size of an ion is finite, this imposes a limit to the maximum concentration at the surface; in addition the electric field encountered in this region may also orient the dipoles of the solvent, altering their arrangement.

The electric field strength in this region is extremely high, with fused silica capillaries the depth of the inner region is typically less than 1nm. Assuming a potential drop of around 100 mV, the field strength would be in excess of 10^6 V cm^{-1}. A potential of this magnitude is vastly in excess of any electric field applied across the capillary and cations in the stern layer remain statically bonded to the capillary wall.

1.3.2. Generation of Electroosmotic Flow in Fused Silica Capillaries.

The pI of fused silica is in the region of 1.5 and as the pH increases above this value silanol groups on the capillary surface begin to ionise, resulting in the build up of an increasingly negative charge. Cations in the electrolyte solution are attracted towards the surface in an attempt to neutralise the surface charge, forming the electrical double layer. When a potential is applied across the capillary, cations in the diffuse layer are drawn towards the cathode, resulting in the bulk flow of solution towards the cathode. Although the diffuse layer is only in the region of 10nm deep, electroosmotic flow is transmitted throughout the entire diameter of the capillary. The reason for this is not well understood, but is generally attributed to hydrogen bonding between water molecules and van der Waals interactions between buffer constituents. Very strong electroosmotic flow rates can be achieved in capillaries due to the high surface to volume ratio.

Because the electroosmotic flow is generated uniformly down the entire length of the capillary, the radial flow profile is uniform across the capillary, apart from very close to the capillary wall, where the flow rate becomes zero, (Figure 1.4(a)). This radial flow profile accounts for the very high efficiencies achievable by CE. Figure 1.4(b) show the effect of electroosmotic and laminar flow on two equal length sample zones. From the figure it can be seen that the boundaries of the sample zone remain flat during electroosmotic flow. Whereas with laminar flow the sample zone becomes distorted due to frictional interaction with the sides of the capillary, which causes the sample zone to become broadened.

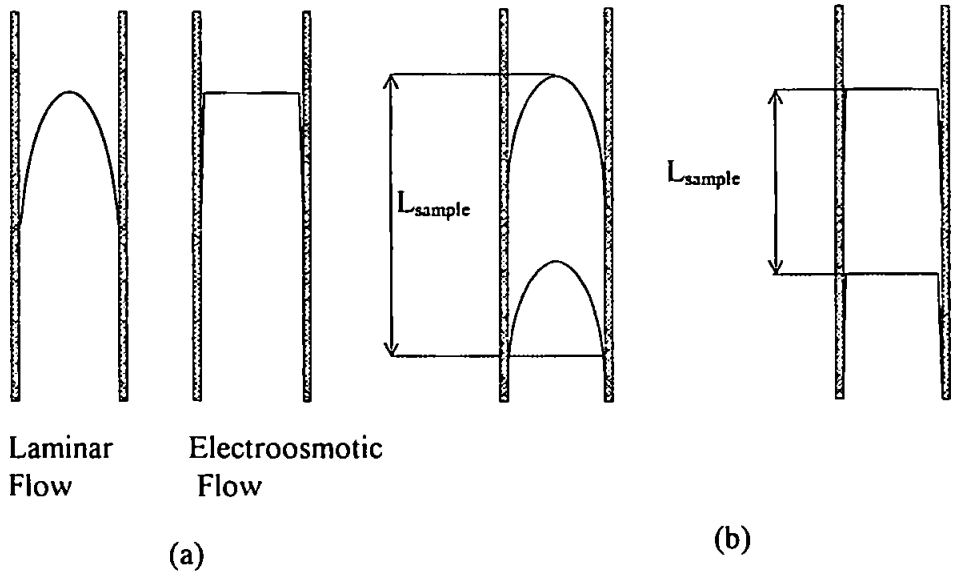

Figure 1.4. (a) Laminar and Electroosmotic Flow Profiles. (b) Sample Zone Shape During Laminar and Electroosmotic Flow. (L_{sample} is the total length of the sample zone during flow)

1.4. Effect of Electrolyte Composition on Electroosmotic Flow.

1.4.1. The pH of the Electrolyte.

As previously mentioned in section 1.3 the rate of the electroosmotic flow is dependent on the electrolyte pH, which is related to the degree of ionisation of the surface silanol groups. Therefore lowering the pH of the electrolyte produces a decrease the rate of the electroosmotic flow. Figure 1.5 shows the effect of pH on the electroosmotic flow in a fused silica capillary. At a pH value of 3 electroosmotic flow is minimal, as the pH rises, the flow increases exponentially until pH 7 when it follows a limited growth pattern, reaching its maximum flow at about pH 8. Hysteresis effects have been

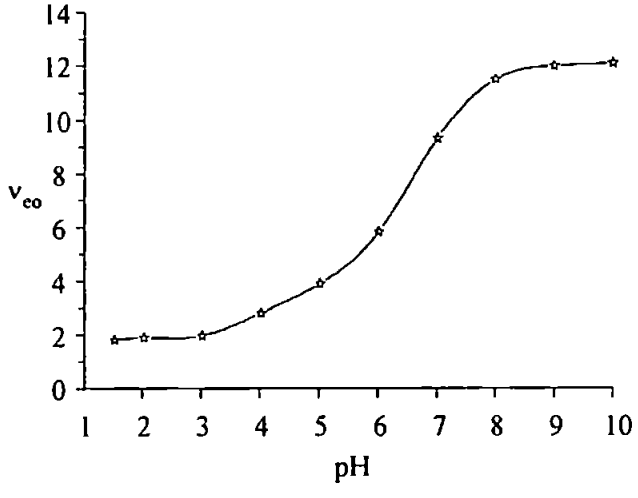

Figure 1.5. Changes in the Velocity of the Electroosmotic Flow (v_{eo} - cm sec^{-1}) with pH

noted [8,9] where the direction of approach to a particular pH value produces a different electroosmotic flow.

Since the mobility of an ion is dependent on its charge, the pH of the electrolyte can also be used to alter the selectivity of a separation by changing the mobility of a solute.

1.4.2. The Ionic Strength of the Electrolyte.

The electroosmotic flow is influenced by the ionic strength of the electrolyte. The electroosmotic flow decreases in proportion to the square root of the electrolyte concentration. This is due to modification of the thickness of the stern layer, which in turn influences the zeta potential.

1.4.3. The Size and Charge of Electrolyte Ions.

The choice of electrolyte co-ion can also be used to manipulate the electroosmotic flow. This is because the size and geometric arrangement of the ions in the Stern layer determine the zeta potential. Small highly charged ions form a dense tight layer, which produces greater shielding the capillary wall, reducing the zeta potential and therefore the electroosmotic flow.

1.4.3. Viscosity Modifiers.

The addition of long chain polymeric additives such as hydroxypropylmethylcellusose can be used to slow the electroosmotic flow by increasing the viscosity of the buffer, retarding the migration of ions by the creation of a physical barrier. The relationship between viscosity and electroosmotic flow is shown in Equation 1.9.

Viscosity modifiers can also be used to increase the resolution of solutes, especially cationic components, by retarding not only the electroosmotic flow but also the migration of the solutes themselves. The relationship between viscosity and mobility is shown in Equation 1.7.

1.4.4. Organic Solvents.

The addition of organic solvents can be used to modify the viscosity of the electrolyte or the zeta potential of the capillary wall. In general linear alcohols such as methanol or ethanol decrease the

electroosmotic flow, whilst solvents such as acetonitrile produces a small increase. Organic solvents can also be used to modify selectivity and aid solubility.

1.5. Joule Heating.

Although the efficiency of a separation improves with the use of higher field strengths, the passage of excessive currents leads to the generation of resistive heat that in turn may decrease the separation efficiency. The generation of this heat is one of the principal reasons for carrying out electrophoresis in a capillary, due to the more effective heat dissipation obtained from the higher surface to area ratio, allowing the use of higher separation voltages.

Joule heating is the result of frictional collisions between mobile ions and electrolyte constituents. One of the major limitations on the speed and resolution of an electrophoretic separation is the inability to efficiently dissipate heat through the capillary wall. Joule heating can adversely affect the efficiency and resolution of a separation in two ways, due to the development of natural convection and radial thermal gradients.

Natural convection is the flow of fluid due to differences in density. The viscosity of most fluids decreases with increasing temperature, causing lower density fluid to 'float' above the cooler more dense fluid. Natural convection is more of a problem with capillary electrophoresis in wide bore capillaries and traditional electrophoresis where gels are used to provide a physical barrier to convection currents.

Since heat is only lost through the capillary wall, the rate of dissipation will be lower at the centre of the capillary and this can lead to the formation of a radial thermal gradient.

As the viscosity of the electrolyte effects the electroosmotic flow and the electrophoretic velocity of a solute, temperature will also influence these factors by altering the electrolyte velocity. When a thermal gradient develops the electroosmotic flow becomes greater at the centre of the capillary than at the wall, resulting in a flow profile similar to that of hydrodynamic flow. The

electrophoretic velocity of the solutes is also influenced by temperature. Reduction in the viscosity of the electrolyte reduces the frictional drag and allows the ions to migrate with greater velocity at the centre of the capillary, causing zone broadening. In severe cases, the buffer may boil resulting in interruption of the electric field.

Joule heating can be reduced by decreasing the applied field, although this decreases the mobility of ions and hence the speed and efficiency of the separation. An alternative method is to use a narrower bore capillary, this has two effects, a decreased cross-sectional area means there are less ions present for the passage of current and also an increased surface to area ratio, improving heat dissipation through the capillary wall.

Alternatively, the capillary can be mechanically cooled by the flow of either fluid or air through an external jacket.

Joule heating can be detected by performing an Ohms Law test on the electrolyte during method development. This entails 'ramping' the voltage across the capillary and plotting the current obtained. The current increase will be linear until joule heating begins to become apparent.

1.6. Diffusion in Capillary Electrophoresis.

The major attraction of CE over other separation techniques is the very high separation efficiency attainable. Under ideal circumstances, where molecular diffusion is the only source of zone broadening, the separation efficiency is proportional to the applied voltage and the migration distance from the injection point to the detector, producing plate numbers in the order of several hundred thousand or more [10]. In reality broadening due to convection, electrodiffusion and wall effects may exceed that caused by molecular diffusion, resulting in lower plate numbers than predicted [5].

1.6.1. Electrodiffusion.

With the analysis of metal ions complexed with ligands additional diffusion may also be encountered due to the instability of the complexes. Complex stability equilibria consider only thermodynamics, it is also assumed that an equilibrium between the complex and the free metal is reached. In reality, the kinetics of a complexation reaction may not be fast enough for equilibrium to be reached during electrophoretic migration. When this takes place the observed migration velocity of the metal complex is not composed of a single velocity attributable to the complex alone but composed of the combined velocities of all the species present in the sample zone. This leads to the introduction of an additional element of zone broadening, which is termed electrodiffusion. Electrodiffusion is defined by Equation 1.10 and is additional to the standard diffusion coefficient.

$$D_e = \frac{E^2 \Delta\mu \, k_1 k_2}{2t} \qquad \textit{Equation 1.10}$$

Where E is the electric field strength, $\Delta\mu$ is the difference between the effective mobility and the mobility of an ion in non-equilibrium, k_1 is the reaction rate for complex formation and k_2 is the rate of complex dissociation.

In equation 1.10 only the kinetics of the complex formation and dissociation are considered, when side reactions with the electrolyte constituents or impurities are involved in reactions with the metal or ligand, the migration mode of the complex becomes very complicated and electrodiffusion can be increased. The passage of current through the capillary generates some heat and the rate of loss will never be as efficient from the centre of the capillary as the edge. The generation of heat is usually considered to be within tolerable levels until it begins to cause peak broadening. But since the rate of a reaction is temperature related even a small amount of heat will result in an increase in the rate of the reaction. This leads to the possibility that a complex that is stable under standard conditions may not be stable during electrophoresis.

In many cases, electrodiffusion can provide a much greater contribution towards zone broadening than other forms of diffusion. During either method of direct detection slow reaction kinetics play a major part in the ability of a complex to survive electrophoresis and slow kinetics of formation can lead to serious electrodiffusion, to the point that the peak becomes totally lost.

Kinetics has been used as a method of manipulating the selectivity of a separation using what was termed the kinetic differentiation mode of CE [11-15] Pre-formed PAR complexes of Co^{3+}, V^{5+}, Fe^{2+}, Cu^{2+}, Ni^{2+}, were separated in an electrolyte devoid of the ligand. Cd^{2+}, Zn^{2+} and Mn^{2+} totally dissociated and were not detected. In this mode, it is highly likely that the thermodynamics stability of the complexes will also play a role in their detection. In addition, the sensitivity of the complexes that are detected is likely to be compromised to some extent by dissociation.

Ideally for electrophoretic migration a metal complex should have high thermodynamic stability, the kinetics of the reaction should be fast in the forward reaction and slow in the reverse. A stoichiometric ratio of 1:1 is also preferred as his reduces the number of possible species and thus the contribution to zone broadening from electrodiffusion.

1.7. Capillaries for Capillary Electrophoresis.

Fused silica, a highly cross linked polymer of silicon dioxide (SiO_2), is the most common material used in the manufacture of capillaries for CE. Fused silica has become widely used for CE, partly due to the ready availability of technology developed in the manufacture of capillary columns used in gas chromatography (GC) and in part due to its properties of UV transparency, zeta potential, high tensile strength and durability, when externally coated with polyamide.

The surface characteristics of the inner wall of a capillary can be highly influential on the efficiency and resolution of a separation, even a small amount of interaction between the solute and wall can cause a significant reduction in resolution and efficiency, particularly with large molecules [16]. The choice of material for capillary construction is therefore of great significance.

Ideally, the internal wall of the capillary should be chemically inert to the solute; however, in this respect fused silica is far from being an ideal material for CE capillaries. The surface of fused silica is very difficult to quantify, being composed of siloxane groups and at least three surface silanol groups, Figure 1.6 [17]. The exact nature and density of these groups can vary considerably, as can be seen from the pK_a values quoted in the literature, which range from 5.3 to 6.3. Deprotonation of these surface groups creates an active anion exchange surface, which is responsible for the creation of electroosmotic flow, however, this surface is also available for interactions with cationic solutes. Cations may also bind to the capillary walls by methods other than electrostatic attraction, which are not well understood [18]. In addition, there appears to be phase-related interactions where hydrophobic molecules can adsorb onto the wall, particularly at low pH [19].

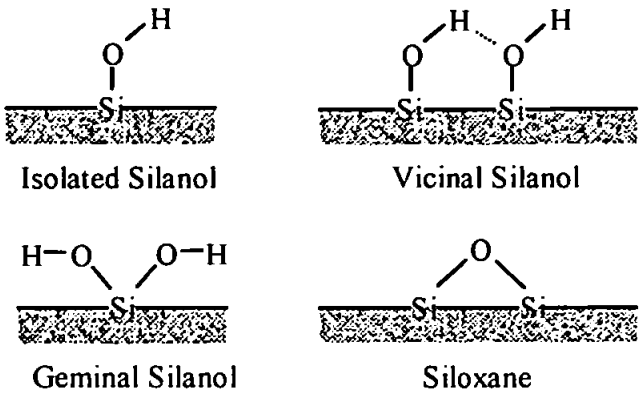

Figure 1.6. Silica Groups on Fused Silica Capillary Walls [17].

A variety of polymeric capillaries have also been used by several workers but as yet have not become a viable alternative to fused silica. Available in a range of materials with varied surface characteristics and chemistries, which include polystyrene, Poly(vinylidene fluoride) (PVDF), Polypropylene [20-22] and polybutylene terephthalate [21]. One of the main reasons these capillaries have not become widely used is due to the poor uniformity of the internal diameter. This can be due to the manufacturing process, but also may occur during handling due to the ductile nature of the materials. Localised heating can cause the capillaries to melt and the electric field generated within the capillaries can cause them to be attracted to metal parts of the instrument resulting in short-circuiting and melting.

1.8. Capillary Coatings.

A wide variety of methods have been developed with the purpose of reducing poor reproducibility of migration times due to variation in the electroosmotic flow and to improve the efficiency of separations by counteracting solute-wall interactions.

In certain circumstances, electroosmotic flow can be a disadvantage, particularly with the analysis of mobile anions. It is possible to reduce, stop or even reverse the electroosmotic flow by modification of the inner wall of the capillary. The electroosmotic flow can be altered in several ways, usually being accomplished by masking the capillary surface with a coating. These coatings can be subdivided into two fields, bonded coatings and dynamic coatings. Bonded coatings can be regarded as those that are permanent and include chemical derivatization of the capillary wall. Dynamic coatings are temporary and need continually or routine regeneration, these coatings usually take the form of additives to the electrolyte.

Surface modification by bonded coatings or electrolyte additives can also be used to eliminate or reduce solute wall interactions and in many instances, this is the primary motivation for their use.

1.8.1 Dynamic coatings

1.8.1.1. Adsorbed coatings

These coatings are used either as electrolyte additives or physically adsorbed onto the capillary wall by flushing through the capillary between runs. Coatings of this type are usually non-ionic surfactants such as Brij-35 [23] and Carbowax [24]. Towns and Regnier [25] studied the adsorption of variety of non-ionic surfactants including Brij-35, Brij-78, Tween-20, Tween-4 and Tween-60 to C18 bonded capillaries. These coatings work by adsorption onto the capillary surface physically masking the ionised surface groups.

1.8.1.2. Cationic Additives

Low concentrations of cationic surfactants such as cetyltrimethylammonium bromide (CTAB) and other tertiary ammonium salts, form ion pairs with anionic silanoate groups on the capillary wall,

masking the negative charge of the wall. In low concentrations, cationic surfactants reduce electroosmotic flow, but as the concentration is increased electroosmotic flow can be eliminated as more or the silanoate ions are masked. Higher concentrations still, result in the formation of hemi-micelles along the capillary wall giving the capillary wall a net positive charge and reversal of the electroosmotic flow, as shown in Figure 1.7. The formation of hemi-micelles most likely occurs prior to the total masking of all the silanoate groups on the capillary wall. This results in the surface being made up of a number of negative charges compensated by a number of positive charges, which could still result in wall effects.

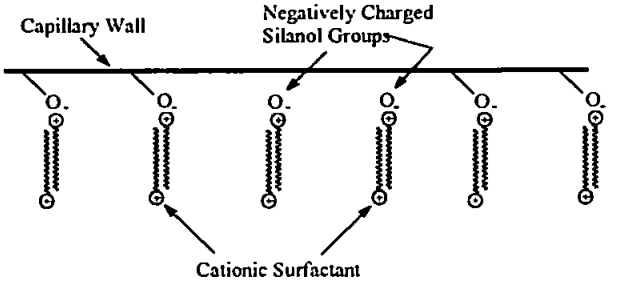

Figure 1.7. Charge Reversal of the Capillary Wall using Cationic Surfactants.

A non-covalently bound high molecular weight coating was used by Chiu *et al.* [26] to create positively charged capillary wall for the separation of cationic proteins. The coating was reported to be stable for several days and easily regenerated by treatment with dilute solutions of polyarginine. Cordova *et al.* [27] examined four cationic polymers, polybrene, polyethylenimine, poly(methoxyethoxyethyl)ethylenimine and poly(diallyldimethylammonium chloride) to stabilise electroosmotic flow and reduce the adsorption of proteins.

These additives are primarily used to reduce solute adsorption and stabilise the electroosmotic flow rather than suppress it. The most frequently used compounds used for this purpose are a variety of relatively low molecular weight amines and amino acids [28, 29].

1.8.2. Bonded Capillary Coatings

A wide range of bonded phase capillary coatings have been developed. The production of these capillaries usually involves chemically bonding a variety of polymers to the capillary wall to produce a wide range of properties, which include hydrophilicity, hydrophobicity and charge.

Many of these phases are derived from technology developed for the production of stationary phases for HPLC and gas chromatography (GC) columns. Although many of coatings have been developed with the purpose of preventing the adsorption of cationic biopolymers on the wall of fused silica capillaries, there are many other situations in capillary electrophoresis when the quality of a separation can be improved by the use of coated capillaries.

1.8.2.1. Non-Ionic Phases.

These coatings are generally used to eliminate electroosmotic flow by reducing the charge on the capillary wall and increasing the viscosity at the electrolyte wall interface. Although the charge on the wall may be entirely eliminated by polymer coatings, in the case of hydrophilic coatings an electroosmotic flow may be present, caused by ions in the electrolyte becoming adsorbed on the polymers thus creating a potential [4]. The major factor concerning the elimination of electroosmotic flow then becomes the increase in the viscosity at the capillary wall caused by the polymer. Non ionic coatings are also frequently employed to prevent the adsorption of cationic solutes such as metals, proteins and peptides.

1.8.2.1.(i). Polyacrylamide Coatings.

Of the non-ionic phases Polyacrylamide has been the most widely investigated for the creation of neutral capillary coatings. Polyacrylamide has been extensively used for the gel electrophoresis of biopolymers, principally because it is hydrophilic and does not interact with these molecules, thus making it an obvious choice for the production of neutral capillaries for protein and peptide analysis. There a several methods of attaching polyacrylamide to the surface of capillaries published in the literature. The main variation in these procedures is the method used to create the bond between the wall and polymer. The first near zero flow capillaries coated with linear polyacrylamide were produced by Hjerten in 1985 [30]. This method is the basis of the commercially available BioCAP capillaries supplied by Bio Rad, with the polyacrylamide being attached to the capillary wall with a Si-O-Si-C bond using γ-methacryoxypropyltrimethoxysilane.

An alternative method reported to provide greater stability of the coating at high pH was developed by Cobb *et al.* [231]. In this method the attachment of the polyacrylamide was achieved by Si-C bond, this was reported to be less prone to hydrolytic cleavage at higher pH values than the Si-O-Si-C bond. The capillary surface was first chlorinated with thionyl chloride then reacted with a Grignard reagent (vinyl magnesium bromide) and subsequently linear polyacrylamide attached.

Kohr and Engelhardt [32] vinylated the capillary surface using trichlorovinylsilane prior to bonding the polyacrylamide with azobisisobutyronitrile and thermal polymerisation. In order to overcome the unpredictable character of the surface of bare fused silica, Schmalzing *et al.* [33] produced a cross-linked polyacrylamide capillary coating with a double layer. The surface was first treated with cross-linked Polyvinylmethylsiloxanediol to create a stable under layer with a high density of bonding sites. Linear polyacrylamide was then grafted on to the double bonds of the siloxanediol and cross-linked with formaldehyde. A coating procedure for linear and cross-linked polyacrylamide capillaries was developed by Huang *et al.* [34]. Fused silica capillaries were pre-treated with 7-oct-1-enyltrimethoxysilane and then statically coated with polyacrylamide. Methylene bisacrylamide was added in the preparation of the cross-linked coating. This method of bonding the polyacrylamide to the capillary wall with hydrophobic alkylsilanes was expanded by Huang *et al.* [35] to include allyltrimethoxysilane (C3) and methyltrimethoxysilane (C1), in addition to the 7-oct-1-enyltrimethoxysilane (C8) already used. The authors reported the greatest stability of the coating was achieved when combinations of the different length alkylsilanes were used.

Cifuentes *et al.* [36] describe a method for the preparation of fused silica capillaries with a cross-linked polyacrylamide coating bonded to the internal wall, which was used in conjunction with cationic additives to the electrolyte in order to mask any residual negative charges on the capillary surface. Chen and Cassidy [37] bonded C1 and C8 linear alkyl chains to the capillary wall with

trimethylchlorosilane and dimethyloctadecylchlorosilane. Chiari *et al.* [38] separated proteins using capillaries modified with poly(acryloylaminoethoxyethanol. The polymer was covalently attached to the capillary surface, which had been modified with an α-methacryloxylpropyl functionality. High efficiency and resolution were reported using this coating.

1.8.2.1.(ii). Carbohydrate Coatings.

Carbohydrates have also been used for capillary coatings due to their neutral, hydrophilic properties.

Methylcellulose and dextran coated capillaries were prepared by Hjerten and Kubo [39] covalently bonding allyl derivitised polymers to the wall which was activated with γ-methacryoxypropyltrimethoxysilane. The methylcellulose capillaries were reported to be stable for upto 16 days at pH 12 and 10 days at pH 0.3. Liao *et al.* [40] fabricated a hydrophilic coating that strongly suppressed electroosmotic flow by covalently coupling a hydroxyl group of methylcellulose to the epoxy group of α-glycidoxypropyltrimethoxysilane. Huang *et al.* [41] describe a stable low flow cellulose derived capillary coating in which hydroxypropylcellulose and 2- hydroxyethyl methacrylate were statically coated onto a hydrophobic alkyl-silane under layer created from 7-oct-1-enyltrimethoxysilane. The capillaries were reported to be stable for several weeks in the pH range 2-10, the authors concluded that the hydrophobic under layer protected the Si-O-Si linkage between the under layer and the capillary wall from hydrolysis at high pH.

Bruin *et al.* [42] modified capillary surfaces with carbohydrate coatings for the separation of proteins. Epoxy-diol coatings were created by bonding γ-glycidoxypropyltrimethoxysilane to the surface followed by acid hydrolysis of the epoxide group using 0.1M HCl. A maltose coating was prepared by first derivitising the surface with 3-aminopropyltriethoxysilane. The capillaries were compared with polyethylene glycol (PEG) modified capillaries, the efficiency of the coated capillaries was reported to be lower than that obtained from the PEG modified capillary and the epoxy-diol coating was found to be unstable above pH 5. Chiari *et al.* [43] coated fused silica

capillaries were with ((N- acryloylamino)ethoxy)ethyl-beta-D-glucopyranose (AEG) to produce a coating with pronounced hydrophilicity. The coating was reported to give very stable migration times with RSD values of around 0.5%. Smith and El Rassi [44] produced zero flow capillaries by bonding high molecular weight hydroxypropyl cellulose to the inner surface of fused capillaries. A two layer approach was used, the capillary surface was first activated with γ-glycidoxypropyltrimethoxysilane, the first layer consisted of covalently bonded medium molecular weight hydroxypropyl cellulose (M.Wt. 30,000 - 50,000) and the second layer contained highly cross-linked large molecular weight hydroxypropyl cellulose (M. Wt. 150,000 - 400,000). The capillaries were reported to exhibit virtually zero flow until pH 8.5 when a slight flow was detected. A simple method for producing coated capillaries by adsorption of thin-film coatings of cellulose acetate, cellulose triacetate or cross-linked hydroxypropylcellulose was detailed by Busch *et al.* [45]. However, these coatings were reported to be unstable above pH 7·5. Mechref and El Rassi [46] fabricated hydrophilic capillaries with reduced electroosmotic flow by covalently attaching high molecular weight branched dextrans to the inner surface of fused silica capillaries. The dextrans were subsequently crosslinked with diepoxypolyethylene glycol. The coating was reported to exhibit reduced electroosmotic flow and was stable over a wide range of conditions including high and low pH.

Bentrop *et al.* [47] fabricated capillaries coated with poly (methylglutamate) by thermal polymerisation of the N-carboxyanhydride of glutamic acid-5- methylester, the authors reported that total shielding of surface silanols was not achieved.

1.8.2.1.(iii). Polymer Oxide Coatings.

Ng *et al.* [48] coated capillaries with triblock copolymers made up of polyethylene oxide-polypropylene oxide-polyethylene oxide (PEO-PPO-PEO). The capillaries, which were pre-derivitised with dichlorodimethylsilane and copolymers, were statically coated on the wall. Various copolymers made up from different PEO-PPO-PEO ratios were assessed for deactivation

of the capillary surface. Iki and Yeung [49] developed a simple method to coat PEO onto the inner wall of a bare fused-silica capillary via hydrogen bonding to the surface silanol groups. The capillary was filled with 1 M HCl solution, then flushed with 0.2% poly (ethylene oxide) solution containing 0.1 M HCl. The coating was reported to be stable in the pH range 3-7 and easily regenerated.

Towns *et al.* [50] prepared surface deactivated capillaries by pre-derivitised with glycidylpropyltrimethoxysilane, followed by deposition of a film of multifunctional oxirane, which was polymerised using either boron trifluoride or a tertiary amine. The coatings were reported to reduce protein adsorption but still allow sufficient electroosmotic flow to carry both positive and negative species past the detector.

1.8.2.1.(iv). Glycol Coatings.

Bruin *et al.* [51] separated proteins in hydrophilic polyethylene glycol (PEG) modified capillaries. The capillary was first silylated using γ-glycidoxypropyltrimethoxysilane prior to grafting with PEG600. Huang *et al.* [52] bonded polyethylene glycol (PEG) and polyethylene imine (PEI) onto the capillary surface pre-derivitised with a highly crosslinked polysiloxane. Zhao *et al.* [53, 54] developed a simple one step method for producing capillaries coated with Superox 0·6 and 4 (PEG) and Ucon (polyethylene-propylene glycol). The capillary surface was derivitised with hexamethyldisilaxane and the polymer immobilised with dicumyl peroxide, both steps being performed simultaneously, the polymers were then cross-linked by slow heating to 150 °C.

A simple method for producing a stable neutral surface coating was developed by Ren *et al.* [55] the capillaries were coated with a thin film of epoxy resin to which polyethylene-propylene glycol was bonded. The coating was reported to be stable in the pH range 4-11.

1.8.2.1.(v). Octadecylsilane Coatings.

Towns and Regnier [25] prepared hydrophilic capillaries by derivatization of the silica surface with octadecylsilane followed by the deposition of a layer of non-ionic surfactant from an aqueous

solution above the critical micelle concentration. The coating was reported to be of sufficient thickness to reduce electroosmotic flow 5-8 fold and the resultant flow was relatively constant throughout the pH range 4-11.

1.8.2.1.(vi). Polyether Coatings.

Fused-silica capillaries with hydroxylated polyether coatings were produced by Nashabeh and El Rassi [56]. The two layer coatings consisted of a glyceropropylpolysiloxane sub-layer covalently attached to the inner surface and a polyether top layer. In a second approach, the capillary wall was coated with polysiloxane polyether chains and both ends of the monomeric units covalently attached to the capillary surface. The coatings were reported to yield capillaries with different electroosmotic flow characteristics. The relatively long polyether chains shielding the unreacted surface silanols, reducing solute-wall adsorption.

1.8.2.1.(vii). Poly (vinyl alcahol) Coatings.

Gilges et al. [57] describe a simple method for the preparation of a water insoluble, permanent coating for fused silica capillaries by thermal immobilisation of Poly(vinyl alcohols) (PVA). A dynamic wall coating was also created using PVA as an additive to the electrolyte. The immobilised coating was reported to provide greater stability over a wider pH range than the dynamic coating.

1.8.2.2. Ionic Phases.

These coatings can be used to prevent solute-wall interactions by producing surfaces with a charge opposite to that of the solutes causing repulsion. Ionic coatings can also be used to stabilise electroosmotic flow and produce a flow that is independent of pH. The flow can be created in either direction dependant on the charge imparted to the capillary wall a switchable flow can also be created by the use of zwitterionic polymers.

1.8.2.2.(i). Cationic Coatings.

A hydrophilic positively charged capillary coating was developed by Towns and Regnier [58] in which polyethyleneimine (PEI) was adsorbed onto the capillary wall and subsequently cross-linked with ethyleneglycol diglycidyl. Physically adsorption of PEI onto the capillary wall was also used by Erim *et al.* [59] to produce coated capillaries with anodal flow. The capillaries were used in a pH range of 3- 11 and during long term stability tests, migration times were reported to increase by 3% over 60 hours leading the authors to conclude that the adsorption of PEI was almost completely irreversible. Smith and El Rassi [44] modified zero flow hydroxypropyl cellulose capillaries by bonding polyethyleneimine to the inner surface of capillaries to produce a pH independent anodal flow, a polyether layer was then covalently attached to reduce solute-wall interactions. The resulting anodal flow was reported to be relatively weak due to the high viscosity produced by the hydroxypropyl cellulose layer. Smith and El Rassi [44] also produced capillaries with relatively strong and constant anodal electroosmotic flow by chemically derivitising the inner capillary surface with methylated polyethyleneimine hydroxyethylated. Polyether chains were then covalently attached to the hydroxyl groups of the polymeric coating to produce a permanently charged coating with pH independent anodal flow and minimal solute-wall interactions.

Liu *et al.* [60, 61] developed capillaries with anodal electroosmotic flow by chemically bonding cationic groups to the capillary wall, the polymers used were poly (2-aminoethyl methacrylate hydrochloride) and poly (diallyldimethylammonium chloride).

A capillary surface derivitised with a quaternary amine was prepared by Huang *et al.* [62] to produce a capillary with anodal flow. The capillary surface was first silylated with iodopropyltrimethoxysilane, and then poly (4-vinylpyridine-co-butylmethacrylate) was immobilised through a reaction between the carbon-iodo bonds and the pyridine groups of the polymer, forming quaternary amine functionalities.

Chiou and Shih [63] bonded the macrocyclic polyether cryptand-22 to fused silica capillaries. At pH below 7, cryptand-22 is protonated and its behaviour is similar to that of quaternary ammonium salts forming complexes with anions, resulting in a reversal of the electroosmotic flow. Sun *et al.* [64] coated fused silica capillaries with the natural polymer chitosan by ionic interaction between the amino group of the polymer and the silanoate anion of the capillary surface. The cationic property of chitosan below pH 6.5 created an anodal electroosmotic flow in the capillary, even at low pH. The coating was reported to be stable for unto 20 hours at pH 2.49 - 5. Cheng *et al.* [65] separated metal ions in a positively charged capillary coated with 3-aminopropyltrimethoxysilane. Improved separation efficiency was reported due to reduced interaction between the cations and the capillary surface. Córdova *et al.* [27] evaluated four non-covalently bound polycationic coatings of differing molecular weight for the separation of proteins. The capillary coatings used were PEI (M. Wt. 15,000) poly (methoxyethoxyethyl) ethyleneimine (M. Wt. 64,000) Polybrene (M. Wt. 25,000) poly (diallyldimethylammonium chloride) (M. Wt. 10,000).

1.8.2.2.(ii). Anionic Coatings.

An anionic capillary coating with a pH independent flow was produced by Huang *et al.* [62]. The capillary was silanized with 7-oct-1-enyltrimethoxysilane followed by copolymerisation of 2-acryloylamido-2-2-methylpropanesulphonic acid and acrylamide mixtures onto the treated surface. The rate of flow could be altered by varying the ratio of the two polymers. The coating was used in electrolytes ranging from pH 3 - 10 and the variation in flow was reported to be within 2% over 80 injections.

Sun *et al.* [47] also used immobilised sulphonic acid groups to create a negatively charged wall with a pH independent flow, the method was based on that developed by Hjerten [30]. A combination of acrylamide and 2-acrylamido-2-methyl-1-propanesulphonic acid (AMPS) were

bonded to the wall, by varying the ratio of acrylamide to AMPS the degree of charge could be controlled, producing different rates of flow.

1.8.2.2.(iii). Coatings with Switchable Charge.

Smith and El Rassi [66] developed fused silica capillaries with switchable electroosmotic flow. A multifunctional surface consisting of unreacted silanol groups, positively charged quaternary ammonium functions, and a hydrophilic layer of long polyether chains was created. The net charge of the capillary surface could be varied from positive to negative by altering the pH of the electrolyte whilst the long polyether chains shielded biomacromolecules from the charged capillary surface. Cryptand moieties were immobilised onto the capillary surface through a cross-linking reaction of a cryptand-containing polymer and co-polymerisation of a cryptand-containing monomer by Huang *et al.* [62]. The resultant coatings provided switchable electroosmotic flow from low to high pH due to the complexing ability of the cryptand moieties with the metal ions from the buffer solution.

Guo *et al.* [67] fabricated a capillary coated with aminopropyltriethoxysilane having switchable electroosmotic flow. The net charge at the surface of the coating being dependent on the degree of protonation of the amino groups and the degree of ionisation of the silanol groups. At pH 6.0 or below, the coating was reported to have a net positive charge, which resulted in anodal flow and at pH 6.5 or above, the coating was negatively charged with flow towards the cathode.

1.8.3. Polymeric Capillaries.

Liu *et al.* [21] coated hollow fibres made from polypropylene and polybutylene terephthalate with polyacrylamide. Surface modification was reported to significantly improve the performance of the capillaries. A later paper [68] details new procedures involving surface activation and in situ polymerisation, using dynamic and static coating of reagents to produce both linear and cross-linked polyacrylamide modified surfaces

Polypropylene hollow fibres modified with ionic functional groups were developed by Ren *et al.* [22]. Polymeric surface coatings containing sulfonic acid and quaternary amine functionalities and a novel polyphosphazene were bonded to the polypropylene surface. The authors report that varying the concentration or mixture of these coatings could be used to change the direction or magnitude of the electroosmotic flow. The authors also developed a hydrophilic zero flow capillary for the separation of basis protein mixtures by modifying polypropylene hollow fibres with hydroxypropylcellulose [69]. Fridstrom *et al.* [20] used polypropylene hollow fibres as columns for micellar electrokinetic capillary chromatography, reporting stable but enhanced electroosmotic flow in the pH range 5.0 –12.0. The surface was also modify with polyacrylamide and charged 2-acryloylamido-2- methylpropane sulfonic acid to lower the strength of the electroosmotic flow. Bayer and Engelhardt tested Polybutyleneterephthalate, ethylene-vinylacetate, polymethylmethacrylate, and nylon, assessing these materials for the reduction of protein adsorption [70].

1.9 Sample introduction.

The use of very narrow bore capillaries leads to certain difficulties involving the introduction of the sample into the capillary. To be of analytical merit, any method of sample injection must be highly reproducible. This requires the precise control of the quantitative aspects of the sample being introduced into the capillary.

Owing to the extremely small volumes of sample injected overloading of the sample onto the capillary can cause a significant increase in band broadening and a reduction in the separation efficiency [71].

Three methods of sample introduction have been developed for used in capillary electrophoresis

1.9.1. Hydrostatic Injection

With this method of sample introduction the sample is introduced by immersing the capillary inlet

into the sample vial and applying a positive pressure to the sample vial. Alternatively, a vacuum is applied to the destination vial drawing the sample into the capillary.

The volume of sample injected can be described by Poisseuille's law and can be estimated using Equation 1.11.

$$V_t = \frac{\Delta P D^4 \pi}{128 \eta L_t} \qquad \textit{Equation 1.11}$$

Where V_t is the volume injected per unit of time in nL s^{-1}, ΔP is the pressure difference between the inlet and outlet of the capillary, D is the internal diameter of the capillary, η is the viscosity of the sample and L_t is the total length of the capillary.

Hydrostatic injection requires precise control of the pressure or vacuum being applied and of the duration that it is applied for. It is important that when the injection is finished that any residual pressure or vacuum is quickly dissipated to prevent further injection of the sample. The method also requires the use of capillaries with internal diameters within certain constraints (between 25 and 100 μm). With wide bore capillaries the flow rate is too great for precise control requiring very low pressures, conversely very narrow bore capillaries require high pressures to inject the sample. Figure 1.8 shows a plot of D against V_t, data being calculated using 1.11. From Equation 1.11 it can be seen that V_t is also influenced by the viscosity of the sample being injected, consequently the viscosity of the samples and standards needs to be matched.

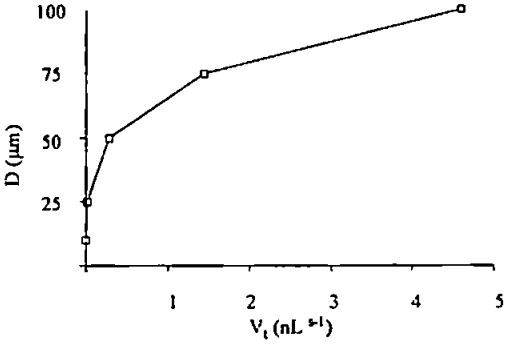

Figure 1.8. Plot of the Volume of Sample Injected with Time

1.9.2. Hydrodynamic Gravity Injection.

Gravity injection is a relatively simple method of sample introduction in which the capillary inlet is immersed in the sample vial and then elevated above the level of the destination vial, allowing the

sample to siphon into the capillary. With this method of sample introduction some means of physically elevating the sample vial to a definable height for a set period of time is required.

Since gravity can be considered a constant, this leaves two variables that need to be controlled during a hydrodynamic injection; the height to which the sample vial is raised; the length of time it is elevated. The raising and lowering of the vial also needs to be precisely controlled, as the sample will begin to siphon as soon as the vial begins to rise.

The volume of sample injected into the capillary can be estimated from Equation 1.11 by exchanging the expression ΔP to take into account the effect of gravity, the height difference and the density of the sample to give Equation 1.12.

$$V_t = \frac{\rho g \Delta h D^4 \pi}{128 \eta L_t} \qquad \textit{Equation 1.12}$$

Where ρ is the density of the sample being injected, g is the gravitational constant and Δh is the height difference between the capillary inlet and outlet.

As with hydrostatic injection methods gravity injection is also constrained to a range of capillary internal diameters. With narrow bore capillaries the length of the injection rises exponentially as the capillary diameter decreases. This is not a problem with the capillaries in common usage at the present but may become so if the trend for using narrower bore capillaries continues.

1.9.3. Electrokinetic Injection.

As with the other methods of injection, the capillary inlet is first immersed in the sample vial, a voltage is then applied across the capillary and sample ions are induced to migrate into the capillary. With regard to instrument design this is the simplest injection method, needing only a controllable high voltage power supply to perform the injection and this is an integral part of the instrument. Because the sample is introduced into the capillary using electophoretic or electroosmotic migration, the more mobile sample components are preferentially migrated into the capillary over the less mobile, this creates a bias towards the more mobile components of the

sample [72]. Consequently, a sample loaded using this method is not quantitatively representative of the sample, unlike hydrostatic or gravity injections, which do not alter the composition of the sample.

The quantity of sample introduced into the capillary is dependent on several parameters, the most important being the electroosmotic flow and the mobility of the sample components. As previously mentioned electroosmotic flow is dependent on the composition of the electrolyte, its pH, ionic strength, and the mobility of its constituents. In addition, the pH and conductivity of the sample matrix will also have an influence on the quantity of sample introduced. A lower quantity of ions will be introduced into the capillary when a high ionic strength sample matrix is used due to the decreased velocity of the sample ions as a result of the reduced field strength they experienced within the sample vial. This bias can be compensated by the use of standard calibrations, although it is very important that the pH and conductivity of the samples and standards are closely matched. This bias created during an EK injection can be used to enhance the detection sensitivity of highly mobile ions.

The amount of sample injected per unit of time can be estimated from the Equation 1.13 [6]

$$V_t = \frac{\pi r^2 C_s (\mu_{ep} + \mu_{eo}) E \lambda_b}{\lambda_s} \qquad \textit{Equation 1.13}$$

Where λ_b is the conductivity of the background electrolyte λ_s is the conductivity of the sample and C_s is the concentration of the sample.

1.9.4. Sample Stacking.

One of the major problems associated with CE is the relatively poor detection limits that are achieved, to a greater extent this is caused by the low volumes of sample that can be injected into the capillary. Simply increasing the volume of sample injected onto the capillary may improve the sensitivity but often at the expense of the separation efficiency. Sample 'stacking' is a term used

to describe methods of injecting larger sample volumes, which subsequently become concentrated into narrow bands, minimising the effects on efficiency.

Stacking is accomplished by hydrostatic or hydrodynamic injection of a sample made up in a lower ionic strength matrix than that of the separation electrolyte. When a voltage is applied this results in a zone of high field strength in which the ionic velocity of the injected sample ions will be accelerated, once these ions migrate out of the injection zone into the separation electrolyte they encounter a lower field strength and their velocity slows. Meanwhile, ions within the sample zone still experience the high field strength and continue to move with accelerated velocity, causing them to catch up and stack into a narrow band. Buffer co-ions and counter-ions will also experience the high field strength as they migrate through the injection zone. In the case of an injection at the cathodic side, anions will stack up in front of the injection zone, cations will stack up behind the injection zone, and when electroosmotic flow is suppressed cations will migrate out of the capillary into the source vial.

Stacking can be used to inject larger sample volumes into the capillary, significantly increasing detection limits, with minimal losses of efficiency. Maximum stacking can be achieved by using a high ionic strength separation electrolyte and low ionic strength sample. However, the ionic strength of the separation electrolyte is limited by joule heating and the injection of large volumes of low ionic strength samples may result in flow disturbances, resulting in poor reproducibility. Ideally, samples should be made up in the lowest possible ionic strength matrix, such as de-ionised water. Since the measured electroosmotic flow is actually the average flow of all zones and as there is an inverse relationship between the ionic strength of a buffer and the zeta (ζ) potential of the capillary wall, the electroosmotic flow in the sample zone will be greater than that of the electrolyte. The effect of this is to introduce a hydrodynamic component to the electroosmotic flow, causing band broadening and a reduction in efficiency. Where electroosmotic Flow is suppressed, for example by using neutrally coated capillaries, this effect is less noticeable due to

the virtual absence of any kind of flow and lower ionic strength injections are possible. Chien and Burgi [73-78] developed a technique of stacking they termed 'field amplified stacking', in which the entire capillary was filled with sample. However this technique requires electroosmotic flow and the ability to switch voltage polarity during the run.

Stacking techniques can also be applied to electrokinetic injections, the principle is the same as with hydrostatic injections. The sample is made up in a low ionic strength matrix, when a voltage is applied ions in the sample vial rapidly migrate into the capillary where they encounter the higher ionic strength separation electrolyte and slow down, stacking into a narrow band. The major disadvantage of this injection method is that it is not reliably quantitative. This is because the number of ions migrating into the capillary is in part a function of time but also strongly influenced by the ionic strength of the sample. Therefore, if the ionic strength of each individual sample varies, then the number of ions migrating into the capillary will be different for each sample. This is a very real possibility when dealing with real samples and calibrating using synthetic standards.

1.10. Detection in Capillary Electrophoresis.

Along with injection problems, sensitive detection has also proved a problem for CE. Although impressive mass limits of detection can be achieved, the concentration limits of detection are relatively poor. The low concentration limits of detection are in part due to the very small volume of sample injected but also due to physical problems with the detectors themselves.

The most common detection method of detection is based on molecular absorption spectrophotometry, where achieving good sensitivity for trace analysis is a major problem. Most commercially available instruments are fitted with on-column photometric detectors as standard. These can contribute to detection problems due to the very short optical pathlength and the poor optical characteristics of the cylindrical capillary surface. The optical pathlength in CE is typically

between 25 and 100 μm, compared with 5 to 10mm for standard HPLC detectors. The sensitivity lost by the short path length is compensated to some extent by the very high efficiencies of CE separations.

Fluorescence and laser induced fluorescence detectors are available on some instruments and highly sensitive conductivity detectors are now available. Capillary electrophoresis has also been interfaced with mass spectroscopy and most recently ICP-MS

The Dionex CES1 is fitted with a variable wavelength dual beam UV/Vis detector. The instrument is fitted with tungsten and deuterium lamps capable of producing wavelengths between 190 and 800nm in 1nm steps. The light source is delivered to the optic bench via fibre optic cable, which is divided to produce the signal and reference beams. The signal beam is composed of seven optical fibres vertical aligned with the capillary window. Light collection is by photodiode placed in close proximity immediately behind the capillary window. The detector employed a smoothing algorithm to reduce detector noise and the user adjustable parameter, the rise time, was set to 0.3 seconds.

One method of increasing the sensitivity of absorption detectors is to increase the optical pathlength. This can be achieved by the use of bubble cell capillaries, Figure 1.9 (a) or the use of 'Z' cell capillaries, Figure 1.9 (b) With these types of capillaries detector sensitivity is offset to some extent by a reduction in the separation efficiency. Rectangular capillaries with improved surface optical characteristics have also been tried.

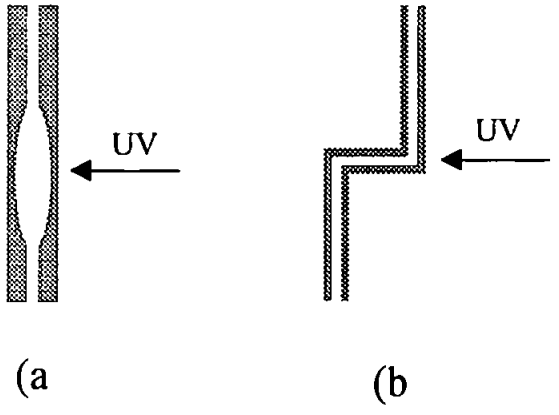

Figure 1.9 Schematic Diagrams of Bubble cell and 'Z' Cell capillaries

Unlike HPLC where all solutes pass the detector window at the same speed, in CE, separation is based on differences in the speed of each solute therefore each solute passes the

detection window with a different velocity and the width of the peaks become progressively broader as the run proceeds. Provided the run to run reproducibility of the migration time is good, this does not pose a serious problem. However, the migration time of a solute can be influenced by several factors including electrolyte viscosity, temperature, sample ionic strength and modification of the capillary wall. When this occurs, variations in the electroosmotic flow rate and migration time of solutes can effect the quantitative aspects of the data obtained. The height of a peak is unaffected by the speed of its passage past the detector window but the integrated area under the peak is. A simple correction can be applied to the data to compensate for any differences in the velocity of the solute. The simplest method of correction is to divide the area under the peak by the migration time in seconds producing a time compensated ratio.

1.10.1. Indirect Photometric Detection.

Up until 1995 the majority of the literature regarding the separation of cations was concerned with indirect detection methods. With this method an electrolyte additive, termed the probe, generates an UV absorbing background at a wavelength at which solute absorption does not occur. Thus when the solute migrates past the detector window a decrease in absorption is detected. The probe must migrate in the same direction as the ions being determined and should also have a similar mobility. This is in order to produce good peak shapes. Although it is not possible to match the mobility of the probe to every solute, a mobility of somewhere between is acceptable. Solutes migrating with a velocity greater than the probe produce fronted peaks and those migrating with velocities lower than the probe have tailing peaks. The degree of fronting or tailing depends on the difference between the migration velocity of the detected ion and the probe. In order to keep the electrolyte conductivity low whilst maintaining its buffering capacity, the probe should if possible be the electrolyte co-ion.

The main advantage of this approach is that it provides a universal detection system for analytes sharing the same displacement mode, thus exploiting the separation power of capillary

electrophoresis. Against is the relatively poor detection limit due to the signal to noise (S/N) ratio. The absorbance limit of detection deteriorates as background absorbance increases, since less light reaches the photodiode. The maximum concentration C_{LOD} can be calculated using Equation 1.14.

$$C_{LOD} = \frac{Cm}{TR \times DR} \qquad \textit{Equation 1.14}$$

Where DR is the dynamic range - the ability to measure a small change on top of a large signal and equal to the S/N ratio of the background signal. Cm is the Concentration of the probe. TR is the Transfer Ratio – the number of molecules of the probe displaced by each solute molecule.

Ideally the TR should be 1:1, but surface and equilibrium effects lower the TR. Increasing Cm does not improve sensitivity because the DR is related to Cm, although increasing Cm can be useful for extending the linear calibration range.

One of the problems of indirect detection is that in order to produce the separation of very large numbers of ions within relatively short times the concentration of each ion often needs to be manipulated. This is because a high concentration of one ion may produce a peak that masks another. Unfortunately, many real samples often contain vastly disparate concentrations of ions leading to the possibility that a separate method may need to be developed for each individual sample that differs in ionic concentration. The short analysis time is in part a product of the requirement for the ions to all migrate at a similar velocity as the visualising co-ion in order to maintain the shape of the peaks.

Although unselective indirect detection is capable of determining a large number of metal species in a single run, but very low detection limits are prevented by the relatively high background noise caused by the probe.

1.10.2. Direct Photometric Detection.

An alternative approach the indirect detection of metal ions by CE is to use direct absorbance

measurement. With this method the lower background noise in comparison to indirect methods should produce better detection limits. For metal ions the direct approach normally involves the formation of a strongly absorbing metal complex, usually with a chelating dyestuff, formed either pre-column or on-column. For example, 4-(2-pyridylazo resorcinol) (PAR) and derivatives have been studied by a number of workers for the direct detection of metal ions [12, 13, 15, 79, 80]. However, a major drawback to this technique is the potential instability of metal complexes during electrophoretic migration and many complexes completely dissociate before they reach the detector [81, 82]. It appears therefore that the complex must have a large stability constant preferably coupled with relatively slow kinetics of dissociation.

The direct detection of metal ions is accomplished by complexing the metal ion with a ligand to produce an absorbing complex and directly detecting this complex. Direct detection offers several advantages over indirect detection. These are principally related to sensitivity and selectivity. The sensitivity of the separation is only limited by the extinction coefficient of the complex. Consequently, very highly absorbing metal complexes can be used to improve the limit of detection.

There is extensive literature concerning the colorimetric determination of metals, which can be applied to the separation and detection of metal ions by CE.

Two methods of complexation can be used in the direct detection of metal ion complexes, being differentiated by where the complexation reaction takes place. Direct detection can be achieved by the injection of pre-formed complexes or by on-capillary complexation.

With the injection of pre-formed complexes the stability of a complex is of great importance. This is because the metal ion and ligand do not share the same migration mode, the metals being cationic have a positive mobility and the ligands being anionic or neutral will have a negative or zero mobility, therefore should they dissociate they will migrate away from each other. This problem can be alleviated to some extent by the addition of a small concentration of the ligand to

the electrolyte; this then introduces an element of on-capillary complexation to the migration of the metal complex. With the addition of reagent to the electrolyte the mode of complexation will become increasingly due to on-column complexation the more labile the complex.

With on-capillary complexation the ligand is present in the background electrolyte and the sample containing the metal ions is injected onto the capillary, where it becomes complexed. With this method of complexation a relatively high concentration of the ligand is required to ensure an adequate supply for the complexation reaction. Unless the absorption of the free reagent is significantly different from that of the complexes, a loss of sensitivity will result due to the high background; consequently some reagents will not be suitable to this method of complexation. Throughout on-column complexation highly labile ligands and metal ions will continuously dissociate and reform causing a retardation of their migration velocity. Even when complexed with anionic ligands, the overall migration velocity of highly labile complexes may be towards the cathode. Macka *et al.* [83] reported that the migration of strontium was cathodal when complexed with the anionic ligand sulphonazo III.

1.11. Related Techniques.

Capillary Electrophoresis is a group of related techniques than can be applied using a CE instrument.

1.11.1. Capillary Zone Electrophoresis (CZE).

Capillary Zone Electrophoresis, also referred to as free solution electrophoresis, is the simplest and most commonly used form of CE. Separations take place in an homogeneous electrolyte with the principal separation mechanism being differences in the electrophoretic mobilities of individual solutes. The parameters governing the conditions used in CZE separations have already been discussed and so will not be repeated.

1.11.2 Micellar Electrokinetic Capillary Chromatography (MECC).

One of the limitations of CZE is the inability to separate neutral compounds. MECC can be used to solve this problem by the addition of a pseudo-stationary phase to the electrolyte to produce separations similar to those obtained using reversed-phase LC. MECC was first introduced in 1984 by Terabe *et al.* [84]. This technique allows the separation of neutral solutes based upon differences in their distribution between the electrolyte and the pseudo stationary phase.

Separation in HPLC is based on differences in the partitioning of solutes between two phases. These phases are descriptively referred to as the stationary and mobile phases, the stationary phase being the chromatographic column packing and the mobile phase being the eluent. Although, referred to as the stationary phase there is no requirement for this phase to be static and in MECC the stationary phase is created by the addition of a surfactant to the electrolyte. The mobile phase is the electrolyte.

Surfactants are long chain hydrocarbons with polar head groups attached to one end. The polar head group imparts a degree of solubility to an otherwise insoluble molecule. In aqueous solution the polar group is solvated but the hydrophobic chain remains unsolvated. In solution at low concentration, the hydrophobic tails of the surfactant are attracted towards each other by van der Waals forces, whilst the polar head groups are repulsed from each other. As concentration increases, the molecules come together to form what is termed premicellar assemblies. As the concentration rises above a specific level, termed the critical micelle concentration (CMC), surfactant molecules assemble to form spherical aggregates called micelles. The exact structure and shape of these micelles is contested, but this is of little concern in this instance. Repulsion of the head groups and Van der Waals attraction of the tail groups determine the shape of the micelle produced. The choice of surfactant for MECC is a balance between solubility in aqueous solution and lipophilicity. With carbon chain lengths of 14 or more, solubility can become a problem. Shorter chain lengths produce smaller micelles of lower lipophilicity. Sodium dodecyl sulphate

(SDS) ($C_{12}H_{25}OSO_3Na$) an anionic surfactant is the most commonly used surfactant for MECC satisfying these requirements in most circumstances. In solution, a double layer similar to that on the capillary wall forms on the surface of the micelle.

1.11.2.1. Separation Mechanism

With fused silica capillaries electroosmotic flow is towards the cathode but SDS micelles are anionic and migrate towards the anode. At neutral to alkaline pH the electroosmotic flow is of sufficient velocity to carry the micelles towards the cathode but with a retarded velocity. An uncharged solute that remains in the electrolyte will migrate with a velocity equal to that of the electroosmotic flow, but a solute that has a greater affinity for the micelle will migrate with a lower velocity. Therefore, solutes with greater affinity for the micelle migrate with lower velocities than those that spend more time in the aqueous electrolyte.

Ionic solutes can also be separated by MECC with the migration order being anions, neutrals then cations. This reversed migration order is because anions are repulsed by the anionic surfactant, neutrals are separated by hydrophobicity and cations migrate last due to ion pairing with the micelles.

1.11.2.2. Choice of Surfactant.

Both cationic and anionic surfactants can be used in MECC with cationic surfactants the electroosmotic flow is reversed and therefore the polarity must also be reversed. Mixed micelles of ionic and non-ionic surfactants can be used. Mixed micelles have a lower surface charge to size ratio and therefore migrate at lower velocities than the corresponding ionic micelle creating a shorter separation window. Resulting in shorter analysis times at the expense of reduced resolution.

1.11.3. Capillary Isotachophoresis (CITP).

This technique, also referred to as displacement electrophoresis, is the separation of solutes in a discontinuous electrolyte system. CITP can be used for the determination of both cationic and

anionic species, although not simultaneously. The term isotachophoresis literally means migration at uniform speed, which is exactly what happens. Commercial instruments for CITP have been available since 1974, but despite this, the technique has failed to become widely accepted in analytical laboratories on a global scale, although the technique has found some favour within academic establishments particularly in Czech Republic.

The basic principles governing separations by CITP have already discussed in section 1.2 and will therefore only be outlined here.

The electrophoretic velocity (v) of a solute is proportional to the electric field strength that it encounters and since field strength is inversely proportional to conductivity, Equation 1.15, the electrophoretic velocity of an ion will decrease as conductivity (κ) increases.

$$v = \frac{I}{\kappa} = \mu_{ep} E \qquad \textit{Equation 1.15}$$

Consequently, when an ion migrates from a region of low conductivity to a region of higher conductivity, the field strength it encounters would be lower causing its velocity to decrease. When the sample itself becomes the conducting electrolyte the independent migration of ions will result in the formation of zones. These zones, consisting of ions of a specific velocity will also have a specific conductivity.

As with other CE modes the separation is based on differences in the mobilities of ions. Two electrolytes of differing mobility are used these are referred to as the leading and terminating electrolytes. The co-ion of the leading electrolyte must have a mobility greater than that of any of

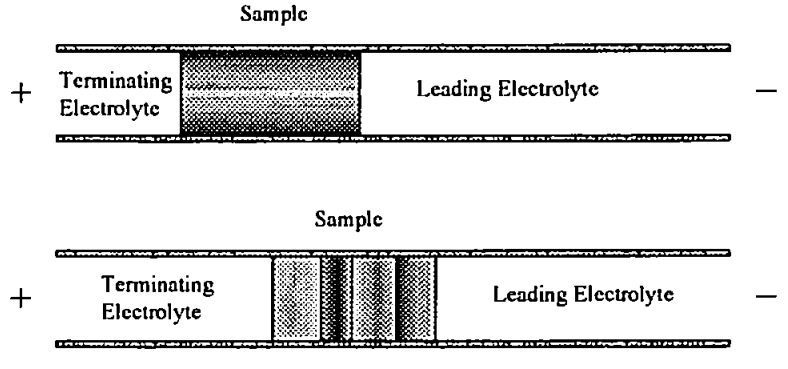

Figure 1.10. Schematic Diagram of a Four Component Cationic Separation by CITP.

the solutes to be separated and the co-ion of the terminating electrolyte must have a mobility of less than that of any of the sample components. To perform the separation, the capillary and destination vial are filled with the leading electrolyte and the source vial is filled with the terminating electrolyte, the sample is then injected into the capillary at the source end, between the leading and terminating electrolytes as shown in Fig 1.10. When a voltage is applied across the capillary, ions in the capillary begin to migrate towards the corresponding electrode, according to their individual mobilities.

As migration proceeds the ions begin to form into bands based on differences in their ionic velocity. However, as the zones develop, the field strength in each zone becomes altered by the ions migrating into it. The more mobile ions create a lower field strength since they are more conductive and since field strength is inversely proportional to conductivity, as a result the velocity of the ions decreases. On the other hand, the less mobile ions create a higher field strength causing their velocity to increase. Eventually a steady state develops in which all the zones migrate with the same velocity. Once the zones are created they remain focused, should an ion diffuse into a adjacent zone its velocity will be altered by the field strength it encounters causing it to migrate back into its own zone.

Since the conductivity of a solute is not just a function of its mobility but also its concentration, it is necessary that the concentration in each zone is uniform. However, there is no requirement for the concentration of each component to be matched at the time of injection, as dilute zones cause high field strengths, resulting in normalisation of the concentration in the zone by compression of the zone into a narrow band. This feature is one of significance for the enrichment of trace constituents.

As the separation does not take place in an homogenous electrolyte, electrical continuity through the capillary is maintained by the components in the sample zones, as a result each zone must remain in contact with those either side of it.

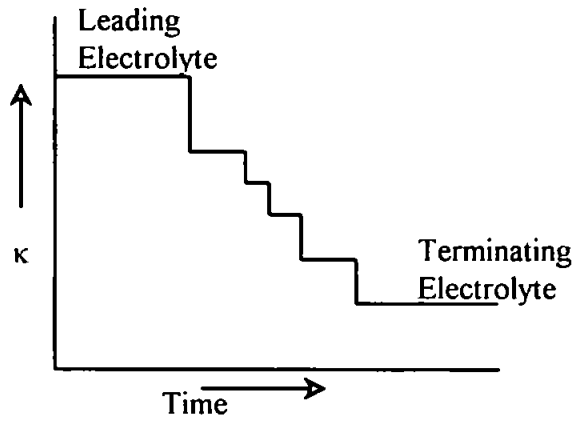

Figure 1.10. Schematic Diagram of Conductivity Detector Output in a Four Component Cationic Separation by CITP.

Since each zone has its own specific conductivity, detection is easily achieved by conductivity detection with the output appearing as a series of decreasing steps, illustrated in Fig.1.11. This means that the detected zones do not appear as the conventional peaks seen in HPLC or other modes of CE but as a series of steps. The implication of this may have some significance on the lack of general acceptance of this mode of CE.

With CITP separations electroosmotic flow is a disadvantage and is usually suppressed.

1.11.4. Capillary Isoelectric Focusing (CIEF)

CIEF is technique used to separation of zwitterionic solutes in a pH gradient. The technique is widely used for the separation of proteins and peptides.

The basic principle behind CE separations is mobility. As previously stated mobility is due to the charge to mass ratio of a solute, consequently, should this ratio be altered the mobility of the solute will also be altered. Correspondingly, if the charge of the solute is reduced to zero during a run then its mobility will also be reduced to zero.

The charge of a zwitterion is pH dependent, at its isoelectric point (pI) the charge is neutral, above this value the charge is negative and below the charge is positive. The charge distribution of a neutral amino acid, above, below and at its pI is shown in figure 1.12.

Due to the pH dependency of charge, a zwitterion encountering a pH greater than its pI will have a negative charge and migrate towards the anode and a zwitterion encountering a pH of less than its pI will have a positive charge and migrate towards the cathode. These zwitterions will

continue to migrate in their respective directions until they reach the point where their pI value is equal to that of the pH of the solution and at this point their mobility will be zero.

CIEF utilises this relationship between the pH and charge to separate the molecules. The pH gradient is created by filling the capillary with a mixture of zwitterions, termed the carrier ampholytes, having a range of pI values, the pH of the solution at this point is an average of the mixture. When a voltage is applied across the capillary, carrier ampholytes with a pI value of less than the pH of the solution will have a positive charge and migrate towards the cathode, while those with a pI value greater than the pH of the solution will have a negative charge and migrate towards the anode, Figure 1.13. Consequently, the pH at the anodic end of the capillary will decrease and the pH at the cathodic end will increase. The pH of the anodic vial needs to be lower than the pI of the most acidic ampholytes and likewise the pH of the cathodic vial must be greater than the pI of the most basic ampholytes to prevent them migrating out of the capillary. The choice of carrier ampholytes is important, obviously the mixture should cover the pH range of the solutes to be separated, but also the prevention of joule heating is an important consideration. For this purpose the conductivities of the carrier ampholytes need to be reasonably matched to provide a uniform field strength and prevent the formation of hot spots (caused by joule heating due to differences in the field strength).

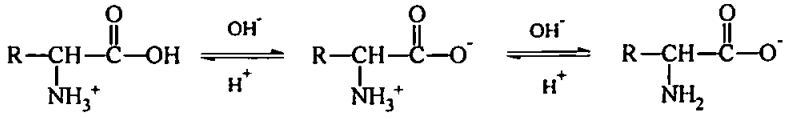

Figure 1.12. The pH dependent charge of a zwitterion.

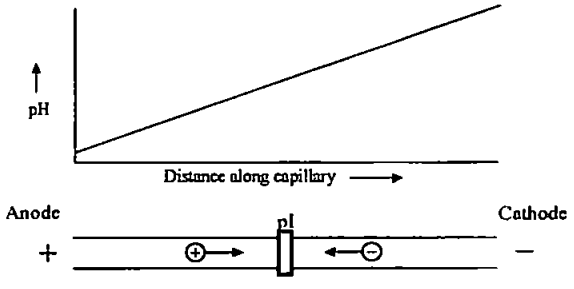

Figure 1.13. The Creation of the pH gradient in CIEF

Were the carrier ampholytes to form tight bands, (this would result in them being sandwiched between low conducting zones of water) the result would be partitioning of the carrier ampholytes between low conducting zones of water, giving rise to a series of hot spots along the capillary due to ohmic resistance. However, due to diffusion, the concentration of the carrier ampholytes in each pH band follows a gaussian distribution, with concentration decreasing away from the mid point this still gives rise to some joule heating. As the ampholytes continue to migrate, the changing pH causes their charge to alter. Eventually the charge will be reduced to zero and the ampholyte will cease migrating.

The separation is achieved by filling the capillary with the carrier ampholytes and sample, the capillary ends are then immersed in the appropriately buffered run vials and a voltage applied across the capillary. The carrier ampholytes and solutes will migrate until a steady state is reached when the mobility of the carrier ampholytes and solutes reaches zero, at this point the observed current will also approach zero. Once the components are focused they remain within their zones, diffusion causes them to drift out of the zone but as they leave it they acquire a charge which causes them to become refocused. Once focusing is complete it is necessary to mobilise the focused zones past the detector window. The most common type of detector used is an UV absorption detector. There are three methods of mobilisation of the focused zones

The first method, hydrodynamic mobilisation, is a relatively simple method in which a pressure [85] or vacuum [86] is applied to the appropriate run vial after focusing. The contents of the capillary can then be eluted past the detector. Band broadening during elution can be minimised by maintaining the focusing voltage.

The second method, electrophoretic mobilisation, is accomplished by the addition of salts [85] or zwitterions [87] to the buffer vial. In order to create the pH gradient the components in the capillary contain basic groups (BH^+) (e.g. NH_3^+) and acidic groups (A^-) (e.g. COO^- SO_3^-). The electroneutrality condition is represented by Equation 1.16.

$$C_{H^+} + \Sigma C_{BH^+} = C_{OH^-} + \Sigma C_{A^-} \qquad \textit{Equation 1.16}$$

Where C is the concentration in equivalents liter^{-1}

If a salt is added to the cathodic vial as shown in Figure 1.14 (a) it provides a source of anions which compete with OH^- for electromigration into the capillary, Equation 1.17 shows Equation 1.16 with the addition of the salt.

$$C_{H^+} + \Sigma C_{BH^+} = C_{OH^-} + \Sigma C_{A^-} + C_{X^{n-}} \qquad \textit{Equation 1.17}$$

where X^{n-} is an anion with a charge of n

In order to balance Equation 1.17, maintaining electroneutrality, the addition of X^{n-} will result in a decrease in OH^-. With less OH^- entering the capillary the pH will decrease causing ampholytes and solutes previously focused at their pI's, to become positively charged and migrate towards the cathode.

$$C_{H^+} + \Sigma C_{BH^+} + C_{Y^{n+}} = C_{OH^-} + \Sigma C_{A^-} \qquad \textit{Equation 1.18}$$

Where y^{n+} is a cation with a charge of n.

Similarly, as depicted in Fig 1.14 (b) and Equation 1.18, if the salt is added to the anodic vial, it produces a source of cations Y^{n+} which compete with H^+ migrating into the capillary, resulting in an increase in pH. Consequently, previously focused ampholytes and solutes become anionic causing them to migrate towards the anode.

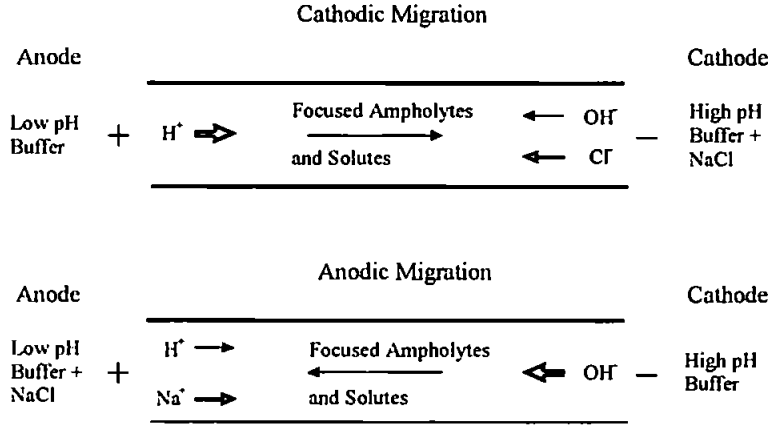

Figure 1.14. Mobilisation in CIEF. (a) cathodic Migration and (b) anodic Migration.

Increasing the concentration of the added salt induces the component mixture to migrate faster but at the expense of increasing joule heating.

The Third method, electroosmotic mobilisation, occurs simultaneously with the focusing step. This is achieved by slowing the electroosmotic flow by the addition of a viscosity modifier such as methylcellulose to the ampholyte mixture. This slows the electroosmotic flow sufficiently to ensure focusing occurs before the solutes migrate past the detector window.

1.11.5. Capillary Gel Electrophoresis (CGE)

Slab-Gel electrophoresis is the principal technique use for the separation of biological macromolecules such as proteins, peptides and polynucleotides. CGE is a direct transfer of this technique to capillaries. With slab-gel electrophoresis, the gel needs to be sufficiently viscous to prevent it flowing off the plates, permitting the prepared plates to be handled, but with CGE the capillary wall provides mechanical support for the gel allowing the use of lower viscosity gels. The gels used in slab-gel electrophoresis, such as agarose and polyacrylamide, can be applied to CGE. Low viscosity gels can be refreshed between runs but high viscosity gel filled capillaries are usually polymerised in situ and must be discarded when the gel deteriorates.

As with slab-gel electrophoresis the separation mechanism for CGE is based on molecular sieving, capillaries are filled with a polymeric gel matrix and solutes are induced to migrate through the gel by the application of an electric field across the capillary. Small molecules pass through the matrix relatively unimpeded but as molecular size increases, their passage through the gel becomes increasingly hindered. Under properly controlled conditions the solutes mobility is inversely proportional to its size.

Due to their shape and charge, proteins need preparation prior to analysis by gel electrophoresis. This involves reduction of disulphide bonds and unfolding of the coiled helix. This is accomplished by heating the proteins in a solution of sodium dodecyl sulphate (SDS) and a reducing agent (usually mercaptoethanol or dithiothreitol). The SDS binds to the proteins by

electrostatic and hydrophobic interactions providing the molecules with a negative charge so they all migrate in the same direction.

CGE is the most recent of all the related CE techniques, but has suffered with several problems such as unexpected gel failures and problems with high viscosity or rigid gels, and has had little success in replacing the more traditional slab-gel electrophoresis.

1.11.6. Capillary Electrochromatography (CEC).

Capillary electrochromatography is technique that combines CE and HPLC for the separation of solutes in capillaries packed with conventional HPLC packings, using electroosmotic flow to generate the flow of the mobile phase. Although the technique was first demonstrated by Pretorius *et al.*[88] in 1974, there has been little interest in CEC until quite recently and the technique is still very much in its development stage. The main advantages of CEC are the increased separation efficiencies achievable, the simplicity of the pumping system, the small quantity of reagents consumed and the requirement of very small sample volumes. The separation mechanism is a combination of electrophoresis and chromatography (the differential partitioning between two phases). CEC can be used to separate neutral and charged solutes. For neutral solutes, selectivity is the same using CEC or HPLC. However, with charged solutes selectivity will differ between CEC and HPLC, as the solutes migrate according to their individual mobilities under the influence of the applied electric field. Standard fused silica capillaries are used to create the separation columns. These capillaries are used because ionisation of the capillary wall and packings allows the generation of high mobile phase flow rates and the capillaries possess sufficient tensile strength to withstand the high pressures used to pack them. The most widely used packings are silica based reversed-phase particles, held in place with retaining frits. The frits are made from silica particles [89] or the stationary phase itself [90], fused in place with heat. Fritless columns have also been produced using chemically bonded charged gels [91].

The parameters influencing the choice of mobile phase for CEC are similar to those in CZE. Separations usually take place under conditions of high pH, when silanol groups of the packing and the capillary wall are ionised to ensure adequate flow rates. Buffering is essential for reproducible separations as variations in the electroosmotic flow will alter the elution times. The ionic strength of the electrolyte must also be controlled to prevent joule heating. The addition of non-aqueous solvents such as methanol or acetonitrile can be used to increase the solubility of less polar solutes. These can also be used to reduce the conductivity of the electrolyte but will also affect the zeta potential and electroosmotic flow.

The major theoretical advantage for using CEC is the increased separation efficiency that can be achieved when compared with HPLC separations. This is in part due to the flat flow profile through the particles imparted by electroosmotic flow and the ability to use smaller particles in the column packing. Over the years smaller particle diameter column packings have increase the efficiency and improved the resolution of HPLC separations. As the particle size has become smaller, the pressure required to drive the mobile phase through the packings at similar velocity increases proportionally to the square of the inverse of the particle size. At particle sizes below 3μm the back-pressure becomes a limiting factor [92]. In CEC, the mobile phase is electrically driven and there is no increase in back-pressure to impede the passage of the mobile phase through the packing, allowing the use of smaller particle size packings. However, the particle size used in packings for CEC columns appears to be limited to a diameter of 40 times the double layer thickness [89]. Smaller sized particles were reported to result in overlap of the double layer on the surface of the particles causing a reduction in the electroosmotic flow rate. This means that smaller particles can be used with higher ionic strength electrolytes, by reason of the thinner double layer, but at the expense of a greater current or reduced electric field.

With packed capillaries, electroosmotic flow is generated by the electrical double layer on the capillary wall and the surface of the stationary phase particles. Furthermore, the frits may also

contribute towards the electroosmotic flow. The maximum efficiency that can be attained from a packed bed column using a pressure driven system is limited by the particle size that can be used. Smaller particles produce higher efficiency, but at the expense of increased back-pressure and a greater pressure drop across the packed bed. With an electrically driven system, the flow is independent of particle size, theoretically allowing the use of sub-micron particle sizes; in addition, there is no pressure drop across the packing.

Dittman *et al.* [93] compared the contributions to band broadening in HPLC and CEC. Values were assigned to each of the contributory factors and applied to models with the same stationary phase, particle size, mobile phase and flow rate. The authors concluded that any factor independent of flow profile would be the same in either system and therefore the major difference between the systems was a reduction in eddy diffusion in CEC due to the electroosmotic flow profile. Eddy diffusion occurs due to unevenness in the packing in the column, resulting in pore sizes of different diameter. In a pressure driven system, the flow velocity is influenced by the channel width, with a wider channel allowing a greater flow, as illustrated in Figure 1.15 (a). These flow inequalities and the parabolic velocity profile contribute towards eddy diffusion. Whereas, with an electroosmotically driven system, Figure 1.15 (b) flow is generated uniformly throughout the packing (except where the channel through the particles is so small that the double layers of adjacent particles overlap) resulting in a uniform velocity profile and a reduction in eddy diffusion.

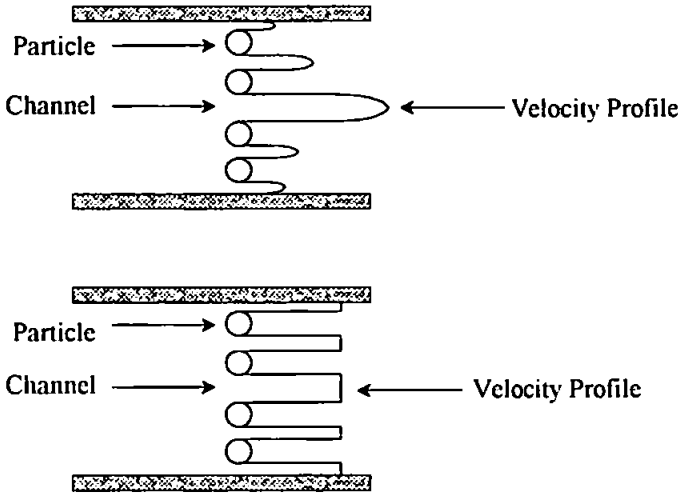

Figure 1.15. Eddy Diffusion and Velocity Profiles in (a) HPLC and (b) CEC.

One of the major problems with CEC is the formation of bubbles within the column when a voltage is applied. Bubble formation is thought to occur due to the heterogeneous nature of the column causing variation in local field strengths, differences in the electroosmotic flow rates and joule heating. The heterogeneity of the columns is due to the unpacked sections, frits and inequity in the distribution of the packing material. Pressurising the capillary prevents bubble formation but at the expense of complicating the system.

Sample introduction can also present a problem owing to the high back-pressure exerted by the packed column. This back-pressure restricts the use of hydrodynamic injection, and requires high pressures or longer injection times with hydrostatic injection. Electrokinetic injection is unaffected by the back-pressure but as previously mentioned introduces a bias with ionic solutes.

1.12. Theory of Coordination Chemistry.

This project concerns the study of the separation and determination of metal ions by capillary electrophoresis. Most of this will be based on the formation of metal complexes with special electrophoretic and spectroscopic characteristics. Consequently, it will be useful to set out the basic principles of metal coordination.

A coordination compound or complex is formed by association between a metal ion or atom and an anion or polar molecule, termed a ligand. The concept of metal complexes originated from the work of Swiss chemist Werner (1891) who proposed that metal ions (in particular transition metals) had two types of valence termed the principal and auxiliary valences. The principal valence is based on the oxidation state of the ion while the auxiliary valence represents the number of ligands bonding to the ion and relates to the coordination number.

Ligands donating a single pair of electrons such as water, ammonia and the halide ions are termed monodentate. Ligands donating more than one pair of electrons are referred to as multidentate. Examples of multidentate ligands include ethylenediamine, which donates two pairs of electrons

and is termed bidentate or ethylenediaminetetraacetic acid (EDTA), which donates six pairs of electrons and is termed hexadentate. When a multidentate ligand bonds to a metal ion, a ring structure of four or more members is produced, this ring structure is called a chelate.

1.12.1. Bonding in Metal-Ligand Complexes.

A simple representation of the nature of the bond between the metal and ligand regards the metal as an electron pair acceptor and the ligand as an electron pair donor. The metal acts as a Lewis acid, while the ligand acts as a Lewis base and the donation of an electron pair by the ligand to the metal creates a coordinate bond.

Trends in the stability of metal complexes can be explained using the Principle of Hard and Soft Acids and Bases (HSAB Principle) [94]. In the HSAB Principle, acids and bases are classified as either 'hard' or 'soft'. Hard acids have acceptor atoms that usually possess high positive charge and small size with no unpaired electrons in the valence shell. Soft acids have acceptor atoms of low positive charge, small size and often have unpaired electrons in the valence shell. Hard acids are not very polarisable whereas soft acids are easily polarisable. The terms hard and soft are derived prom the polarisability of an acid or base. Polarisability relates to deformation of the electron cloud and the ability to become deformed can imply softness, accordingly polarisable acids or bases are referred to as soft and non-polarisable acids or bases are referred to as hard. Chemical hardness or softness is not an inherent property of an acid or base but can be influenced by the substituent atom. For example tri-valent boron is borderline between hard and soft but the addition of three fluoride ions makes it a hard acid. Conversely, the addition of three hydride ions softens the boron.

The general concept of the HSAB Principle is that hard acid prefer to coordinate with hard bases and soft acids prefer to coordinate with soft bases. Table 1.1 displays a list of metal ions classified as hard or soft acids and Table 1.2 classifies a range of ligands as hard or soft bases. Soft acids tend to form covalent bonds with soft bases and hard acids form ionic interactions with

hard bases. Although, there are many examples of strong bonds between mismatched pairs and other factors which determine bond energies must be taken into account, such as the charges and size of the acids and bases, the electronegativities of the donor and acceptor atoms, orbital overlap and steric repulsion. However, the HSAB Principle refers to an additional stabilisation of hard-hard and soft-soft, or destabilisation of hard-soft pairs [94].

Table 1.1. Classification of Metal Ions as Hard or Soft Acids [95].

Hard	Soft
H^+ Li^+, Na^+, K^+, Rb^+, Cs^+	Pd^{2+}, Pt^{2+}, Pt^{4+}
Be^{2+}, Mg^{2+}, Ca^{2+}, Sr^{2+}, Ba^{2+}, Ra^{2+}	Cu^+, Ag^+, Au^+, Cd^{2+}, Hg^+, Hg^{2+}
Sc^{3+}, La^{3+}, Ce^{4+}, Gd^{3+}, Lu^{3+}, Th^{4+}	CH_3Hg^+, BH_3, Te^{4+}, Tl^+,
U^{4+}, UO_2^{2+}, Pu^{4+}, Ti^{4+}, Zr^{4+}, Hf^{4+}	
VO^{2+}, Cr^{3+}, Cr^{6+}, MoO^{3+}, WO^{4+}	
Mn^{7+}, Mn^{2+}, Fe^{3+}, Co^{3+}, BF_3, BCl_3	
Al^{3+}, $AlCl_3$, Ga^{3+} In^{3+}, Si^{4+}, Sn^{4+}	
Borderline	
Cr^{2+}, Fe^{2+}, Co^{2+}, Ni^{2+}, Cu^{2+}, Zn^{2+}, Rh^{3+}	
Ir^{3+}, Ru^{3+}, Os^{2+}, Sn^{2+}, Pb^{2+}, Sb^{3+}, Bi^{3+}	

Table 1.2. Classification of Ligands as Hard or Soft Bases [96]

Hard	Soft
H_2O, OH^-, F^-	R^-, C_2H_4, C_6H_6, CN^-, RNC, CO
CH_3COO^-, PO_4^{3-}, SO_4^{2-}	SCN^-, R_3P, $(RO)_3P$, R_3As
Cl^-, CO_3^{2-}, ClO_4^-, NO_3^-	R_2S, RSH, RS^-, $S_2O_3^{2-}$
ROH, RO^-, R_2O, O^2	I^-, R^-, H^-
NH_3, RNH_2, N_2H_4	
Borderline	
$C_6H_5NH_2$, C_5H_5N, N_3^-, N_2	
NO_2^-, SO_3^{2-}, Br^-	

In aqueous solution soft acids and bases tend to form stable complexes but hard acids form only moderately stable complexes, even with hard bases. This is because water acts as a hard molecule, both as an acid and as a base, competing with the ligand.

1.12.2. Stability of Metal Complexes.

A quantitative description of the extent to which an aqueous metal ion bonds to a ligand can be gained by using the appropriate equilibrium constants.

In aqueous solutions, metals exist in the hydrated form, consequently when a ligand bonds to a metal (M) it has to displace a water molecule. For a monodentate ligand (L) the formation of the complex proceeds in a stepwise manner with successive replacement of water molecules, as in Equation 1.19 –1.20, (for simplicity the charges of the metal and ligand have been omitted).

$$[M(H_2O)_x] + L \rightleftharpoons [ML(H_2O)_{x-1}] + H_2O \qquad \textit{Equation 1.19}$$

$$[ML(H_2O)_{x-1}] + L \rightleftharpoons [ML_2(H_2O)_{x-2} + H_2O \qquad \textit{Equation 1.20}$$

The reaction continues until the coordination number of the metal is reached. For reactions in dilute aqueous solution, the activity of water remains essentially constant and is therefore usually omitted from equations defining stability constants.

1.12.2.1. Concentration Stability Constants.

For a mononuclear complex, assuming the resultant complex does not precipitate, the coordination of a metal and ligand can be described by the equilibrium expressions in Equation 1.21- 1.23.

$$M + L = ML \qquad K_1 = \frac{[ML]}{[M][L]} \qquad \textit{Equation 1.21}$$

$$ML + L = ML_2 \qquad K_2 = \frac{[ML_2]}{[ML][L]} \qquad \textit{Equation 1.22}$$

$$ML_{n-1} + L = ML_n \qquad K_n = \frac{[ML_n]}{[ML_{n-1}][L]} \qquad \textit{Equation 1.23}$$

These reactions continue until the number of ligands equals the coordination number of the metal ion. K_1, K_2 ..... K_n are the stepwise formation constants for each reaction. There are n equilibria for each reaction where n represents the coordination number of the metal ion M, for

the ligand L. The coordination number of the metal may vary according to the ligand to which it is coordinated. For example, the coordination number of aluminium (III) is 4 when complexed with the chloride ion and 6 when complexed with the fluoride ion forming the complexes $AlCl_4^-$ and AlF_6^{3}, respectively.

An alternative way of expressing the equilibrium relationship is shown in Equation 1.24 – 1.26

$$M + L = ML \qquad \beta_1 = \frac{[ML]}{[M][L]} \qquad \textit{Equation 1.24}$$

$$M + 2L = ML_2 \qquad \beta_2 = \frac{[ML_2]}{[M][L]^2} \qquad \textit{Equation 1.25}$$

$$M + nL = ML_n \qquad \beta_n = \frac{[ML_n]}{[M][L]^n} \qquad \textit{Equation 1.26}$$

β values are termed the overall formation constants. The relationship between K values and β values can be expressed as $\beta_1 = K_1$, $\beta_2 = K_1 \times K_2$ and $\beta_3 = K_1 \times K_2 \times K_3$ and the general relationship is expressed in Equation 1.27.

$$\beta_n = K_1K_2K_3.....K_n = \prod_{i=1}^{i=n} K_i \qquad \textit{Equation 1.27}$$

Table 1.3 shows the values for the stepwise and overall formation constants for a variety of metals complexed with ammonia and ethylenediamine. Expressed as a logarithm, the value for K usually decreases with each progressive step.

Table 1.3. Stability Constants of Metal Ions Complexes with Ammonia and Ethylenediamine

Metal	Ligand	$LogK_1$	$LogK_2$	$LogK_3$	$LogK_4$	$LogK_5$	$LogK_6$	Logβ
Ag^+	NH_3	3.30	3.89					7.19
Zn^{2+}	NH_3	2.59	2.32	2.00	1.70			8.61
Cu^{2+}	NH_3	4.28	3.59	3.00	2.17			13.04
Ni^{2+}	NH_3	2.80	2.23	1.73	1.18	0.74	0.04	8.72
Cu^{2+}	en	10.70	9.30					20.00
Ni^{2+}	en	7.52	6.28	4.25				18.05

This can be simply explained in statistical terms. The ligands approach to the metal ion is a random event. As each water molecule is replaced, the number of sites on the coordination sphere where a ligand can attach decreases. As more sites become occupied the probability of finding an unoccupied site decreases.

Determinations of the stepwise stability constants are usually made in solutions of constant ionic strength, usually though not exclusively in 0.1M solutions. These constants are referred to as the concentration stability constants. The value of the concentration equilibrium constant varies with the ionic strength of the medium in which it is measured, due to this a conversion factor may be needed to compensate for reading taken at different ionic strengths. Figure 1.16 shows the approximate conversion factor for converting activity constants to concentration constants. From Figure 1.16, it can be seen that the correction for the 1^+ metal ions measured in 0.1 M solution and those measured in 0.5 M solution is minimal. For metals with higher charge the correction for constants measured at different ionic strength is much larger and usually needs to be taken into account. With increasing dilution, the concentration stability constant becomes the same as the activity constant.

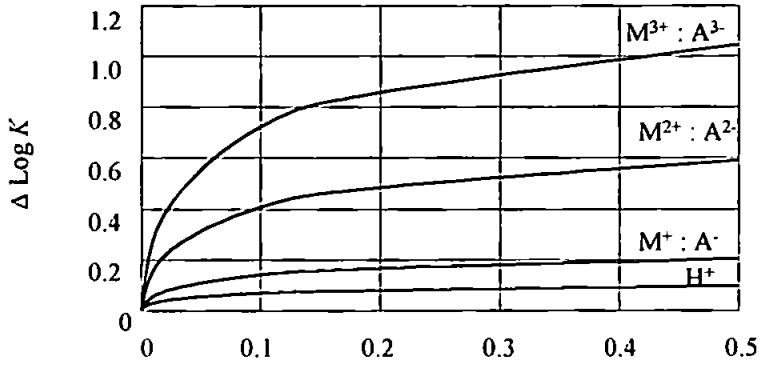

Figure 1.16. Diagram giving the Approximate Conversion of Activity Constants into Concentration Constants.[97]

1.12.2.2. The Chelate Effect.

Chelates tend to be more stable than metal complexes with monodentate ligands. From Table 1.3 it can be seen that the stability constants for ethylenediamine are much higher than those for ammonia. Using nickel as an example, in both complexes the number of ligand-acceptor bonds is

the same and both involve nitrogen groups, yet the $Nien_3^{2+}$ complex is approximately 10^{10} times more stable than the ammonia complex. This increased stability is termed the chelate effect.

$$[Ni(H_2O)_6]^{2+} + 6NH_3 = Ni(NH_3)_6^{2+} + 6H_2O \qquad Log\ \beta_6 = 8.7 \quad \textit{Equation 1.28}$$

N° of Particles: 1 + 6 1 + 6

$$[Ni(H_2O)_6]^{2+} + 3en = [Ni(en)_3^{2+} + 6H_2O \qquad Log\ \beta_3 = 18.0 \quad \textit{Equation 1.29}$$

N° of Particles: 1 + 3 1 + 6

When a monodentate ligand such as NH_3 displaces a water molecule from the coordination sphere of Ni^{2+}, (Equation 1.28) the entropy change ($\Delta S°$) is small (same number of particles on each side of the equation). When a three bidentate ligands such as ethylenediamine displace six water molecules as in Equation 1.29 a large increase in entropy is encountered (four particles on the left yield seven on the right).

A simple explanation is that when an ammonia molecule dissociates from the complex it is free to diffuse away or reform the complex. On the other hand when one of the nitrogens from the ethylenediamine molecule dissociates from the complex it is held in place by the second nitrogen bond and the probability of the complex reforming is much higher.

1.12.2.3. Conditional Stability Constants.

The effect of then ionic strength on the stability constant is often insignificant compared to the effect of competing side reaction from other ligands present in the solution. The stepwise and overall formation constants assume that the reactants, or products, are in one form, but in reality the amount of metal or ligand available for complexation may be lower due to these side reaction from 'interfering' ions. Common side reactions are those caused by hydrogen ions, hydroxide, buffer constituents and impurities.

Due to interference from side reactions the concept of the conditional stability constant, (K′) defined in Equation 1.30 has been developed [98].

$$K' = K_{ML'} = \frac{ML}{[M'][L']} \qquad \textit{Equation 1.30}$$

Where [M′] represents the concentration of not only the free metal ion but also all the metal in solution that has not reacted with the ligand and [L′] denotes the concentration of the ligand and the concentration of all species of unbound ligand in the solution. The conditional constant gives the relationship between the concentration of the product formed [ML] and the total concentration of uncomplexed metal [M′] and the total concentration of uncomplexed ligand [L′]. The total concentration of uncomplexed metal is in relation to the primary reaction and includes all metal complexed by the competing ligands. For example, shown in Equation 1.31, when zinc is titrated with EDTA (H_4Y) in an ammonia-buffered solution, NH_3 and OH^- will enter into side reactions with the zinc and H^+ will have side reactions with the EDTA, Equation 1.32 (the charges are omitted from the equations for simplicity).

$$[Zn'] = [Zn] + [Zn(NH_3)] + \ldots\ldots [Zn(NH_3)_4] + [Zn(OH)] + \ldots\ldots + [Zn(OH)_4] \qquad \textit{Equation 1.31}$$

$$[Y'] = [Y] + [HY] + [H_2Y] + [H_3Y] + [H_4Y] \qquad \textit{Equation 1.32}$$

The conditional constant is not a real constant, but depends on the experimental conditions, especially the concentrations of other species in the solution. In the above example, at a constant temperature, the pH and concentration of ammonia in the solution will determine the value of K′ ($K_{Zn'Y'}$). Conditional stability constants can be used to predict the stability of metal complexes in the presence of competing ligands and under different pH conditions and produce species distribution plots using computer programs such as Mineql. For example, Figure 1.17 shows the stability of various metals

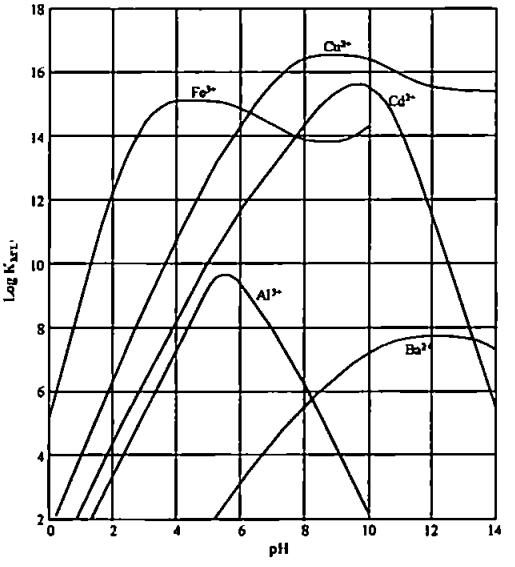

Figure 1.17. Conditional stability constants, $K_{M'L'}$ of various metal EDTA complexes as functions of pH [99].

complexed with EDTA as a function of pH, calculated using conditional stability constants, $K_{M'L'}$ [99].

1.13. Review of Metal Ion Determination by Capillary Electrophoresis.

The determination of metal ions by CE is a comparatively new area of study and the quantity of published work is relatively small, but is sufficient to provide a basis for the work developed here. The capillary electrophoresis separation of metal ions is based on the differences in the electrophoretic mobilities of the ions. However, a problem with metal ion analysis is that in some cation groups the electrophoretic mobilities of the individual hydrated metal ions are similar, due to equal charge and similar radii. To achieve the separation it is necessary to introduce additional chemical interactions to the system, forming complexes to modify the mobilities of the different metals. Direct and indirect absorption detection can then be used depending on the spectroscopic properties of the ligand.

1.13.1. Indirect detection

Foret *et al.* [100] used creatinine as the background electrolyte, with α-hydroxyisobutyric acid (HIBA) as the complexing agent, separating fourteen lanthanides. 4-methylbenzylamine has been widely used as the electrolyte probe and is patented by Waters (Millford, MA) under the brand name UV-cat 1. Jandik *et al.* [101] first used 4-methylbenzylamine as an electrolyte in 1991 with HIBA as the complexing agent to separate alkali and alkaline earth metals. Since then 4-methylbenzylamine has been used by several other workers. Shi and Fritz [102] used 4-methylbenzylamine with lactic acid and 18-crown-6 as the complexing agents. Riviello and Harrold [103] used an electrolyte consisting of cupric sulphate, formic acid and 18-crown-6 to separate common inorganic cations and low molecular mass amines. Yang *et al.*[104] used an imidazole-H_2SO_4 buffer with HIBA to optimise the separation of alkali and alkaline earth metals in the presence of high sodium concentrations. Simunicova *et al.*[105] used benzimidazole with

tartaric acid and 18-crown-6. Aluminium ions were sensitively detected in the presence of other metals by Barger *et al.* [106] using ephedrine as the probe and HIBA as the complexing ion. Chen and Cassidy [107] assessed a range of chromophoric reagents, creatinine, benzylamine, N-methylbenzylamine, N-1-naphthylenediamine dihydrochloride, benzyltrimethylammonium chloride, N,N-dimethylbenzylamine and naphthene methylamine, with the best results gained using N,N-dimethylbenzylamine and HIBA. Beck and Engelhardt [107] reported a system for the separation of some transition metals using 4-aminopyridine and HIBA. Vogt and Werner [108] determined arsenic and selenium species by indirect detection at 254nm using chromate as the probe.

Gross and Yeung [109] used indirect laser induced fluorescence detection using quinine sulphate, in the separation and sensitive detection of alkali and alkaline earth metals. Bächmann *et al.* [110] used cerium (III) as the background fluorescing agent in the separation of alkali and alkaline earth metals. Recently, Desbène *et al.* [111] reported the indirect laser induced fluorescence detection of Ba(II), Ca(II), Mg(II), Fe(III), Zn(II) and Cu(II) using fluorescein (as sodium salt), the separation was optimised using ethylenediaminetetraacetic acid (EDTA).

1.13.2 Direct detection

T. Saitoh *et al* [80] separated metal chelates of 4-(2-pyridlyazo)resorcinol (PAR) by micellar electrokinetic capillary chromatography (MECC). D. Saitoh *et al.* [112] also investigated the MECC separation of porphinato chelates of Mn(II), Cu(II), Co(III) and Mn(III), with direct detection at 422nm. Highly stable complexes were formed using α,β,γ,δ-tetrakis(4-carboxyphenyl)porphine and a minimum detectable amount of 4.8×10^{-16} moles was found for the zinc chelate.

Chen *et al.*[113] separated transition metal complexes of PAR using modified capillaries containing NH_2 and COOH functional groups with direct visible detection at 520nm. Regan *et al.* [79] investigated the separation of PAR chelates of Co(II), Fe(II), Cu(II) and Zn(II) using pre-formed complexes and on capillary complexation methods. Lower detection limits were obtained

with on capillary complexing using trace enrichment by peak stacking, $1x10^{-8}$ M for Co, Fe and Zn, although greater linearity and precision were obtained by pre-capillary complexation. Timerbaev *et al.* [114] reported the separation and direct UV detection of transition and alkaline earth metals as pre-formed chelates of 8-hydroxyquinoline-5- sulphonic acid (8-HQS)

K. Saitoh *et al.* [115] separated electrically neutral acetylacetonato complexes of Cr(II), Co(II), Rh(III), and Pt(II) or Pd(III) by MECC, with direct UV detection at 230nm, in another paper [116] they report the separation of Sc(III), V(IV), Cr(II), Mn(III), Fe(III), Co(III), and Cu(II) by the same method.

Timerbaev *et al.* [117] determined Co(II), Cu(II), Cd(II), Fe(III), Hg(II), Mo(VI), Sc(III), U(VI), V(V), Y(III) and Zn(II) after chelation with 2,6-diacetylpyridine bis(N-methylenepyridiniohydrazone) and direct UV detection at 254nm. Separation was aided by the addition of a surfactant, and detection limits were in the mid ppb range. Timerbaev *et al.* [118] examined a range of aminopolycarboxylic acids as chelating reagents for the determination and direct UV detection of metal ions. Pre-formed complexes of lanthanoid metal ions and nitrilotriacetic acid (NTA), ethylenediaminotetraacetic acid (EDTA), cyclohexanediaminotetraacetic acid (CDTA), diethylenetriaminopentaacetic acid (DTPA) and triethylenetetraaminohexaacetic acid (TTHA) were tried. CDTA provided the optimum separation conditions, separating thirteen of the lanthanoids (not Pm), yttrium and scandium. Timerbaev *et al.* [119] also separated and detected lanthanoid metals as PAR and Arsenazo III complexes, only a limited number of metals were separated due to loss of labile complexes during the electrophoresis conditions.

Motomizu *et al.* [82] used the visible light absorbing chelating agent 2-(5-bromo-2-pyridylazo)-5-(N-propyl-N-sulphopropylamino)phenol to separate fourteen metals with direct visible detection at 550nm. Iki *et al.* [120] separated pre-formed chelates of Al(III), Co(III), Cr(III) and Fe(III) with 2,2'-dihydroxyazobenzene-5-5'-disulphonate. The separation and direct UV detection of

negatively charged cyanide complexes of Fe(II), Fe(III) and Zn(II) in metal plating solutions was reported by Aguilar *et al.* [121] in 1989.

Buchberger *et al.* [122] also report the separation of cyanide complexes of Fe(III), Fe(II), Cu(II), Ni(II), Cr(III), Hg(II), Pd(II), Ag(II),Cd(II), Zn(II) Co(II) and Co(III), with direct UV detection at 214nm.

Medina *et al.* [123] determined organic mercury species as cysteine complexes by direct UV detection, the technique was applied to real samples and reference materials producing reasonable results.

Swaile and Sepaniak [81] separated zinc, calcium and magnesium using 8-HQS in the background electrolyte with on column complexation and direct fluorescence detection.

1.14. Aims and Objectives.

One of the main problems of capillary electrophoresis is the relatively poor concentration limits of detection that are achieved. In addition, of the publications detailing the separation of metal ions by capillary electrophoresis very few have been applied to real samples.

Indirect photometric detection provides an universal detection method for ions sharing the same displacement mode. With this method the maximum sensitivity of the separation can be calculated using Equation 1.14. However, this theoretical sensitivity is not realistically attainable due to wall effects and diffusion. In addition, the maximum theoretical sensitivity only applies to ions with mobilities closely matched to that of the probe. Ions migrating with velocities of either greater than or less than that of the probe produce fronted or tailing peaks respectively, causing a reduction in their sensitivity. The lack of selectivity inherent in this mode of detection makes it difficult to apply to environmental samples. Due to these limitations this work will concentrate on the direct detection of highly absorbing metal ion complexes.

The direct detection of metal complexes has several advantages over indirect detection. The technique is potentially more sensitive due to the lower background adsorption of the electrolyte. The limit of detection with direct detection methods is essentially limited by the extinction coefficient of the metal complex and the greater the absorption of the complex the greater the sensitivity of the separation. Direct detection also offers greater selectivity over indirect detection, which should make the separation methods more applicable to the analysis of a wider range of environmental samples. The major disadvantage of this detection strategy is due to the instability of the metal complexes during electrophoretic conditions, although several workers have used this as a means of enhancing selectivity in what is referred to as kinetic differentiation mode.

The main aim of this study was to investigate the spectroscopic and electrophoretic properties of a range of metal ions complexed with selected chelating dyestuffs with the objective of developing highly sensitivity methods for the separation and detection of metal ions in a range of samples.

The work will involve an investigation into the stability of metal ions complexed with chelating dyes, the optimisation of direct photometric methods and the application the most successful of these methods to the analysis of environmental samples.

Post column reaction detection is commonly used as a method of detection in the ion chromatographic separations of metal ions. This work will also involve an investigation into the transfer of this approach to a capillary electrophoresis system and the development of a post-capillary reaction trace metal detection system for capillary electrophoresis.

CHAPTER 2.0. THE SPECIATION OF MERCURY.

2.0 Introduction

The environmental behaviour and toxicity of a metal are often related to the specific form or species in which it occurs [125]. It is generally recognised that the organometallic species of certain metals are far more toxic than the inorganic forms due to their greater biological compatibility [126]. The determination of total metal concentrations do not reflect this important information and this has led to the need to distinguish between the different species. There has been a continuing interest in the speciation of mercury for a number of years now owing in part to the high toxicity of methylmercury and the tendency towards bio-magnification as it passes through the food web [127]. This bio-magnification is particularly large in marine ecosystems and leads directly to human exposure through the fish food chain.

2.0.1. Mercury in the Environment.

The occurrence of mercury in the environment is widespread. An estimated average of 3,000 tons of mercury is released into the atmosphere by natural degassing from the earth's crust and oceans [128]. A further 3,600 to 4,500 tons are contributed to the annual atmospheric loading by anthropogenic activities which represents some 50-75% of the annual total input from all sources [128]. This atmospheric mercury can be transported great distances resulting in a wide distribution. Point sources, particularly industrial effluent discharges, can lead to localised increases far greater than those of natural background levels giving rise to potentially dangerous levels.

2.0.2. Chemistry of Mercury.

With a melting point of –38.87°C mercury is the only metal that exists as a liquid at room temperature or below. It has a density of 13.59 g cm^{-1} and a low vapour pressure (0.001201

mm Hg at 20°C) [129].

Mercury has two principal oxidation states +1 and +2. Mercury (I) forms the diatomic ion with a metal-metal covalent bond, Hg_2^{2+} and mercury (II) forms the ion, Hg^{2+}.

Mercury forms amalgams with many other metals, some of which are of commercial value, the principal uses being in dental amalgam and the gold extraction industry. Mercury and organomercury species are *soft* acids and tends to form covalent bonds with *soft* ligands.

Table 2.0. The stability of various ligands with methyl mercury and protons [130].

Ligand	Coordinating atom	pK $(CH_3Hg^+)^a$	pK $(H^+)^a$
F^-	F	1.5	2.85
Cl^-	Cl	5.25	-7.0
Br^-	Br	6.62	-9.0
I^-	I	8.6	-9.5
OH^-	O	9.37	15.7
HPO_4^-	O	5.03	6.79
S^{2-}	S	21.2	14.2
SCN^-	S	6.05	4.0
SO_3^{2-}	S	8.11	6.79
NH_3	N	7.6	9.42
$(CH_3CH_2)_3P$	P	15.0	8.8
CN^-	C	14.1	9.14

[a] $pK(CH_3Hg^+) = \log \frac{[CH_3HgB]}{[CH_3Hg^+][B^-]}$ and $pK(H^+) = \log \frac{[HB]}{[H^+][B^-]}$

From Table 2.0, it can be seen that methyl mercury tends to form very stable complexes with sulphur containing ligands, as do other mercury species. The sulphide ion forms very strong complexes with the methyl mercury cation, it also forms a stable bond with protons but the mercury bond is greatly favoured. Phosphorus can also forms stable complexes with mercury as shown by the high stability constant for triethylphosphine in Table 2.0. Cyanide bonds through the carbon atom to form a stable complex with methyl mercury. The stability of the mercury-carbon bond gives rise to the large number of organic mercury compounds. Methyl mercury also forms complexes with the halides with the exception of fluorine, which is a very

hard base. The hydroxide is a relatively strong base with regard to the methyl mercury but vastly stronger towards the proton.

Equation 2.0 explains the complexation of methyl mercury with in terms of the HSAB principal. The sulfonate is a soft base towards the methyl mercury whereas chloride acts as a hard base.

$$CH_3HgCl + HSO_3^- \longrightarrow CH_3HgSO_3^- + HCl \qquad \textit{Equation 2.0}$$

Soft – hard Hard – soft Soft – soft Hard - hard

2.0.3. Methylation of Mercury in the Environment.

Mercury is methylated in a wide variety of environments with much of the focus of research being on fresh water and estuarine environments [128]. Mono-methyl mercury is the only organic species detected in freshwater but in open oceanic environments, di-methyl mercury has been detected in significant concentrations. Mono and di-methyl mercury are both formed by similar processes, with di-methyl mercury being formed from Hg (II) and mono-methyl mercury by demethylation of the dimethyl mercury. Although it is not known if mono-methyl mercury is the final product of bacterial methylation, or whether di-methyl mercury is the final product, which then rapidly demethylates to mono-methyl mercury [131]. The greater concentration of mono-methyl mercury over di-methyl mercury at the sediment water interface and in water column is thought to be due to its greater stability [132]. In the aquatic environment sulphate-reducing bacteria have been identified as the principal mercury methylating organisms [133] and methylcobalamin (CH_3-Co(III)-5,6-dimethyl benzimidazoyl-cobamide) as the main source of the methyl group [134]. Mercury is also demethylated by mercury resistant microbial species. This demethylation occurs mainly at the oxic/anoxic interface and the total concentration of methyl mercury in the water column is an equilibrium between methylation and demethylation.

The methylation of mercury occurs in both aerobic and anaerobic conditions, with the latter being more favourable. The pH of the system also influences speciation of organo-mercury, as methyl mercury is more stable in neutral to acidic conditions, whereas di-methyl mercury is more stable in basic conditions. This may explain why di-methyl mercury is detected in seawater and mono-methyl mercury is the only species detected in freshwaters, which tend to be more acidic. A low pH has also been noted to correlate with the release of mono-methyl mercury from the sediment surface [131] in lacustrine systems. A reduction of the pH at the aerobic/anaerobic water sediment interface was reported to produce a two to three fold increase in the rate of methyl mercury production [135,136]. Acidification of lakes has also been reported to promote methylation of mercury in the water column [131]. This was thought to be due to sedimentation of dissolved organic matter as aluminium complexes. This results in the loss of Hg^{2+} binding sites and promotes the methylation of mercury in the water column due to the greater availability of inorganic mercury.

The concentration of mercury in an aquatic environment can influence the production of methyl mercury. Furutani and Rudd [137] reported that in non mercury contaminated lakes the production of methyl mercury was 10 times faster than in mercury contaminated lakes. This increase in production was ascribed to the absence mercury resistant bacteria in the pristine lakes and it is these microbes that are responsible for the demethylation the mercury.

Sulphide concentrations can also influence methyl mercury production, with high sulphide concentrations being reported to reduce the rate of methylation. This was thought to be due to precipitation of the stable HgS making it unavailable for methylation [138,139].

The methylation of mercury was reported to increase with temperature to an optimum of 35°C [140]. The colder climate of the Northern Hemisphere, particularly during the winter, does not favour microbial activity. However, the production of methyl mercury continues throughout the year, suggesting that the methylation of mercury may also be abiotically

mediated. The main sources of abiotic methylation are reported to be humic substances [141, 142] and rain [143, 144].

2.0.4. Bio-accumulation of Mercury and Methyl Mercury

Mercury methylated by bacterial activity in sediments can be absorbed or ingested by benthic organisms. This methyl mercury is then passed on to and accumulated by fish feeding on these organisms. Methyl mercury is also released into the water column from the sediment where it may be absorbed as it passes through the gills of fish.

The bio-magnification of MeHg in the marine ecosystem is generally thought to result from its lipophilic character. However, the prevalence of MeHg in fish muscle rather than in fat tissue indicates its adsorption may not be entirely controlled by lipid solubility [145]. Although, the lipophilicity of methyl mercury is likely to play an important role in its preferential absorption across the gut wall when compared with inorganic mercury [146].

In vitro studies have shown that both inorganic and organic mercury accumulate in phytoplankton by passive diffusion across the cell membrane, however, zooplankton feeding on the phytoplankton tend preferentially accumulate methyl mercury rather than inorganic mercury [147]. This is because methyl mercury passes into the cytoplasm of the phytoplankton whereas the inorganic mercury tends to be retained in the cell membrane, most likely through thiol bonding [148]. Zooplankton feeding on the phytoplankton digest the cytoplasm but defecate the cell membrane. Consequently, this first step in the food chain is highly significant with regard to the bioaccumulation of methyl mercury in preference to inorganic mercury.

Nearly all species of fish contain trace amounts of methyl mercury but in regions with elevated mercury levels either from natural sources or form industrial pollution the levels of mercury in fish may pose a threat to humans. The US Food and Drug Administration (FDA) limit in fish

flesh for human consumption is 1ppm and in general, methyl mercury levels in most fish range from 0.01 ppm to 0.5 ppm. In a few species of fish the FDA limit is reached or exceeded, usually in top predatory species such as shark, swordfish and some large species of tuna.

The data in Table 2.1 shows the correlation between elevated mercury concentration and fish size, a good indication of the age of the fish. This data can be interpreted as a good indication of bioaccumulation in these top predatory species.

Table 2.1 Mercury Levels in Commercial Marine Species [149]

Species	Size in lbs	Mean Mercury concentration (mg Kg^{-1})
Swordfish	Under 50	0.55
	50 - 100	0.86
	Over 100	1.08
Bluefin Tuna	Under 10	0.37
	10 - 30	0.51
	Over 30	0.89
Yellowfin Tuna	Under 70	0.21
	Over 70	0.62
Skipjack Tuna	Under 9	0.17
	Over 9	0.21

2.0.5. Analysis of Mercury Speciation

A great deal of effort has been put into developing methods to differentiate and determine organomercury species in biological and environmental samples. Analytical methods for the determination of mercury speciation up to 1994 have been critically reviewed by Puk and Weber [150]. In general, methods for the speciation of mercury can be divided into two major fields, selective reduction and chromatographic methods.

2.0.5.1. Selective reduction Methods.

Selective reduction methods are based on the procedure proposed by Magos [151], which makes use of the differing reduction behaviours of inorganic and organo-metallic species in the presence of reducing agents. Hg(II) is reduced to Hg(0) by stannous chloride alone whereas alkylmercury compounds are only reduced to Hg(0) by stannous chloride in the presence of

cadmium chloride. The mercury vapour generated is then detected by cold vapour atomic absorption spectrometry (CVAAS) [152-154] and cold vapour atomic fluorescence spectrometry (CVAFS) [155]. There are several variations to this method, mainly differing in the choice of reductants [151, 155, 156]. A major drawback to this method is that it only distinguishes between inorganic and organic mercury and does not differentiate the individual organic species.

2.0.5.2. Gas Chromatographic Methods

The other common approach for the determination of methylmercury is based on the gas chromatographic (GC) method originally developed by Westoo [157, 158], with detection of the organomercury halide by electron capture detection. Initial GC work utilised packed columns and suffered problems with low column efficiencies, sample loss and severe peak tailing leading to poor reproducibility [159]. These problems were principally due to interactions between the organomercury compounds and the chromatographic support and have been solved to some extent by the use of column conditioning [160] and capillary columns [161].

High performance liquid chromatography (HPLC) methods have also been developed using a variety of detection systems including reductive electrochemical [162], inductively coupled plasma mass spectrometry (ICPMS) [163], UV/Vis [164, 165] and CVAAS [166].

2.0.5.3. Capillary Electrophoresis Methods.

Lai and Dabekzlotorzynska [167] developed a method for speciation of mercury using pulsed amperometric detection, although this method was not applied to the determination of methyl mercury in fish flesh.

Medina *et al.* [123] developed a CE method for the determination of organomercury species based on the direct measurement of the UV absorbance of cysteine complexes at 200nm. This

technique has been further investigated with respect to sample stacking [168] and validation [169] by Carro-Díaz *et al.* Although good results were obtained in this work, a detection wavelength of 200nm is not ideal since many inorganic and organic species absorb strongly in this region. This may result in problems when applied to real samples due to interference and high baseline noise, especially when extraction from large sized samples for the purpose of pre-concentrating the methyl mercury. This ultimately could affect the measurement of samples with very low concentrations of MeHg.

The work described here uses a similar approach, but involves mercury complexes that are highly absorbing in the visible region. This approach should be less prone to interference by organic impurities, providing some potential for an improvement in the detection sensitivity.

2.0.6. Dithizone Sulphonate.

Dithizone is one of the most studied chelating dyestuffs and forms intensely coloured and very stable complexes with a wide range of metals including the heavy elements. A further important characteristic of dithizone is its ability to form strong complexes with organometallic species, particularly organo mercury compounds [170]. Most dithizone complexes are uncharged and insoluble in water making them unsuitable for CE separation. Tanaka *et al* [171] described the synthesis of a water soluble derivative of dithizone called dithizone sulphonate (DzS). Being soluble in aqueous solution, DzS was considered to be highly favourable for application to the direct detection of metal species by CE, with particular attention paid to mercury species because of the environmental concern discussed above. The free acid of DzS was reported to be unstable but the

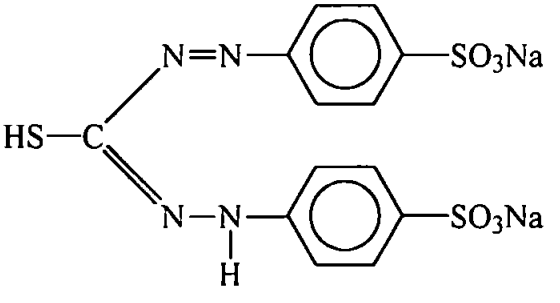

Figure 2.0. The Structure of Disodium Dithizone Sulphonate.

disodium salt, shown in Figure 2.0, was reported to be stable in aqueous solution and the dry state.

2.0.7. Extraction of Methyl Mercury from Fish Flesh.

The Westoo extraction procedure [156, 157] for environmental samples is well established and a number of modifications have been published since its first use in the late 1960s. For fish flesh, it is essentially based on a three-stage solvent extraction process. The first stage results in release of the MeHg as the halide from the fish flesh in strong acid, with extraction into toluene. In the second stage, MeHg is back extracted into an aqueous layer as the thiosulphate or cysteine complex to isolate it from the large quantities of fat that will also be extracted into the toluene. Finally, in the third stage, the complexed organomercury species are back extracted into toluene ready for gas chromatographic analysis. Since CE is mainly applied to aqueous samples, the third stage may not be necessary, as long as the methyl mercury complex is stable and can be detected. Medina *et al.* [123] used a simplified two-stage extraction procedure for their determination of organo mercury species in fish flesh by CE.

2.1 Experimental

2.1.0 Instrumentation and separation conditions.

All experiments were carried out on a Dionex CES 1 capillary electrophoresis system (Dionex, Sunnyvale, CA) equipped with a reversed polarity power supply. Sample injections were performed hydrostatically at the cathodic side from a height of 100mm for a period of 30 seconds. A constant voltage of -25kV was used throughout. Detection was carried out by on-column spectrophotometric measurements at 480 nm. Fused silica capillaries of 100μm internal diameter were supplied by Dionex (Dionex UK, Camberley, Surrey.) Data was

recorded by a Dionex ACI computer interface, and processed using Dionex AI450 automated chromatography software, sampling at a rate of 50Hz.

2.1.1. Reagents and Solutions.

A 1000 μg ml^{-1} mercury (II) nitrate standard was obtained from BDH (British Drug Houses, Poole, Dorset). Methyl mercury, ethyl mercury and phenyl mercury, as the chloride salts, were obtained from Shell UK. 1000 μg ml^{-1} standard solutions of each was prepared by dissolving the appropriate amount in MilliQ water, with dissolution aided by sonification. All mercury standards were stored in the dark and fresh solutions prepared monthly. Sodium acetate, sodium hydroxide, acetic acid and hydrochloric acid were of Aristar Grade and obtained from BDH (Poole, Dorset, UK). HPLC grade Toluene was obtained from BDH. Acrylamide, potassium persulphate, N,N,N',N', tetramethylethylenediamine (TEMED) and γ-methacryloxypropyltrimethoxylsilane were obtained from Sigma (St. Louis, MO). Dithizone sulphonate was manufactured in house, using a modified method based on that developed by Tanaka *et al.* [171]. All water used was 18-MΩ cm^{-1} obtained from a MilliQ high purity water system (Millipore, Bedford, MA). A variety of samples of tinned tuna, salmon and crab meat samples were obtained from three national supermarkets, samples of locally caught fresh cod and haddock samples were also obtained from a local fish monger. A certified reference material, DORM 1 was obtained, which is freeze-dried dogfish muscle distributed by the Canadian National Research Council.

2.1.2. The Preparation of Coated Capillaries.

The capillaries were coated using a procedure based on that developed by Hjertén [30]. Fused silica capillaries with detection windows 5 cm from the end were flushed with 1 M NaOH for 30 minutes, then rinse with MilliQ water for 15 minutes. The capillaries were then filled with a 1% (v/v) γ- methacryloxypropyltrimethoxylsilane solution, adjusted to pH 3.5 with acetic

acid. The silane solution was allowed to react at room temperature for 1 hour, the capillaries were then rinsed with MilliQ water for 15 minutes. A 3% (w/v) solution of acrylamide was prepared by dissolving 0.3g acrylamide in 10 ml water, this was degassed by sonification and helium sparging. 10 μg of potassium persulphate and 10 μl of TEMED were added to the degassed acrylamide solution and thoroughly mixed. The capillaries were filled with the acrylamide solution, both ends sealed, and placed in an oven at 40°C for 1 hour. At the end of this period unbound polyacrylamide was removed from the capillaries by flushing them with water, using an HPLC pump. The coated capillaries were then dried by allowing nitrogen to flow through them overnight. The dried capillaries were sealed by joining the two ends together using a short length of 0.3mm ID PTFE tubing and stored until required.

2.1.3 Fish Sample Preparation.

2.1.3.1. Freeze-dried Samples.

Excess liquid was drained from a 185g can of tuna, which was freeze dried and ground to a fine powder using a mortar and pestle.

2.1.3.2. Wet Canned Samples.

Excess liquid was drained from the can, the contents then emptied into a beaker and thoroughly mixed using a spatula. An aliquot of this was then used for the extraction.

2.1.3.3. Fresh Fish.

A sample of fish muscle (ca.30g) was skinned and finely ground using a hand held homogeniser, an aliquot of this was then used for the extraction.

2.1.4. Extraction Procedure.

The extraction procedure was based on the classical method of Westöö [156], with the exception that a two-stage extraction was used and DzS was used in place of cysteine to back extract the methyl mercury from the toluene.

The procedure for wet fish samples is outlined below and in Figure 2.1. 20ml water and 10ml HCl were added to a beaker, a weighed sample of fish flesh was added to the beaker and the contents homogenised for 5 minutes using an homogeniser. The contents of the beaker were transferred to a 100ml conical flask and 40ml of toluene was added. The flask was then placed in a Gallenkamp flask shaker and shaken for 5 minutes. The contents of the flask were transferred to a glass centrifuge tube, which was sealed and centrifuged at 3000 rpm for 5 minutes. An aliquot of the supernatant was then transferred to a conical flask containing 1ml of 500 mg l^{-1} DzS. The flask was shaken for 2 minutes, the aqueous layer was then removed by pipette and transferred to a 2 ml glass centrifuge tube and centrifuged at 3000 rpm for 5 minutes. 0.5 ml of the dye was removed and analysed by CE. The procedure for freeze-dried samples was essentially the same, differing only in that the homogeniser was not used.

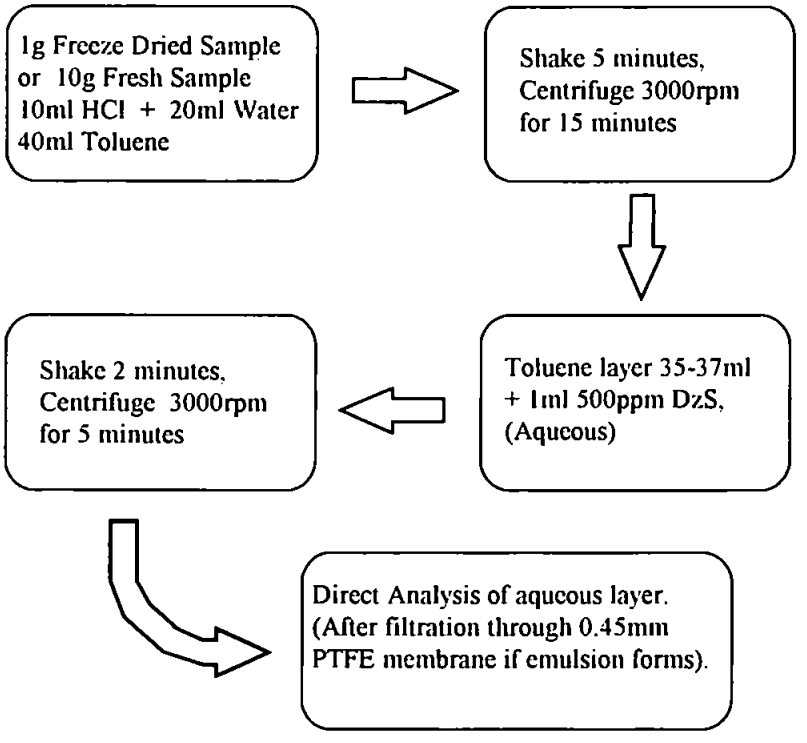

Figure 2.1. Schematic diagram of the extraction proceedure.

2.2. Results and discussion.

2.2.1. Optimisation of the CE separation

Throughout this work, the DzS metal complexes were pre-formed prior to CE separation. On-column complexation was used since the injection of pre formed complexes was a requirement of the proposed extraction procedure. Four mercury cationic species were investigated, namely, inorganic mercury (Hg (II)), methyl mercury, ethyl mercury and phenyl mercury. All the mercury DzS complexes were found to be highly stable even in strong acid conditions. However, the dye itself was unstable below pH 4, though it did not begin to degrade rapidly until below pH 3. The stability of the dye at low pH values did not preclude the use of mildly acidic separation conditions provided the metal complex in the sample vial was not made up in the low pH electrolyte.

Initial studies were carried out with uncoated fused silica capillaries. The initial attempts at separation were conducted using a sodium acetate electrolyte at pH 5. At this pH, the electrophoretic velocity of the complexes was insufficiently different from the velocity of the electroosmotic flow. Since the direction of migration of the complexes was opposed to that of the flow, the sample zones migrated away from the detector and no peaks were detected within a reasonable time frame. A lower pH of 3 was then tried since the electroosmotic flow is much reduced due to minimal ionisation of the surface silanol groups on the capillary wall. An example of the separation obtained is shown in Figure 2.2. Under these conditions, a good separation of the three organo-mercury complexes was achieved, although a 'bridge' was observed between the ethyl and phenyl complexes. Injection of either the ethyl or the phenyl complex individually did not produce any significant tailing or fronting and it was assumed this was an interaction between the two complexes. The separation of the methyl and ethyl mercury complexes was better than expected, given their equal charge and relatively small

difference in molecular weight. This gives some indication that the stability of the complexes may also be playing some role in their separation. From the electropherogram it was clear that the dye was not very pure, producing a large number of impurity peaks. However, these impurity peaks were not found to be a serious problem since they were sufficiently well separated from the organomercury complexes.

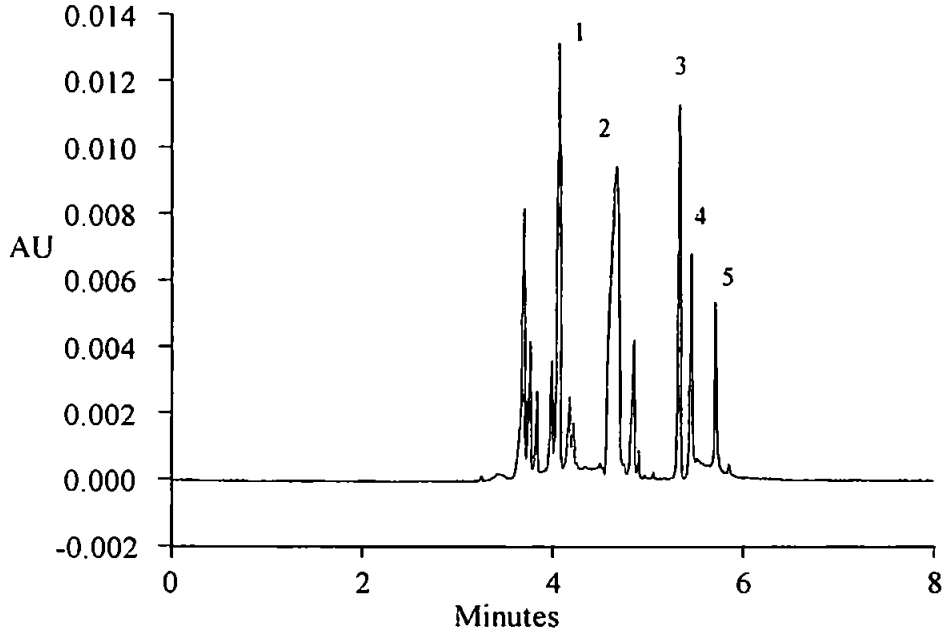

Figure 2.2. Electropherogram showing the separation of inorganic and organo mercury species (1 μg ml^{-1} each) as the DzS complexes. Separation conditions: Electrolyte 10mM Sodium acetate pH 3; Capillary fused silica L_d 50cm 100μm ID; Voltage - 25kV; Detection 480nm. Key: 1 inorganic mercury, 2 DzS (20 μg ml^{-1}), 3 methyl mercury, 4 ethyl mercury and 5 phenyl mercury. Unlabeled peaks due to dye impurities.

The plotted calibrations curves were linear, with high correlation coefficients, although a large negative intercept was found for all the organomercury species, shown in Figure 2.3. Since the calibration was linear, the negative intercept seemed to indicate that a constant subtraction from each sample was occurring. This loss was noted to significantly decrease the sensitivity of the separation to the point that ethyl and phenyl mercury complexes could not be detected at concentrations below 200 μg l^{-1}. The reduction in sensitivity was noted to correlate with

increasing migration time and the size of the complex, with methy mercury being the least effected and phenly mercury the most.

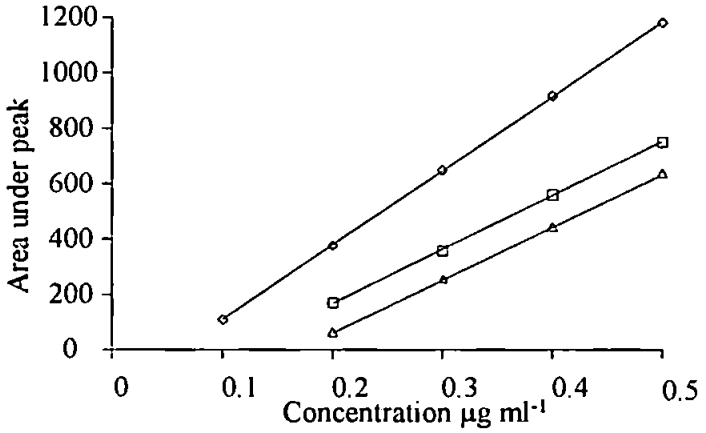

Figure 2.3. Calibration of Organo Mercury Species at pH3. Separation Conditions; Voltage 25kV; Capillary, Fused Silica 55cm Ld, 100µm ID; Electrolyte, 10mM Sodium Acetate. Detection, 480nm
Key: ◇ *MeHg* □ *EtHg* △ *PhHg*

2.2.2. Losses of Organomercury Species.

The capillary surface was a constant factor in each separation and it was thought that capillary wall interactions might be a possible cause of the loss. Interactions between the capillary wall and solutes are a common problem in CE but are usually accompanied by tell tale signs such as peak tailing, but this did not appear to be the case. The dye should be repelled by the wall, as it is anionic, although the mercury species may themselves be attracted to the wall. In general, mercury has little attraction for oxygen containing ligands but it was thought that there might have been some ionic interaction with the wall. Increasing the ionic strength of the electrolyte should suppress wall interactions by increasing the quantity of the sodium ion, which should force the equilibrium away from the mercury species, Equation 2.1

$$RHgSiO + Na^+ \rightleftharpoons SiONa + RHg^+ \qquad \textit{Equation 2.1}$$

However, increasing the ionic strength of the electrolyte was found to cause an increase in the negative intercept, seriously decreasing the sensitivity, Figure 2.4 (squares). Whereas

reducing the ionic strength of the electrolyte caused a decrease in the negative intercept and an improvement in sensitivity (Figure 2.4, diamonds). The results of this experiment seemed to discount wall interactions, certainly those of an ionic nature. Although at this pH, hydrophobic interactions between the wall and either the organomercury species or the DzS could not be ruled out completely.

The influence of the ionic strength of the electrolyte on the negative intercept was thought to be due to trace metal impurities in the electrolyte, which were exchanging with the DzS mercury complexes. This would produce a constant subtraction of a small amount of the mercury species over the whole calibration range, resulting in a negative intercept.

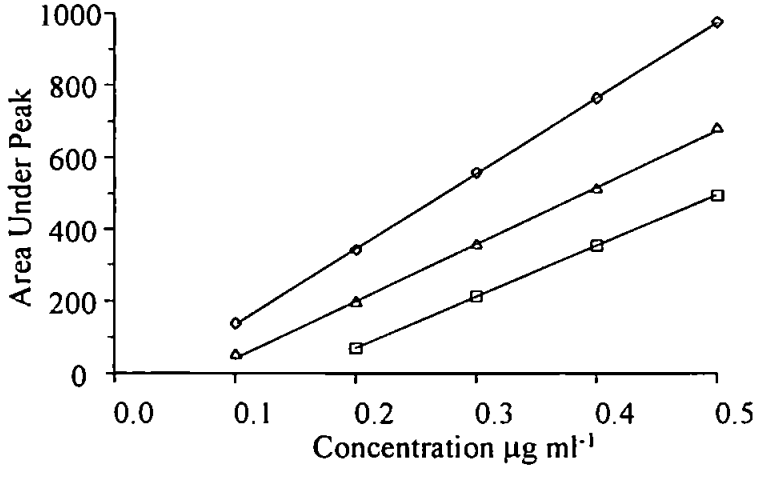

Figure 2.4. The Effect of the Ionic Strength of the Electrolyte on the Negative Intercept Obtained for Methyl Mercury.
Separation Conditions; Voltage -25kV; Capillary, Fused Silica 55cm Ld 100µm ID; Electrolyte, Sodium acetate pH 3. Key ; ◇ = 5 mM. △ = 10 mM. □ = 20 mM.

Lowering the concentration of the electrolyte would decrease the concentration of the impurities and therefore the degree of competition. Low concentrations of impurities in the electrolyte would have an exaggerated effect owing to their opposing mobility, which would essentially provide a constant steam of metals migrating from the destination vial into the sample zone. On entering the sample zone, these metals would accumulate due to the retardation or reversal of their electrophoretic velocities upon complexation with the excess

DzS. Some of the dye impurity peaks shown in Figure 2.2 may be due to this factor. Further evidence of this theory may be attributable to the fact that the losses are greatest with PhHg and least with MeHg. As the PhHg zone would be the first that the metal impurities encountered, retardation of their migration would mean it would take longer for them to reach the next zone. This would result in a smaller effect on the EtHg and still lesser effect on the MeHg. The areas used in Figure 2.3 are not corrected for migration velocities so an increase in area under the peak might be expected due to the slower passage past the detection window.

Even Aristar Grade sodium hydroxide and acetate contain relatively high levels of metal impurities. In order to reduce the impurity levels to a point where they no longer interfere in the separation, the electrolyte concentration would have to be reduced to less than 1mM. It should be noted that in terms of overall system sensitivity, low ionic strength electrolytes should be avoided due to the decreased stacking effect and low buffering capacity. An alternative solution to the problem is the addition of a low concentration of DzS to the electrolyte. This would have the effect of complexing the metal impurities in the electrolyte preventing them from accumulating in the migrating sample zones.

Dissociation of the metal complex was also considered a potential problem since the DzS and uncomplexed mercury species have an opposite charge and therefore opposing mobilities. When they are first injected, the organomercury complexes are in an excess of DzS but when the voltage is applied across the capillary, the DzS migrates with a greater velocity than the complexes leaving them behind. When dissociation of the complex within the sample zone occurs, the mercury species will reverse their mobility moving away from the detector and the free DzS will move with an accelerated velocity towards the front of the sample zone. When this happens, the organomercury ion will rapidly encounter another dye molecule, reform the complex and begin migrating towards the detector again. However, at the rear of the

migrating sample zone, mercury species migrating out of this zone would not encounter any dye molecules and are free to continue migrating away from the detector. Conversely, free DzS at the front of the sample zone would not encounter any more metal ions and continue to migrate with accelerated velocity. The loss of the organomercury species would not be constant but dependent on the concentration of the mercury species in each sample zone. Consequently, the calibration would be linear, though biased.

The addition of small concentrations of DzS to the separation electrolyte should also be effective in preventing this problem since the mercury species would always encounter a constant supply of DzS molecules migrating into the sample zone.

When 5mg L^{-1} of DzS was added to the electrolyte, the negative intercept was virtually eliminated while still maintaining linear calibrations. Nonetheless, adding DzS to the electrolyte gave rise to another problem connected with its instability at low pH values. Whereas instability was not a problem with pre-column formation of the complexes, having DzS in the electrolyte for long periods at pH 3 resulted in significant degradation within a few hours, reducing its effectiveness in eliminating the negative intercept. Increasing the pH to reduce the degradation of DzS would solve this, but at the expense of increasing the electroosmotic flow significantly increasing the separation time. Suppression of the electroosmotic flow using coated columns appeared to be the solution.

2.2.3. Separations using Coated Capillaries.

There are two methods of capillary coating routinely use in CE, dynamic coatings and bonded coatings. With dynamic coatings, suppression of the electroosmotic flow is achieved by the addition of low concentrations of trimethylalkyl ammonium salts to the electrolyte [172, 173]. 0.2mM hexadecyltrimethylammonium bromide was added to a 10mM sodium acetate buffer at pH 5 and a series of methyl mercury standards were injected into the instrument. This

approach proved to be unsuccessful, possibly due to an electrostatic interaction between the positively charged surfactant coating the capillary wall and the negatively charged dye and complexes. It was therefore decided to investigate chemically coated capillary technology. Capillaries coated with neutral hydrophilic coatings have been developed in the field of protein separations [30, 58, 31, 32]. These have been designed to suppress EOF and eliminate surface interactions. A polyacrylamide coating was chosen for its neutral charge, relatively hydrophilic properties and the comparative ease of in-house manufacture.

A series of experiments were performed using polyacrylamide coated capillaries prepared as described in the Experimental (Section 2.1.2). A sodium acetate electrolyte at pH5 with the addition of 5mg l^{-1} DzS was used throughout. These capillaries were found to give very good separations (Figure 2.5).

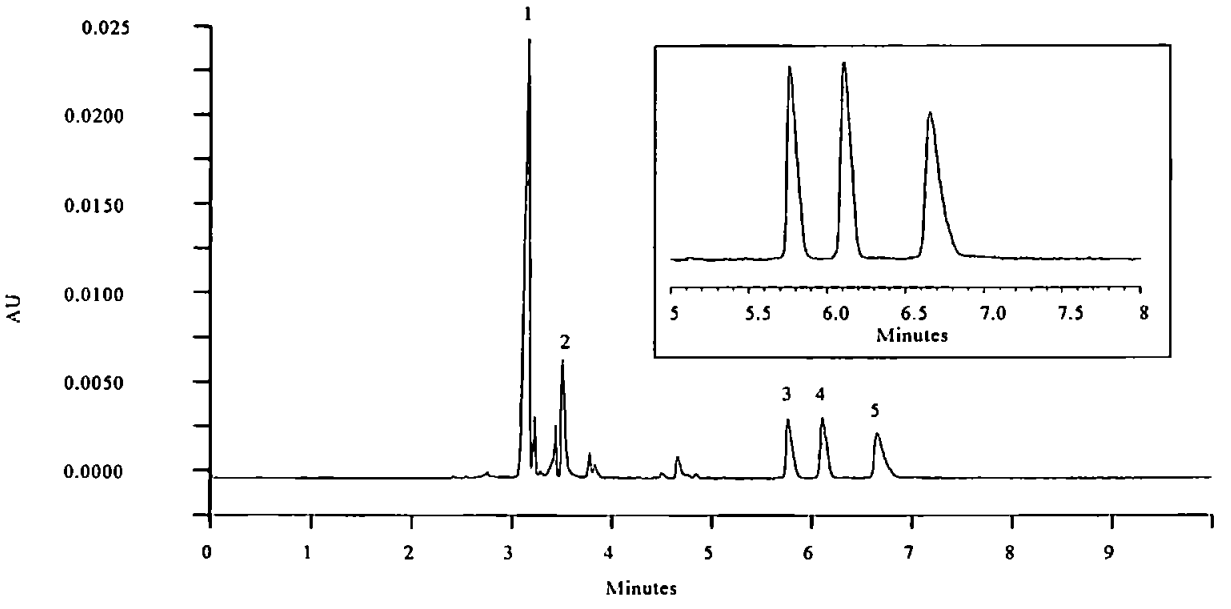

Figure 2.5. Electropherogram showing the separation of inorganic and organo mercury species (1 μg ml-1 each) as the DzS complexes, with inset of organomercury separation.
Separation conditions: Electrolyte 10mM Sodium acetate pH 5 containing 5μg ml^{-1} DzS; Capillary polyacrylamide coated fused silica 65cm L_b 60cm L_d 100μm ID; Voltage -25kV; Detection 480nm. Key: 1DzS (20 μg ml-1), 2 inorganic mercury, 3 methyl mercury, 4 ethyl mercury and 5 phenyl mercury. Unlabeled peaks due to dye impurities.

The coated capillaries and higher pH electrolyte produced an improvement in the separation of the organo mercury cations from the dye and its impurities. The increased pH appeared to cause a further deprotonation of the DzS, producing an increase in its migration velocity. The migration velocity of the organomercury complexes was largely unaffected by the increased pH. The inorganic mercury although still not fully resolved from the impurity peaks was sufficiently resolved to obtain quantitative information.

2.2.4. Quantitative Performance.

All the mercury DzS complexes exhibited similar lambda (λ) max. values close to 480nm. The absorbance spectrum of DzS and its impurities seriously overlapped those of the mercury complexes, but this was not a problem as long as they were all separated from each other during electrophoresis. Calibration curves were found to have excellent linearity for all four species. Peak areas have been used for quantitative data calculations throughout. Although peak height generally gives greater precision, it has been observed that at concentrations above 1mg l^{-1} a non-linear response to concentration has been reported [174]. For the low range calibration, a slight negative intercept was found showing the inclusion of DzS in the electrolyte did not entirely solve this problem. Nevertheless, this did not prevent determinations down to low μg l^{-1} levels as can be seen in Figure 2.6 for methylmercury giving a negative intercept of 5.5 μg l^{-1}.

This negative intercept was probably due to overlap in the absorption of the mercury complexes and the DzS in the electrolyte. The possibility of the formation of an organomercury complex with one of the DzS impurities could not be entirely ruled out. This could result in a small net subtraction from each sample. Increasing the concentration of DzS in the electrolyte was found to increase the negative intercept, although this would be expected in either of the above cases.

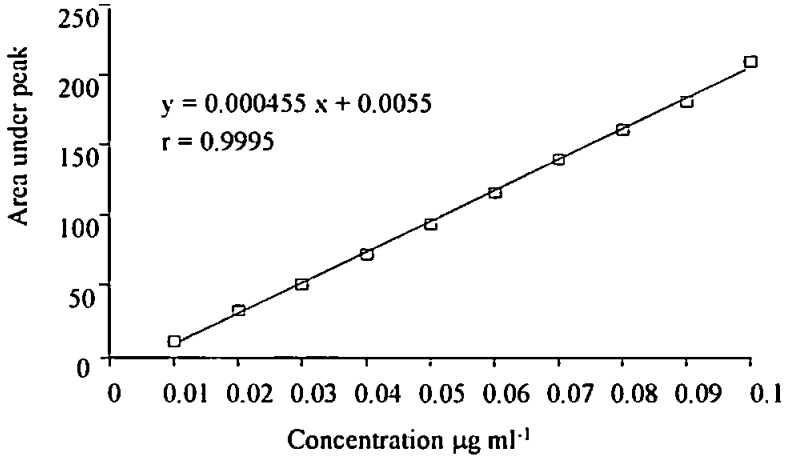

Figure 2.6. Low level methyl mercury calibration. Separation conditions: Electrolyte 10mM Sodium acetate pH 5, containing 5µg ml^{-1} DzS; Capillary polyacrylamide coated fused silica L_d 60cm 100µm ID; Voltage -25kV; Detection 480nm.

Figure 2.7 shows the improved calibrations for the ethyl and phenyl mercury.

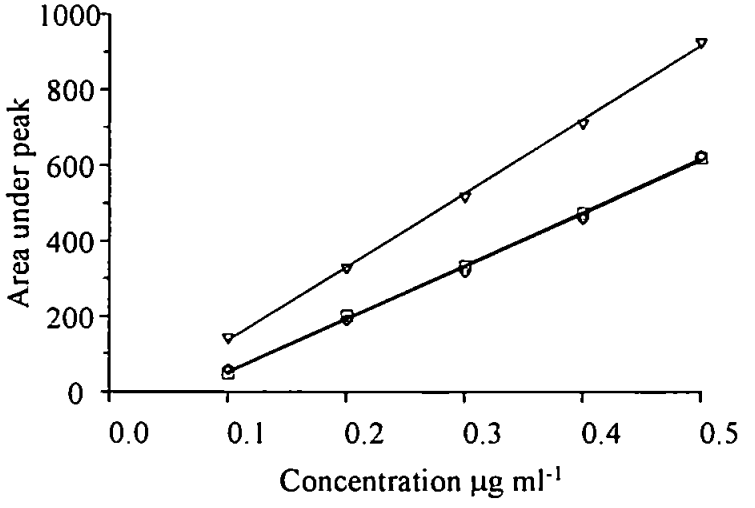

Figure 2.7. Calibration of Organomercury complexes at pH5 Electrolyte. Separation conditions: Electrolyte 10mM Sodium acetate pH 5, containing 5µg ml^{-1} DzS; Capillary polyacrylamide coated fused silica L_d 60cm 100µm ID; Voltage -25kV; Detection 480nm.

2.2.5. The Migration of Organo-mercury DzS Complexes.

It was initially assumed that the organomercury complexes were highly stable during electrophoresis but the excellent resolution of these complexes suggests that this may not have been the case. Had these complexes been inert it is highly unlikely that the MeHg and EtHg

would have been fully resolved. The separation of ions is based on the differences in their charge to mass ratio. Although a simplistic view, in this case it should be applicable since the shape of the molecules is not significantly different. Since all the organomercury complexes have the same charge, separation would be effected purely by differences in their mass. However, the masses of MeHg, EtHg and PhHg complexes are 620, 634 and 682 respectively. The mass of MeHg is 98% of that of EtHg with a t_m of 330 seconds this would give a peak to peak difference of only 7 seconds, whereas the observed difference is nearer to 20 seconds. Again with PhHg the predicted difference between the MeHg and PhHg peaks is 30 seconds but the observed difference is around 50 seconds. This apparent retardation of the migration velocity of the organomercury complexes was more apparent when compared to that of the free DzS. The charge to mass ratio of the DzS and MeHg was 1:202 and 1:310 respectively. Consequently, the t_m of 188 seconds for DzS would translate to a t_m of 290 seconds for the MeHg complex but the observed tm for MeHg was 330 seconds. This calculations should not be taken a absolute but provide a useful guide since it is assumed that the charge on the dye was exactly minus 2 although this may not have been the case.

The migration of these metals is a function of an equilibrium between the dye and metal ion. Because the metal ion spends at least some time in an uncomplexed state, its mobility is continually reversing causing the complex to migrate with an overall retarded velocity.

The peaks were slightly broader than expected indicating that electrodiffusion as well as standard diffusion was occurring. Wall interaction, probably of a phase-related nature, as indicated by the greater broadening of the phenyl mercury may also have been responsible.

2.2.6. Limit of Detection.

The background noise was found to be exceptionally low in all studies emphasising the potential advantage of direct absorbance methods over indirect methods. This is clearly seen

in Figure 2.5 with organomercury concentrations at the 1 mg l^{-1} level and also in Figure 2.8 showing mercury and methyl mercury at the 0.01 mg l^{-1} levels, close to the limit of detection. The noise levels were found to be ± 0.00002 absorbance units coupled with very flat baselines. In fact, the limit of detection in this case was controlled by the extent of the negative intercept rather than the noise. Thus, the detection limit found for methyl mercury was less than 0.01 μg ml^{-1}.

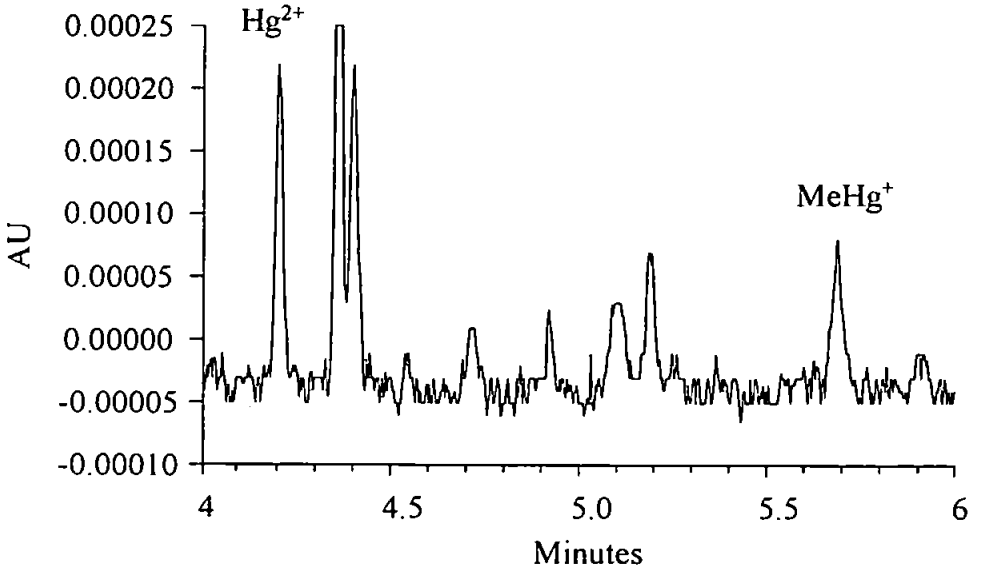

Figure 2.8. Electropherogram of inorganic mercury and methyl mercury near the limit of detection. Separation conditions are the same as in Figure 2.5. Hg^{2+} concentration = 0.01mg l^{-1} and MeHg concentration = 0.01mg l^{-1}.

2.2.7. Electrophoretic Properties of DzS and its Mercury Complexes.

DzS is relatively new and unstudied and there is no data concerning stability or acid dissociation constants. Tanaka *et al.* [171] reported that Hg (II) formed a complex with a mole ratio of 1:2 (M:2L) and it was assumed the dye formed a 1:1 complex with the organic mercury species. This appeared to be confirmed by experimental observations.

From the observed electrophoretic velocities of the dye and its complexes at pH 3, it was estimated that the dye had a charge of approximately minus one and formed the following complexes with the mercury species at pH 3.

$$Hg^{2+} + 2HL^{-} \rightleftharpoons HgL_2^{2-} + 2H^{+} \quad \text{and} \quad RHg^{+} + HL^{-} \rightleftharpoons RHgL^{-} + H^{+} \qquad \textit{Equation 2.2}$$

Based upon the electrophoretic velocities of the dye and its complexes at pH 5 it was estimated that the dye had a double negative charge and co-ordination with the mercury species gave the following complexes.

$$Hg^{2+} + 2\,HL^{2-} \rightleftharpoons HgL_2^{4-} + 2H^{+} \text{ and } RHg^{+} + HL^{2-} \rightleftharpoons RHgL^{2-} + H^{+} \qquad \textit{Equation 2.3}$$

As with dithizone it was assumed the mercury species bonded to the sulphide group rather than the sulphonic acid groups due to the greater stability of this bond over the latter. Although the formation of a chelate between inorganic mercury and the sulphonic acid groups may increase this stability, this complex was discounted due to the resultant charge of the migrating complex.

2.2.8. Other Metals Complexing with Dithizone Sulphonate.

A brief study was carried out involving the CE of other metals as their DzS complexes which might produce potential interference in the determination of mercury species. Ag, Au, Bi, Cd, Co, Cu, In, Ni, Pb, Pd, Mn, Tl and Zn were investigated. Most were found not to show any peaks at all even at the 10ppm level, indicating that complete dissociation had taken place before the detector. Some of the metals Ag, Au, Cd, Co and Pd gave distorted peaks close to inorganic mercury but well away from the organomercury peaks which are the main ones of interest for this work.

2.3. The determination of Methyl mercury in Real samples.

Despite numerous papers describing separation by capillary electrophoresis the technique has failed to become accepted as a tool for routine analysis. One of the major reasons for this lack of acceptance is the general lack of robustness of capillary electrophoresis when applied to the analysis of real samples. The resolution and detection sensitivity are highly influenced by a number of parameters among which include the ionic strength and pH of the sample. One of the principal advantages of this work is that the methyl mercury is isolated from any ionic sample constituents during the sample preparation therefore the samples are low in ionic strength and more importantly are easily matched to the ionic strength of the calibration standards.

Although methylmercury is the only mercury species expected to be present in biological samples, it is important to show that a clear separation of different organometallic forms is possible. The method was found to be quantitative and very sensitive, due not only to the highly absorbing DzS complexes, but also the extremely low and stable absorbance background. The detection limit of less than 10 $\mu g\ l^{-1}$ for methyl mercury was more than adequate for the investigation of marine organisms. All results were calculated from calibrations obtained by adding DzS to aqueous organo mercury standards.

2.3.1. Extraction Efficiency.

All solvent extraction processes involve losses, whether due to less than 100% partition efficiency or reduction in volume due to emulsion formation etc. It is therefore important to obtain a reliable overall extraction efficiency and to assess the reproducibility of the technique. The extraction efficiency was determined by adding 1μg MeHg to a solution containing 20ml MQ water and 10ml HCl. 40ml of toluene was added to this and placed in a flask shaker for 5 minutes. The mixture was then transferred to a 100 ml glass centrifuge tube, sealed and

centrifuged at 3000rpm for 5 minutes. An aliquot of the toluene layer was transferred to a conical flask containing 1ml of DzS and placed in the flask shaker for 2 minutes. The mixture was then centrifuged at 3000rpm for a further 5 minutes and 0.5ml of the DzS layer was analysed. This procedure was replicated 15 times giving a mean recovery of 82.5%, with a standard deviation of 1.63 and relative standard deviation (RSD) of 1.98%. It was considered that the extraction efficiency could have been improved by extracting the toluene layer a second time. However, this was found to reduce the reproducibility of the extraction technique without producing any significant increase in the overall efficiency. It was decided to use a single extraction in this work as the recovery was sufficiently high and that good reproducibility was more important for the application to real samples. To assess the concentration of DzS to use in the extraction, a series of injections of increasing reagent concentration were made. There was some concern that very high concentrations of dye may produce interference problems due to impurity peaks that went undetected at lower concentrations. However, the lack of interference in region of interest allowed the use of a vast excess of DzS, which was hoped, would increase the efficiency of the transfer of methylmercury from the organic phase.

2.3.2. Fish and Crab Meat Results

The types and properties of samples analysed are summarised in Table 2.3. Canned fish samples, where possible, were obtained in brine owing to the higher solubility of MeHg in vegetable oils. It was thought that oil might leach out some of the MeHg making it necessary to analyse the oil portion as well. All samples were extracted from the wet fish sample, except tuna number four which was freeze dried prior to extraction. Canned tuna is principally composed of the smaller species of tuna such as skipjack and albacore. These species tend to have much lower levels of methyl mercury, averaging only about 0.17 ppm, than the larger

species which tend to be sold as fresh tuna meat and steaks [175]. It was intended to analyse fresh tuna or swordfish steak in addition to the canned samples but unfortunately, these were unavailable at the time.

Table 2.3. Origin and characteristics of samples analysed.

Sample	Origin of Can	Matrix in Can
Tuna Fish 1	Philippines	Spring Water
Tuna Fish 2	Thailand	Brine
Tuna Fish 3	Spain	Brine
Tuna Fish 4	Philippines	Vegetable Oil
Crab	Thailand	Brine
Salmon	Alaska	None

During the extraction, certain samples caused the formation of persistent emulsions between the aqueous and organic phases. In the worst cases an emulsion also developed between the toluene and dye. The formation of an emulsion between the acidified aqueous layer and toluene was not a problem since not all the toluene layer was removed. During the development of the extraction procedure, it was found that the total recovery of the toluene layer was not feasible. This was in part due to difficulties in pipetting from the relatively broad surface of the centrifuge tube and losses due to the formation of emulsion. Attempts at total recovery were not always possible and time consuming resulting in evaporation of the toluene making it impossible to quantify the recovered volume. It was far easier to rapidly remove a quantifiable volume, ca. 30 ml and use this for the extraction.

The formation of an emulsion between the toluene and DzS layers was more of a problem. Initially a small volume of methanol was found to disperse the emulsion. Although this method was very successful at dissolving the emulsion it was realised that it introduced a quantitative problem. Although a known volume of methanol was added to the sample, it was not known how much of the Methyl mercury DzS complex was partitioning into the toluene due to the addition of the methanol. An alternative solution to the problem of emulsion formation in the sample was found by filtration of the DzS layer through a 0.45 μm PTFE

membrane. This additional step was not found to affect the overall recovery of the extraction procedure. However, a significant correlation was found between the formation of this emulsion and the higher residual standard deviations (RSD) obtained with some samples. With the freeze-dried samples, very little emulsion was formed, resulting in greater precision than the wet samples. It was assumed that the freeze-drying process may remove some of the more volatile organic components of the samples. The greater physical quantity of methyl mercury in the freeze-dried sample may also have influenced the precision with these samples, since a greater RSD would be expected when approaching the limit of detection.

During the extraction efficiency experiments no emulsion was produced and it was thought that the emulsion formed during the extraction of real samples might adversely effect the result The effect of the matrix on the extraction procedure was assessed by spiking 10g portions of a tuna sample (No. 3) with 2.5μg of MeHg. The results displayed in Table 2.4 show good quantitative recoveries were obtained.

Table 2.4. Recovery results for a tuna sample spiked with 2.5 μg of MeHg.

Sample Spiked	Mass of Sample (g)	Spike μg Kg^{-1}	Found (μg Kg^{-1})	Sample (μg Kg^{-1})	Amount Recovered (μg Kg^{-1})	% Recovery [a]
Tuna 3	10.20	245	435	193	242	98.7
Tuna 3	10.04	249	455	193	262	105.2
Tuna 3	10.12	247	444	193	251	101.6

[a] 82.5% extraction efficiency taken into account. Mean Recovery = 102 ± 3.2%

A certified reference material was also investigated to assess the overall accuracy of the technique. DORM 1 is freeze-dried dogfish muscle with a MeHg value of 731 ± 60 μg kg^{-1}. Four extractions were performed using 0.5 g of DORM 1 for each. The results gave an average of 714 +/- 12 μg Kg^{-1} (1.7% RSD). Although this value is slightly lower than the certified mean value, the concentrations found were well within the certified range.

The fish and crab results are summarised in Table 2.5. From the data it can be seen that as expected the tuna contains the highest concentration of MeHg. These levels are within the US Food and Drug Administration action level of 1000 μg Kg^{-1} (wet weight) for Hg in fish and the 500 μg Kg^{-1} limit set in Canada [176]. The concentration of methyl mercury found in the freeze dried tuna was surprisingly low, considering this relates to approximately 45 μg Kg^{-1} wet weight. The low result is possibly due to losses of MeHg to the oil in the can, but unfortunately the oil was discarded and could not be analysed. A more likely source of any loss was the freeze drying process, which could cause volatilization of the MeHg. Losses of up to 60% have previously been reported during freeze drying [177].

Table 2.5 MeHg concentrations found in fish and crab meat

Sample	Mean mass (g)	Mean Concentration[a] (μg Kg^{-1})	Standard Deviation	Replicates	RSD %
Tuna Fish 1	10.33	113	3.86	4	3.4
Tuna Fish 2	10.62	218	11.5	4	5.5
Tuna Fish 3	10.53	193	9.5	4	4.9
Tuna Fish 4	10.51	469[b]	4.5	4	0.95
Cod	21.02	70	0.5	2	1.4
Haddock	23.47	58	3.5	2	6.0
Crab	10.26	2.8	0.1	2	3.5
Salmon	10.19	3.7	0.1	2	2.7

[a] Assuming 82.5% extraction efficiency. [b] Dry weight (Freeze dried sample)

The levels found in the cod and haddock are lower, consistent with their position in the food chain. Figure 2.9 shows the electropherograms of methyl mercury in cod and haddock meat. These electropherograms illustrate the high efficiency and good peak shapes obtained for methyl mercury, which were well separated from the dye impurity peaks.

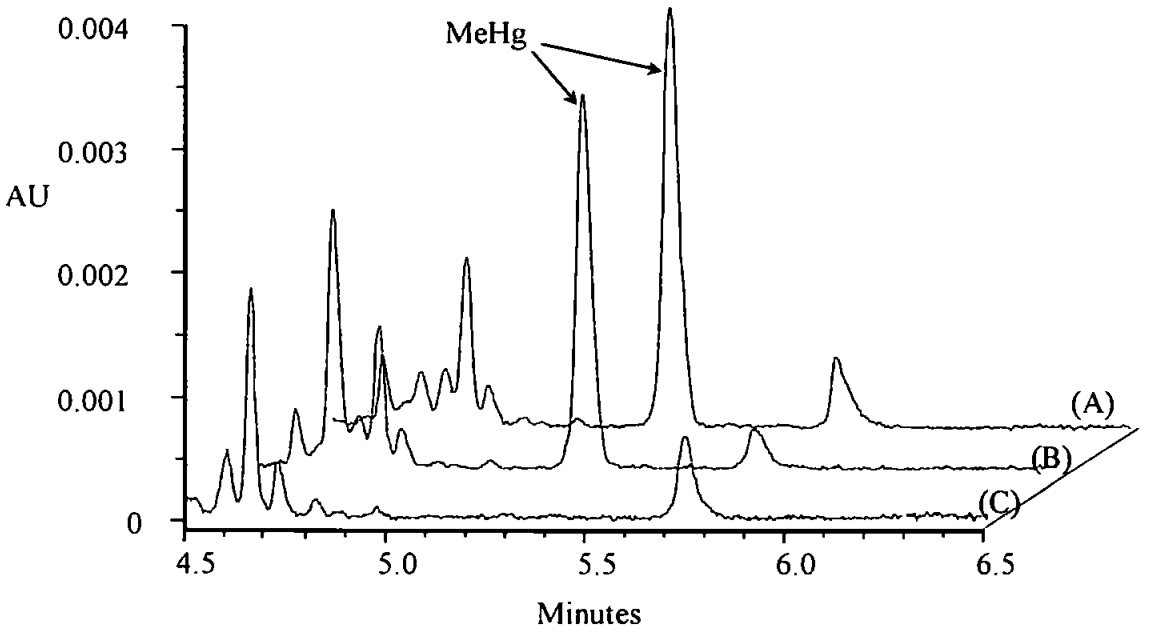

Figure 2.9. Electropherograms showing the MeHg peaks obtained after extraction of cod and haddock meat. Separation conditions: Electrolyte 10mM sodium acetate pH 4.5.containing 5μg ml^{-1} DzS; Capillary, polyacrylamide coated fused silica 65cm L_t, 60cm L_d 100μm ID; Voltage -25kV; Detection 480nm. Key: (A) - cod, (B) - haddock, (C) - blank.

The impurity peaks shown in the electropherogram were almost exclusively derived from the DzS, with few if any resulting from the extractions. These impurities are constant for a particular batch of DzS and have a fixed relationship to the mercury species in terms of migration time. Interestingly, they actually help by acting as "markers" for the inorganic and organo mercury positions. This can be seen in Figure 2.10 which shows the electropherograms for salmon and crab meat where the MeHg peaks are a constant 0.4 minutes from an impurity peak.

The methyl mercury concentration of the salmon was surprisingly low considering its predatory nature, but may reflect its relatively short life span. MeHg was even detected in crabmeat, which has been used as a control sample in the past, as the methylmercury concentration is usually below the detection limit of the method used [170]. This is an indication of the very high sensitivity of the method, where the base line is flat even when the sensitivity control is increased so that the clipped digitised noise is seen. The average peak to

peak noise was 0.00004 absorbance units and defining a detection limit as twice this figure, corresponds to a minimum detectable concentration of 2 μg Kg^{-1} MeHg for a 10g sample.

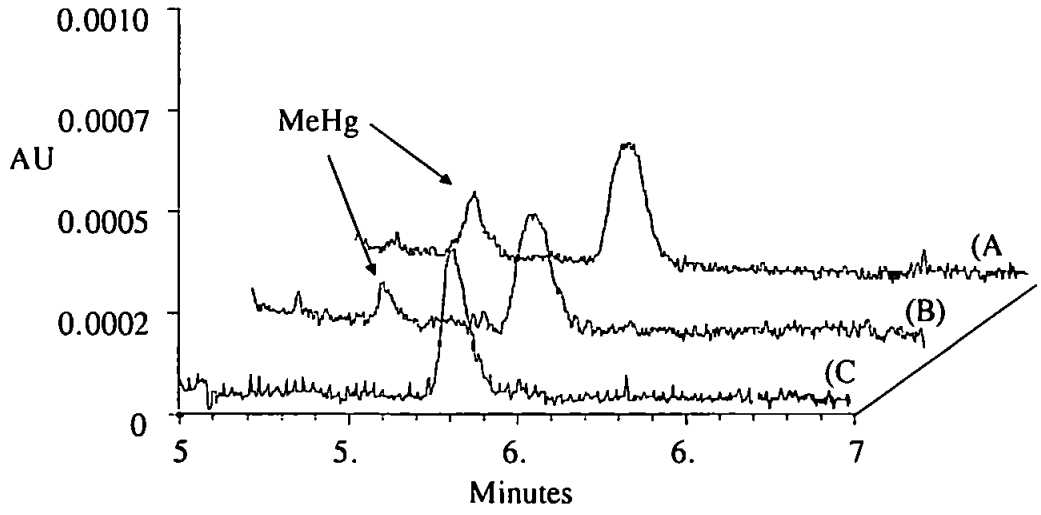

Figure 2.10. Electropherograms showing the MeHg peaks obtained after extraction of salmon and crabmeat. Separation conditions: Electrolyte 10mM sodium acetate pH 4.5.containing 5μg ml^{-1} DzS; Capillary, polyacrylamide coated fused silica 65cm L_b 60cm L_d 100μm ID; Voltage -25kV; Detection 480nm. Key: (A) - salmon, (B) - crab, (C) - blank.

2.4. Summary.

A good quality separation of inorganic and three organo mercury species as their dithizone sulphonate complexes was achieved using coated capillary columns. The complexes were pre-formed before injection and detection was by direct measurement of the absorbance of the complexes. Good linear calibration curves were obtained for all the mercury species studied and the exceptionally low background noise and straight base lines meant that detection limits in the low μg l^{-1} range could be obtained.

Dithizone sulphonate (DzS) was used in place of cysteine to extract methyl mercury from fish flesh in the final stage of a simplified Westoo extraction procedure. The intensely absorbing methyl mercury DzS complex was then separated by CE using a coated capillary and

determined by direct absorption measurement at 480nm. Good quantitative performance was demonstrated by spiking experiments and the analysis of DORM-1, a certified reference material. Values found ranged from 18 μg Kg^{-1} for a tuna fish to 2.8 μg Kg^{-1} for a crab sample. The very stable base line and lack of interfering peaks meant that a low detection limit of 2 μg Kg^{-1} could be achieved for a 10g sample. The method developed here should also be suitable for the determination of methyl mercury in other environmental samples, such as sediments. However, the method is not suitable for the direct determination of di-methyl mercury without prior demethylation of the di-methyl mercury to mono-methyl mercury, since di-methyl mercury does not form a complex with the dithizone sulphonate.

CHAPTER 3. THE DETERMINATION OF URANIUM.

3.0 Introduction.

3.0.1. Environmental Occurrence, Toxicity and Uses of Uranium.

Uranium (U) is a member of the actinide series of elements. It is a radioactive metal with a high specific gravity of 18.7 g cm^{-3}. It was first discovered in the mineral pitchblende by Martin Klaproth in 1789 and was named after the planet Uranus. Naturally occurring uranium consists of a mixture of three isotopes in the following proportions; ^{238}U 99.27%, ^{235}U 0.72 % and ^{234}U 0.0057%. With ^{235}U being the only naturally occurring fissionable element. The half lives in years of these isotopes are; ^{234}U 2.48×10^5, ^{235}U 7.13×10^8 and ^{238}U 4.51×10^9 [178].

Uranium is the forty-eighth most abundant element in the earth's crust, with an estimated concentration of 2.4 μg g^{-1} [179], which is similar to that of tin, tungsten and molybdenum. In excess of 150 uranium-bearing minerals have been identified, the primary sources being uraninite (A complex mixture of the oxides, UO_2 and UO_3 with a formula ranging from $UO_{2.25}$ to $UO_{2.67}$, commonly expressed as the simplified formula U_3O_8), pitchblende (a fine-grained variety of uraninite), brannerite (a complex oxide of uranium, lanthanides, iron and titanium) and coffinite (uranium silicate). With the principal source of the world's uranium being produced from pitchblende ores. The most important secondary minerals are carnotite (potassium uranium vanadate), autunite (calcium uranium phosphate), davidite (a complex mix of metal oxides principally iron, titanium, uranium and lanthanide metals), gummite (uranium and thorium oxides), torbernite (copper uranium phosphate) and uranophane (calcium uranium silicate) [180]. Major global uranium deposits occur in the former Soviet

Union, Canada, Australia, South Africa and the USA. Global production of uranium was 34,400 tonnes in 1992 (equivalent to 40600 tonnes U_3O_8) with the former Soviet Union accounting for 32%, Canada 27%, Africa 21%, Australia 7%, France 6% and the USA 5% [181].

Uranium is widely distributed throughout the environment and human exposure is inevitable. Table 3.0 shows the distribution and isotopic abundance of uranium in the marine environment. The approximate mean concentration of uranium in seawater is 3 $\mu g\ l^{-1}$.

Table 3.0. The Isotopic Abundance of Uranium in the Marine Environment.[182]

Isotope	Range of concentrations found in the ocean $\mu g\ l^{-1}$	Range of concentrations found in oceanic sediments $\mu g\ kg^{-1}$
^{234}U	0.00016 - 0.00021	0.024 - 4.9
^{235}U	0.019 - 0.025	2.8 - 580
^{238}U	2.7 - 3.4	400 - 80,000

Typical concentrations of uranium in the terrestrial environment are: river water ~0.5 $\mu g\ l^{-1}$, soil 3.4-10.5 $\mu g\ g^{-1}$ dry weight and granite rock 15-80 $\mu g\ g^{-1}$ [179].

Uranium and its compounds are toxic to humans by virtue of both their chemical toxicity and radiological toxicity. Uranium daughter products are mostly alpha emitters and are also potentially hazardous to humans. The most notable being radon gas, which has a sufficiently long half life to permit it to permeate from the soil where it can build up to dangerous concentrations in buildings without adequate ventilation [183]. The oral toxicity of uranium was reported to be low [178]. The toxicity of inhaled uranium compounds was reported to be fatal to several laboratory species when exposed for one month at a concentration of 20mg m^{-3} although inhalation of 0.05mg m^{-3} resulted in no histological damage. The intravenous toxicity of uranium was reported to be very high [178]. The critical organ in uranium toxicity is the kidney, which is the major route of excretion. The radio toxicity of uranium has not

been well established due to difficulties in differentiating between radiocarciogenisis and metallocarcinogenisis in laboratory studies [178]. Uranium tends to be deposited in skeletal tissue accounting for 66% of the body burden, which has been estimated at between 100-125μg for a standard human [184]. The major source of uranium and its compounds in humans is from diet, with the average intake in the UK estimated at 1.2 μg per day [184]. Table 3.1 show the distribution of uranium in human tissue.

Table 3.1. Uranium in Human Tissue [183].

Tissue	Average Burden (ng g^{-1} wet tissue)
Liver	0.23
Lung	1.08
Kidney	0.44
Blood	0.46
Muscle	0.19
Heart	0.16
Spleen	0.42
Gonad	0.60
Fat	0.60
Bone	25.0

Table 3.2 gives the average concentration of uranium in some important dietary groups.

Table 3.2. Uranium Concentrations in Food Groups [184]

Food Group	Average Uranium Concentration ng g^{-1}
Sea Fish *	21.0
Table Salt	40.0
Tea	5.0
Coffee	6.0
Thyme	90.0
Parsley	60.0
Meat	0.4
Vegetables / fruit	0.8
Milk	0.01
Eggs	0.4

* [185]

A study in the USA by Welford and Baird [186] concluded that potatoes, meat, fish, vegetables and bakery products contributed over seventy percent of annual uranium

intake in humans. This study found that the concentration of uranium in tap water was negligible.

The principal use of uranium is as the fuel in nuclear power reactors to generate electricity. Uranium is also used in the manufacture of radioisotopes used in the production of nuclear weapons and as radiolabelled tracers.

The natural abundance of uranium isotopes has been used to estimate the age of the earth and to date rocks and minerals [187].

Uranium oxides are also used in small quantities to produce pale yellow and green coloured glass, which fluoresces in UV light and similarly coloured ceramic glazes.

Depleted uranium, a form of recycled radioactive waste is used in the cones of armour piercing shells capable of piercing all known tank armour. An estimated 25 tonnes of depleted uranium was used in the Gulf war [179].

3.0.2 Chemistry of Uranium

Uranium has four known oxidation states, (+III), (+IV), (+V) and (+VI), with the ions formed being U^{3+}, U^{4+}, UO_2^{+} and UO_2^{2+} respectively. In the environment, uranium exhibits only two principal oxidation states, U^{4+} and UO_2^{2+}. Oxidation-reduction reactions between $U^{3+}$and U^{4+} or UO_2^{+} and UO_2^{2+} are rapid, since these reactions only involve the transfer of an electron. Whereas, the oxidation of U^{4+} to UO_2^{2+} is much slower as this reaction involves a structural reorganisation around the metal ion.

In aqueous solution, UO_2^{2+} is the most stable form. U^{3+} is oxidised, slowly by water, but rapidly by air, to U^{4+}, which is itself slowly oxidised to UO_2^{2+} by air. UO_2^{+} is a transient species and disproportionates to U^{4+} and UO_2^{2+}.

The standard reduction potentials (E^0/V) for uranium are shown in Figure 3.0 below.

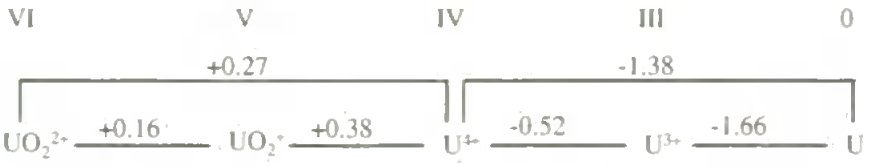

Figure 3.0. The standard Reduction Potentials for Uranium [188]

The radioactive decay series of ^{238}U ends in a stable isotope of ^{206}Pb, shown in Figure 3.1, whereas the decay series of ^{235}U ends in ^{207}Pb [187]. ^{235}U is of special importance since this isotope undergoes nuclear fission with slow neutrons to yield enormous amounts of energy. The fission process of ^{235}U may produce other actinides, and the neutron capture of $^{238}_{92}U$ in the system can be used to produce ^{239}Pu [189].

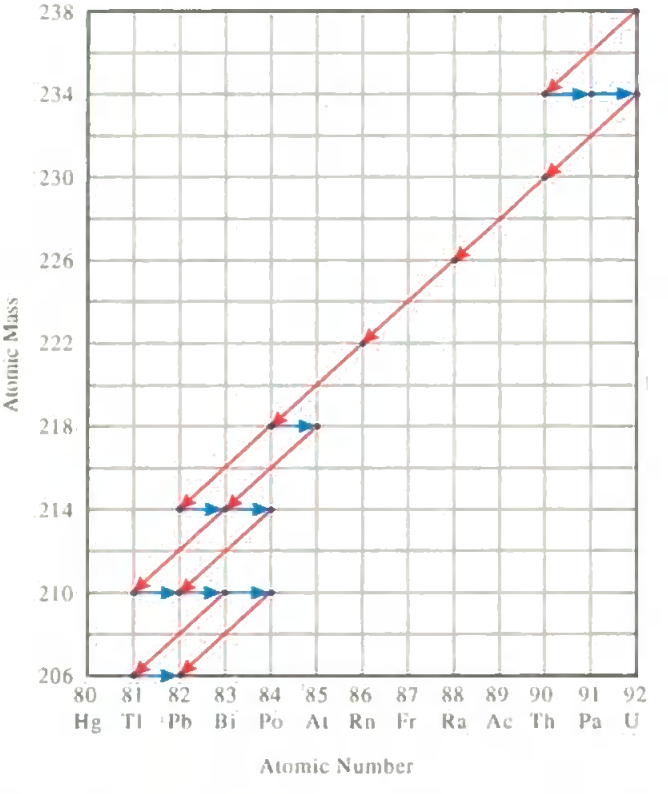

Figure 3.1 ^{238}U Radioactive Decay Series. (The diagonal arrows represent α-particle emissions and the horizontal arrows represent $\beta-$ emissions).

3.0.3 Methods for the Determination of Uranium.

Numerous methods for determination of uranium have been described in the literature. Owing to the low concentrations of uranium and the presence of high levels of interfering ions, many of these methods employ separation or pre-concentration techniques prior to analysis [190] including solvent extraction techniques [191] and pre-concentration on ion exchange resins [192]. A large number of

spectrophotometric methods have been described using among others, Arsenazo III [193-196], Chlorophosphonazo [197-199], Malachite Green [200] and PAR [201]. More recently a wide range of instrumental methods have also been developed including, HPLC [192, 201 202], flow injection analysis [190, 204], isotope dilution mass spectrometry [205], X-ray fluoresence [206], inductively coupled plasma atomic emission spectrometry (ICP-AES) [207], inductively coupled plasma mass spectrometry (ICP-MS) [207] and laser ablation - ICP-MS [208].

Uranium has also been determined by capillary electrophoresis. Colburn *et al.* [209] injected pre-formed uranyl-Arsenazo III complex and a detection limit of 10 $\mu g\ l^{-1}$ was achieved using the field amplified sample stacking technique developed by Chein and Burgi [78, 74, 210]. This method used bare fused silica capillaries but failed to separate the uranyl complex from the excess reagent.

Macka *et al.* [24] used on-capillary complexation for the detection of the uranyl and lanthanide Arsenazo III complexes. This method used gravity injections into a capillary dynamically coated with carbowax 20M, the detection limit for uranium was reported to be 60 $\mu g\ l^{-1}$.

Liu et *al.* [211] separated pre-formed uranium, thorium and lanthanide metal complexes of 2-[(2-arsenophenyl)-azo]-1,8-dihydroxy-7-[(2,4,6-tribromophenyl)azo]-naphthalene-3,6-disulfonic acid. This method used bare fused silica capillaries and hydrostatic injections. The lanthanide metals were not resolved from each other but were separated from uranium and thorium. Detection limits of 200 $\mu g\ l^{-1}$ and 40 $\mu g\ l^{-1}$ were reported for uranium and thorium, respectively. From the above it appears that Arsenazo III requires a more detailed study for the capillary electrophoresis determination of trace metals.

3.0.4. Arsenazo III

Arsenazo III has been reasonably well documented as a spectrophotometric reagent forming complexes with wide range of metals notably, Ca, Ba, Sr, Fe, Cu, Al, Th, U, Zr, Pd, Sc and the lanthanide metals [212, 213]. Arsenazo III reacts with the acid hydrolyzing metals Hf, Np, Pa, Pu, Th, U(IV) and Zr in strongly acidic solution. Arsenazo III is relatively soluble in aqueous solution. In acid solution the reagent is red/pink but begins to turn blue at pH values above 5.

The dye is usually impure, although a highly purified product can be obtained, the main impurity being Arsenazo I. There are numerous inconsistencies in the literature, regarding the stoichiometry of metal complexes with Arsenazo III [214]. These discrepancies have been attributed to the impure state of the reagent and recent studies on lanthanide metals indicate these metals only form 1:1 complexes [214, 215]. Arsenazo III forms a stable complex with the uranyl cation, with a molar ratio of 1:1, the structure of the complex is shown in Figure 3.2. The kinetics of the complexation reaction was reported in the literature to be fast for the formation of the complex but slow for the dissociation reaction [212]. The dye is also reported to form 1:1 and 1:2 complexes with quadrivalent metal ions such as Th and U(IV) [216].

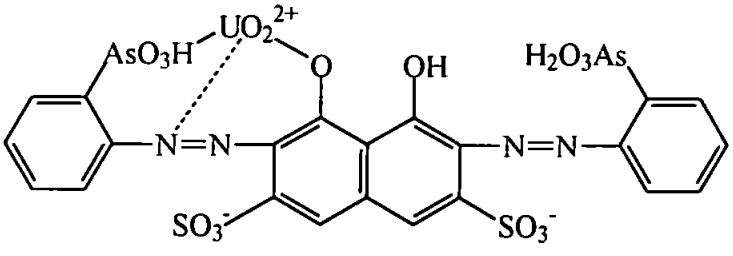

Figure 3.2. Structure of Uranyl-arsenazo III complex

Literature values of the protonation constants of Arsenazo III also show considerable variation, as illustrated in Table 3.3. The source of this variation is also thought to be due to the impurity of the reagent [215].

Table 3.3. Literature Values for the pK_a Values of Arsenazo III

pK_n	[217]	[218]	[219]	[220]	[221]	[222]
1	-2.6	-1.3	0.60	1.89	0.8	<1.3
2	0	-0.6	0.80	2.96	2.9	<1.3
3	2.4	3.8	1.60	3.64	3.5	2.60
4	2.4	5.2	3.40	5.05	5.0	4.29
5	5.3	7.1	6.27	6.77	7.0	6.70
6	5.3	9.0	9.05	7.64	8.4	8.79
7	7.5	11.7	11.98	9.30	10.2	10.58
8	12.3	14.6	15.10	11.85	12.4	10.99

More recently, the absorbance changes of a standardised solution of the free reagent were determined as a function of pH in the range 1- 11, by Rohwer and Hosten [215]. This data, shown in Table 3.4, was used to calculate acid dissociation constants from the absorbance changes.

Table 3.4. pK_a and ε Values of Arsenazo III [215].

		ε (10^4 l mol^{-1} cm^{-1})			
Species	pK_n	536nm	565nm	605nm	650nm
LH_n		3.91	3.33	0.559	0.061
LH_{n-1}	3.36	3.93	3.56	0.756	0.099
LH_{n-2}	4.32	3.99	3.66	0.818	0.188
LH_{n-3}	7.77	2.97	3.03	1.38	0.384
LH_{n-4}	10.38	2.86	3.34	2.89	1.54

Unfortunately, the correlation between the data in tables 3.3 and 3.4 is relatively poor, and little confidence can be used when estimating the charge of the reagent at different pH values.

The charge of the free reagent and the metal-Arsenazo III complexes were estimated from Figure 3.3 which shows a species distribution diagram of the

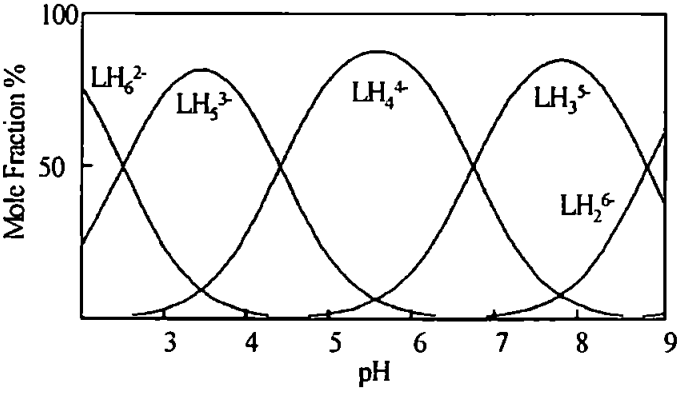

Figure 3.3 Distribution Diagram of Arsenazo III as a function of pH. [222]

different protonation states of Arsenazo III between pH 2 and 9. The diagram was constructed using the Log β values given by Nemcova *et al.* [222].

Preliminary experiments showed that a number of metal ions, notably U(VI) formed complexes with Arsenazo III which were stable enough to survive separation by capillary electrophoresis and the following study focuses on the development of a capillary electrophoresis method for the determination of uranium as U(VI).

3.1 Experimental.

3.1.1 Instrumentation.

All experiments were carried out on a Dionex CES 1 capillary electrophoresis system (Dionex, Sunnyvale, CA) using the reversed polarity power supply. Sample introduction was performed by either gravity or electrokinetic injection from the cathodic end of the capillary. Detection was carried out by on-column spectrophotometric measurements at 654nm unless otherwise specified. Data was recorded using a Dionex ACI computer interface, and processed using Dionex Peaknet automated chromatography software, sampling at a rate of up to 50Hz.

Fused silica capillaries of 100μm, 75 μm and 50μm internal diameter were supplied by Dionex (Dionex UK, Camberley, Surrey.) and internally coated with polyacrylamide using the method described in Chapter 2. A 100μm capillary internally coated with an unspecified neutral hydrophilic polymer and polymeric capillaries manufactured from polyacrylimide with an internal diameter of 0.004", polystyrene and poly(vinylidene fluoride) (PVDF) with 0.003" internal diameters, were a gift from Dionex (Sunnyvale, CA).

3.1.2. Reagents and Solutions.

All reagents used were of analytical grade or better. 1000 mg l^{-1} standard solutions of uranium (VI) and thorium (IV) were obtained from May and Baker (Dagenham U.K. 1000 mg l^{-1} standard solutions of lanthanide metals obtained from Johnson and Matthey.

A 1000 mg l^{-1} Spectrosol standard solution of Iron III was obtained from BDH (British Drug Houses, Poole, Dorset, UK). Sodium acetate and acetic acid were of Aristar Grade also obtained from BDH. All water used was 18-MΩ cm^{-1} obtained from a MilliQ high purity water system (Millipore, Bedford, MA). Arsenazo III (2,7-Bis(2-arsonophenylazo)chromotropic acid) of 98 % and approximately 60% purity was obtained from Aldrich (Gillingham, Dorset) and 95% purity Arsenazo III was obtained from ICN (ICN Pharmaceuticals, Basingstoke, UK). Tartaric, citric and ascorbic acids and sulphur dioxide solution were obtained from BDH (British Drug Houses, Poole, Dorset, UK). Hydroxylamine hydrochloride was purchased from Aldrich (Gillingham, Dorset).

3.2. Results and Discussion.

3.2.1. Capillary Wall Chemistry.

The electroosmotic flow generated by bare fused silica capillaries can be detrimental to the detection of anions and anionic chelates, due to increased analysis times or the possibility of ionic interactions between metal ions and the capillary wall. For these reasons, neutral hydrophilic coated capillaries were chosen for the analysis of the Arsenazo III-uranium complexes. Although these capillaries should suppress ionic interactions, phase related interactions could become significant. Uncoated fused silica capillaries are known to have hydrophobic interaction sites and when using very large

organic reagents such as Arsenazo III, adsorption of the reagent onto the capillary wall could result in the formation of a chelating surface. It was considered that a hydrophilic coating should reduce any phase related interactions between the reagent and the capillary surface. While possessing many advantages, coated fused silica capillaries are more expensive than bare fused silica or time consuming to manufacture. The coatings have limited durability and are susceptible to damage by electrolyte additives or extremes of pH. The surface characteristics may also be altered by the precipitation of solutes or electrolyte components. For this reason, polymeric capillaries were also investigated since these are available with a range of surface properties and are relatively cheap.

An alternative method of suppressing or reversing the electroosmotic flow is the use of dynamic coatings. These can be used either as electrolyte additives, such as cationic [223], or fluorinated surfactants [224], or for preconditioning the capillary prior to a run using either cationic [225], or non-ionic surfactants [24].

Dynamic coatings were not investigated in this study because it was thought that the use of surfactants might increase the possibility of interactions between the Arsenazo III and the capillary wall. It was considered that dynamic coatings requiring the pre-conditioning of the capillary between runs would add an additional step to the procedure and unduly increase the analysis time. On the other hand, a significant advantage of using these types of dynamic coatings is that the capillary surface is renewed prior to each run.

3.2.2. The Composition of the Electrolyte.

Initially a sodium acetate electrolyte was investigated for the determination of uranium in the presence of interfering ions. With a pK_a value of 4.76 sodium acetate buffers

within the region of interest and with a maximum mobility of -42.4 x 10^{-5} cm^2 V^{-1} s^{-1} produced a relatively low current, allowing the use of high separation field strengths. Furthermore, the pH range of this buffer can be easily extended to pH 2.5 or less by the addition of HCl or chloroacetic acid.

Tartrate and citrate electrolytes were also investigated for the separation of uranium and thorium, the pK_{a1} values are 3.04 and 3.13 and the pK_{a2} values 4.75 and 4.76 respectively. Both these buffers are more complexing than acetate and produce greater currents due to their greater charge and mobilities. In addition, phosphate and KCl - HCl electrolytes were investigated for the determinations of thorium in the pH range 2.2 - 3.

The uranyl complex was found to be sufficiently stable to survive the electrophoretic conditions without the addition of reagent to the electrolyte. However, the addition of 5 mg l^{-1} (6.09 x 10^{-9} M) Arsenazo III to the electrolyte was found to produce a marginal improvement in peak efficiency. Although photometric absorption of the Arsenazo III and its uranyl complex is different by almost 100nm, a slight increase in the background would be expected due to the inclusion of the dye in the electrolyte. The sensitivity of the uranium peak was found to be largely unaffected by the inclusion of reagent in the electrolyte and was possibly offset by the gain in peak efficiency. Lanthanide and alkaline earth metals failed to produce any peaks without the addition of reagent to the electrolyte. The thorium complex although detectable at concentrations above 2ppm was greatly improved by the inclusion of reagent.

The concentration of reagent added to the electrolyte was increased to 50 mg l^{-1} (60.9 x 10^{-9} M) for on-column complexation studies.

3.2.3. Determination of Uranium.

3.2.3.1. Initial Conditions.

The detection of uranium is most sensitive as the uranium (IV) Arsenazo III complex in strongly acidic solutions (>3M HCl). Unfortunately, these conditions are far from ideal for CE, owing to the very high conductivity of the electrolyte. Uranium (VI) forms a stable complex with the reagent at pH values between 1-5, although at these pH values several other metals also form complexes which may interfere.

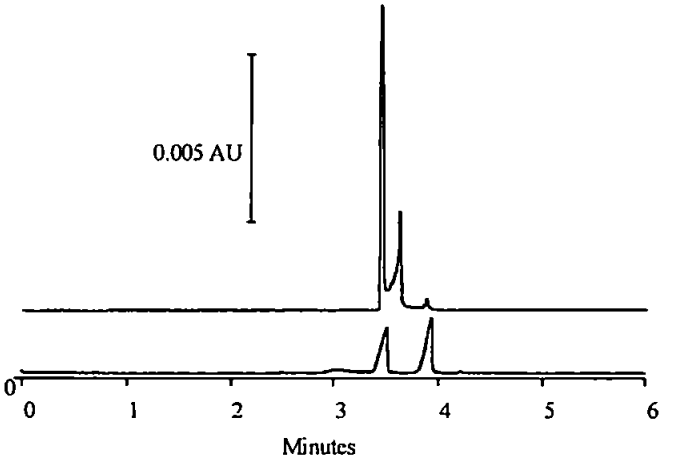

Figure 3.4. Electropherogram of Uranium using low Purity Arsenazo III. Separation conditions. Electrolyte, 10mM Sodium acetate, pH 3.5 with 5 mg l^{-1} Az III; Voltage, -30 kV; Injection Gravity, 100mm, 30 second; Detection 660nm; Capillary 65cm L_t 100mm ID. Key: Lower Trace, Az III. Upper Trace Az III and uranium

Initially, the 60% purity Arsenazo III was injected onto the capillary and a series of injections were made using 10mM sodium acetate electrolyte at pH values from pH 2.5 -5. Using a detector wavelength of 660nm the dye was found to produce two main peaks, these were assumed to be Arsenazo III and Arsenazo I. Injection of the uranium complex was found to produce a single peak poorly resolved from the reagent, shown in Figure 3.4. These complexes failed to resolve from the free reagent peaks until the electrolyte pH was increased above 4. Although manipulation of the electrolyte pH could be used to resolve the uranyl-Arsenazo III complex the formation of the uranyl-Arsenazo I complex presented a serious problem to the sensitivity of the method due to the large proportion of the

uranium that was being complexed by the Arsenazo I. The high purity reagent was obtained and used for all subsequent work.

3.2.3.2. High Purity Arsenazo III

The 98% purity reagent was found to produce a single peak but unfortunately this dye was found to be very expensive, a separate source of 95% purity dye was located at a much reduced cost from ICN (ICN Pharmaceuticals, Basingstoke, UK). Although the 95% purity reagent was found to contain an impurity that produced a small peak, this did not interfere with the separation and did not appear to complex with the uranium.

3.2.3.3. Effect of Electrolyte pH and Concentration

At pH values below 3.5 the uranyl-complex and free reagent were found co-migrate although the complex appeared as a separate sharp peak on the shoulder of the free reagent, shown in Figure 3.5. This peak was found to be both reproducible and quantitative.

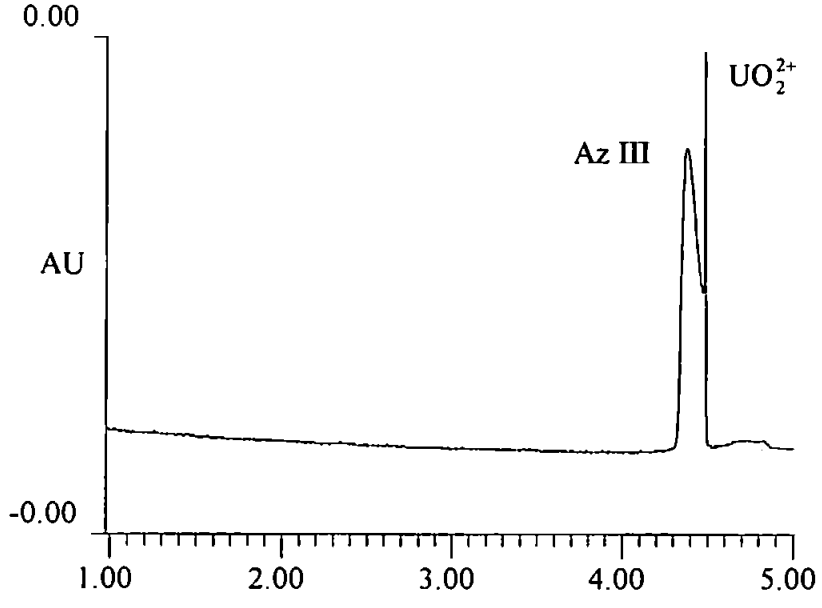

Figure 3.5. Electropherogram showing the Arsenazo III and Uranyl complex at pH 3. Separation conditions: Electrolyte, 10mM Sodium acetate pH 3 with 5 mg l^{-1} Az III; Voltage, –25 kV; Injection Gravity, 100mm, 30 second; Detection 654nm; Capillary 50cm L_t 100mm ID acrylamide coated.

When the pH of the electrolyte was increased above 4 the uranyl-complex and the free reagent peaks were fully resolved. Reducing the pH below 3 was found to reduce the mobility of both the reagent and the complex but had no influence on their resolution. Figure 3.6 shows the effect of pH on the mobility of the free Arsenazo III and the uranyl-Arsenazo III chelate. From the Figure it can be seen that the free reagent become progressively more mobile with increasing pH, whereas the mobility of the complex was far less influenced throughout the pH range examined. The increase in the mobility of the reagent was attributed to increasing ionisation of the molecule. The lower susceptibility of the complex to changes in pH was thought to be because the complexation reaction itself caused the deprotonation of the group responsible for the increase in the mobility of the free reagent.

The chelate would always be expected to have a lower mobility than the reagent considering the increase in size and decrease in the overall negative charge. Consequently the co-migration of the chelate and free reagent was somewhat surprising. The chelate was expected to have a charge of n-2, where n is the charge of the free reagent, which coupled with the greater size of chelate it should give a lower mobility. Assuming that the chelation reaction causes deprotonation of the arsenic acid and phenolic groups (Figure 3.2) then the charge of the chelate may be similar to that of the protonated reagent, although co-migration is still unlikely due to the greater size of the chelate. The co-migration of the uranyl-complex

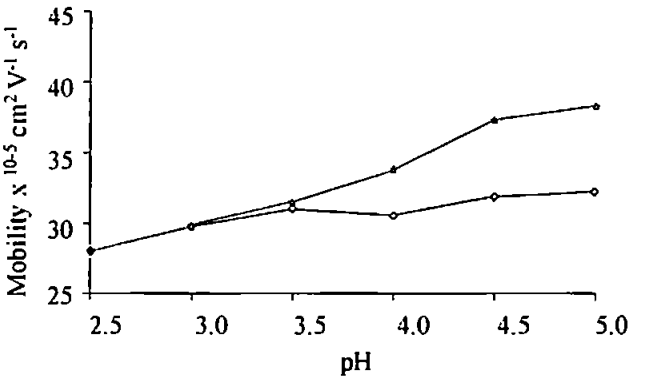

Figure 3.6. Changes of mobility as a function of pH. ☆ = *Free arsenazo III and* ◇ = *uranyl-arsenazo III complex*

and the free reagent remains unexplained and could not be ascribed to lower stability of the complex at pH 3, since this would result in the complex migrating with a cathodal mobility. The formation of the 1:2 complex was also though unlikely as this would still result in a molecule with a lower charge to mass ratio than the free reagent.

The data in Figure 3.6 was obtained from a new capillary using a 10mM sodium acetate electrolyte containing no Arsenazo III. When this experiment was repeated with a previously used capillary, the mobility of the free reagent was found to remain relatively constant and the mobility of the uranyl chelate was found to decrease as the pH increased. The reason for this was put down to the development of a cathodal electroosmotic flow, which would be opposed to the mobility of the sample zones. Previous workers have shown that acrylamide coated capillaries generate some electroosmotic flow [226, 227] and with long-term use this flow has been noted to increase due to degradation of the coating, particularly at high pH. However, in this instance the generation of electroosmotic flow was attributed to adsorption of Arsenazo III onto the wall. Evidence of wall adsorption was ascertained by performing a series of repeat injections into a new acrylamide coated capillary using a pH 5 sodium acetate electrolyte containing no Arsenazo III. The migration times of the uranium and Arsenazo III peaks were noted to be relatively constant, but when 50 mg l^{-1} Arsenazo III was added to the separation electrolyte the migration time of the uranium-Arsenazo III peak was found to progressively lengthen. Adsorption of the reagent onto the capillary wall would be expected to cause significant broadening and loss of sensitivity, as dissociated uranium would be chelated by the adsorbed Arsenazo III. Although some loss of sensitivity and broadening was found this was not a significant as might be expected, possibly due to the high stability or favourable kinetics of the uranyl-Arsenazo III chelate.

The optimum peak resolution was obtained using an electrolyte of between pH 4.0 and 5.0. In terms of sensitivity and peak efficiency there was little difference between the different electrolytes in this range. A 10mM electrolyte at pH 5 produced 36-38μA of current from a 30kV separation voltage. Although this current was greater than that obtained from the lower pH electrolytes and getting towards the upper limit before joule heating would become a problem, it was still usable and there was no advantage to be gained from using the lower pH electrolytes.

The photometric absorption of the Arsenazo III at 654 nm increases rapidly above pH 5 and begins to overlap with that of the uranyl-complex causing an increase in the background absorption and corresponding reduction in sensitivity.

The ionic strength of the electrolyte was varied to find a compromise between buffer capacity, field strength and efficiency. Low ionic strength electrolytes allow the use of high field strengths, but peak efficiency may be compromised due to a reduction in the stacking effect when large injection volumes are used. Sodium acetate electrolytes of 5, 10 and 20mM and pH 4.5 were used for a series of injections of the pre-formed uranium-Arsenazo III complex. The current obtained using the 20mM electrolyte necessitated a reduction in the separation voltage. As a result of this the expected increase in peak efficiency was not experienced. The lower ionic strength of the 5mM electrolyte did not produce any advantage, since the maximum voltage of the instrument (30kV) could be used with the 10mM electrolyte. Consequently, the 5mM electrolyte was rejected due to its lower buffering capacity and stacking ability. A 10mM sodium acetate electrolyte at a pH of 4.5 – 5 was found to produce the best results with respect to resolution, separation current, peak shape, and sensitivity, consequently this was the principal electrolyte used for the analysis of uranium.

3.2.3.4. Quantitative Performance.

Figure 3.7 shows the separation of the uranyl-Arsenazo III complex from the free reagent. This separation was performed using the 98% purity reagent and shows the very flat baseline achieved and the absence of interference peaks.

Good symmetrical peak shapes were obtained for the uranyl-complex and peak efficiencies of in excess of 500,000 plates per meter could be obtained with new capillaries. The peak efficiency of the capillaries was noted to decline during the first week of use but then remained constant for several weeks. Batches of fresh capillaries were frequently made and used as required. Linear calibrations were obtained for the uranyl-Arsenazo III complex from 2 mg l^{-1} down to 0.01 mg l^{-1} with correlation coefficients (r) of 0.999 or higher. Using a detection limit twice the base line noise a concentration of 0.01 mg l^{-1} was obtained with gravity injections of 30 seconds at a height of 100mm.

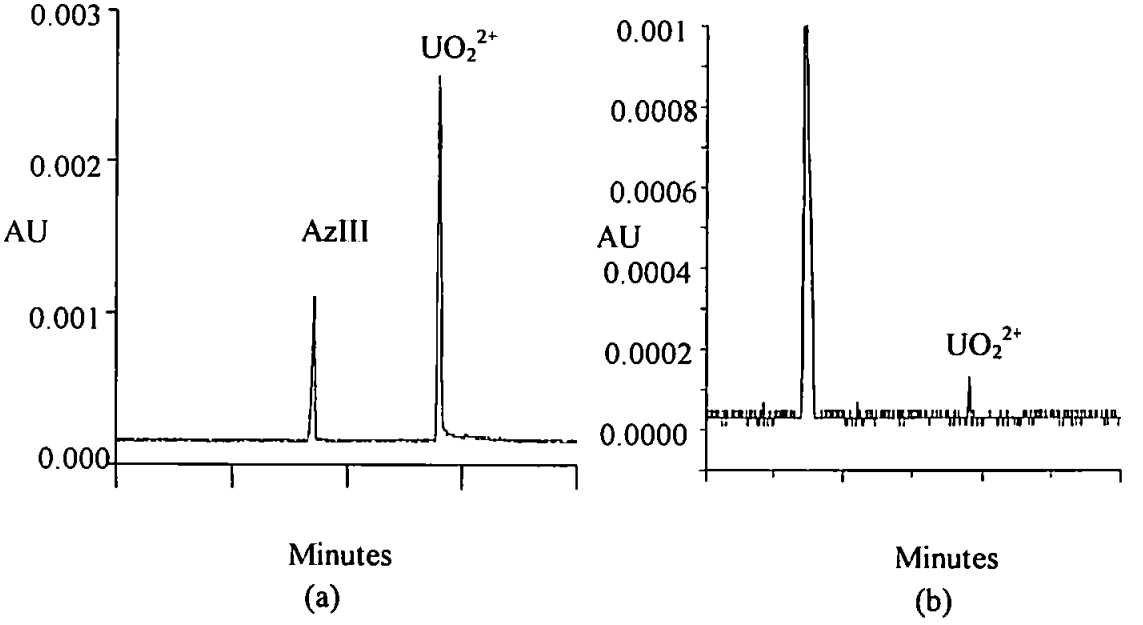

Figure 3.7. Electropherogram of Uranium Separation. Separation conditions Electrolyte, 10mM Sodium acetate pH 5 with 5 mg l^{-1} AZ III; Voltage, –25 kV; Injection Gravity, 100mm, 30 second; Detection 654nm; Capillary 65cm L_t 100mm ID Key (a) 1mg l^{-1} and (b) 0.01 mg l^{-1}

3.2.4. Improvement of the Limit of Detection.

3.2.4.1. Gravity Injection.

In CE an increase in the detection limit can be achieved by the injection of very large sample volumes onto the capillary. The samples can be 'stacked' into narrow bands by injection of the sample in a low ionic strength matrix. The degree of stacking is proportional to the ratio of the resistivities between the sample matrix and the separation electrolyte. Consequently, a sample made up in water and injected into a column filled with high ionic strength buffer should achieve maximum stacking. With these methods, the maximum volume of sample that can be injected into the capillary is principally limited by flow disturbances. These flow disturbances are caused by a local increase in the electroosmotic flow velocity within in the sample zone.

The use of coated capillaries, where electroosmotic flow is absent or at least significantly reduced, can be a significant advantage in sample stacking techniques. This is because the injected water plug remains immobile or at least moves with a much reduced velocity, thus allowing larger volumes of sample to be injected without significantly effecting the efficiency or resolution of the separation. This supposition was tested by performing a series of gravity injections of increasing injection time whilst maintaining a constant height. Figure 3.8 shows the effects of increasing the injection volume by gravity injection. All injections were performed at a fixed height of 100mm and only the time was varied. The Figure shows that the increase in the integrated area under the peak with increasing injection time is linear, but peak height follows a limited growth pattern, increasing in a reasonably linear manner up to 60 seconds but then falling off. Peak efficiency declines rapidly with increasing injection

time but peak resolution is not significantly affected, as even with a 240 second injection the peak width at the base line was only 9 seconds wide.

Some loss of efficiency was considered an acceptable trade off against an increase in detection sensitivity. In terms of sensitivity, peak height was considered the most important parameter. From Figure 3.8 it can be seen that was little gain in sensitivity beyond a 60 second injection. The peak height obtained with an injection of 60 second was found to be three times that of a 15 second injection. Whereas, the height obtained with a 240 second injection was found to be only 1.5 times that obtained for 60 seconds. The integrated area under the peak although significantly increased was of little consequence in the improvement of detection sensitivity, due to the increased broadening of the peaks.

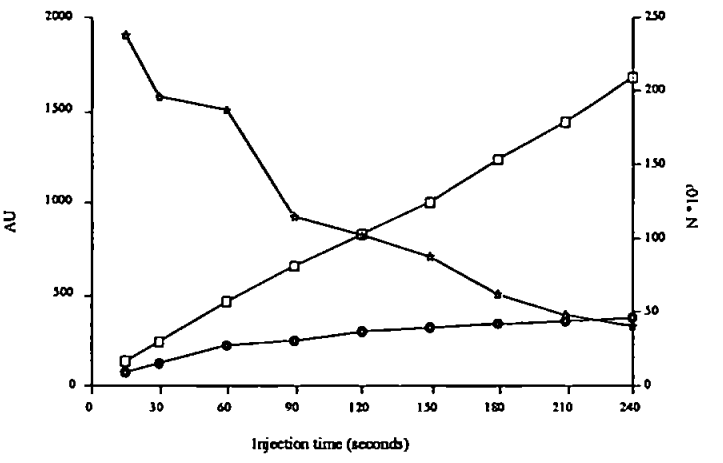

Figure 3.8. The Effect of increasing the injection time on peak response and efficiency using gravity injection. Where O = peak height, □ =integrated area under the peak and ☆ = Plate number per 75μm ID, 50cm L_d capillary. Uranium concentration 0.5mg l^{-1}.

3.2.4.2. Electrokinetic Injection.

The electrokinetic injection of samples has also been used as a means of sample pre-concentration in CE by injecting samples prepared in low ionic strength matrices [76, 228]. Referred to as field amplified injection by Chien and Burgi [76] the method can yield several hundred fold increase in the number of ions injected. The increased field strength encountered in the low ionic strength sample causes an increase in the velocity

of ions. Differences between field strength encountered in the sample and separation electrolyte cause the sample ions to stack into a narrow band once they encounter the higher conductivity of the separation electrolyte inside the capillary.

In the absence of electroosmotic flow, ions migrate into the capillary solely under the influence of their own mobility and therefore only one type of ion can be injected at a time. The quantity of ions migrating into the capillary is primarily a function of the length of the injection time and the field strength they encounter in the sample zone, with the field strength being determined by the ionic strength of the matrix and the applied voltage.

Figures 3.9 (a)-(d) show the results for the electrokinetic injection study. In each study a fixed injection voltage was used and the length of the injection time varied.

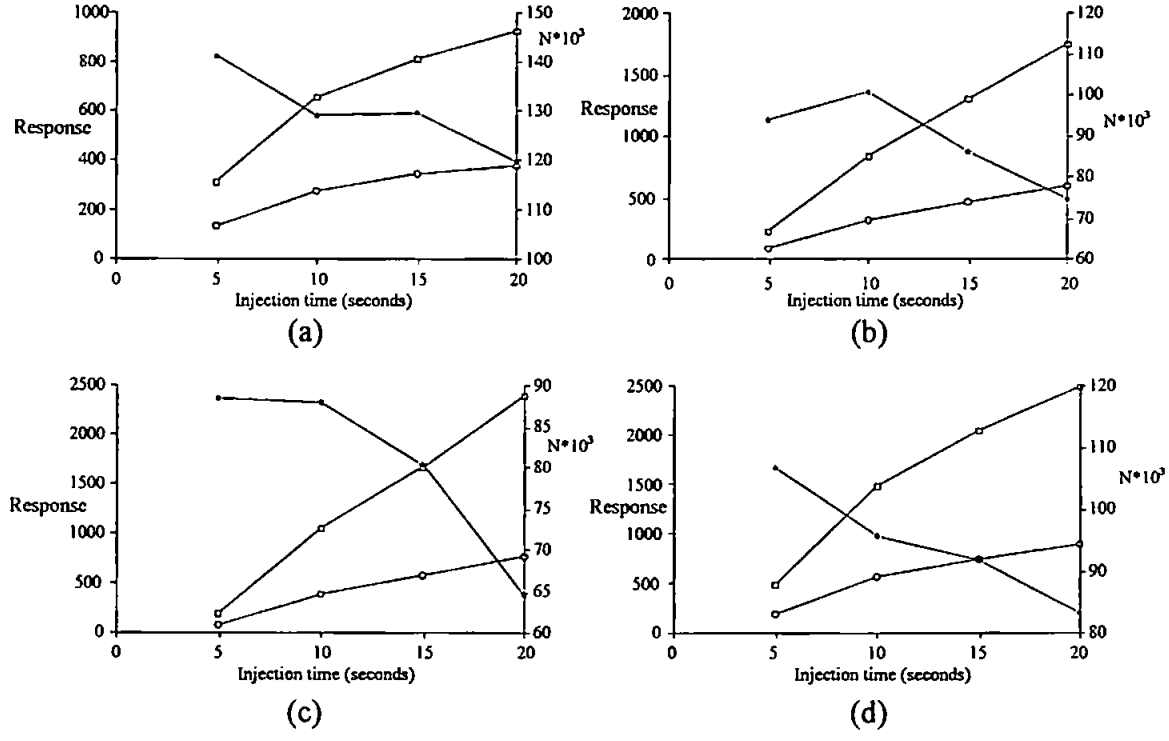

Figure 3.9. Effect of increasing the injection time on peak response and efficiency with electrokinetic injection. Where ○ = peak height (AU x10⁻⁵), □ =integrated area under the peak and ☆ = Plate number per 50μm ID, 50cm L_d capillary. Uranium concentration 0.1mg l⁻¹. Injection Voltages; (a) 5Kv, (b) 10Kv, (c) 15Kv, (d) 20Kv.

It can be seen from each figure that increasing the injection time results in an increase in the detector response. The most significant increase in peak height was obtained using 10 second injections, above this time the increase in response was found to decline. The figures also show that as the injection voltage is increased there is also a gain in response, but to a lesser extent than that due to injection time. The plate number was found to reduce with injection time but not to such an extent as with gravity injection. With respect to injection time, voltage and plate number, 10 second, 10 kV injections were found to be best compromise. Injection times of greater than 20 seconds resulted in a rapid falling off in the increase in peak area and height at all voltages. A detection limit of less than 0.001 mg l^{-1} could be obtained using electrokinetic injection. Figure 3.10 shows a comparison of the peaks obtained by gravity and electrokinetic injection for uranium at a concentration of 0.01 mg l^{-1}.

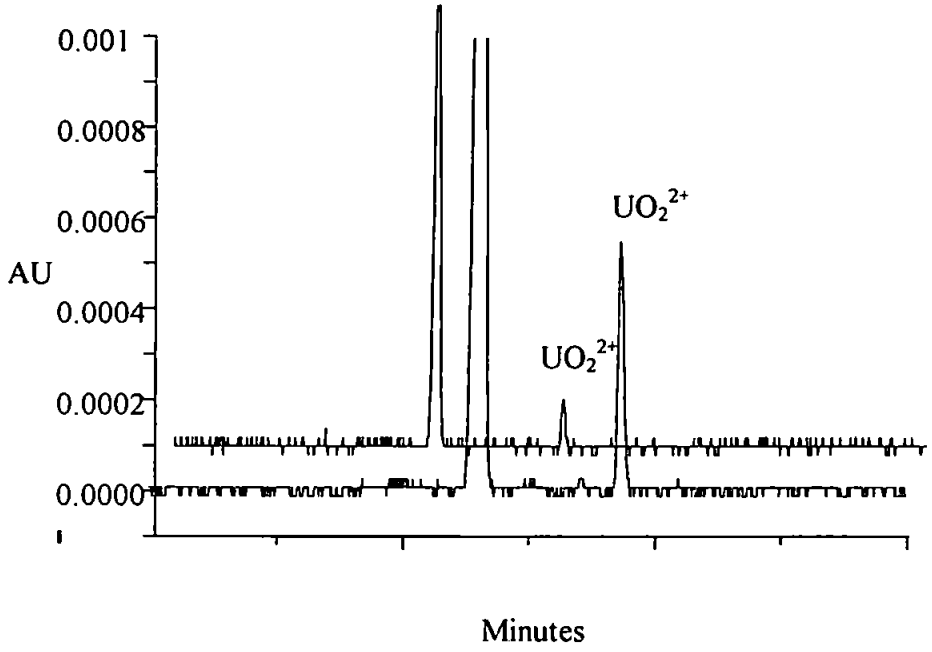

Figure 3.10. Electropherograms showing a Comparison of Gravity and Electrokinetic injection of 0.01mg l^{-1} UO_2^{2+}. Separation conditions: Electrolyte, 10mM Sodium acetate pH 4.5 with 5 mg l^{-1} AZ III; Voltage, –30kV; Detection 654nm; Capillary 60cm L_t 100mm ID Key (a) and Upper Trace, 100mm, 30 second Gravity Injection. Lower Trace, 10kV, 10 second Electrokinetic injection.

3.2.4.3. Peak Splitting During Electrokinetic Injections.

Initially, injections of over 10 seconds, at voltages of 15kV and above were found to produce split peaks for the uranyl-Arsenazo III complex and free reagent peaks. This was a curious phenomenon and not fully understood although it was remedied relatively easily by providing mixing in the sample vial or repositioning the electrode. Mixing in the sample vial was accomplished by running a separate 100 μm ID capillary parallel to the separation capillary and extending this to the bottom of the sample vial. Helium was then bubbled through this capillary during the sample injection.

The position and shape of the electrode with respect to the capillary entrance was also found to be influential in the formation of these split peaks. In general practice the ends of the electrode and capillaries are aligned. However, when the capillary end was raised above the level of the electrode tip, the split peaks were no longer formed. Bending the electrode to form a loop through which the capillary was inserted was also found to eliminate the formation of the split peaks.

The peak splitting appeared to be caused by rapid localised depletion of ions in the high field strength region between the electrode and capillary entrance. If this were the case, mixing of the sample vial would provide replenishment of the zone between the capillary tip and electrode. By placing the capillary higher up the electrode, or creating a loop, the electrode may increase the size of the pool from which ions were drawn. That is from both above and below the capillary tip in the case of the repositioned capillary or all around the capillary tip with the looped electrode. However, with all these methods, peak splitting still occurred intermittently when using 25kV injections of over 10 seconds. The frequency of the peak splitting was noted to be worst when repeat injections were made from the same sample vial with no mixing of the sample between injections.

3.2.5. Interferences.

At the pH values optimal for the determination of uranium several other metals also form complexes with Arsenazo III. Under the conditions used for the determination of uranium, the calcium–Arsenazo III complex was found to be extremely labile and could only be detected by reversal of the power supply, as the migration mode of the calcium complex was cathodal. Although a pre-formed complex was injected, the detection of calcium was essentially due to an on-column complexation reaction. Without the addition of dye to the electrolyte, the calcium and dye, having opposing mobilities, would migrate away from each other and the calcium would not be detected.

Complexes of intermediate stability, such as lead were lost through diffusion and only iron and the lanthanide metals were found to produce a response. The mobility of the lanthanide metal complexes was lower than that of the uranyl complex producing peaks significantly later that did not interfere. This behaviour was predicted, since a 1:1 complex with a 3+ metal would be expected to have a lower anionic charge than the uranyl complex. Although all the lanthanide metals injected produced a response, the peaks were severely broadened and unsuitable for quantification. Under the conditions used for the uranium analysis, the lanthanide chelates were all found to have similar mobilities and were not resolved.

3.2.5.1. Separation of Iron and Uranium

Figure 3.11 shows the separation of the uranyl and iron (III)-Arsenazo III chelates. Like thorium, the iron III complex was found to migrate with a greater velocity than that of the free Arsenazo III. Also, in common with thorium, iron produced a broad response composed of more than one peak. The chemistry of iron is highly

complicated and it is known to form polymeric hydroxide species. It was considered that the broad, highly anionic response for iron was probably due to the inclusion of hydroxide ions in the coordination sphere.

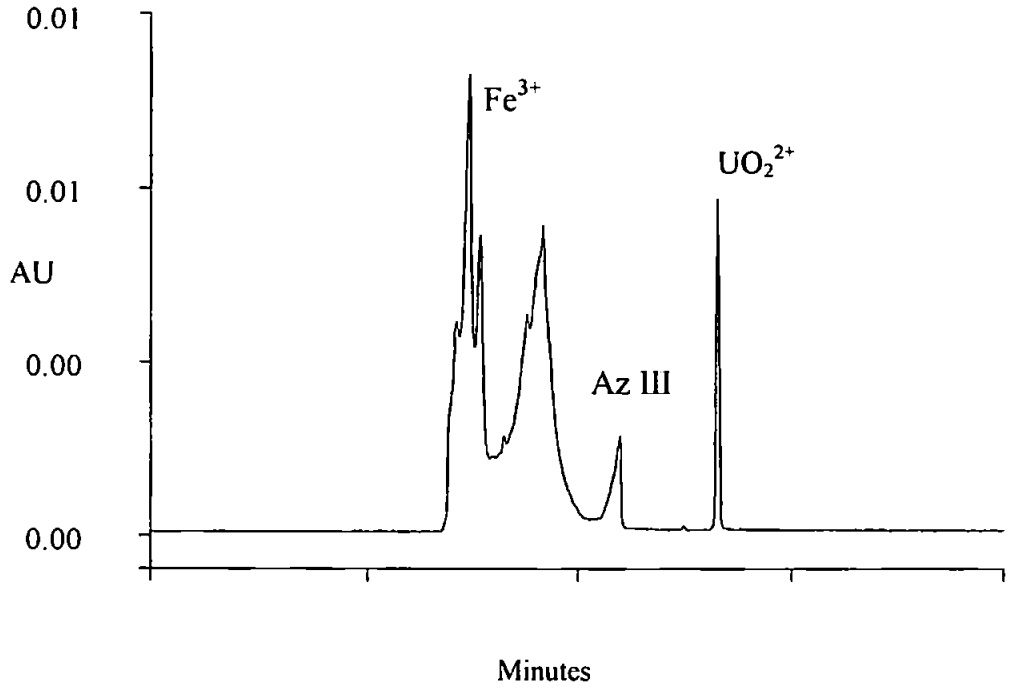

Figure 3.11. Separation of Uranium and Iron III. Separation conditions: Electrolyte, 10mM sodium acetate pH 4.5 and 5 mg l^{-1} arsenazo III; capillary, 100μm ID 65 cm L_t; applied voltage 30kV; Sample Fe^{3+} & UO_2^{2+} 2mg l^{-1}; injection, gravity, 30 seconds @100mm.

The iron response was well separated from the uranium peak and was not found to interfere in the determination of uranium provided that the concentration of the iron did not exceed 2ppm. Unfortunately, real samples containing uranium, particularly those of geological or biological origin, tend to contain iron in vastly greater concentrations, with up to six orders of magnitude difference in concentration not unusual.

Although the iron peaks did not interfere in the determination of uranium, excessive Fe^{3+} in the sample was found to cause the formation a dark blue precipitate. The speed of formation of the precipitate was noted to be a function of the concentration of iron present in the sample and the concentration of the dye added. When concentrations of

2 mg l^{-1} or less Fe^{3+} were present in the sample the complex remained in solution for at least 24 hours and no loss of signal for uranium was detected within eight hours. At concentration of 200 mg l^{-1} Fe^{3+} the precipitation reaction was virtually instantaneous. Significantly, the uranium appeared to have been co-precipitated with the Fe^{3+} arsenazo complex as subsequent analysis of precipitated samples resulted in total loss of the uranium peak. The addition of more Arsenazo III to the sample prior to analysis still failed to produce a response for uranium confirming that the uranyl-arsenazo complex was being co-precipitated and not just starved of reagent.

The injection of uranium and iron (III) in concentrations above 1 mg l^{-1} also caused a reduction in the response of uranium using on-column complexation. This technique was only briefly investigated owing to modification of the capillary surface by the precipitation and subsequent adsorption of the Fe^{3+} complex. This resulted in a significant reduction in the efficiency of the capillary and the capillary had to be discarded.

Many methods for the determination of uranium use a sample pre-treatment step to remove interferences. However, this adds a further time consuming step to the analysis, therefore several attempts were made to eliminate interference from iron without the need for a separate sample clean up step. Unfortunately, these attempts were only met with limited success.

The simplest method that was used to minimise the impact of iron was by the addition of low concentrations of Arsenazo III to the mixed UO_2^{2+} and Fe^{3+} standards. It was hoped the stability of the uranium complex might be sufficiently larger than that of the iron to cause an equilibrium shift allowing the uranium to be complexed in preference to the iron. No reagent was added to the electrolyte to prevent the iron from becoming complexed on-column. Although this method was found to significantly

reduce the iron response, the uranium peak was also reduced, seriously affecting the detection limit.

3.2.5.2. Reduction of Iron with Sulphur Dioxide.

An alternative strategy used in an attempt to improve the iron tolerance of the system was by reduction of the Fe^{3+} to Fe^{2+}. Although Fe^{2+} also forms a complex with Arsenazo III, the complex was found to be more soluble than the Fe^{3+} complex and might solve the problems of precipitation. The choice of reducing agent is important since it needs to be sufficiently powerful to reduce the Fe^{3+} to Fe^{2+} but not UO_2^{2+} to U^{4+}.

Initially, the iron was reduced by the addition of SO_2 solution to the sample vial and a low concentration added to the electrolyte to prevent re-oxidation of the iron. Although the solubility of the iron-Arsenazo III complex appeared to be significantly improved by this, the addition of 1mM SO_2 solution to the electrolyte caused an increase in the conductivity of the electrolyte, necessitating the use of lower separation voltages. The addition of 10mM SO_2 solution to the sample also caused a significant increase in the ionic strength of the sample resulting in serious broadening of the uranium peak and a reduction in sensitivity. Despite these problems, the iron was found to produce a single very sharp peak migrating slightly in front of, but unresolved from, the free Arsenazo III. Although reduction of the iron with SO_2 increased the iron tolerance of the system to 50 mg l^{-1}, unfortunately the detection limit for uranium was raised to 0.1 mg l^{-1}.

3.2.5.3. Reduction of Iron III with Ascorbic acid.

Ascorbic acid has been reported to reduce UO_2^{2+} to U^{4+} [229] but under the conditions used here, this was not found to be the case. Figure 3.12 illustrates an electropherogram of the separation of the reduced iron and uranium at concentrations of 50 mg l^{-1} and 1 mg l^{-1} respectively. As with the SO_2 solution iron II produces a very sharp peak migrating slightly ahead of the free Arsenazo III.

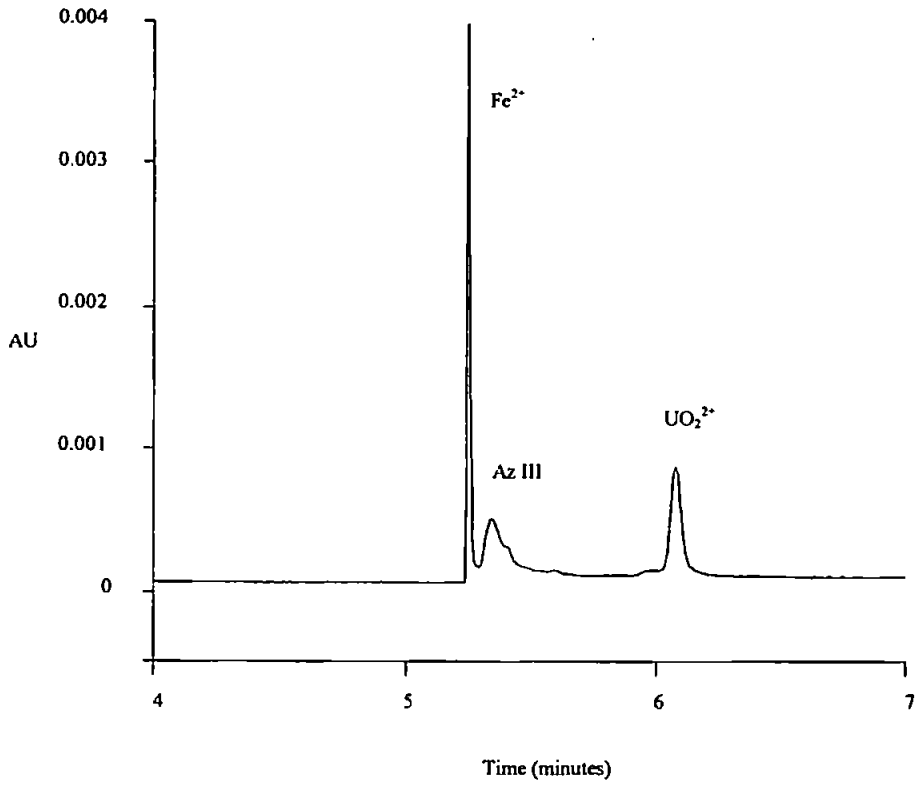

Figure 3.12. Separation of 1 ppm Uranium and 50 ppm Iron III. Separation conditions: Electrolyte, 10mM sodium acetate pH 4.5 + 1mM ascorbic acid and 5 mg l^{-1} arsenazo III; capillary, 100μm ID 65 cm L_t; applied voltage 25kV; sample, 1 mg l^{-1} UO_2^{2+} and 50 mg l^{-1} Fe^{3+} made up in 10 mM ascorbic acid; injection, gravity, 30 seconds @100mm.

Using ascorbic acid the uranium peak was also detected and in terms of peak height the results were in reasonable agreement with those obtained without the addition of ascorbic acid to the sample or electrolyte. However, the uranium peak was broader and plate numbers were approximately one third of those obtained without the reducing agent. The reduction of the iron did not totally solve the problems of precipitation but a concentration of 50 mg l^{-1} of iron was found to be the tolerable.

Even with 10 mM ascorbic acid in the sample, precipitation of the iron complex began to occur at a concentration of 100 mg l^{-1}. Increasing the concentration of ascorbic acid in the sample resulted in a decline in the uranium sensitivity due to broadening of the peak. Although ascorbic acid has a low mobility, an increase in the separation current was noted limiting the concentration in the separation electrolyte to 2mM.

The limit of detection for this system was found to be 0.05 mg l^{-1}. This somewhat unsatisfactory value was the result of the reduced separation efficiency and the inability to resolve a small broad peak migrating with a velocity slightly greater than that of the uranium peak.

3.2.5.4. Masking of Iron with 1, 10 Phenanthroline.

Many spectrophotometric methods utilise masking agents to eliminate interferences and this technique was applied to the CE method. Iron II forms strong complexes with 1, 10 phenanthroline, which may be stable enough to prevent the iron from complexing with the Arsenazo III. A further advantage of 1, 10 phenanthroline was that the iron complexes would also be cationic and therefore would migrate out of the capillary. A series of standards containing 1 mg l^{-1} UO_2^{2+} and Fe^{3+} at concentrations between 0 - 200 mg l^{-1} were made up. The Fe^{3+} was reduced to Fe^{2+} by the addition of ascorbic acid, which is reported to reduce the iron but not the uranium. The reduced iron was then pre-complexed with 1,10 phenanthroline. The iron-1,10 phenanthroline reaction is kinetically much slower than the Arsenazo III reaction therefore the standards were left to stand for 1 hour before the addition of the Arsenazo III. 1mM 1,10 phenanthroline was also added to the electrolyte to help maintain the stability of the iron complex. Although the addition of this reagent was unlikely to have much effect it did not contribute to the ionic strength of the electrolyte and therefore did not

increase the current. The addition of Arsenazo III to the standards caused the colour to change to blue although either the uranium or the iron could have caused this.

The injection of the standards containing the reduced and pre-complexed Fe^{3+} and UO_2^{2+} produced a single very broad hump on the baseline, which started at around 5 minutes and was over 3 minutes in width. No peaks were detected for either the free Arsenazo III or the uranyl-Arsenazo III complex. This broad peak was thought to be due to the formation of a ternary complex, between the iron, Arsenazo III and 1,10 phenanthroline resulting in an anionic complex which appeared to be only moderately stable as indicated by the severe broadening of the peak. Injection of Arsenazo III and the uranyl-Arsenazo III complex, made up in the same way as the iron-uranium standards, produced peaks that appeared to be largely unaffected by the addition of 1,10 phenanthroline. However, these peaks were found to be slightly broader than those obtained without the addition of the 1,10 phenanthroline to the sample and electrolyte.

3.2.6. The Separation of Uranium and Thorium

Figure 3.13 illustrates the separation of uranium, thorium and the free Arsenazo III as the pre-formed complexes. Thorium produces a broad hump with several peaks that were only partially resolved from the free Arsenazo III peak.

The shape of the thorium peak was highly influenced by the concentration of thorium being injected onto the capillary. At a concentration of 1 mg l^{-1} or greater, three small peaks (labelled as 1, 2 and 4 in Figure 3.13) and one main peak (labelled as peak 3) were detectable. Below this concentration, the thorium peak deteriorated extensively and was detectable as little more than a hump on the baseline. Figure 3.14 shows that increasing the thorium concentration above 1 mg l^{-1} caused a significant increase in the

response of peak 3. The smaller peaks labelled 2 and 4, either side of peak 3 were also noted to increase proportionally.

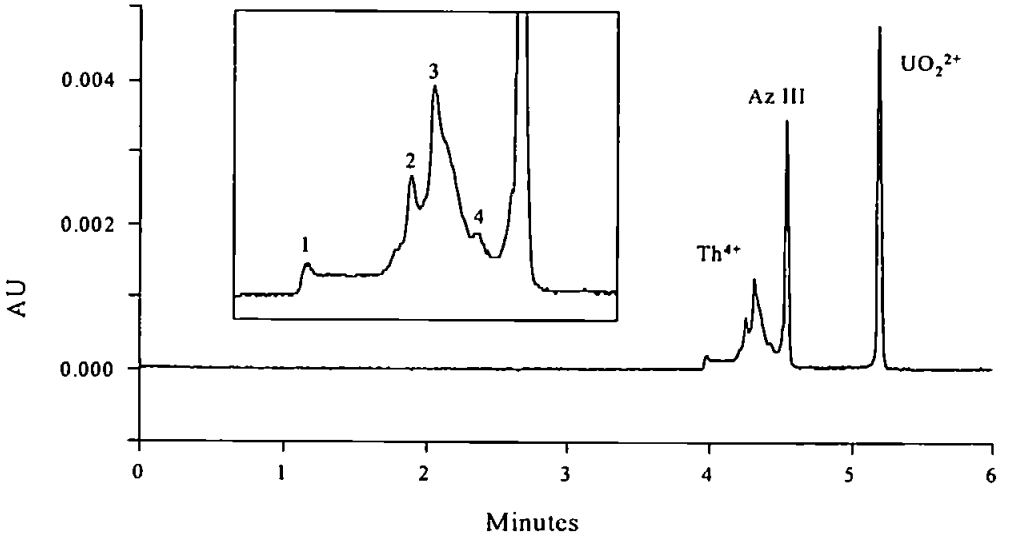

Figure 3.13. Electropherogram of Uranium and Thorium Separation, with inset giving detail of the four thorium peaks. Separation conditions: Electrolyte, 10mM sodium acetate pH 4.5 and 5 mg l^{-1} arsenazo III; capillary, 100μm ID 65 cm L_t; applied voltage -25kV; injection, gravity, 30 seconds @100mm. Detection, 654 nm. Sample, 1 mg l^{-1} UO_2^{2+} and 2 mg l^{-1} Th^{4+}.

Leaving the thorium complex to stand for several hours prior to injection was found to increase the size of peak 1. This may have been an indication that this peak was due to the 1:2 complex and that the formation of the 1:1 complex was fast (a colour reaction was obtained instantly the metal and reagent were mixed) but the formation of the 1:2 complex was relatively slow.

The greater mobility of the thorium over the free Arsenazo III, indicated that the complex carried a very high negative charge. This negative charge could not be attributed solely to the thorium-Arsenazo III complex due to the high positive charge of the thorium. Assuming the Arsenazo III carried a charge of minus four at pH 5, the 1:2 complex with thorium would then have a charge of minus four but with a mass of over twice that of the Arsenazo III. In order for the complex to have a greater

mobility than the free reagent it would need to have a negative charge of greater than 2.25 x that of the free reagent.

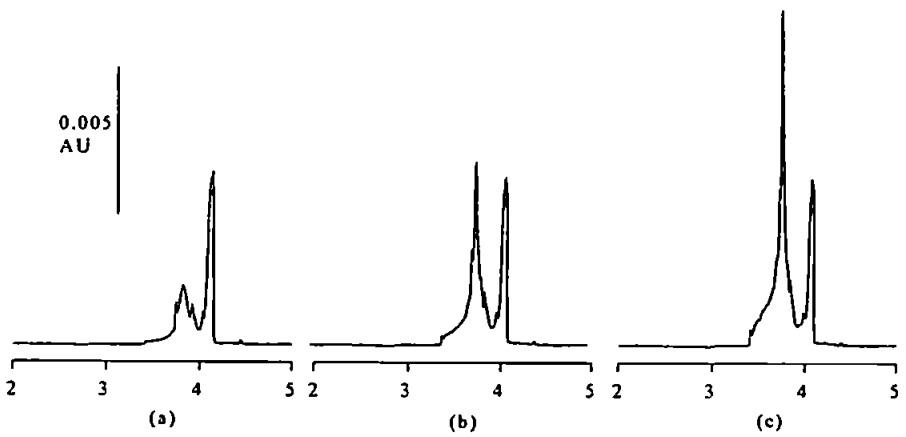

Figure 3.14. The Effect of the Injected Concentration of Thorium on Peak Shape.
Separation conditions: Electrolyte, 10mM sodium acetate pH 4.5 and 5 mg l^{-1} Arsenazo III; capillary, 100μm ID 65 cm L_t; applied voltage 30kV; injection, gravity, 30 seconds @100mm; metal concentrations. (a) 2 mg l^{-1} (b) 4 mg l^{-1}(c) 6 mg l^{-1}.

The high mobility of the thorium complex cannot be explained in terms of complex stoichiometry. The formation of a 1:3 complex was not reported in the literature and seemed unlikely due to steric hindrance. It seemed most likely that electrolyte constituents were involved in the thorium complex, with the smaller side peaks being attributable to the to the formation of mixed ligand complexes containing acetate or hydroxide.

The effect of changing the electrolyte to one containing a competing ligand forming stronger complexes than acetate was investigated to see the effect on these side peaks. Figure 3.15 (a) shows that some improvement in the peak shape was produced using a sodium tartrate electrolyte, with a single tailing peak being detected. The separation between the free reagent and the thorium peak was observed to be greater using this electrolyte, implying that the tartrate was involved in the complex. Figure 3.15 (b) shows an electropherogram of thorium using a sodium citrate electrolyte. As with tartaric acid a single tailing peak was detected although this peak was less well

separated from the free reagent, signifying that the mobility of this peak was lower than that of the thorium - Arsenazo III - tartrate peak.

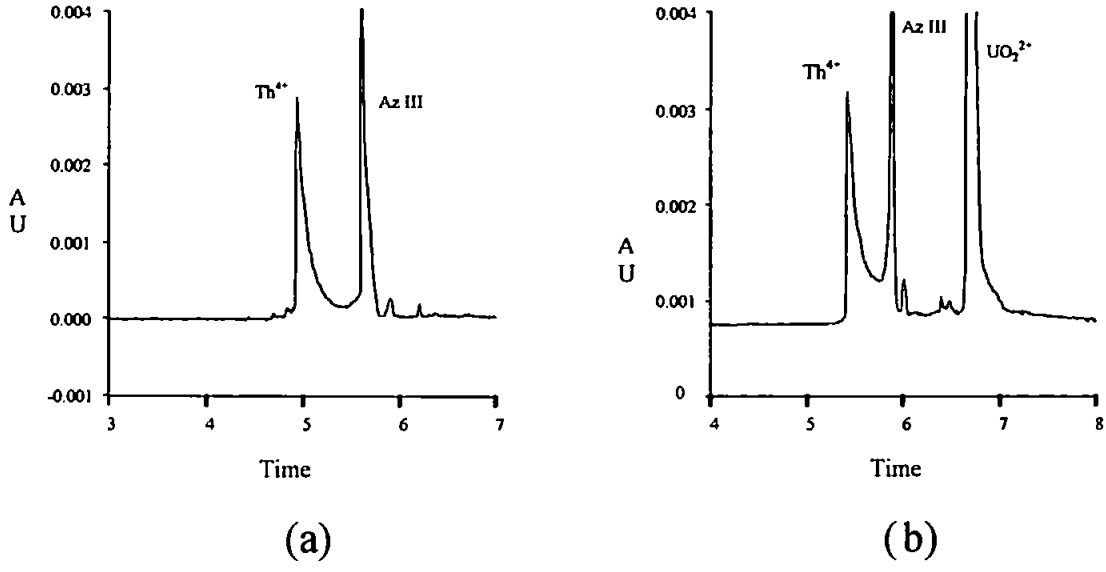

Figure 3.15. Effect of competing ligand on the thorium peak. Separation conditions: capillary, 100μm ID 65 cm L_b; injection, gravity, 30 seconds @100mm; metal concentrations 2 mg l^{-1}. Electrolyte, (a) 5mM sodium tartrate pH 4.5 and 5 mg l^{-1} Arsenazo III; applied voltage 30 kV (b) 5mM sodium citrate pH 4.5 and 5 mg l^{-1} Arsenazo III; applied voltage 25 kV.

Under these conditions both ligands have the same charge. The ternary complex involving the citrate would be expected to have the greater mobility due to its higher stability constant, although this could be offset by the larger size of the citric acid, which may be subject to more steric hindrance. Although a minor improvement of the thorium peak could be gained this experiment points to the involvment of other ligands in addition to the Arsenazo III in the formation of the thorium complex.

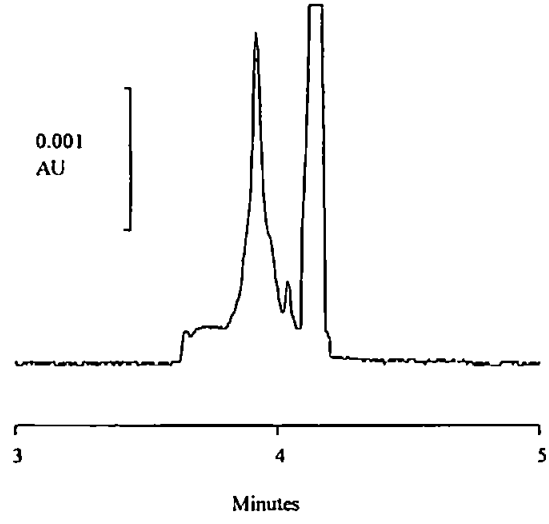

Figure 3.16. Effect of electrolyte pH on the thorium peak. Separation conditions: Electrolyte, 5mM KCl pH 2.2 and 5 mg l^{-1} arsenazo III; capillary, 100μm ID 65 cm L_b; applied voltage 25kV; injection, gravity, 30 seconds @100mm; metal concentration, 2 mg l^{-1}.

The peak shapes also indicated that the stability of the thorium complex was also a problem.

A lower pH electrolyte was tried since the thorium-Arsenazo III complex is reported to be more stable under acidic conditions [230]. Figure 3.16 shows an electropherogram of thorium at pH 2.2. A reduced pH should provide some indication to the extent at which hydroxide is involved in the formation of the complex. Although some improvement in peak shape was obtained, a much lower pH appeared to be needed before any significant improvement could be obtained. However, the use of a lower pH electrolyte was found to be impractical owing to the very high current obtained.

3.2.7. The Analysis of Uranium in Real Samples.

The low tolerance to iron in the CE determination of uranium made it impractical for the analysis of certain types of environmental samples, without some form of sample pre-treatment to isolate the uranium. The detection limits achieved with this method although good by CE standards were too high for the direct analysis of many real samples without some from of pre-concentration. To test the performance of the method in the analysis of real samples, a mineral and a tap water sample were spiked with uranium. Although this was not as good as the analysis of an environmental sample containing uranium, the mineral water was high ionic strength and gave some indication of the robustness of the method.

3.2.7.1. Sample Preparation.

3 x 10ml of tap water and Badoit Mineral water samples were titrated to pH 4 with 0.1M HCl. 100 µL of 1mg l^{-1} uranium standard was added to the samples giving a final concentration of 0.01mg l^{-1}, followed by 100 µL of 500mg l^{-1} Arsenazo III

solution. Tap and mineral water blanks containing only the reagent were also made up. The samples and blanks were injected onto the capillary using 30 second 100mm gravity and 10kV 10 second electrokinetic injections.

3.2.7.2. Spiked Sample Results.

The averaged data for the gravity injections is shown in table 3.5 and the data for the electrokinetic injections is shown in table 3.6. The number of replicates was three in all cases.

Table 3.5. Data for Spiked Water Sample by Gravity Injection.

Sample	RSD	% Recovery
Tap Water	6.98	93.2
Mineral Water	12.72	86.7

Table 3.6. Data for Spiked Water Sample by Electrokinetic Injection.

Sample	RSD	% Recovery
Tap Water	19.80	56.8
Mineral Water	32.75	34.6

From the data in Tables 3.5 and 3.6 it can be seen that gravity injection was the better injection technique being far less susceptible to differences in the ionic strength of the sample and standards. Some peak broadening was observed with the

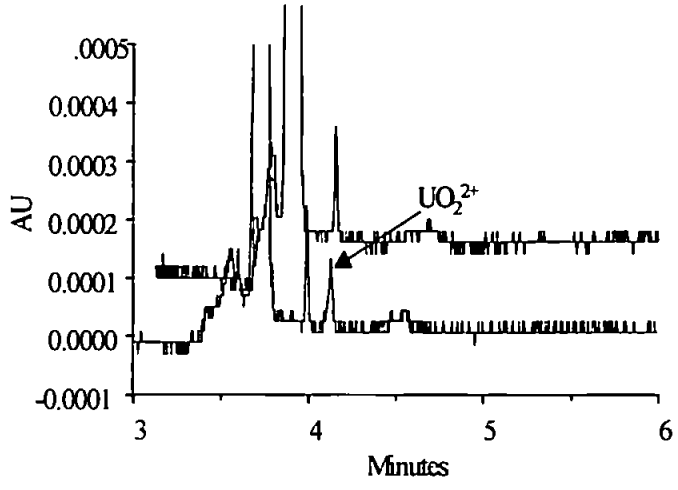

Figure 3.17. Comparison of Tap Water Sample and Tap Water Spiked with 0.01 mg l^{-1} UO_2^{2+}. Separation conditions: Electrolyte, 10mM sodium acetate pH 4.5 and 5 mg l^{-1} arsenazo III; capillary, 100μm ID 50 cm L_t; applied voltage 30kV; injection, gravity, 30 seconds @100mm; Lower trace Spiked tap water. Upper trace, Sample blank.

gravity injections, particularly the mineral water which was higher in ionic strength than the tap water sample and this is reflected by the lower recovery and greater RSD obtained with this sample. Figure 3.17 shows an electropherogram of the spiked tap water and tap water injected by gravity injection.

The recoveries and reproducibility of the electrokinetic injections was poor despite the potentially lower limits of detection that can be obtained from this method under ideal circumstances. Consequently, this method of injection would not be quantitative when applied to the analysis of environmental samples. Making up the samples and standards in a buffer was found to reduce this bias but increased the detection limit to almost 100 $\mu g\ l^{-1}$.

3.3. Capillary Study.

The high stability of the uranyl – Arsenazo III complex during electrophoresis made it ideal to assess the suitability of a variety of capillaries with differing internal chemistries for the separation of metal chelates.

Two internally coated fused silica capillaries and three polymeric capillaries were assessed for the determination of the uranium-Arsenazo III complex. In so far as possible all the conditions used to assess the different capillaries were kept constant, the only exception being the internal diameter of the capillaries. The electrolyte was 10mM sodium acetate at pH 4.5 containing 5 mg l^{-1} Arsenazo III. A constant voltage of - 30kV was used throughout. Gravity injections of a pre-formed 1.0 mg l^{-1} uranyl-Arsenazo III complex were performed at a height of 100mm for 30 seconds. The data presented in Tables 3.7 – 3.10 was obtained from three runs and the efficiency is given as plates per 60 cm L_d (65cm L_t) column. Peak heights are given in absorbance units (AU). Area under the peak is given in arbitrary units and corrected areas under the

peak are peak areas divided by the migration time to give data that is independent of mobility. Comparison of the plate numbers obtained from fused silica and polymeric capillaries should only be taken as a guide. This is because the precision of the internal diameter of fused silica capillaries is reported to be far more accurate than that of polymeric capillaries, in which case there may be considerable variation from one polymeric capillary to the next. The source of this imprecision is in part due to the manufacturing processes and also the ductile nature of the capillaries.

3.3.1. Polyacrylamide Coated Fused silica Capillaries.

Polyacrylamide coated fused silica capillaries had been used for the bulk of the uranium study prior to the acquisition of the polymeric and hydrophilic coated capillaries. The coating is moderately hydrophilic and provided the best results of all the capillaries tested. The internally coated polyacrylamide capillaries used for this study were 65cm L_t and 100 μm internal diameter. Although good results were obtained using these capillaries, a reduction in efficiency became evident with long term use, indicating that the coating was either being degraded or subject to solute adsorption. The coating was known to have limited durability, but in this situation solute adsorption was suspected since the reduction in efficiency was accelerated when using high concentrations of dye in the electrolyte during an on-column complexation study or when injecting high concentrations of dye during the iron (III) study. Typically, new capillaries produced plate numbers in the region of 450,000 plates per 60 cm (L_d) capillary and a detection limit of 5μg l^{-1} using 30 second gravity injection at a height of 100mm for the uranyl-chelate. Some variation in the efficiency of the new capillaries was found, with 'good' capillaries giving peak efficiencies of greater than 600,000 plates per 60 cm (L_d). The capillary used in this study had been previously used for

nearly one month and the separation efficiency was lower than that obtained when new. However, the capillary was still functioning well and a 10μg l^{-1} uranium peak was easily detected. The data obtained using this capillary is presented in Table 3.7. The capillary gave good precision in terms of migration time and peak height.

Table 3.7. Polyacrylamide Coated Fused Silica Capillary Data.

Polyacryamide	t_m	Peak Area	Corrected Peak Area	Peak Height	Efficiency (N)
Mean	4.79	1071.0	223.3	905.8	349542.0
St Dev	0.03	81.8	18.6	33.8	38069.4
RSD	0.66	7.6	8.35	3.7	10.9

3.3.2. Neutral hydrophilic coated fused silica capillaries.

The exact polymer coating used in this capillary was unknown, but was stated by the donor to be considerably more hydrophilic than polyacrylamide. A hydrophilic coating was chosen to try to assess the degree of hydrophobic adsorption of the Arsenazo III onto the capillary wall. The data obtained from this capillary is shown in Table 3.8. These capillaries produced poor results in terms of sensitivity and efficiency. The peaks were found to be symmetrical but broader, with peak areas similar to those obtained using acrylamide capillaries but much lower peak heights. The precision of migration times and peak heights were also found to be similar to those obtained using the acrylamide coated capillaries.

Table 3.8. Neutral Hydrophilic Coated Fused Silica Capillary Data.

NHP	t_m	Peak Area	Corrected Peak Area	Peak Height	Efficiency (N)
Mean	4.63	1237	266.2	223.3	14423
St Dev.	0.07	117	21.62	5.8	1604
RSD	1.5	9.5	8.1	2.6	11.1

3.3.3. Polystyrene Capillaries.

These capillaries were supplied with an internal diameter of 0.003" (76μm). The capillaries were highly ductile and difficult to install in the instrument, particularly with

regard to threading the capillary through the injection head. The capillaries were reasonably transparent to visible light and there was no need to create a window. A major problem with these capillaries became apparent when a voltage was applied across the capillary. The voltage created a strong electrostatic field around the capillaries causing them to be strongly attracted to the metal injection arm of the instrument. Contact with the arm eventually resulted in a short circuit, which blew a hole in the capillary wall with a loud report. High detector noise in the early stages of a run seemed to indicate that the capillaries were earthing through the detector. A reduction in this noise was found to correlate reasonably well with the capillary coming into contact with the injector arm, which may have provided better earthing. A shield was placed around the injection arm to prevent the capillary coming into contact with it. However, the shield did not always remain in place due to the movement of the arm during an injection. The flexible nature of the capillary made it difficult to prevent it from coming into contact with some part of the instrument and invariable the capillaries blew within a few runs. For this reason long term studies could not carried out on these capillaries.

From the data in Table 3.9 it can be seen that the polystyrene capillaries produced poor results, with migration times far greater than expected and sensitivity of approximately one order of magnitude lower than that obtained using the polyacrylamide coated capillaries. The decreased sensitivity is most likely due to a high level of capillary surface interaction that would also account for the increased migration times due to the generation of electroosmotic flow.

Table 3.9. Polystyrene Capillary Data.

Polystyrene	t_m	Peak Area	Corrected Peak Area	Peak Height	Efficiency (N)
Mean	10.2	306	29.95	68.67	143891
St Dev	0.275	35.8	2.795	2.887	7816.2
RSD%	2.69	11.7	9.33	4.20	5.43

3.3.4. Poly(vinylidene fluoride) (PVDF).

These capillaries were supplied with an internal diameter of 0.003" (76μm). As with the polystyrene capillaries, PVDF is transparent and the creation of a window was unnecessary. These capillaries were somewhat more rigid than the polystyrene and as a result were easier to install. The insulation capacity of PVDF was found to be greater than polystyrene under the influence of high voltages and no earthing problems were encountered with these capillaries. Fluorinated polymers tend to be very hydrophobic and hydrophobic interactions between the capillary surface and Arsenazo III would be expected to be greatest in these capillaries. The increased migration times may be an indication of hydrophobic adsorption but the corrected peak areas were larger than those obtained with the acrylamide capillary. The precision of the migration time and peak height was relatively poor and the plate numbers obtained were only about one third of those using the acrylamide capillary. The data obtained from the PVDF capillaries is shown in Table 3.10.

Table 3.10. Poly(vinylidene fluoride) Capillary Data.

PVDF	t_m	Peak Area	Corrected Peak Area	Peak Height	Efficiency (N)
Mean	6.23	1832	294.1	560.7	110197
St Dev	0.132	66.2	11.4	63.04	28929
RSD%	2.12	3.61	3.87	11.24	26.25

3.3.5. Polyacrylimide Capillaries.

The polyactilimide capillaries were supplied with an internal diameter of 0.004" (102 μm). Unlike the other polymeric capillaries, these capillaries were not transparent and a window was created by attaching a section of 100 μm acrylamide coated fused silica capillary to the end. The junction was made by insertion of the two capillary ends into a short section of PVC tubing. However, no peaks were obtained using this type of capillary. This was thought to be due to the formation of a positive charge on the

surface. A positively charged surface should result in the generation of an anodal electroosmotic flow thus sweeping the anionic reagent and complex past the detector window with accelerated velocities. Since no peaks were detected it was suspected that the reagent was adsorbing on to the capillary wall creating a negatively charged chelating surface. In which case any flow generated would be cathodal preventing both reagent and the uranyl-chelate from migrating past the detector window.

3.4. Summary.

The high stability of the uranium-Arsenazo III complex during electrophoresis produced very sharp peaks in new polyacrylamide-coated fused silica capillaries. The long-term use of these capillaries was found to causes a reduction in sensitivity and peak efficiency. This reduction in peak efficiency was noted to be more rapid during the on-column complexation study indicating that the reduction in sensitivity and peak efficiency was due to the adsorption of Arsenazo III onto the capillary walls. The stability of the complex also appears to minimise zone broadening due to wall interactions allowing sensitive determinations to be made with the same capillary for at least one month.

Highly sensitive determinations of uranium can be achieved especially when using electrokinetic injection. Although in terms of the analysis of environmental samples, electrokinetic injection was found to be less quantitative, being highly dependent on the ionic strength of the sample being injected. The precision of the electrokinetic injections was also found to be poor when high ionic strength samples were used. Gravity injection provided a less sensitive means of sample loading but the technique was found to be more reproducible and resilient to high ionic strength samples than electrokinetic injection. In the analysis of the tap water and mineral water samples

gravity injection proved to the more reproducible than electrokinetic injection. Although even with gravity injection the higher ionic strength of the mineral water was noted to reduce the precision and recovery of uranium spike. The high calcium concentration of the water samples was not found to be a problem, as the calcium Arsenazo III complex was found to be highly labile and migrated with a cathodal mobility

The problems of iron interference could not be overcome to such an extent that geological samples could be directly analysed without some form of sample pre-treatment. However, many sample pre-treatments such as pre-concentration on an ion-exchange column may not be ideal for analysis by capillary electrophoresis due to the resultant low pH or high ionic strength of the sample.

Concerning the reducing agents used to decrease the interference from iron (III), ascorbic acid was found to produce the best results, in terms of electrolyte conductivity and interference with the uranium peak. Although the problems of co-precipitation of the iron and uranium Arsenazo III chelates could not be entirely eliminated by reduction of the iron (III) to Iron (II).

The shape of the thorium Arsenazo III chelate peak was found to be too poor for quantitative analysis although the thorium (IV) peak was well separated from uranyl chelate and was not found to interfere.

In the capillary study the polyacrylamide coated fused silica capillaries were found to give the best results with respect to peak efficiency. The more hydrophilic capillary supplied by Dionex was found to produce peaks with migration times similar to those obtained from the polyacrylamide capillaries but these peaks were significantly broader.

The extended migration times and the low corrected area under the peak obtained from the polystyrene capillaries indicate that a high degree of adsorption is taking place in these capillaries. Due to this adsorption, the polystyrene capillaries were found to be unsuitable for the analysis of metal ions complexed with large organic molecules such as Arsenazo III.

The PVDF capillaries were the most hydrophobic of those assessed. The corrected area under the peak obtained from these capillaries was the highest of all the capillaries indicating a lower degree of wall interaction. However, the peaks obtained were significantly broadened.

The polyacrylimide capillaries were not transparent and required the insertion of a section of polyacrylamide coated fused silica capillary for detection. Even with this these capillaries were found to produce no peaks.

CHAPTER 4. THE DEVELOPMENT OF A POST-CAPILLARY REACTION DETECTION SYSTEM FOR CAPILLARY ELECTROPHORESIS.

4.0 Introduction.

Post-capillary reaction systems have been routinely used as a means of detecting metal ions separated by liquid chromatography (LC) for many years now [231]. Those based on 4-(2-pyridylazo) resorcinol (PAR) have been the most popular combined with high efficiency ion chromatography columns. When capillary electrophoresis was first investigated for trace metal determinations, post-capillary reaction (PCR) systems were little studied presumably because of the more difficult technical problems involved in their construction. Therefore, most of the work focused on the separation and detection of metal complexes formed either pre-capillary [15, 123, 232] or on-capillary [24, 79, 233]. Indirect detection techniques usually involving a UV-Vis absorbing buffer containing weak complexing acids gave good separations, but sensitivity can be limited by the relatively low molar absorptivities of visualising agents such as imidazole and creatinine. More importantly perhaps, the unselective nature of indirect methods could be a serious disadvantage when looking for traces of transition metals in the presence of large amounts of alkali and alkaline earth metals. The direct detection of highly absorbing metal complexes seemed a better way of obtaining better selectivity and sensitivity and a number of studies have been published mainly involving highly coloured organic chelating agents [24, 79, 82, 233]. Although several of these produced good separation and detection characteristics using pre-capillary or on-capillary chelation, there are several problems limiting this approach. Unless the complexes are kinetically or thermodynamically very stable, dissociation could occur, producing

broad peaks or no peaks at all. Interaction with the capillary wall was also possible, again broadening peaks.

In an attempt to overcome the problems of complex dissociation, a PCR system for the detection of metal ions separated by CE was investigated. The transfer of post-column technology from HPLC to CE is not straightforward. The smaller scale of CE makes the construction of a post-capillary reactor technically much more difficult and since one of the major attractions of CE is the high efficiency of the separations, the requirements in terms of preventing peak broadening are far more critical than in LC. Several designs for post-capillary reactor systems developed for CE have been published in the literature [234 - 241]. The merits and drawbacks of each of these systems were examined prior to the construction of a post-capillary reaction system for the determination of metal ions. Several physical constraints were placed on the design of the post-capillary reactor system. These include the availability of materials and technology for the construction of the post-capillary reactor system and the adaptation of the system to operate on the Dionex CES 1 without permanently altering the instrument.

All but one of the post-capillary systems described in the literature have been designed for use with fluorescence detectors, with the majority of these being applied to the detection of *ortho*-phthaldialdehyde (OPA) derivatised amino acids. Fluorescence detection has the obvious advantage of a very low background, which potentially leads to superior sensitivity. However, for the determination of metal ions, absorbance detection has a number of attributes that make it the preferable method. The most widely used approach for the PCR detection of metal ions separated by liquid chromatography is based on the formation and detection of metal chelates. There are several compelling advantages in using this method of detection for the

post-capillary detection of metals in CE. The chemistry of metal chelate formation has been extensively studied and has been well documented in the literature. Many metal chelates have intense absorbance in the visible range, which minimises the background contribution from other electrolyte components. This allows the use of the existing absorbance detectors, which are fitted as standard to many commercial CE instruments. Many metal chelate reactions are very fast, essentially forming on mixing, allowing the use of relatively short reaction capillaries. There is also the potential to alter selectivity by the use of different post-capillary reagents.

Reagents forming fluorescent chelates with some metals are available but these tend to be highly selective making them less attractive as post-capillary reagents.

4.1 Capillary Electrophoresis Post-Capillary Reaction Systems.

Most approaches to the design of PCR systems for CE, have used a capillary as both reactor and detection cell. In these systems, the separation capillary is coupled to a reaction capillary and the post-capillary reagent is introduced into the reaction capillary usually via a junction between the two capillaries. The derivatised solutes are then detected using an on-capillary window. These systems can be sub-divided into two categories, being termed according to the mode of fluid transport in the reaction capillary as either voltage or pressure driven systems.

Voltage driven systems are distinguished by the presence of an electric field in the reaction capillary. In this type of system, the transport of solutes in the reaction capillary is due to a combination of the electroosmotic flow generated by the capillary wall and the individual electrophoretic velocities of the solutes. In a pressure driven system the electric field is de-coupled at the junction between the capillaries and the transport of the solutes in the reaction capillary is achieved entirely by laminar flow.

The alignment of the reaction and separation capillaries in either PCR system is critical in order to minimise disturbance of the flow across the junction. Kuhr *et al.* [242] demonstrated the importance of capillary alignment, reporting significant diffusion away from the gap when two 75μm ID capillaries with a 10μm gap between them were misaligned by as little as 1-2μm.

The length of the gap between the capillaries can also influence the efficiency of transfer across the junction. Under normal conditions, radial diffusion is insignificant in CE as the solute is constrained by the capillary walls. However, when a gap is introduced between two capillaries, this boundary is removed and the solute is free to diffuse away from its normal path. The major factor affecting radial diffusion is the residence time of the solute in the gap; consequently, radial diffusion can be reduced by increasing the flow rate across the gap or by reducing the distance between the capillaries. In a voltage driven system, radial diffusion may be countered to some extent by the focusing effect of the electric field experienced in the gap.

4.1.1. Voltage Driven Systems.

In a voltage driven system, the grounding electrode is located in the destination vial at the exit of the reaction capillary. The reagent is introduced into the capillary by the application of pressure or siphoning. The pressure can be created by either elevating the reagent reservoir above the level of the capillary junction (height difference) or the application of gas pressure to the reagent. With either method of reagent addition, there is an increase in the volume of fluid entering the reaction capillary. It is important that this increased flow is directed into the reaction capillary, as any back pressure exerted on the separation capillary would be detrimental to the separation. Excessive pressure would cause laminar flow in the separation capillary and in serious case could result in complexation of the metal ions in the separation capillary. To

accommodate this increased volume, either the velocity of the flow in the reaction capillary must be increased or the internal diameter of the capillary must be greater than that of the separation capillary. The increased flow rate in the reaction capillary can be created by increasing the electroosmotic flow in this region or by the pressure used to introduce the reagent. Siphoning of the reagent into the reaction capillary can also be achieved by increasing the rate of the electroosmotic flow in the reaction capillary.

Technically, the least complicated PCR system for CE described in the literature is the free solution approach adopted by Rose [234], in which a single separation capillary is terminated in a reservoir of *ortho*-phthaldialdehyde, shown in figure 4.0. The sample zones migrating out of the capillary, mixed and reacted with the reagent to produce fluorophores, which were detected just beyond the capillary outlet. Although simple in design, the system is restricted to very fast derivatisation reactions, since the zones become rapidly diluted on exiting the capillary. The system also requires a reaction cell capable of holding sufficient volume of reagent to prevent depletion during a run. Replenishment of the reagent at the capillary exit is due solely to turbulence caused by the flow exiting the capillary. Since this is the only source of mixing in the reaction cell, several closely migrating zones may lead to localised depletion of the reagent at the capillary exit, resulting in a decline in response over

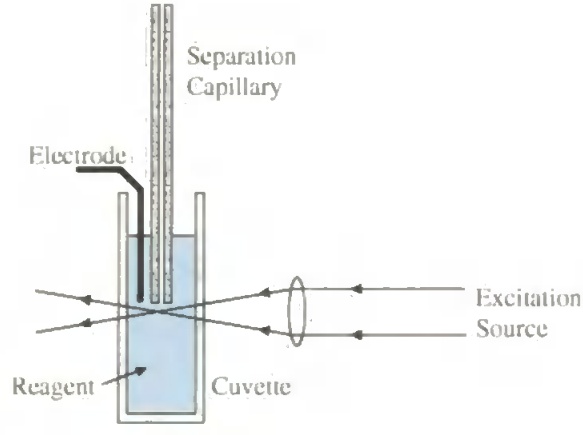

Figure 4.0. Free Solution Post Column Reactor Detector [234]

time. This system also requires accurate focusing of the excitation source close to the capillary exit, which is difficult to achieve using standard fluorescence detectors. Although suitable for use with in-house manufactured CE systems, the requirements of the reaction cell make this system difficult to apply to most commercial instruments. This is due to the focusing requirements of the excitation source and the need for both the inlet and outlet of the capillary to be at the same height if siphoning is to be avoided.

Jorgensen and co-workers [235, 236] applied a coaxial arrangement in which a smaller outside diameter (OD) capillary was inserted into a larger ID capillary, with a sheath flow of reagent driven by pressure running through the outer capillary. This arrangement, shown in Figure 4.1 is essentially an improvement of the free solution approach described previously, in which the reactor and detector cells are created from a section of capillary.

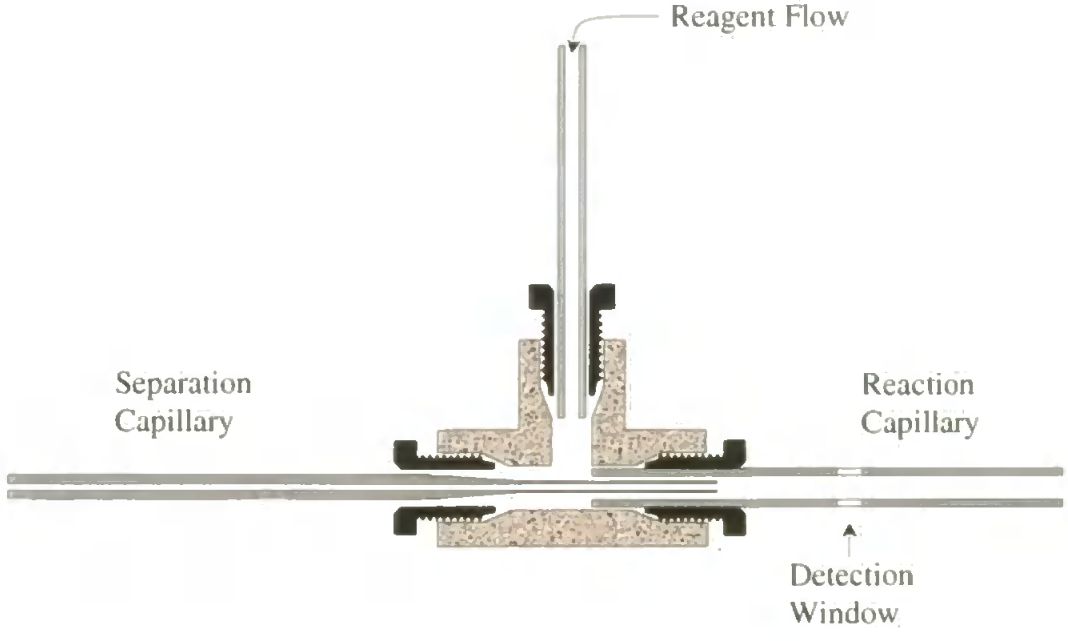

Figure 4.1. Coaxial Post Column Reactor System Designed by Jorgensen et al. [235].

This arrangement provides a continually replenished supply of reagent and allows the use of on-capillary detection using standard CE detectors. Zone broadening was minimised by closely matching the internal diameters of the separation and reaction capillaries. Matching of the inner dimensions of the capillaries was achieved by etching the outside of the separation capillary with hydrofluoric acid to reduce the wall thickness. The end of this capillary was also tapered to reduce turbulence cause by the blunt end. With this system, the grounding electrode is situated at the outlet of the reaction capillary and the transport of solutes and electrolyte in reaction capillary is a combination of electrophoretic processes and laminar flow.

Provided the reaction capillary is kept reasonably short and comparatively low flow rates are used to deliver the post-column reagent, the application of a compensating pressure to the inlet of the separation capillary can be avoided. This is due to the minimal back pressure exerted on the separation capillary because of the shorter length and greater flow rate of the wider bore reaction capillary. The main problems associated with a co-axial system are difficulties in centring the end of the separation capillary inside the reaction capillary and the extreme fragility of the etched capillaries, which makes assembly of the components very intricate.

Electroosmosis was used to introduce the reagent in to the reaction capillary in the design of Albin *et al.* [239], which is shown in Figure 4.2. A 50μm ID separation capillary and 75μm ID reaction capillary were in inserted into PTFE tubing sleeves to allow the use of a standard LC four-way connector to be used as the reactor. A small gap of between 10 and 50 μm was left between the capillaries. The cross channel of the reactor was connected to PTFE tubes allowing the reactor to be flushed with reagent and electrolyte. The reagent was reported to enter the capillary by virtue of the greater volumetric flow rate of the electroosmotic flow in the reaction capillary.

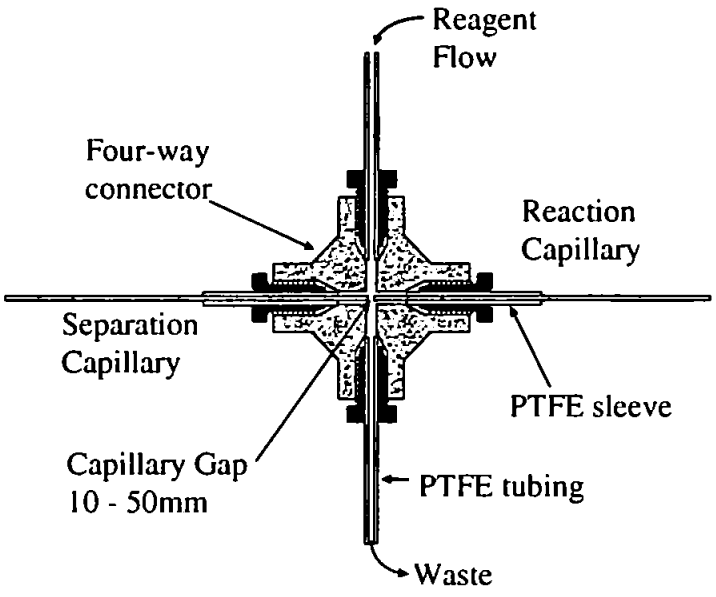

Figure 4.2. Cross Flow Post Column Reactor designed by Albin et al. [239]

Although the reagent was drawn into the reaction capillary in this system, the mechanism used to describe the introduction of the reagent is, in the authors opinion, incorrect, since the electroosmotic flow in the reaction capillary would be proportionally lower than that encountered in the separation capillary. Derived from Ohms Law, Equation 4.0 describes the relationship between field strength (E) and cross sectional area of the capillary.

$$E = \frac{i}{\kappa \pi r^2} \qquad \textit{Equation 4.0}$$

Since the current (i) and the specific conductivity (κ) of the electrolyte should be the same in either capillary, it can be seen that an increase in the cross sectional area of the capillary results in an inversely proportional decrease in field strength. The lower field strength in the larger internal diameter capillary produces in proportional decrease in the electroosmotic flow and corresponding reduction in the volumetric flow rate through the reaction capillary. A probable cause of the introduction of

reagent is due to dilution of the electrolyte by the reagent. This results in a reduction of the ionic strength of the electrolyte and corresponding increase in field strength.

Pentoney *et al.* [238] designed a simple method for introducing the reagent into the capillary via a cross or tee junction. The junction was made by boring a hole through the capillary wall with a laser and bonding the reagent delivery capillary or capillaries at right angles to the separation capillary. The reagent flow was driven by pressure created by height difference in this system. This system is essentially an electroosmotic system with the transport of solutes in the reaction capillary due to the electrophoretic velocity of the derivatised solutes and electroosmotic flow, with a hydrodynamic element superimposed over these. The major advantage of this system is the minimal loss of efficiency achieved, which can be attributed to the low dead volume of the capillary junction and the perfect alignment of the separation and reaction capillaries. However, lasers capable of boring holes with this precision are highly specialist and not readily available.

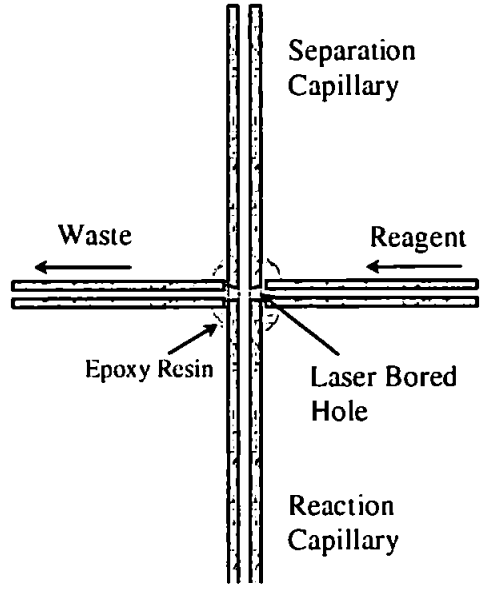

Figure 4.3. Laser Bored Cross Flow Post Column Reactor System developed by Pentoney et al. [238]

An alternatively approach, providing a controllable means of reagent introduction was developed by Cassidy *et al.* [240] in which a second independent voltage source is employed to create an ancillary potential across the reaction capillary. In this system, shown in Figure 4.4 the electroosmotic flow and hence the volume of reagent drawn

into the reaction capillary could then be controlled by variation of the field strength in the reaction capillary.

The system was used to separate carbohydrates, which were detected by electrochemical detection. The major drawback of this system is that in order to allow the use of an increased field strength in the reaction capillary, the field strength employed for the separation has to be less than optimal if joule heating is to be avoided in the reaction capillary.

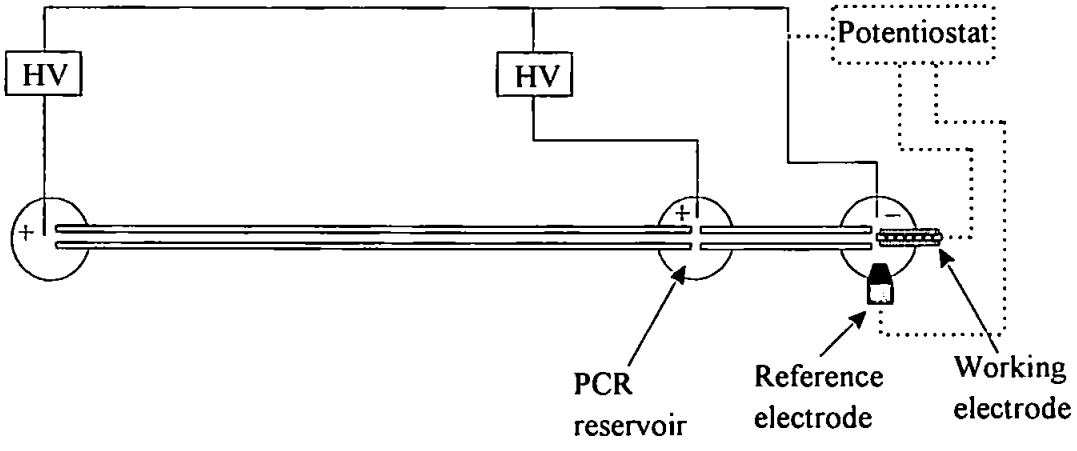

Figure 4.4. Post Column Reactor System Employing a Second HV Power Supply for the Introduction of the Reagent. [240]

4.1.2 Pressure Driven Systems

With a pressure driven system, the grounding electrode is placed at the junction between the separation and reaction capillaries. Since there is no electric field in the reaction capillary the transport of solutes in this zone is achieved entirely by laminar flow. The reagent is introduced into the reaction by the application of pressure to the reaction cell. As a result, the total flow in the reaction capillary is made up of electroosmotic flow exiting the separation capillary and the inflow flow reagent.

Since the electrode situated is outside the capillary junction, the bulk flow of electrolyte due to electroosmotic flow, and the migration of cations due to their electrophoretic velocities, will be towards the grounding electrode. Therefore, the electroosmotic flow and migrating cations need to be redirected towards the reaction capillary. This requires a minimum pressure to be applied to the reaction cell. The minimum pressure (P_{min}) needed to prevent electroosmotic flow dispersing into the reaction cell can be calculated from the Equation 4.1.

$$P_{min} = 32\eta\mu_{eo} V \frac{L_2 d_1^2}{L_1 d_2^4} \qquad \textit{Equation 4.1}$$

Where η is the electrolyte viscosity, μ_{eo} is the electroosmotic flow, V is the applied voltage and L_1 L_2 d_1 and d_2 are the lengths and internal diameters of the separation and reaction capillaries, respectively.

The pressure applied to introduce the reagent across the junction will be transmitted to both the separation and reaction capillaries, which may result in a laminar flow element in the separation capillary. From Equation 4.1, it can be seen that most of the pressure applied to the reaction cell will be dispersed through the reaction capillary, provided the length of the capillary is kept short, or the bore of the capillary is greater than that of the separation capillary. This is by virtue of the lower frictional resistance encountered in these capillaries.

Laminar flow in the separation capillary would be in opposition to the electroosmotic flow and would adversely affect the separation efficiency. In extreme cases, laminar flow could cause the flow of post-column reagent into the separation capillary. The problem of laminar flow in the separation capillary can be overcome by the application of a compensating pressure to the capillary inlet.

The absence of an electric field in the reaction capillary means that the electrolyte and solutes move with a uniform velocity. Due to this, there is no need to correct peak area for differences in migration velocity. A significant advantage of this system for metal ion separations is that should a complex have rapid dissociation kinetics, the metal ions and ligand are no longer induced to migrate in opposite directions. Therefore, provided the reaction capillary is long enough or the reaction kinetics fast enough, this should permit the formation of an equilibrium between the metal and ligand.

Tsuda *et al.* [237] developed a system which coupled CE to a conventional LC post-column set-up. The solutes were first separated in a fused silica capillary that was co-axially coupled to a piece of 0.5 mm PTFE tubing via a four-way connector. One of the free ports of the connector was used to ground the capillary and the other was used for the introduction of an alkaline buffer to the PTFE tubing. A fluorimetric reagent was subsequently added via a T-junction and the derivatised solutes detected using a standard HPLC fluorescence detector. The instrumentation, schematically illustrated in Figure 4.5 was relatively complicated. In this system three HPLC pumps were used, one to deliver the alkaline buffer, a second for the fluorescent reagent and the third to provide a compensating pressure to the capillary inlet.

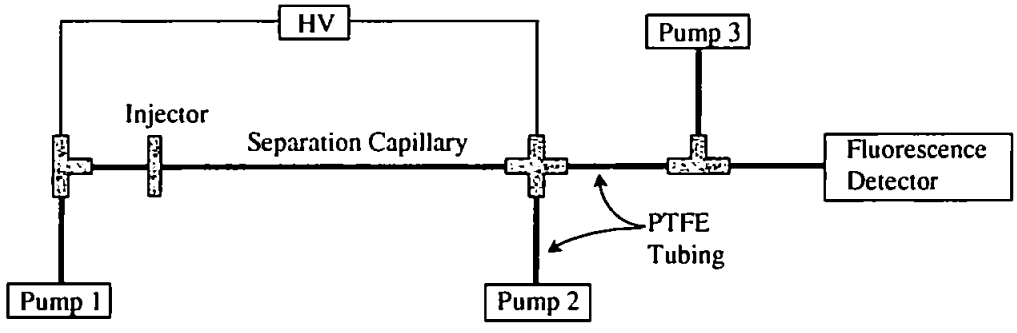

Figure 4.5. Diagram of Coupled CE Separation and HPLC Post Column Reactor System Developed by Tsuda et al. [237]

The grounding electrode was immersed in the alkaline buffer, whereas the capillary was filled with a different electrolyte resulting in a discontinuous electrolyte, more indicative of CITP than CZE. This would result in a progressive change in the pH and conductivity of the separation electrolyte. The transfer of the solutes from the small internal diameter capillary to the larger diameter PTFE tubing in conjunction with the separation in a discontinuous electrolyte are factors likely to contribute to the relatively poor efficiency attained using this system.

Zhu and Kok [241] developed a pressure driven system in which the junction between the separation and reaction capillaries was made by inserting the capillaries into a porous PTFE tube, shown in Figure 4.6.

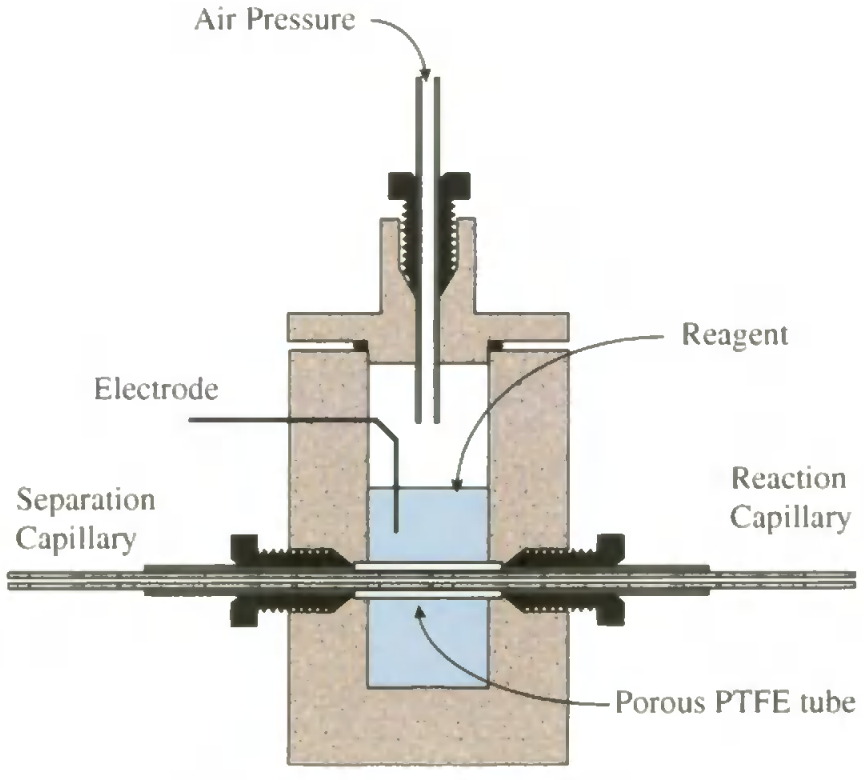

Figure 4.6. Diagram of the Reactor Cell in the Pressure Driven System Developed by Zhu and Kok [241]

The coupled capillaries were fixed inside a grounded reagent vessel of approximately 1ml capacity with finger-tight fittings. The porous PTFE tube was principally used to

align the capillaries and was reported to offer little or no resistance to the flow of fluid, except when high flow rates were used. The reagent was driven through the porous tube by air pressure applied to the reagent vessel. This air pressure was simultaneously applied to the reagent vessel and the capillary inlet to counteract Poisseuille flow in the separation capillary. Improved efficiencies were reported by coupling 75μm ID separation capillaries to 50 μm ID reaction capillaries and enhanced sensitivity was obtained using 'bubble-cell' capillaries. The only real drawbacks of this system were the inability to flush the reagent vessel and that the gap between the coupled capillaries could not be accurately controlled, consequently, reproducibility from one assembly to another may be a problem.

This aim of this work was the construction and investigation of a post-capillary reactor for the determination of trace metals by UV-Vis absorption after formation of intensely coloured complexes.

Two post-capillary reagents were chose for the study, namely, xylenol orange (XO) and 4 (2-pyridylazo) resorcinol (PAR). These reagents were chosen for their ability to form complexes with a range of transition metals and to investigate the performance of the post-capillary reactor at different pH values and electroosmotic flow rates.

4.2. Experimental.

4.2.1. Instrument Considerations and Modifications

A Dionex CES 1 (Dionex, Sunnyvale, CA, USA) was used for all experiments. The CES 1 rinses the capillary by pressurising the destination vial, which forces electrolyte through the capillary towards the source vial. Using this feature would

result in post-capillary reagent being drawn into the separation capillary from the reaction cell, resulting in the possibility of on-capillary complexation during a run. To prevent this problem the capillary was rinsed from source to destination by performing 120 sec pressure injections from a carousel vial containing electrolyte. Using this method reagent may be drawn into the reaction capillary but this is of no consequence to the separation. The capillary rinse was performed after the destination vial had been rinsed and refilled since the destination vial is emptied by the application of pressure to the vial which forces some electrolyte into the separation capillary.

Minor modifications were made to the instrument to allow automated operation with the post-capillary system installed. Figure 4.7 shows a schematic diagram of the modifications to the instrument. A low-pressure helium line providing pressure to the reagent vessel was created by detaching the helium line from one of the spare electrolyte bottles.

A manually operated pressure reduction valve was placed in line to allow independent control of the pressure applied to the reagent vessel. A low-pressure line could also be connected to the capillary inlet via the pressure injection line. To facilitate automatic switching between the pressure injection and the inlet low-pressure system, a three ported, electrically operated low-pressure gas valve was inserted in the pressure injection line. The second inlet of the valve was connected to the low-pressure line. This valve was operated by the switch normally used to operate the capillary cooling valve on the instrument. During a run, the low-pressure system could be automatically switched to the capillary inlet and when the run was complete the capillary inlet was reconnected to the pressure injection line. The manually operated valve was designed for use with pressures above 1.0 psi and operation at

pressures below this, although usable, provided poor precision. A more precise, electrically operated pressure controller was made available for a short period and used to control the pressure to the capillary inlet and reagent vessel. This device, an integral part of an alpha version of the Dionex CES 2, was able to control pressure in 0.1 psi steps from 0.1psi upwards and was used to evaluate the effect of pressure on the separation efficiency.

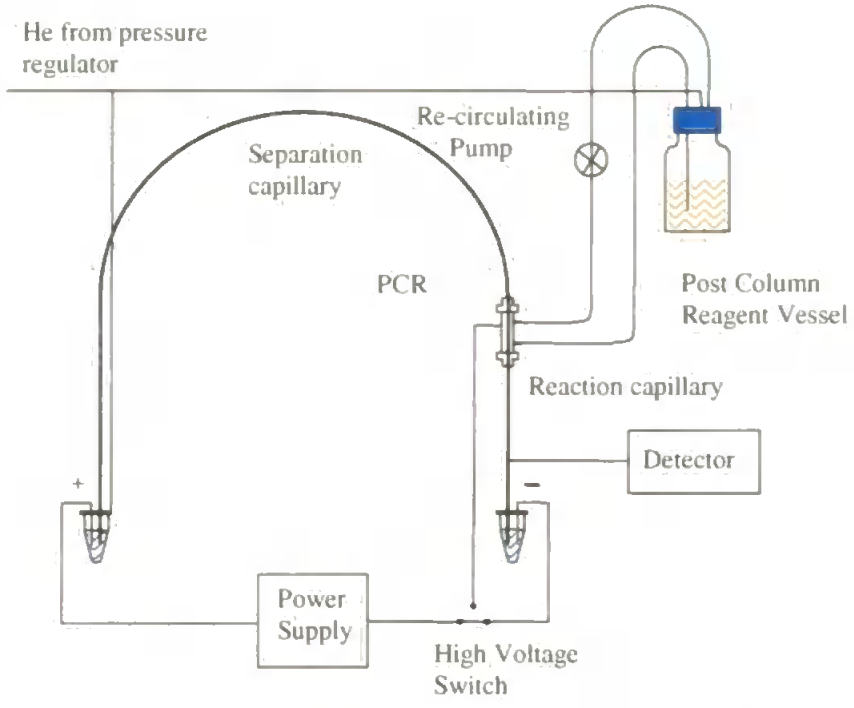

Figure 4.7. Schematic Diagram of the CES 1 with PCR Cell Installed.

The location of the ground on the instrument's power supply is inaccessible, being situated below the optical bench. To enable easy switching of the grounding electrode from the destination vial to the cell, a wire was connected to the power supply ground and soldered to the 'female' part of a push-in connector. The connector was then insulated and fixed to the instrument in an accessible position. The grounding wire from the destination vial was disconnected from the power supply, lengthened and a 'male' push-in type connector soldered to the end. A similar connector was also soldered to the wire from the cell electrode.

4.2.2. Materials and Chemicals.

Fused silica capillaries were obtained from Polymicro Technologies (Phoenix, AZ, USA). Polysulfone hollow fibre membranes with internal diameters of 0.5 and 0.25mm and a nominal molecular weight cut-off of 10,000 were a gift from A&G Technology Corp. (Needham MA, USA).

All chemicals were of analytical-grade purity. Sodium oxalate, citric acid, pyridine-2,6-dicarboxylic acid (PDCA) and xylenol orange (XO) (o-cresolsulfonphthalein-3′-3′′-bis(methyliminodiacetic acid)) were obtained from Fluka (Buchs, Switzerland). Glycine and 2-(N-morpholino)ethanesulphonic acid (MES) were obtained from Sigma (St. Louis, MO, USA).Sodium hydroxide, sodium tetraborate decahydrate, boric acid, tartaric acid, disodium hydrogen phosphate, ammonium dihydrogen phosphate and ammonium hydroxide solution were obtained from BDH (British Drug House, Poole, Dorset, UK). 4-(2-pyridylazo) Resorcinol (PAR) was a gift from Dionex (Sunnyvale, CA.).

4.3. The Design of the Post Capillary Reactor.

Any post-capillary reaction system for CE needs to be easy to operate and simple to install. The separation and reaction conditions must to be controlled for reproducible results. For these reasons, an on-capillary reactor system was chosen. Both electroosmotically and pressure systems offer advantages over each other, therefore the ability to operate in either mode was incorporated the design of the post-capillary reactor.

Unlike ion chromatography-PCR systems, where the separation of the metal ions and the post-column reaction can be performed under different pH and ionic strength conditions, these factors need to be kept similar with a CE-PCR system, to avoid the formation of 'hot spots' caused by joule heating.

4.3.1. Capillary Junction Design.

The original idea for introducing the reagent into the capillary was by inserting a short section of hollow fibre porous membrane between two capillaries. This assembly would then be fitted into a cell filled with reagent, which could then be introduced across the membrane by the application of pressure. This idea is similar to the LC-PCR system developed and marketed by Dionex [627]. The introduction of the reagent from virtually all around the junction may have the advantage of improved mixing over a single point of introduction as in the system developed by Pentoney *et al.* [238]. It was considered that in order to minimise the contribution to zone broadening by the reactor, the internal diameter of the hollow fibre should be closely matched to that of the fused silica capillaries. However, these hollow fibres are manufactured by a very limited number of companies and their availability is severely limited. The fibres are manufactures for specific purposes such as ultra-filtration and dialysis and are not usually available individually, but supplied as expensive units containing multiple bundles of the fibres. The availability is further limited by 'legal' requirements restricting the use of these fibres. An example being Hoerst Celenese, who manufacture a hollow fibre from polypropylene but restrict its use solely to blood dialysis. After an extensive search, only one company (A&G Technologies) was able to provide a sample. This sample was made from polysulfone with an 0.5mm internal diameter. Later a membrane with an internal diameter of 0.25 mm, made from the same material was also made available.

To accommodate the large internal diameter of these fibres, the design of the PCR system was altered, utilising the membrane as a sleeve over a pre-fabricated capillary junction. The internal diameter of the sleeve allowed a brace, made from a small section of 100μm outer diameter capillary, to be glued between the capillary sections,

fixing the gap between them and providing some resistance to lateral twisting. This brace also served to increase the outside diameter of the capillary assembly to nearly that of the internal diameter of the sleeve, reducing the dead volume inside the capillary junction.

4.3.2. Construction of capillary junction.

The adhesive used to construct the capillary assemblies and reactor cells was Loctite, UV curing acrylic adhesive. This adhesive was fully cured within a few seconds by exposure to an intense UV light source, in the region of 285nm.

A schematic diagram of the capillary assembly is shown in Figure 4.8. The junction was constructed from two sections of 100 μm internal diameter capillary of approximately 60cm and 15cm in length, which were cut using a ruby capillary cutter. One end of each capillary was polished, initially using the face of a ceramic capillary cutter, then finished with an ultra fine abrasive film. A small hand held chuck was used to ensure the polished faces of the capillaries remained as perpendicular to the longitudinal plane as possible. Holding the capillaries by hand tended to produce a slightly rounded face due to flexing of the capillary. The capillaries were checked under a microscope to ensure the ends were as smooth and perpendicular as possible. The capillaries were aligned by inserting a piece of 96.52μm diameter tungsten wire into the unpolished end of the 15 cm capillary until a short length protruded. The wire was then threaded into the polished end of the 60cm capillary. The cut end of the tungsten wire was first smoothed with the abrasive film to prevent scratching of the inner surface of the capillaries. The gap between the capillaries was fixed by inserting a short length of tungsten wire of the appropriate diameter (50.08μm and 10.16μm) between the two sections of capillary. The capillaries were then joined

together by bonding a short section of 100 µm outer diameter fused silica capillary between them. A sleeve of 0.5mm internal diameter polysulfone hollow fiber was slipped over this assembly and bonded in place.

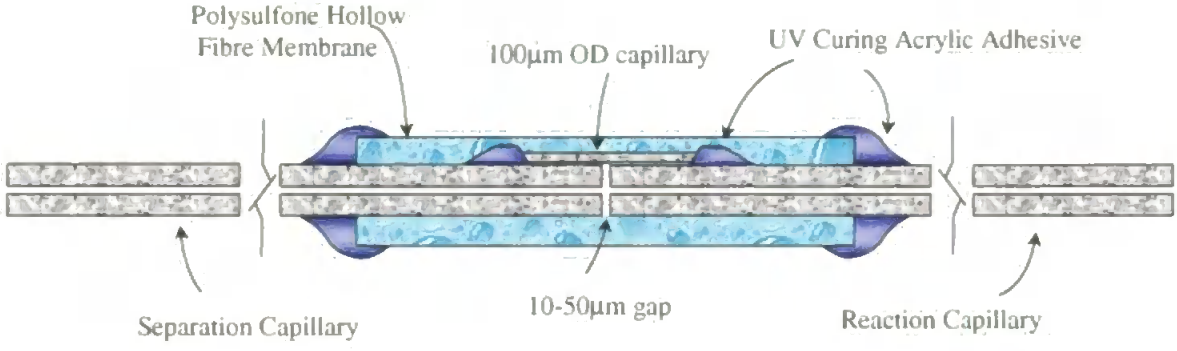

Figure 4.8. Schematic Diagram of the Capillary Junction Assembly.

Prior to use the capillaries were cut to the desired lengths then conditioned by flushing with 0.01M HCL for 30 minutes, followed by 0.5M NaOH for 60mins, then rinsing with MilliQ water. The on-capillary window was made by removing 2-3mm of the polyimide coating with a razor blade. This method of making the on-capillary window is preferable to burning the capillary, which appears to make the capillary brittle and produces windows that are larger than necessary.

4.3.3. PCR Cell Design.

The optical detector on the CES1 is contained inside a light box. There is a gap of approximately 60mm between the light box and the top of the optical bench, which is sufficient room to accommodate a reaction cell. The PCR cell must either fit inside the light box or above it. Placing the cell inside the box means that the length of the reaction capillary is determined within a narrow range. Whereas placing the cell outside the box allows greater reaction capillary lengths to be used but with the

imposition of a greater minimum length. Since the flow in the reaction capillary was expected to be less than 5mm s^{-1}, a solute would still have a residence time of at least 6 seconds in a 30mm reaction capillary. Consequently, it was decided to situate the reaction cell inside the light box.

The cell was connected to an inlet from the reagent reservoir and outlet, which could be run to waste, enabling the cell to be flushed with fresh solution between runs. The ability to flush the cell is more important in a pressure driven system as the reaction cell replaces the destination vial and in order to maintain the buffering capacity of the electrolyte, the cell should be replaced between runs.

4.3.4. PCR Cell Construction

Initially, a suppresser cell, manufactured by Dionex for CE suppressed conductivity detection in the CES2, was utilised as the reagent cell. Schematically illustrated in Figure 4.9(a), the cell included an inlet and outlet allowing the cell to be flushed and refilled with reagent between runs. A platinum wire electrode was also fitted, permitting the cell to be grounded. In use, this cell proved to be too bulky and heavy, frequently causing the reaction capillary to snap at the detection window.

A smaller, lighter cell was constructed from a section of 4mm ID plastic tubing and is illustrated in Figure 4.9(b). In this cell, the minimum effective length of the reaction capillary was 30mm. The capillary assembly was inserted into the cell and glued in place to prevent leaks. This cell design was simple to make and reusable, although since the capillaries were glued into the cell they were difficult to remove without damage and new capillary assemblies had to be used each time

A 40mm section of tubing was cut and the ends taped to allow barbed nipples to be screwed in. Two 1.5 mm holes were drilled and barbed fittings were bonded into these to allow the cell to be filled with reagent.

A third cell design, shown in Figure 4.9(c), was constructed from an unpacked 50mm length, 4 mm internal diameter, liquid chromatography column. This design allowed the capillary assemblies to be installed and removed from the cell without damage, using finger-tight fittings.

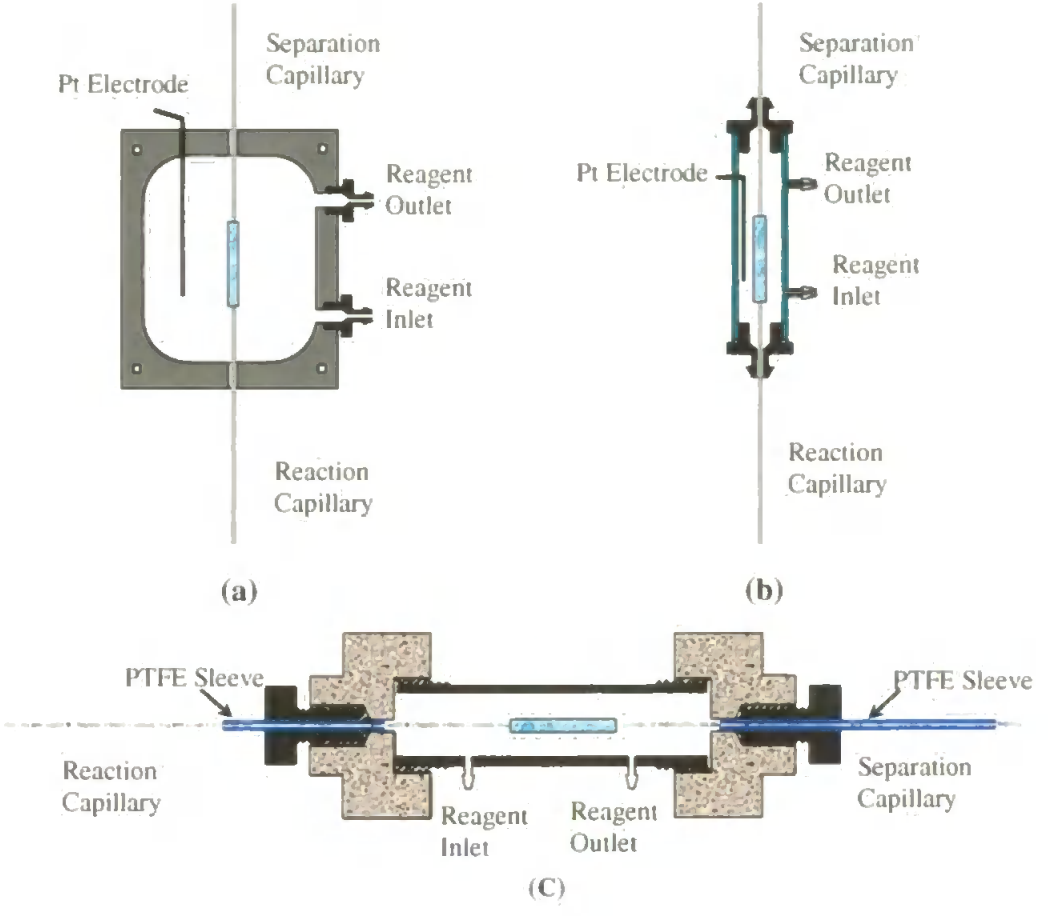

Figure 4.9. Schematic Diagrams of the PCR Cell Designs.

The length of this cell was longer than in the previous cells, requiring alteration of the light box to allow the upper column cap to protrude slightly. The increased cell length also allowed the effective length of the reaction capillary to be increased to 50 mm.

Care was needed when inserting the capillary assembly into the cell to prevent the capillaries becoming unaligned due to twisting when the finger-tight fittings were fastened. This was done by tightening the lower fitting first then gently gripping the

PTFE sleeve of the upper fitting in a pair of pliers as it was gently tightened. The lower fitting was tightened more than the upper, since leakage from this fitting would be unseen, running directly into the detector, whereas leakage from the upper fitting was easily visible and of far less consequence.

A reservoir of reagent was stored in a 100ml glass bottle which was connected by tube, to the inlet of the cell. The outlet of the cell could be run to waste or crimped as needed. The reagent reservoir was also connected to a low pressure helium line controlled by a manually operated pressure reduction valve, allowing the bottle to be pressurised.

4.4 Results and Discussion.

4.4.1. Post Column Reagent.

Although there is a very wide range of colorimetric reagents to choose from, in practise there are only a few which meet the requirements of post-capillary reactors. The reagent needs to be water soluble, form intensely coloured metal complexes and react with a large number of metal ions. Furthermore, for use in CE, the presence of an electroosmotic flow puts a further restriction on the number of suitable chelating agents. This is because the best arrangement for the separation of metal cations in CE is to inject into a buffer containing a weak complexing acid in the presence of a cathodal electroosmotic flow. However, many water soluble colorimetric reagents and their complexes are negatively charged and their migration is directed towards the anode, against the electroosmotic flow. A relatively strong electroosmotic flow is therefore required to ensure the metal chelates are directed towards the detector and to prevent the ligand from migrating into the separation capillary. This electroosmotic

flow requirement limits the choice of chelating ligand to those that form stable complexes at neutral or slightly basic pH.

Two dyes were examined for suitability as post column reagents, 4-(2-pyridylazo) Resorcinol (PAR) and xylenol orange (XO) which form complexes in basic and slightly less than neutral pH conditions, respectively.

PAR forms intensely coloured, water soluble chelates, with a wider range of metal ions than any other commonly available reagent, Table 4.0 shows the range of metals in the form of an annotated periodic table. Although the unselectivity of PAR may pose problems for spectrophotometric determinations, this reagent is ideal for detection in separation systems and has been frequently used as a post-column reagent for the detection of metal ions separated by liquid chromatography.

Table 4.0. Metals forming complexes with PAR.

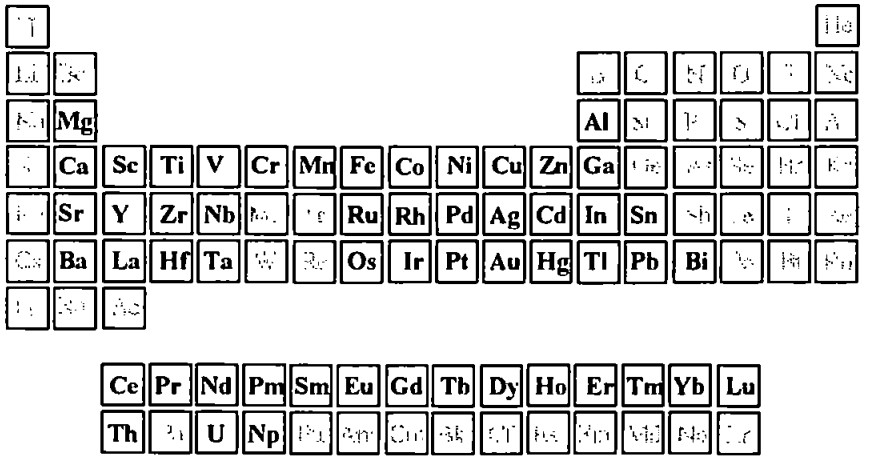

PAR is sparingly soluble in aqueous media but slightly more soluble in basic solutions. The dye forms stable complexes with transition metals in the pH range 8 - 10, bonding through the ortho hydroxyl group, the pyridine nitrogen and the azo nitrogen farthest away from the pyridine ring. The acid-base dissociation steps of PAR are shown in figure 4.10. Although there is some variation in the acidity

constants for PAR, at pH values of between 8 and 10 the ligand will be in the HL^- form.

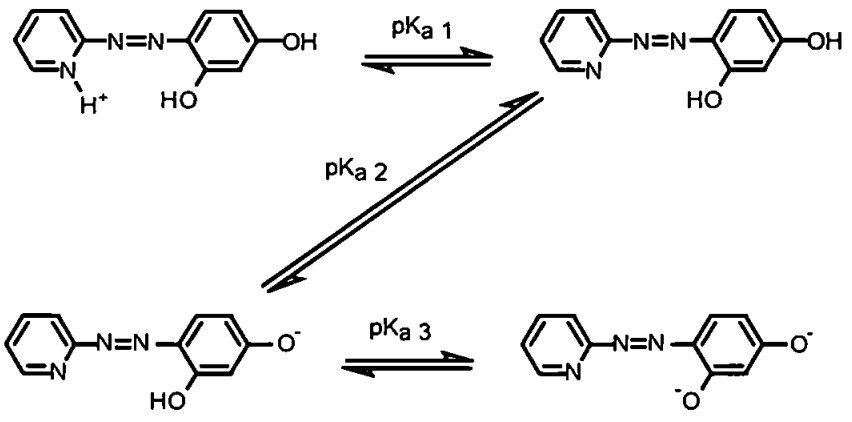

Figure 4.10. The Acid-Base Dissociation Steps of PAR. pK_{a1} = 2.69, pK_{a2} = 5.5 and pK_{a3} = 12.31 [244]

The lambda max. of PAR is 414nm at a pH value of 8.6 and the maximum absorption of the metal complexes is between 490 and 510 nm. To avoid an increased background contribution from the ligand, detection of the PAR metal chelates was performed at 530nm. The molar absorptivity of PAR solutions has been reported to decline with time [244], therefore fresh solutions were prepared regularly.

A suite of six divalent metals was chosen to assess the post-capillary reaction system, these were copper, cadmium, cobalt, zinc, manganese and Nickel. The stability constants of the metal-PAR complexes are shown in table 4.1 below.

Table 4.1. Stability Constants of PAR Chelate [244].

Metal Ion	Log K_1	Log K_2	Log β_2
Zn^{2+}	10.5	6.6	17.1
Cd^{2+}	11.5	10.1	21.6
Ni^{2+}	13.2	12.8	26.0
Co^{3+}	10.0	7.1	17.1
Cu^{2+}	14.8	9.1	23.4
Mn^{2+}	9.7	9.2	18.9

Usually, PAR forms complexes with molar ratios of 1:1 and 1:2 with divalent metals, the structures of the 1:1 and 1:2 complexes are shown in Figure 4.11. The 1:1 complex is cationic with the formation given by Equation 4.2 and the 1:2 complex is anionic with the formation expressed in Equation 4.3

$$M^{2+} + HL^{-} \rightleftharpoons MHL^{+} \qquad \textit{Equation 4.2}$$

$$MHL^{+} + HL^{-} \rightleftharpoons ML_2^{2-} + 2H^{+} \qquad \textit{Equation 4.3}$$

Cobalt II is an exception to this assertion as during the electrophoretic separation of PAR complexes, assuming equal charge, the mobility of the cobalt complex is notably lower than that expected based on size alone. This was thought to be due to oxidation of the cobalt II to cobalt III on chelation, producing an overall charge of one minus for the 1:2 cobalt complex [79, 119]. The chelation reaction between PAR and most of the metals used is very fast, occurring essentially on mixing, with the exception of nickel in which a slight delay was observed.

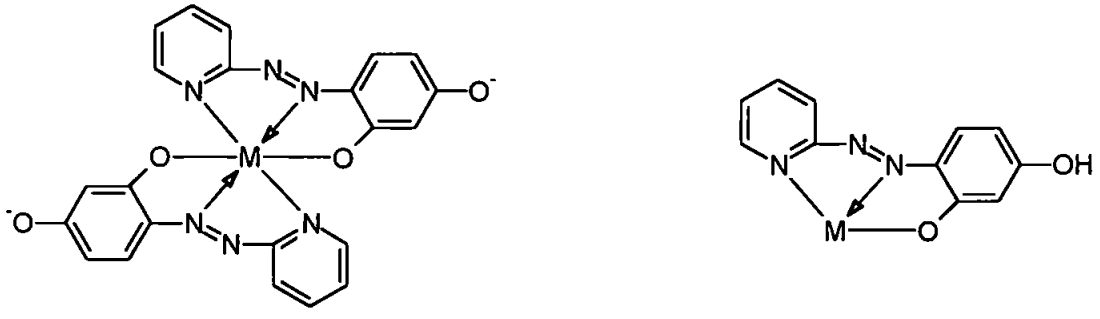

Figure 4.11. The Structure of The 1:2 and 1:1 PAR Chelates.

The triphenylmethane dye xylenol orange is soluble in aqueous solutions, forming red coloured complexes in the pH range 0-6. The dye is yellow in colour below pH 6 and red-violet above pH 7. The structure of xylenol orange is shown in Figure 4.12. Metal chelates are formed with the iminodiacetic acid functional groups. Xylenol orange obtained from commercial sources is often impure containing semixylenol

orange, which contains only one iminodiacetic acid group, cresol red may also be an impurity. The purity of the reagent is of less consequence in a pressure driven system, at worst resulting in some reduction in sensitivity. But in an voltage driven system it may cause problems due to differences in the mobility of the xylenol orange and semixylenol orange chelates.

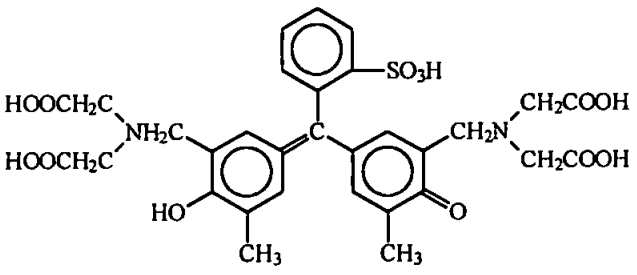

Figure 4.12. The structure of Xylenol Orange

The acid base dissociation values (pK_a) for xylenol orange quoted in the literature are given in table 4.2 below.

Table 4.2. Protonation Constants for Xylenol Orange.

	Functional Group	[245]	[246]	[247]
pK_{a1}	SO_3H	-	-	-1.74
pK_{a2}	$=OH^+$	-	-	-1.09
pK_{a3}	- COOH	-	-	0.76
pK_{a4}	- COOH	2.06	2.00	1.15
pK_{a5}	- COOH	2.16	2.74	2.58
pK_{a6}	- COOH	3.56	4.49	3.23
pK_{a7}	-OH	7.34	7.50	6.40
pK_{a8}	$\equiv NH^+$	9.68	10.30	10.50
pK_{a9}	$\equiv NH^+$	12.61	12.00	12.6

Xylenol orange usually forms metal complexes with the molar ratios of 1:1 with transition metals, the stability constants of the metal xylenol orange complexes are given in Table 4.3 below.

Table 4.3 Stability Constants of Metal-Xylenol Orange Chelates [248]

Metal Ion	Log K_1
Co^{2+}	12.63
Ni^{2+}	12.37
Zn^{2+}	13.41
Cu^{2+}	12.52
Cd^{2+}	9.67
Pb^{2+}	13.68

The dye has a mobility of 43.68 x 10^{-5} cm^2 V^{-1} s^{-1} and at pH 5.5 should have a charge of minus three. The 1:1 complexes are anionic with the formation expressed by Equation 4.4.

$$M^{2+} + HL^{3-} \rightleftharpoons ML^{2-} + H^+ \qquad \textit{Equation 4.4}$$

4.4.2. Sources of Zone Broadening in CE-PCR Systems

In addition to the sources of zone broadening in CE already discussed in Ch1, the introduction of a reagent across a junction contributed further sources.

The principal influences on zone dispersion in a coupled-capillary post-capillary reactor system are dependent on the efficiency of mass transfer across the junction between the coupled capillaries and the kinetics of the derivatisation reaction.

In a pressure driven system, zone broadening is caused by the laminar flow in the reaction capillary. Whereas, there is no contribution from the flat flow profile in a voltage driven system, laminar flow may be created by introduction of the reagent by pressure. Zone dispersion due to laminar flow in the reaction capillary can be described by the Taylor- Aris equation (Equation 4.5).

$$\sigma^2 = \frac{d_c^2}{96D} t_R \qquad \textit{Equation 4.5}$$

Where σ^2 is the increase in the peak width, d_c is the internal diameter of the reaction capillary, D is the diffusion coefficient of the derivatised solute and t_R is the reaction time. From Equation 4.5 it can be seen that zone broadening is reduced when smaller ID capillaries are used and when the rate of the derivatisation reaction is greater.

The mass transfer across the junction is influenced by the alignment of the capillaries and the derivatisation reaction.

The derivatisation reaction may contribute to zone dispersion in a voltage driven system, since altering the size or charge of a solute will also change its electrophoretic velocity. When the velocity of the derivatised solute is greater than that of the solute, zone dispersion will occur as the derivatised solute speeds up causing it to migrate away from the remaining underivatised solute. On the other hand, when the velocity of the derivatised solute is lower than that of the solute, stacking may occur as the derivatised solute slows down, allowing the underivatized solute to catch up. Although stacking is usually a desirable effect in CE, in this instance it may occur at the expense of peak resolution.

Similarly, the kinetics of the reaction can cause a significant contribution to band broadening when the mobilities of the derivatised solutes differ from those of the underivatised solutes.

4.4.3. The Separation of Metal ions.

At the pH values optimal for the PAR metal chelate formation, the silanol groups on the capillary wall are highly ionised, leading to a number of potential problems. Ionisation of the wall provides a large number of cation exchange sites where metal ions can adsorb. These solute-wall interactions contribute to zone broadening and may cause a decrease in detector response. The adsorption of cations may also cause a reduction in the electroosmotic flow due to masking of the silanoate anions on the capillary wall. In addition, some metal ions form insoluble hydroxide species at this pH, causing them to precipitate. At these pH values, the magnitude of the electroosmotic flow is such that the metal ions will be rapidly swept towards the detector with insufficient time for them to separate. Lengthening the capillary increases the separation time but only up to the point that the maximum voltage limit of the instrument is reached, from then on, the field strength in the capillary decreases

as the capillary is lengthened. Lengthening the capillary also increases the surface area of the capillary and consequently, the cation exchange capacity of the column. These problems can be avoided to some extent by pre-complexing the metal ion with a ligand, to form an anionic species. This has the effect of altering the mobility of the metal ion, reducing solute-wall interactions by repulsion between the wall and the anionic species, and may also help to maintain the solubility of the metal ions.

The stability of the ligand used for the separation is of considerable importance, since the complex must be stable enough to perform the above functions, but should not be so stable that the complex does not exchange with the post-capillary detection ligand.

4.4.4. PAR Post-Capillary Reactor System.

4.4.4.1. Initial Testing of the Capillary Assembly.

Initial testing of the design of the capillary junction was performed in the voltage driven mode. In this mode the grounding electrode was placed in the destination vial and a series of injections of metal standards of Cu^{2+}, Zn^{2+}, Mn^{2+}, Co^{2+}, Cd^{2+} and Ni^{2+} were made. The metal ions were complexed with pyridine-2,6-dicarboxylic acid (PDCA) which at the pH values used forms reasonably stable chelates with the metal ions. The formation of the 1:1 complex is shown in Equation 4.6 and when an excess of PDCA is present, the 1:2 complex is formed (Equation 4.7).

$$M^{2+} + L^{2-} \rightleftharpoons ML \qquad \textit{Equation 4.6}$$

$$ML + L^{2-} \rightleftharpoons ML_2^{2-} \qquad \textit{Equation 4.7}$$

At pH values above pH 7, PDCA is fully deprotonated and has a mobility -56.0×10^{-5} $cm^2\ V^{-1}\ s^{-1}$. From Table 4.4, it can be seen that the stability constants for PDCA are sufficiently lower than those of PAR (Table 4.1), allowing the formation of the metal-PAR complexes in the reaction capillary.

Table 4.4. Stability constants of Metal PDCA chelates [249]

Metal ion	Log. K_1	Log.β_2
Zn^{2+}	6.35	11.88
Cd^{2+}	6.75	11.15
Ni^{2+}	6.95	13.5
Co^{2+}	6.65	12.70
Cu^{2+}	9.14	16.52
Mn^{2+}	5.01	8.49

The electrolyte was 10mM sodium tetraborate at pH 8.6 containing 0.5mM PDCA. The post-column reagent was 0.5mM PAR made up in 10mM sodium tetraborate with pH adjusted to 8.6 and a pressure of 0.5psi was applied to drive the reagent across the membrane. The capillary assembly dimensions were; 50cm separation capillary (L_{sep}), 8cm reaction capillary (L_r), giving a total length (L_t) of 58cm, with the length to the detector (L_d) 53 cm. The effective length of the reaction capillary (R_d) was 3cm with a 50μm gap between the capillaries. Injections were performed by gravity injection at a height of 100mm for 20seconds and a separation voltage of 20kV was applied. On-capillary detection was performed at 530nm.

Injections of the individual metals at a concentration of 10 mg L^{-1} were performed and peaks were detected for all the metals. The manganese peak was seriously broadened and detected as little more than a 'hump' in the baseline. The sensitivity of the nickel peak was considerably lower than that of the other metals. The lower sensitivity of nickel was thought to be due to the slower rate of formation of the Ni-PAR complex. Both cobalt and zinc produced partially split peaks. Reducing the concentration of metal ions injected caused the peaks the merge until a single peak was produced at 1 mg L^{-1}.

Figure 4.13 shows the effect of the concentration of zinc on peak splitting. It was thought that this peak splitting may be due to insufficient PAR entering the capillary leading to the formation of the 1:1 and 1:2 complexes which then begin to separate in

the reaction capillary. The dip in the baseline prior to the 10 ppm zinc peak, Figure 4.13(a), tends to support this theory being caused by depletion of the dye due to an excess of the metal.

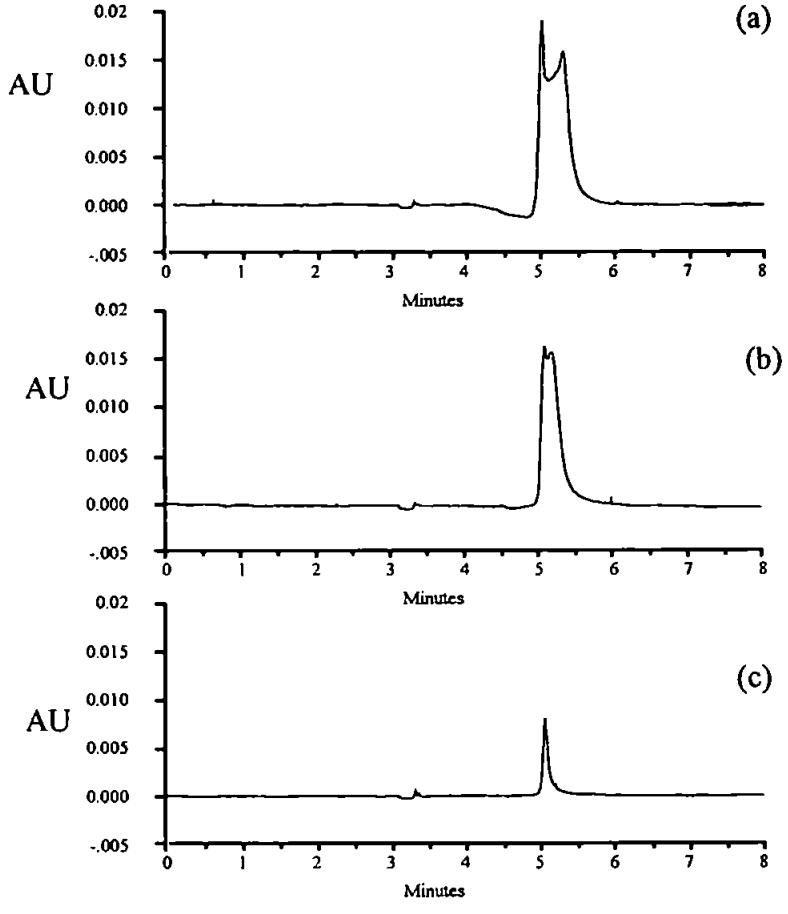

Figure 4.13. The Effect of the Concentration of Zinc on Peak Splitting (a) 10ppm (b) 5ppm (c) 1ppm.

The PAR concentration in the PCR was increased to 5mM and injections of the individual the metal standards were repeated, shown in Figure 4.14. This time single peaks of reasonable efficiency were detected for all the metal ions apart from manganese (not shown) which was again severely broadened, being detected as a slight mound on the baseline. However, from Table 4.5 it can be seen that the migration times of the different metals were similar, and no separation was obtained when a mixture of cobalt, nickel, copper, zinc and cadmium was injected.

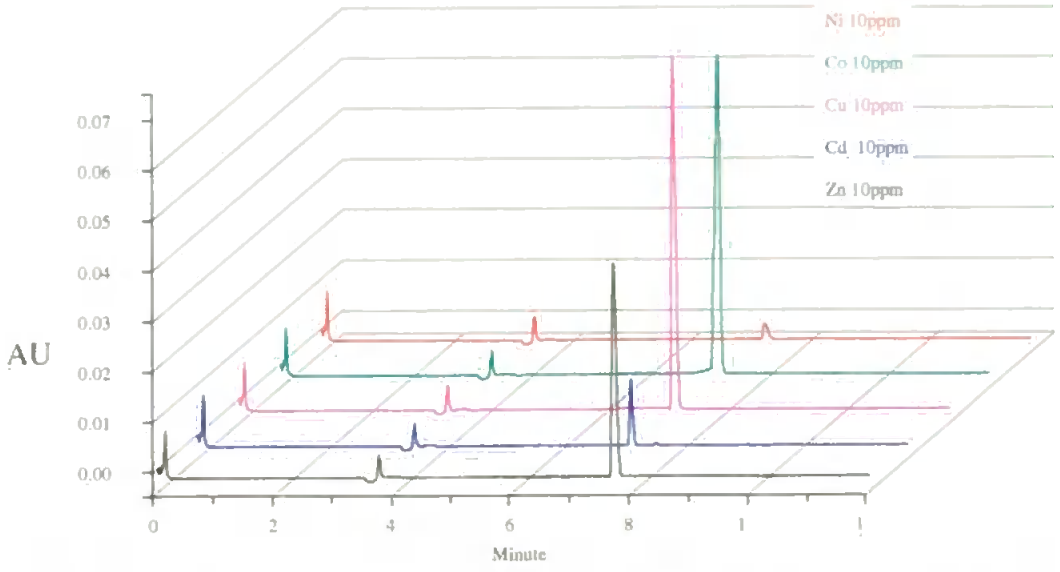

Figure 4.14. Electropherograms of Individual Metal Ion Injections. Separated in 10mM Sodium Tetraborate pH 8.6 with 0.5mM PDCA.

Table 4.5. Peak data relating to Figure 4.13

Metal Ion	t_m	EOF	Peak Height	Peak Area	Corrected Area	N m^{-1}
Zn^{2+}	7.70	3.54	4,274	21,111	2,738	89,398
Cd^{2+}	7.39	3.56	1,334	4,305	586	175,536
Ni^{2+}	7.61	3.54	294	1,644	219	67,377
Co^{2+}	7.56	3.56	6,314	35,852	4,838	82,574
Cu^{2+}	7.55	3.56	7,041	33,192	4,509	81,462

The possibility that the peak splitting was caused by insufficient PDCA in the electrolyte was investigated by increasing the concentration to 1mM. This was found to have no effect on the splitting of the zinc and cobalt peaks although some improvement of the manganese peak was observed. Using the speciation program Mineql with a concentration of 0.5mM PDCA, all the metals were found form the 1:2 complexes with PDCA, apart from manganese which was shown to form the neutral 1:1 and anionic 1:2 complexes in the respective percentage ratio of approximately 40:60. Electrodiffusion caused by differences in the mobility of the two species was thought to be the cause of the broadening of the manganese peak.

Increasing the concentration of the PAR results in higher background absorbance and as expected, the sensitivity of the metal peaks was slightly lower than using 0.5mM PAR. The migration times of the peaks were noted to increase, as were the peak efficiencies. The increased migration times were probably to be due to a small reduction in the electroosmotic flow rate in the reaction capillary caused by the increased ionic strength of the reagent. This would allow the metal-PAR chelates to migrate with an increased negative velocity.

Using the stability constants, the predicted migration order would be cadmium, zinc, cobalt, nickel and copper migrating last. The stability constants for nickel, cadmium, cobalt and zinc are reasonably similar, only copper differs significantly. Due to the greater stability of the copper complex, this metal at least, was expected to separate from the other metals, but no separation was achieved.

An ammonium phosphate buffer at pH 8.6 containing 1mM PDCA was tried. Initially the concentration of this buffer was set at 10mM but a current of 48μA was observed when a voltage of 15kV was applied. The buffer concentration was subsequently reduced to 5mM allowing a voltage of 20kV to be applied.

The precision of the electroosmotic flow was improved with this electrolyte but again no significant difference in the migration time of the metal complexes was noted as shown in Table 4.6.

Table 4.6. Peak Data for Metals separated in 5mM Ammonium Phosphate Electrolyte Containing 1mM PDCA.

Metal Ion	t_m	EOF	Peak Height	Peak Area	Corrected Area	N m^{-1}
Zn^{2+}	6.47	3.12	3,962	24,693	3817	86964
Cd^{2+}	6.15	3.12	2,606	10,394	1690	188380
Ni^{2+}	6.52	3.12	881	6,032	925	74136
Co^{2+}	6.49	3.12	3,680	25,514	3931	82120
Cu^{2+}	6.57	3.12	2,887	18,055	2748	84156

The electroosmotic flow was faster due to the greater mobility of the co-ion. The peak heights were noted to be lower but the corrected areas were found to be similar to those obtained with the borate electrolyte but the peak heights were lower.

When the PDCA complexes were injected into the capillary, where the reagent vessel contained electrolyte with no added PAR and detected at 260nm, the metal ions were observed to produce severely broadened peaks. This behaviour is characteristic of ligands that form complexes of intermediate stability where broadening of the migration sample zone is caused by electrodiffusion.

The increased efficiency of the metal-PAR chelate peaks over the PDCA complexes provides an indication of the importance of the mobility of the derivatised metals in the reaction capillary. Although the free PDCA has a greater mobility than PAR, the metal complexes formed with PDCA are less stable. Consequently, the PAR complexes migrated with greater mobilities than the PDCA complexes, which caused their effective velocity to slow. Although this resulted in sharper peaks, this was at the expense of resolution.

The dip followed by a peak on the electropherograms, occurring just before four minutes was found to coincide with the migration of benzyl alcohol, a neutral marker detected at 260nm. This dip was attributed to the migration of water from the injected sample, which caused a decrease in the background absorbance. The peak migrating immediately behind the water dip was attributed to stacking of the reagent due to its increased mobility in the high field strength region of the water plug. This provides a useful indicator of the rate of the electroosmotic flow during a run. The width of the dip found to correlate with the length of the injected sample plug.

4.4.4.2 The effect of different complexing agents added to the electrolyte.

Since no separation was obtained using PDCA, several other complexing agents were

assessed for suitability in the PCR system.

4.4.4.2(i). Tartaric Acid.

L-Tartaric acid forms much weaker complexes with the metals than PDCA, the stability constants are shown in Table 4.7. The acid dissociation values for tartaric acid are; pK_{a1} 3.04 and pK_{a2} 4.3. At pH 8.6, tartaric acid is in the form L^{2-} and has a mobility of -60.5 x 10^{-5} cm^2 V^{-1} s^{-1}.

Injections of the metals using an electrolyte consisting of 10mM ammonium phosphate at pH 8.6 and 5mM tartaric acid failed to produce any peaks. This was thought to be due to very weak nature of the complexes, leaving the metals free to interact with the capillary walls or precipitate. Increasing the concentration of tartaric acid in the electrolyte was unfeasible due to current considerations and it was decided to try a complexing agent forming slightly more stable complexes with the metals.

Table 4.7. Stability Constants for Metals Complexed with Tartaric Acid [250], Citric Acid [250] and Oxalic Acid [251].

Ligand	Tartaric Acid	Citric Acid	Oxalic Acid	
Metal ion	Log. K_1	Log. K_1	Log. K_1	Log.β_2
Zn^{2+}	2.68	4.98	3.7	6.0
Cd^{2+}	-	3.75	2.9	4.7
Ni^{2+}	2.06	5.4	4.1	7.2
Co^{2+}	2.19	5.0	3.5	5.8
Cu^{2+}	3.39	5.9	4.5	8.9
Mn^{2+}	2.49	4.15	2.7	4.1

4.4.4.2(ii). Citric acid

The acid dissociation values for citric acid are; pK_{a1} 3.13, pK_{a2} 4.76 and pK_{a3} 6.4. At pH 8.6 citric acid is in the form L^{3-} and has a mobility -74.4 x 10^{-5} cm^2 V^{-1} s^{-1}. The stability constants for the citrate complexes are shown in table 4.7.

Initially 5mM citrate was added to a 10mM ammonium phosphate electrolyte titrated to pH 8.6 but this resulted in an excessive current requiring the use of low field strengths (less than 150 V cm^{-1}). Under these conditions, a relatively slow electroosmotic flow was produced and it was thought that if the 1:2 complex ML_2^{4-} was formed its mobility may be sufficiently rapid to prevent the metals from reaching the reaction capillary. Reducing the concentration of citric acid to 1mM allowed the use of increased field strengths but again no peaks were detected.

4.4.4.2(iii). Oxalic acid

The metal complexes with oxalic acid are weaker than those of PDCA and citric acid, but more stable than the complexes with tartaric acid. The acid dissociation values for oxalic acid are pK_{a1} 1.25 and pK_{a2} 4.29 [252] and at pH 8.6 it is fully ionised with a mobility of -74.6 x 10^{-5} cm^2 V^{-1} s^{-1}. The stability constants for oxalic acid are given in table 4.7.

A 10 mM ammonium phosphate buffer at pH 8.6 containing 1mM oxalate produced a peak for each metal when injected individually but failed to effect a complete separation of all the metals when injected together. Figure 4.15 shows the separation of the six metals at a concentration of 1 mg L^{-1}. The capillary assembly dimensions were 50cm L_{sep}, 8cm L_r, 53cm L_d, 3cm R_d and with a 50μm gap, with the grounding electrode placed in the destination vial. The other separation conditions were; gravity injection at 100mm for 20 seconds, applied voltage 15kV, on-capillary detection at 530nm and the PCR reagent was 5mM PAR made up in 10mM ammonium phosphate at pH 8.6. Under these conditions cadmium and manganese were found to co-migrate, cobalt was partially resolved from cadmium, only the nickel and copper peaks were well separated. No peak was detected for zinc within the time scale of the electropherogram.

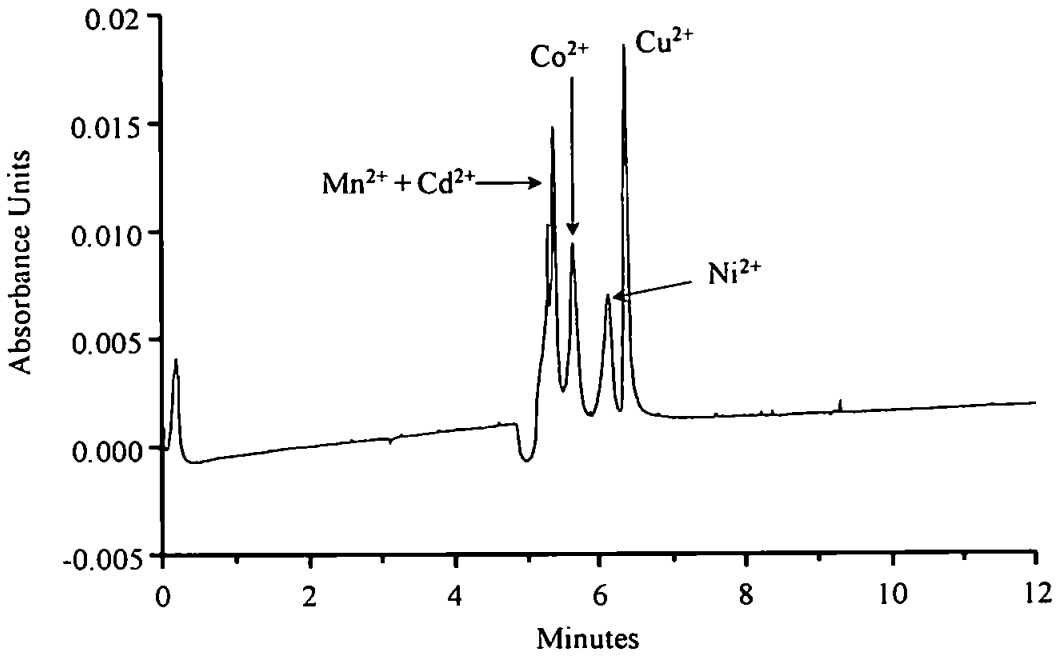

Figure 4.15. The Effect of 1mM oxalic acid on the separation of 1ppm Zn^{2+}, Mn^{2+}, Co^{2+}, Cd^{2+} Ni^{2+} and 2 ppm Cu^{2+}.

Table 4.8. Peak data relating to Figure 4.14

Metal Ion	t_m	Peak Area	Corrected Area	Peak Height	N m^{-1}
$Mn^{2+} + Cd^{2+}$	5.38	2,761	513	968	-
Co^{2+}	5.65	4,775	845	731	20,302
Ni^{2+}	6.14	4,581	746	546	13,003
Cu^{2+}	6.37	8,080	1268	1,698	45,877

Increasing the concentration of oxalic acid to 5mM was found to improve the separation, but at the expense of an increase in the ionic strength of the electrolyte, requiring the use of lower field strengths. To compensate for this increase in ionic strength, the ammonium phosphate electrolyte concentration was reduced to 5mM allowing a separation voltage of 15kV to be used. Under these conditions, all the metals were separated within a reasonable time span, Figure 4.16. The Mn^{2+} peaks Cd^{2+} migrated just after the electroosmotic flow, occurring on the tailing of the reagent peak but were well separated from Cu^{2+}, Co^{2+}, Ni^{2+} and Zn^{2+}. The separation selectivity was within the parameters predicted by the stability constants with the

exception of zinc, which was much later than expected and severely broadened. The retardation and shape of the zinc peak was unexplained, but was thought to be probably due to wall interactions.

The possibility of the formation of the hydroxide species could not be ruled out, but other metals, such as manganese, form weaker complexes with oxalic acid, yet were unaffected. The solubility of many oxalic acid complexes is relatively low and precipitation is reported to be a problem, although the concentration of the zinc was not found to affect the peak shape, as would be expected were this the case.

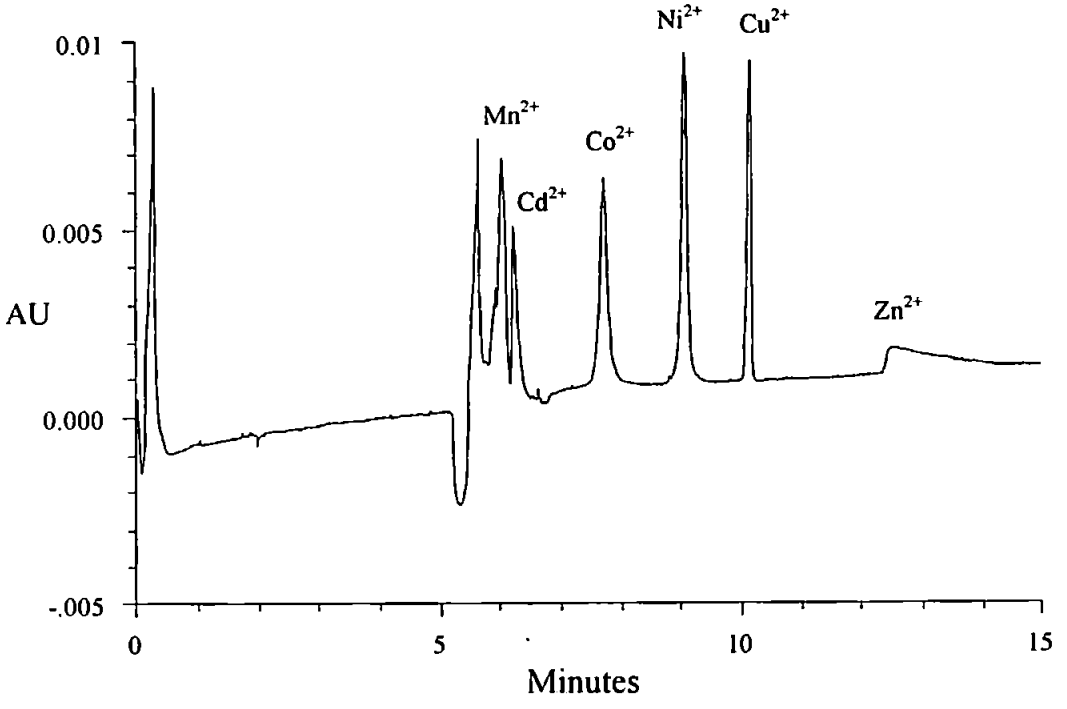

Figure 4.16. The Effect of 5mM oxalic acid on the separation of 1ppm Cu^{2+}, Zn^{2+}, Mn^{2+}, Co^{2+}, Cd^{2+} and Ni^{2+}.

Table 4.9 Peak data relating to Figure 4.16.

Metal Ion	t_m	Peak Area	Corrected Area	Peak Height	N m^{-1}
Mn^{2+}	6.06	5,540	914	655	25,236
Cd^{2+}	6.25	2,699	432	438	46,823
Co^{2+}	7.75	5,167	667	564	39,164
Ni^{2+}	9.11	6,264	688	864	81,304
Cu^{2+}	10.17	3,842	378	854	201,168
Zn^{2+}	12.63	3,680	291	70	1,066

Increasing the length of the reaction capillary from 3 to 5cm was found improve the separation of all the metals, in particular Cd^{2+} and Mn^{2+} were now fully resolved, Figure 4.17.

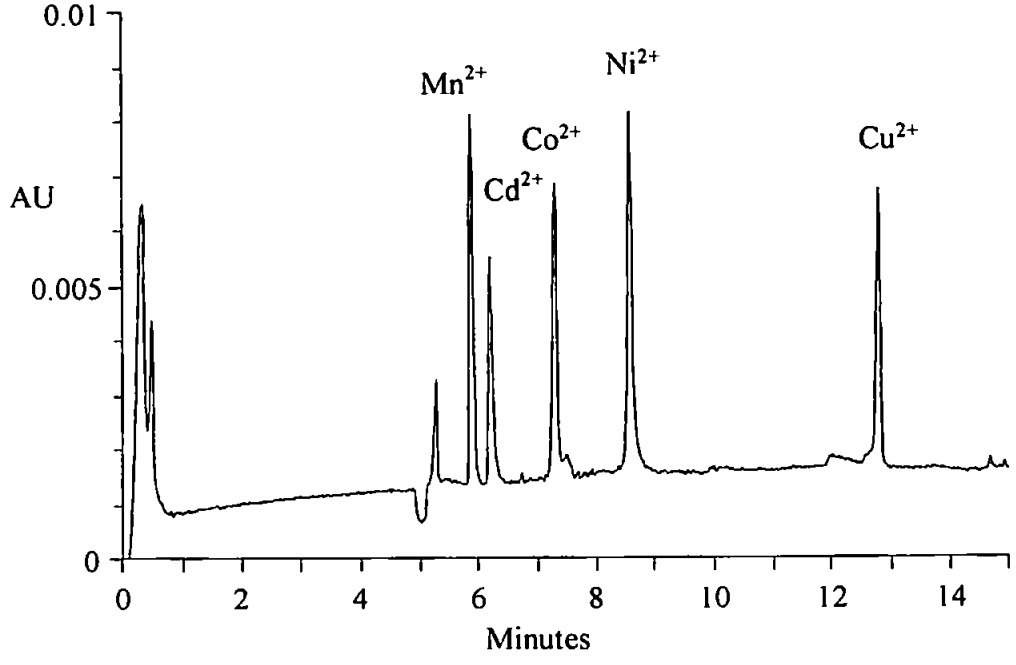

Figure 4.17. Separation of 1ppm Cu^{2+}, Zn^{2+}, Mn^{2+}, Co^{2+}, Cd^{2+} and Ni^{2+}. Separation Conditions; Electrolyte, 5mM Sodium Phosphate with 5mM oxalic acid, pH 8.6. Post Column Reagent, 5mM PAR in 5mM Sodium Phosphate, pH 8.6. Capillaries, L_{sep} 50cm L_d 55cm R_d 5cm, 100μm ID 50μm Gap. Injection, Gravity 20 seconds @ 100mm. Voltage. 15kV. Detection, 530nm.

The data in Table 4.10 shows that the efficiencies of all the peaks were increased although response of the metal complexes was lower than that obtained with the shorter reaction capillary. The migration time of the copper peak was significantly increased becoming further separated from the other metals. Zinc was not detected within the time span of the electropherogram. The improved resolution obtained from increasing the length of the reaction capillary gives a clear indication that the electrophoretic migration of the metal-PAR complexes in this capillary is playing a

significant role in their separation, a situation similar to the separation of pre-formed complexes.

Table 4.10. Peak Data from Figure 4.17

Metal ion	t_m	Peak Area	Corrected Area	Peak Height	N m^{-1}
Mn^{2+}	5.90	3,132	531	681	68,267
Cd^{2+}	6.22	2,037	327	418	79,531
Co^{2+}	7.32	3,231	441	541	84,409
Ni^{2+}	8.59	3,778	440	660	121,220
Cu^{2+}	12.82	2,406	188	498	269,933

4.4.5. Introduction of the Post-column Reagent in the Voltage Driven Mode.

The factors influencing the introduction of the post-column reagent that were investigated, were the effect of the application of pressure to the reaction cell and the ionic strength of the reagent matrix.

4.4.5.1. The Introduction of the Reagent by Syphoning.

Since electroosmotic flow is generated in both the separation and reaction capillaries, the ionic strength or conductivity of the reagent can be used to control the electroosmotic flow in the reaction capillary and therefore the quantity of reagent migrating into the capillary. Under normal circumstances, electroosmotic flow is generated uniformly along the wall of a capillary but when a gap is introduced into the capillary, no electroosmotic flow is generated in this region because there is no wall. In this situation, fluid exiting the separation capillary passes into a static pool of electrolyte. On the other hand, electroosmotic flow is generated by the wall of the reaction capillary, which causes the electrolyte to be drawn out of the gap and into the reaction capillary. When the conductivity of the electrolyte in the gap is the same as that of the separation electrolyte, the volume of fluid transiting the junction will be balanced, since the flow rate entering the gap is equal to that exiting it. If however,

the conductivity of the electrolyte in the gap is higher than that of the separation electrolyte (Figure 4.18 top), the conductivity of the electrolyte in the reaction capillary will gradually increase as the higher conductivity electrolyte is drawn in. When this happens the zeta potential on the capillary wall is suppressed causing a corresponding decrease in the electroosmotic flow, consequently the volume of fluid entering the gap will exceed that exiting it. Conversely, when the conductivity of the electrolyte surrounding the junction is lower than that of the separation electrolyte, (Figure 4.18 bottom) dilution of the electrolyte in the reaction capillary leads to an increase in the electroosmotic flow and siphoning of the gap electrolyte into the reaction capillary.

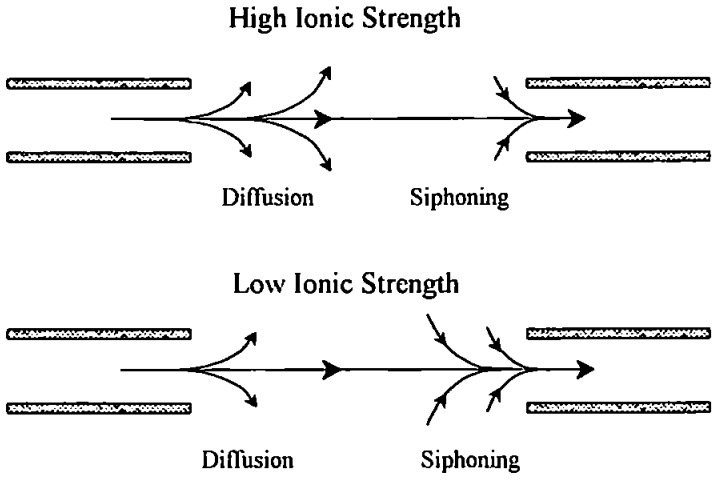

Figure 4.18. Influence of the Ionic Strength of the Electrolyte in the Gap on the Fluid Dynamics Across a Capillary Junction, [402].

The effect of the ionic strength of the reagent was investigated by injecting the six metal ions and progressively reducing the ionic strength of the reagent whilst maintaining constant electrolyte conditions in the source and destination vials. A 5mM sodium phosphate electrolyte at pH 8.6 containing 5mM oxalic acid was used throughout this experiment. The capillary assembly was constructed from a 50cm L_{sep} and 8cm L_T capillaries both with 100μm ID. In this study, reducing the ionic strength of the reagent was found to make very little difference on either the peak efficiency or the resolution. Even when the reagent was

made up in MilliQ water, dilution of the electrolyte in the reaction capillary would be expected to cause an increased flow in the reaction capillary. This faster electroosmotic flow was expected to result in broadening of the solute zones as each zone became 'stretched' when it encountered the more rapid electroosmotic flow. However, this expected broadening was not as pronounced as anticipated. This was thought to be due to two opposing factors that would influence the migration of the metal complexes in the reaction capillary. Firstly, the higher field strength experienced in this capillary caused the negative electrophoretic velocity of the metal PAR complex to increase, producing a greater stacking effect. Secondly, the higher electroosmotic flow in this region would increase the velocity of the zone as it transits the detection window producing a sharper peak. On the other hand, when the ionic strength of the reagent electrolyte was greater than that of the separation electrolyte, peak broadening was accompanied by a significant reduction in sensitivity and loss of resolution. This was attributed to dispersion of the flow from the separation capillary into the reaction cell caused by the build up of backpressure due to the slower rate of electroosmotic flow in the reaction capillary.

4.4.5.2. The Introduction of the Reagent by Pressure.

Initial experiments to observe the effect of pressure applied to the reaction cell on the separation capillary were conducted by observing the electroosmotic flow as the pressure was varied. Excessive pressure on the capillary junction would result in some of this pressure being transmitted to the separation capillary. This should then be detectable as a reduction in the rate of the electroosmotic flow or increase in the migration time of a metal ion. The separation electrolyte was 5mM sodium phosphate at pH 8.6 containing 5mM oxalic acid, the capillary assembly was the same as used in

the ionic strength experiment above. The reagent reservoir and reactor cell were filled with 0.5mM PAR which was made up in the separation electrolyte but without the addition of the oxalic acid. This ensured the ionic strength of the reagent was lower than that of the separation electrolyte and would ensure a flow of reagent into the reaction capillary, without the aid of pressure. A series of injections of 10 mg l^{-1} copper were performed to monitor the rate migration time of the complex and the electroosmotic flow. In the initial injection, the reagent reservoir was placed slightly below the level of the cell to ensure that no pressure was exerted on the junction. A series of injections were made in which the reservoir was increasingly elevated until a height difference of 15cm was attained. No difference in the migration time of the copper was observed. (The height of 15cm above the reaction cell was for convenience, as this allowed the reagent vessel to be situated on the top of the instrument.) Next, a series of injections were performed, during which helium pressure was applied to the reservoir.

Figure 4.19 shows that only at pressures above 2 psi were the migration time of the copper complex and electroosmotic flow observed to increase. This ability to use pressures of up to 2 psi without effecting the separation was attributed to the flow resistance of the polysulfone membrane and the suction caused by the electroosmotic flow

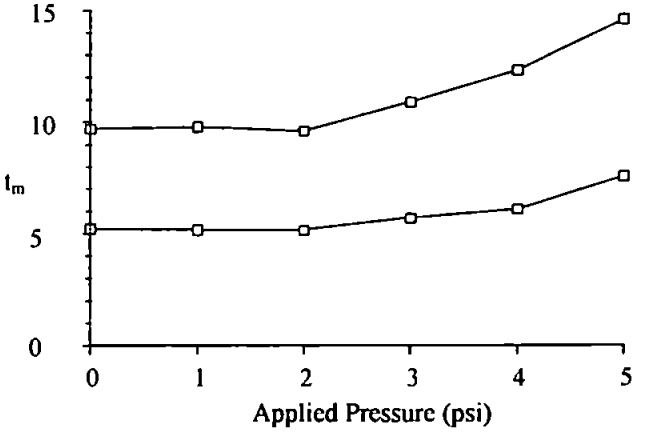

Figure 4.19 the Effect of Pressure Applied to the reaction Cell on the Migration Time of Copper and the Electroosmotic Flow in a Voltage Driven System

generated in the reaction capillary.

The pressure applied to the reaction cell was not found to be overly critical provided pressures of less than 2 psi are used. If higher pressures are used a compensating pressure must be applied to the inlet of the separation capillary to prevent laminar flow in the separation capillary. A certain amount of laminar flow is inevitable in the reaction capillary, even when low pressures were used. However, this did not appear to adversely affect the peak efficiency, probable due to the increased speed of the sample zones as they transit the detection window.

4.4.6. Limits of Detection.

The calibration range of this system was found to be linear over two orders of magnitude, which was narrower than that found with the detection of pre formed complexes. Figure 4.20 shows a calibration curve for nickel, cadmium and cobalt from 0.1mg l^{-1} to 10mg l^{-1}.

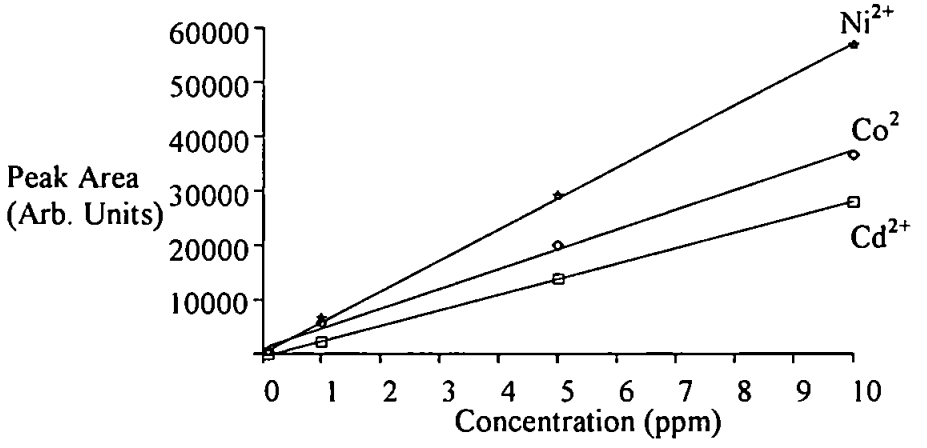

Figure 4.20. Calibration of Ni^{2+}, Co^{2+} and Cd^{2+} from 0.1 to 1.0 mg l^{-1}.

In the post-capillary system, the linear range and the limits of detection were found to be highly dependent on the concentration of the post-column reagent. To ensure an excess of reagent for the complexation reaction relatively high concentrations of reagent were used which produced an increased contribution to the background

absorption. Large negative intercepts were noted in the lower concentration metal calibrations when high concentration reagents were used. These negative intercepts were noted to decrease when the concentration of the post-capillary reagent was reduced. Consequently, the gradients obtained using 5mM and 0.5 mM PAR were found to be independent. The lower reagent concentration was found to produce more sensitive determinations of the metals below the 1mg l^{-1} level. However, the separation resolution could be adversely affected when one of these metals was in a much higher concentration due to the broader and sometimes split peaks produced. Figure 4.21 shows the separation of the metals at a concentration of 0.1mg l^{-1} with a reagent concentration of 5mM.

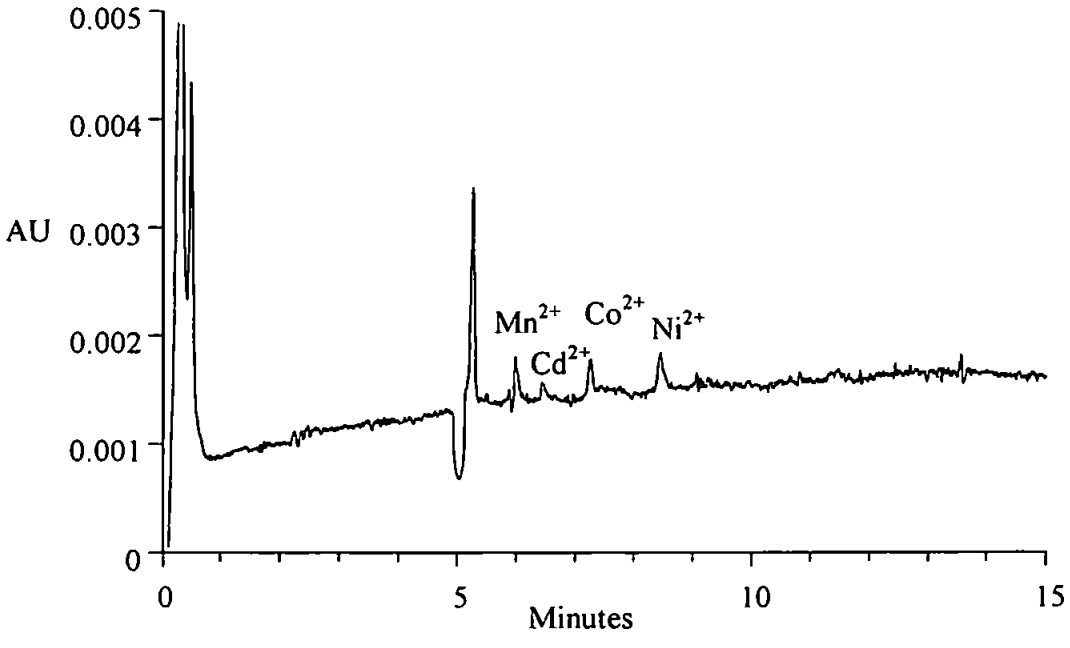

Figure 4.21. Separation of 0.1mg l^{-1} Cu^{2+}, Zn^{2+}, Mn^{2+}, Co^{2+}, Cd^{2+} and Ni^{2+}.
Separation Conditions; Electrolyte, 5mM Sodium Phosphate with 5mM oxalic acid, pH 8.6. Post Column Reagent, 5mM PAR in 5mM Sodium Phosphate, pH 8.6. Capillaries, L_{sep} 50cm L_d 55cm R_d 5cm, 100μm ID 50μm Gap. Injection, Gravity 20 seconds @ 100mm. Voltage. 15kV. Detection, 530nm

The response for copper was found to decline rapidly at concentration below 1mg l^{-1} and was not detected at 0.1mg l^{-1}, the linearity of the calibration for this metal was also found to be poor at the higher concentrations. Surprisingly Nickel could easily

be detected at a concentration of 0.1mg l^{-1} although cadmium is approaching its detection limit. Using a reagent concentration of 0.5mM the detection limit for cadmium, manganese, nickel and cobalt could be reduced to 0.05mg l^{-1}. Unfortunately, the reproducibility of the peak height and area was found to be inferior using the lower reagent concentration.

4.4.7. Pressure Driven Post-Capillary Reactor System.

By decoupling the electric field from the reaction capillary, the migration of the metal complexes is purely due to laminar flow and the mobility of the complex no longer plays a part in the separation. Since the electroosmotic flow exiting the separation capillary is able to disperse into the gap between the capillaries as well as through the reaction capillary the flow from the separation capillary must be directed towards the reaction capillary. This was achieved by the application of pressure to the reaction cell. The minimum pressure needed to prevent the flow dispersing into the cell was calculated using Equation 4.1. The value for P_{min} was calculated at 6.5 mbar (0.11psi) using 100μm internal diameter separation and reaction capillaries with lengths of 50cm and 8 cm, respectively and the electroosmotic flow generated with an applied voltage of 15kV. This equation takes into account the different flow resistances of the capillaries but does not account for restriction of flow across the membrane due to its impermeability. Although this should only become a factor when high flow rates or high pressures are involved. The equation also assumes that there is no contribution to electroosmotic flow from the membrane although this was unlikely.

The pressure applied to the junction is transmitted equally to the separation and reaction capillaries. Provided this pressure is not excessive, the electroosmotic flow exiting the separation capillary will prevent the flow of reagent into the separation capillary. The applied pressure will exert some back pressure on the separation

capillary. This back pressure superimposes a laminar flow element on the electroosmotic flow, which can retard the flow. In a pressure driven system, the introduction of the PAR is achieved by two mechanisms. Reagent flows across the membrane when pressure is applied to the cell and since the PAR is anionic; it will also be induced to migrate across the membrane electrophoretically when a voltage is applied.

The pressure system was examined using the 5mM sodium phosphate electrolyte containing 5mM oxalic acid at pH 8.6. The reaction cell was filled with the same electrolyte, which also contained 0.5mM PAR. The capillary was then grounded in the reaction cell and a series of individual metal ions injected into the capillary. An increased current was observed due to the shorter total length of the electric field necessitating a reduction in the applied voltage to 12kV.

The injection of the individual metals produced peaks for each metal with the exception of zinc, which was not detected in the time span on the electropherogram. The migration time of all the metals detected was noted to be significantly increased when compared to the voltage driven system and the peaks were noted to be broader. The increased migration times were found to be due to back pressure exerted on the separation capillary by the pressure used to prevent the dispersion of the electroosmotic flow across the membrane. Thus emphasising the need for a compensating pressure to be applied to the inlet of the separation capillary.

Broader peaks were expected with this system, owing to the lack of electroosmotic flow in the reaction capillary. Additional broadening was also expected in this system due to the loss of the stacking experienced by the increased electrophoretic velocity of the metal PAR complexes in the reaction capillary. An injection of all six of the metals failed to resolve manganese and cadmium. Cobalt and nickel were only

partially resolved and only copper separated from the other metals. Figure 4.22 shows the separation of copper, nickel and cobalt at 1mg l^{-1} and Table 4.11 shows the peak data for the electropherogram.

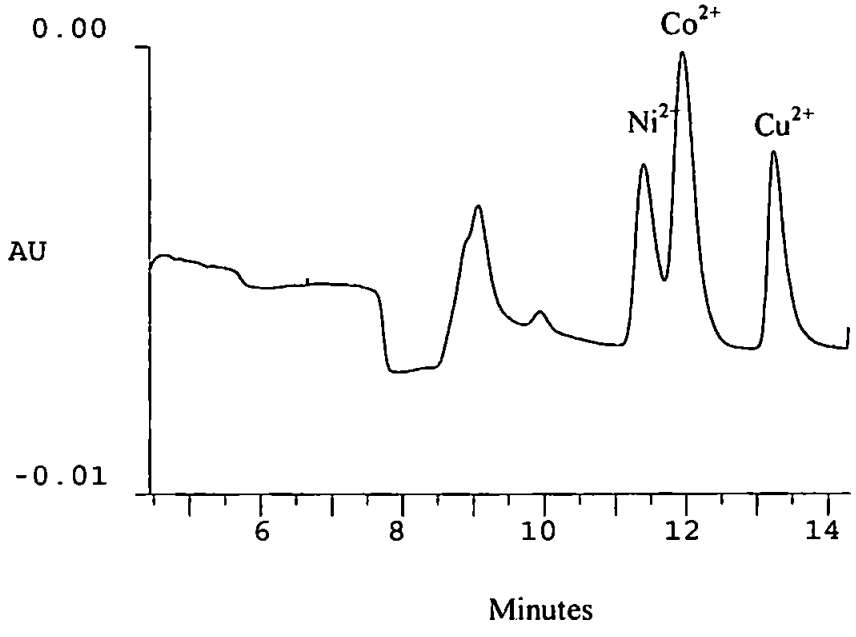

Figure 4.22. Electropherogram Showing the Separation of 1mg l^{-1} Ni^{2+}, Co^{2+} and Cu^{2+} in a Pressure Driven System.

Table 4.11. Peak data for Figure 4.22.

Metal Ion	t_m	Peak Height	Peak Area	Corrected Area	N m^{-1}
Ni^{2+}	11.4	665	12634	1108	13774
Co^{2+}	11.95	1076	22783	1906	14828
Cu^{2+}	13.23	719	11822	894	30234

During the first run using the pressure driven system it was noted that large spikes began to appear on the electropherograms after 14 minutes and with each subsequent injection these spikes began to appear earlier. Initially the spikes were spaced but with each subsequent injection, the spikes rapidly became more frequent until the electropherogram was obliterated by a 'forest' of spikes. It was noted that on leaving the instrument for extended periods between runs, the onset of the spikes could be delayed. This seemed to suggest that the problem was temperature related.

Continuous circulation of the reagent through the cell appeared to produce a slight improvement but, this was at best a temporary measure as with continued use the injected metal peaks became increasingly broadened accompanied by a severe loss in sensitivity.

Examination of the membrane revealed that the exterior had become discoloured by the PAR. The membrane was then cut longitudinally with a scalpel blade and examined under a microscope. The internal surface and interior of the membrane were found to be highly discoloured by the PAR. A capillary assembly used solely in a voltage driven system was also examined, this membrane was also found to be coated with PAR but to a much lesser extent. Although higher concentrations of PAR were used in the voltage driven system, the electrophoretic introduction of PAR across the membrane appeared to be a major factor in the adsorption of the PAR on the membrane. Washing the membrane in methanol and 1M NaOH failed to remove the PAR indicating it was firmly bound.

Once a capillary assembly had been used in a pressure system, it had to be discarded, as when the capillary was subsequently used in the electrophoretic mode the efficiency of the assembly was found to be significantly reduced. This increase in zone broadening was possibly due to some interaction between the metal ion and PAR adsorbed on the membrane.

The initial assumption was that the spikes were caused by voltage leakage, which was earthing through the detector. However, an earth leakage test showed this was not the case. It was later concluded that the spikes were due to refractive index changes caused be small gas bubbles transiting the detector window. These bubbles were thought to originate in the membrane and the mechanism of their formation was probably similar to the formation of bubbles encountered in CEC separations.

Dittman *et al.* [93] attribute the formation of bubbles to the heterogeneous nature of the capillary packings, which can lead to differences in the electroosmotic flow and localised field strengths [93]. It was thought that the situation inside the membrane was similar to that of a packed capillary. The PAR appeared to be attracted to the structure of the membrane creating a negatively charged surface with a very high surface area. It was not known whether this caused an increase or reduction in the electroosmotic flow across the membrane. A reduced flow was thought to be more likely due to the small size of the pores causing an overlap in the electrostatic double layers.

Reducing the concentration of PAR in the reagent electrolyte was found to delay the onset of the spikes although the phenomena still occurred, the spikes were more widely spaced. Decreasing the ionic strength of the reagent matrix was found to have the most significant effect on the formation of these spikes although it still did not entirely cure the problem.

4.4.8. Separation Using Glycine Electrolyte.

The addition of complexing agents to the electrolyte causes an increase in the conductivity of the electrolyte, this appears to create joule heating in the membrane resulting in the formation of bubbles in the electrolyte preventing detection of the metal complexes. A glycine (aminoacetic acid) electrolyte was investigated to examine the effect of low conductivity electrolyte on the pressure driven system using PAR. Glycine buffers in the range 8.24-10.14, it also forms complexes with the metals. The second acid dissociation value (pK_{a2}) of glycine is 9.78 and at pH values above this glycine predominantly exists as the L^- species with a mobility of -37.4 x 10^{-5} cm^2 V^{-1} s^{-1}. At pH values below the pK_{a2}, glycine exists as the zwitterionic species. The lower mobility and ionic strength of the electrolyte resulted in a

significant reduction in the conductivity, causing a corresponding increase in the electroosmotic flow. Although the residence time in the reaction capillary is reduced, the use of higher field strengths should improve the efficiency of the separation.

Glycine forms 1:1 and 1:2 complexes with the metal ions, Cd^{2+}, Co^{2+} and Mn^{2+} may also form the 1:3 complex. At pH 9, below the $pK_{a\,2}$ the metal complexes formed are shown in Equations 4.8-4.10;

$$M^{2+} + HL \rightleftharpoons MHL^{2+} \qquad \textit{Equation 4.8}$$

$$MHL^{2+} + HL \rightleftharpoons MH_2L_2^{2+} \qquad \textit{Equation 4.9}$$

$$MHL_2^{2+} + HL \rightleftharpoons MH_3L_3^{2+} \qquad \textit{Equation 4.10}$$

At pH values above the pK_{a2} value the complexes formed are given in Equations 4.11-4.13

$$M^{2+} + L^- \rightleftharpoons ML^+ \qquad \textit{Equation 4.11}$$

$$ML^+ + L^- \rightleftharpoons MHL_2 \qquad \textit{Equation 4.12}$$

$$ML_2 + L^- \rightleftharpoons MHL_3^- \qquad \textit{Equation 4.13}$$

At pH 9 the glycine was only partially ionized and the species formed with the metal ions were expected to carry a charge somewhere between the two sets of equations above.

Table 4.12. Stability Constants for Metal Glycine Complexes.

Metal ion	Log K_1	Log β_2	Log β_3
Zn^{2+}	5	9	
Cd^{2+}	4.3	7.8	10
Ni^{2+}	5.6	10.5	
Co^{2+}	4.6	8.5	10.8
Cu^{2+}	8.2	15	
Mn^{2+}	2.7	4.8	5.6

The electrolyte was made from 10mM glycine adjusted to pH 9 with sodium hydroxide. Gravity injections of the individual metals performed at a height of 100mm for a period of 20 seconds and a separation voltage of 30kV was applied across the capillary, producing a very low current of 10 μA. The PCR reagent was made from 0.1mM PAR in 10mM glycine at the same pH as that of the electrolyte and introduced across the membrane by the application of pressure to the reagent vessel.

The electroosmotic flow was measured by injecting benzyl alcohol and detected at 254 nm. An electroosmotic flow of 96.9×10^{-5} cm^2 V^{-1} s^{-1} was found which required a P_{min} of 13.9 mbar (0.2psi) which was applied to both the reagent vessel and the capillary inlet.

Injections of the individual metals produced peaks for all the metals with the migration order being Cu^{2+}, Cd^{2+} + Co^{2+}, Ni^{2+}, Zn^{2+} and Mn^{2+}. The copper peak was found to tail seriously but the cobalt, cadmium and nickel peaks were reasonably sharp, while the zinc and manganese peaks were severely broadened. The migration order was significantly different from that expected with regard to the stability constants. Manganese, which forms the weakest complex, migrated last and copper, which has the highest stability constant, migrated first. The selectivity can be explained to some extent by plotting the species distribution curves against pH using the computer program Mineql. This showed that copper predominantly forms the 1:1 complex and would be expected to have a slight positive charge. The stability constants for the complexation of manganese II with hydroxide was found to be greater than that of the glycine complex, K_1 for hydroxide 3.4 [252]. Consequently, manganese (II) was shown to exist predominantly as the hydroxide species at pH

values of 9 and 10. Zinc (II) was also noted to coordinate with hydroxide under conditions of high pH. The broad peaks observed with managanese (II) and zinc (II) were most likely to be due to wall interactions due to the weak nature of the complexes formed in this electrolyte.

An injection of a mixture of the metals, shown in Fig. 4.23 produced a separation of the metals apart from cobalt and cadmium, which were found to co-migrate. The sensitivity was expected to be relatively low due to the short residence time in the reaction capillary. However, nickel could be easily detected at a concentration of 0.5 mg l^{-1} or above.

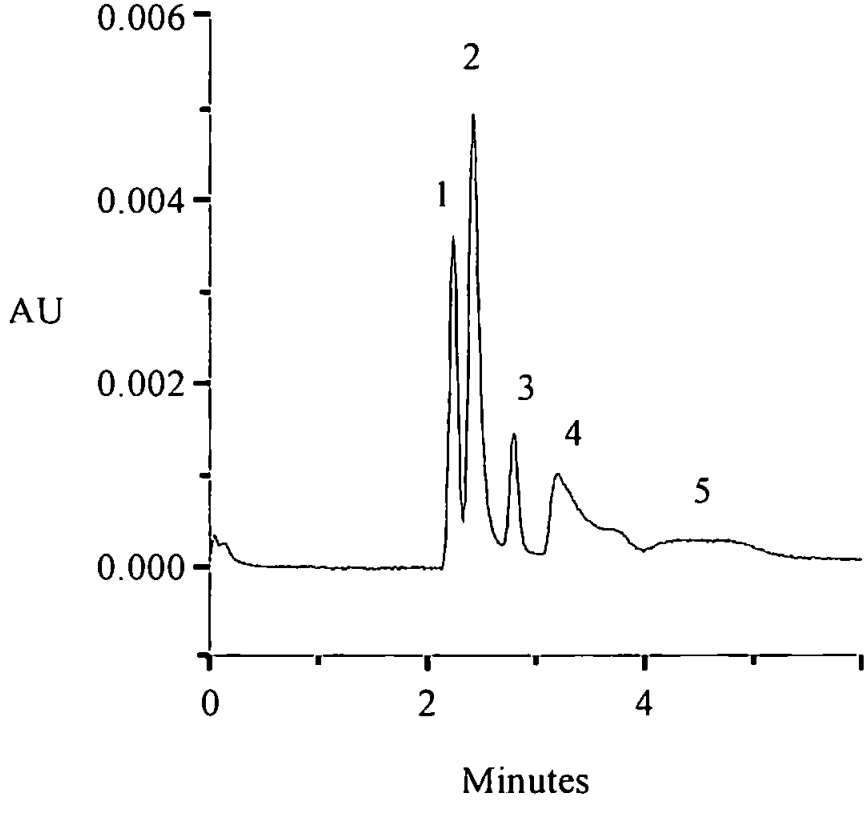

Figure 4.23. Metal Ion Separation in a Glycine Electrolyte at pH 9. Key to peak numbering; 1 Cu^{2+}, 2 Co^{2+} + Cd^{2+}, 3 Ni^{2+}, 4 Zn^{2+}, 5 Mn^{2+}, all at a concentration of 2mg l^{-1}.

At pH 9 the electroosmotic flow of the glycine buffer was at or near its maxima due to the complete ionization of the capillary wall and the low ionic strength of the

electrolyte. Increasing the electrolyte to pH 10 increases the mobility of the glycine due to its greater ionisation, which was thought may help to resolve cobalt and cadmium.

At pH 10 the electroosmotic flow was found to be slower than that observed at pH 9. This was attributed to the increase in the ionic strength of the electrolyte due to the addition of NaOH and the greater ionisation of the glycine.

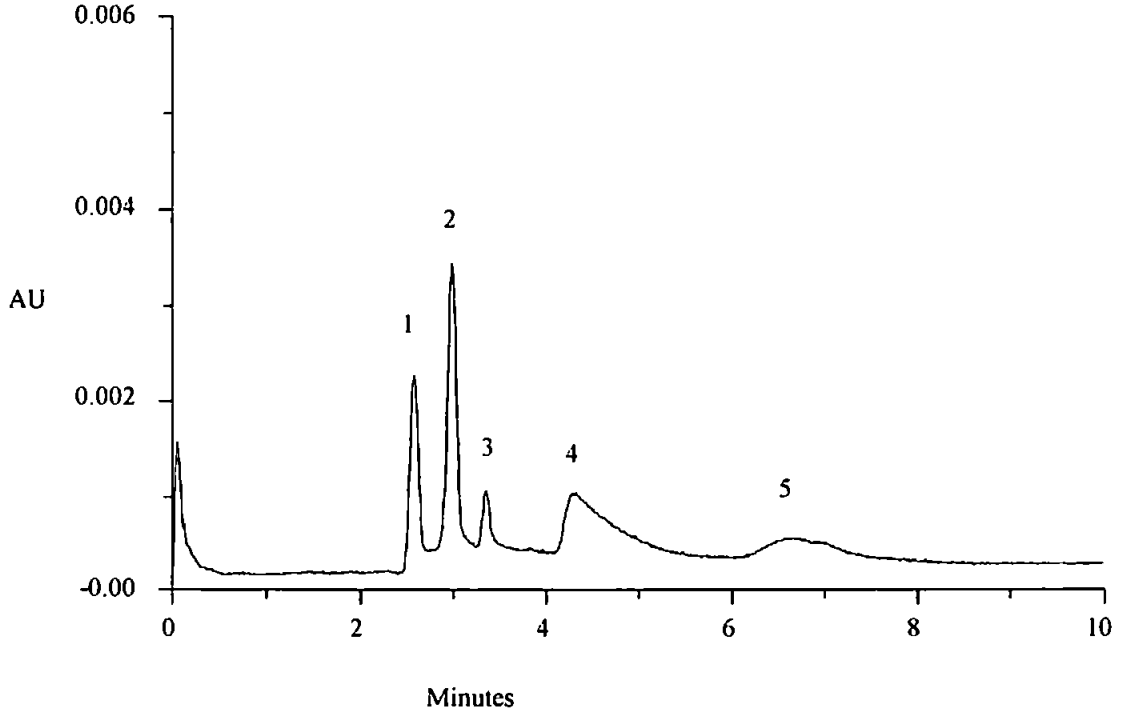

Figure 4.24. Metal Ion Separation in a Glycine Electrolyte at pH 10. Key to peak numbering; 1 Cu^{2+}, 2 Co^{2+} + Cd^{2+}, 3 Ni^{2+}, 4 Zn^{2+}, 5 Mn^{2+}, all at a concentration of 2mg l^{-1}.

Under these conditions, the migration time of the metals was increased to some extent with the greatest effect being on zinc and manganese, shown in Figure 4.24. However, cobalt and cadmium were still found to co-migrate. The peak shapes were found to remain the same with zinc and manganese excessively broadened and the tailing of the copper peak.

Table 4.13. Peak Data for the Injection of Metals in Glycine Electrolyte at pH 10

Metal Ion	Migration Time	Peak Height	Peak Area	Corrected area
Zn^{2+}	4.13	91.3	2588	629
Cd^{2+}	2.87	195	1215	423
Ni^{2+}	3.34	85	449	135
Co^{2+}	2.98	372	2943	988
Cu^{2+}	2.56	212	1478	577
Mn^{2+}	6.64	25	1948	291

4.5. Xylenol Orange Post-Capillary Reactor System.

Although PAR showed some potential as a sensitive spectrophotometric reagent in a post-capillary reactor, it was considered that it would be interesting to investigate a system where the pH was lower and the electroosmotic flow not so strong. The possibility for hydrolysis of metal ions and wall interactions should therefore be less at the lower pH. Xylenol orange is another well studied and used classical spectrophotometric reagent. It also reacts with a wide spectrum of metals, but at a lower pH than PAR, though the molar absorptivities of the xylenol orange metal complexes are significantly lower.

The optimum pH for the reaction of xylenol orange with dipositive metal ions is between 5.5 and 6. The buffer chosen for both the post-capillary and separation solutions was (N-morpholino)ethanesulphonic acid (MES). The pKa of MES is 6.1, which is ideal for use in the xylenol orange system. The fully ionised form also has a relatively low mobility of -26.8 x 10^{-5} cm^2 V^{-1} s^{-1}, which allows the use of high field strengths. As with the PAR system, a complexing acid is required in the separation electrolyte to effect the separation of the metal ions. Preliminary experiments showed that unlike the PAR system, weaker complexing acids such as tartaric acid in the separation buffer produced a response. However, the separation efficiency and detection sensitivity was poor. This can be seen in Figure 4.25(a) where cobalt and

nickel could not be resolved, though lead was well separated. Oxalic acid produced a better separation (Figure 4.25(b)), but the peaks were even broader with a consequent further loss in sensitivity. The only advantage over the PAR reagent was the response to lead, though the sensitivity was not very good.

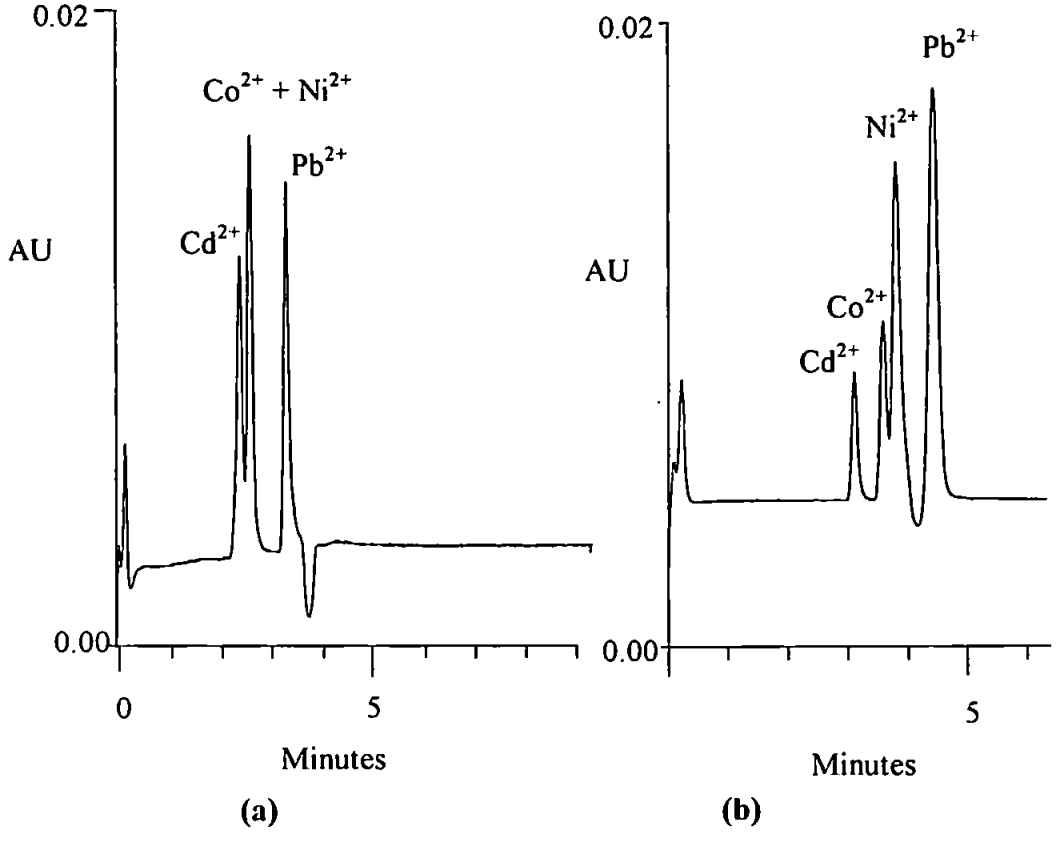

Figure 4.25. Electropherograms of the Separation of Four Metal Ions in the Xylenol Orange Post-Capillary Reactor System. (a) Separation Conditions; Electrolyte, 10mM MES and 1mM Tartaric Acid, pH 5.8; Injection, Gravity 100mm 15 second; Voltage, 30kV; Post-Capillary Reagent; 10mM MES and 0.1mM XO pH 5.8 Metal Concentrations, Cd^{2+}, Co^{2+} and Ni^{2+}, 2mg l^{-1}, Pb^{2+} 20mg l^{-1}. (b) Separation Conditions; Electrolyte, 10mM MES and 0.5mM Oxalic Acid, pH 5.8; Injection, Gravity 100mm 15 second; Voltage, 30kV; Post-Capillary Reagent; 10mM MES and 0.1mM XO pH 5.8 Metal Concentrations, Cd^{2+}, Co^{2+} and Ni^{2+}, 5mg l^{-1}, Pb^{2+} 50mg l^{-1}.

It is interesting to note the relationship between the migration times of the peaks and the electroosmotic flow marker, which again was indicated by a dip in the baseline. For tartaric acid, all four peaks come out before the electroosmotic flow marker, denoting that the tartrate complexes are positively charged, so migrate ahead of the

electroosmotic flow. When using oxalic acid, the Cd^{2+}, Ni^{2+} and Co^{2+} peaks migrate before the electroosmotic flow marker and the Pb^{2+} peak migrates after it. This shows that at the oxalic acid concentration used, only the lead oxalate complex had an overall negative charge. Increasing the concentration of oxalic acid was not investigated in any detail as both the peak shape and sensitivity worsened considerably. This also happened, although to a lesser extent, with an increase in concentration of tartaric acid. Clearly, the xylenol orange reactor is much more effected by these carboxylic acids than the PAR reactor. Presumably because the xylenol orange metal stability constants are much lower than those of PAR.

4.6. Summary.

A post-capillary reactor for capillary electrophoresis was constructed and investigated for the determination of trace metals detected as intensely coloured complexes by UV-Vis absorption. The main principle of operation is based on the infusion of the colorimetric reagent into a small 50 μm gap between the separation capillary and the reaction capillary. The gap is enclosed by a permeable membrane and the flow of reagent is aided by a slight overpressure in the post-capillary reactor cell. Careful choice of colorimetric reagent, EOF and pH was required to prevent the post-capillary reagents from migrating in the wrong direction. Two reagents were studied in detail, namely, xylenol orange (XO) and 4 (2-pyridylazo) resorcinol (PAR). The best separation and detection characteristics were obtained with PAR using oxalic acid for the separation of Cu^{2+}, Cd^{2+}, Co^{2+}, Ni^{2+}, Zn^{2+}, and Mn^{2+}. Good linear calibrations were obtained down to the 0.1ppm level for all the metals except Cu. The xylenol orange system was less sensitive than the PAR but proved useful for the separation and determination of lead (II). The lower electroosmotic flow of this system allowed the use of weaker complexing agents to effect the separation of the metals. Oxalic

acid again proved the most effective complexing agent although at a much lower concentration than in the PAR system.

Little success was made in the pressure driven mode mainly due to the adsorption of PAR onto the polysulphone membrane

CHAPTER 5.0. CONCLUSIONS AND FURTHER WORK.

5.0.1. Mercury Speciation.

Good separations were obtained for the organomercury complexes, proving that the DzS complexes degrade very little during electrophoretic migration. Neutral coated capillaries were found to be essential, as a significant electroosmotic flow prevented detection of the complexed organomercury species. The coated capillaries are also useful in reducing solute wall interactions. DzS was required in the separation electrolyte to suppress large negative intercepts in calibration curves, but did not appear to have any effect on background noise. The capillary electrophoresis method showed high sensitivity and selectivity. The day to day reproducibility of the method was excellent and good linearity was obtained from the calibrations. Very low noise levels were found emphasising the major advantage of direct over indirect absorbance detection. Detection limits were in the low $\mu g\ l^{-1}$ range and were found to be more than adequate for the study of organo mercury species in environmental and biological samples.

The DzS was successfully substituted for cysteine in the Westoo extraction procedure without any problems and the omission of a third extraction stage made the overall process more efficient and relatively simple. Good quantitative results were obtained for methyl mercury in fish flesh indicating that the method can be used, with some degree of confidence, for the analysis of methyl mercury in biological materials of marine origin. The low detection limits are sufficient to allow the technique to be applied to wide variety of marine flora and fauna to study the bioaccumulation of methyl mercury in food chains. Other environmental samples, such as natural waters and sediments should also be capable of being adapted to this capillary

electrophoresis method. The lack of a substrate and the fact that conditioning the capillary is unnecessary makes the technique potentially a viable alternative to gas chromatographic or liquid chromatographic methods.

5.0.2. Uranium.

The capillary electrophoresis determination of uranium as the Arsenazo III complex was found to be highly sensitive. A detection limit of 5 $\mu g\ l^{-1}$ was achieved using gravity injection and less than 1 $\mu g\ l^{-1}$ when using electrokinetic injection. The calibrations were found to be linear over three orders of magnitude, and returned very high correlation coefficients.

A small degree of adsorption of the Arsenazo III onto the capillary wall of the polyacrylamide coated capillaries was noted to occur with continued use. This adsorption was found to decrease the efficiency of the capillary and slightly reduced the sensitivity of the uranium- Arsenazo III complex. However, the adsorption of the dye was not found to be a serious problem with the injection of pre-formed complexes since capillaries could easily be used for several weeks before needing replacement. The adsorption of Arsenazo III was a more serious problem with on-capillary complexation. The peak efficiency of the capillaries was observed to decline rapidly with this complexation method, due to the higher concentration of dye used in the electrolyte.

Iron (III) proved a serious problem for the analysis of environmental samples due to precipitation of the iron-Arsenazo III complex in the sample vial. Alone, the precipitation of the iron would not be a serious problem, however, the uranium complex was found to co-precipitate with it. The problems of iron interference could not be overcome to such an extent that geological samples could be directly analysed without some form of sample pre-treatment. Sample pre-treatments such as pre-

concentration on an ion-exchange column may not be ideal for analysis by CE due to the resultant low pH and high ionic strength of the sample. Of the reducing agent used to decrease the interference from iron, ascorbic acid was found to produce the best results, in terms of electrolyte conductivity and interference with the uranium peak. The use of reducing agents increased the iron tolerance of the system by almost fifty times, but there was still a sample limit of 50 mg l^{-1} iron (III).

The shape of the thorium arsenazo III complex peak was too poor for quantitative analysis, although the thorium peak was well separated from uranium and did not cause interference.

The analysis of spiked tap water and mineral water samples showed good recoveries with gravity injection, indicating that the method could have some use for the analysis of relatively high ionic strength samples provided the iron (III) concentration was low. The recoveries and reproducibility of the electrokinetically injected spiked water samples was poor and this technique, although able to increase the sensitivity when injecting from very low ionic strength samples, was found to be insufficiently robust for the analysis of environmental samples.

5.0.2.1. Injection Study.

Very sensitive determinations of uranium can be achieved using electrokinetic injection. However, electrokinetic injection is less quantitative than gravity injection, being highly dependent on the ionic strength of the sample being injected. With an electrokinetic injection, the number of ions migrating into the capillary is dependent on the velocity of the ions and the injection time. Since the velocity of the ions is a function of the field strength they experience, which is itself determined by the ionic strength of the sample matrix. It can be seen that if the ionic strength of the sample

matrix between two samples is different, the number of ion migrating into the capillary with time will also be different, introducing a bias.

The quantity of ions entering the capillary is not influenced by the ionic strength of the sample with gravity injection. However, during a run, the degree of stacking with a gravity injection is dependent on the ratio of resistivities between the sample matrix and the separation electrolyte. Consequently, the ionic strength of the sample matrix influences the degree of stacking and therefore the sharpness of the peak. This reduces the peak height and diminishes the sensitivity of the separation. Since the area under the peak is influenced to a lesser extent than the peak height, the area under the peak is the more useful parameter for quantitative analysis. This is of importance when considering the injection of real samples calibrated against synthetic standards made up in matrices with ionic strengths differing from those of the sample.

Although gravity injection provided a less sensitive means of sample loading than electrokinetic injection, the technique was found to be more reproducible and resilient to high ionic strength samples than electrokinetic injection.

5.0.2.2. Capillary Study.

The use of highly absorbing organic photometric reagents provides a means of sensitive determination for metal ions. However, with very large molecules, wall adsorption and precipitation can become a problem and the choice of capillary wall chemistry is critical. In the case of the uranium-arsenazo III complex, the high stability of the complex appears to minimise wall adsorption problems, although long term use of the capillary was found to causes a reduction in sensitivity. The suitability of several capillaries with differing surface chemistries were assessed for the separation of metal ions complexed with Arsenazo III. The principal differences

between the capillaries, with the exception of the polyacrylimide, was in their degree of hydrophobicity

In this study, the polyacrylamide coated fused silica capillaries were found to produce the best results. Both the neutral hydrophilic fused silica and the PVDF capillaries produced greater sensitivity with respect to area under the peak, but in both these capillaries the peak height and efficiency was lower than that obtained from the polyacrylamide capillaries. The broadening of the peaks was most marked in the neutral hydrophilic capillaries, which was unexpected since hydrophobic interactions were predicted. PVDF is extremely hydrophobic yet still produced slightly broader peaks than the polyacrylamide.

The polystyrene capillaries returned poor results with a significant increase in migration time and a marked reduction in sensitivity. It was suspected that the electrostatic nature of the capillaries when exposed to an applied electric field was causing strong interactions with the capillary walls.

The polyacrylimide capillaries produced no results presumably due to charge related adsorption of the Arsenazo III.

The polymeric capillaries proved difficult to handle and required considerable care when inserting into the instrument to prevent distortion of the tubular shape. Polystyrene capillaries required an insulating shield to prevent them from coming into contact with the instrument, but even when shielded, earthing through the detector produced noise on the electropherogram. Fused silica capillaries were found to be more suited to the instrument, which required a degree of stiffness to install the capillaries and the internal diameter of these capillaries is more constant than that of polymeric capillaries.

The adsorption of the solutes on the capillary wall appears to be more complicated than just simple phase related adsorption and the choice of wall chemistry can have a significant effect on the sensitivity of a separation method. The choice of polyacrylamide coated capillaries appeared to provide a reasonable compromise between the different wall adsorption mechanisms producing the sharpest peaks of all the capillaries tested.

2.0.3. Post-Capillary Reactor.

The principle of using a small inter-capillary gap surrounded by a permeable membrane to introduce the colorimetric reagent worked successfully, though a slight overpressure was required to ensure a reproducible flow into the reaction capillary. The fabrication of a demountable cell was particularly convenient as the capillary assemblies could be changed when necessary, though some care was needed in the installation of the capillary assembly. Grounding the electrode at the end of the reaction capillary rather than in the reaction cell gave the best results, showing that an electroosmotic flow right through to the detector window was required to keep peak broadening to a minimum. As anticipated, PAR gave the most sensitive reaction for most of the metal ions studied. However, some results were unexpected, such as the broadness of the zinc peak and non-linear calibration for copper. The poorer results for xylenol orange could be due to the lower stability of the metal complexes resulting in more dissociation, i.e. more peak dispersion in the reaction capillary, before reaching the detection window.

5.1 Further Work.

Sensitivity can be a problem in the capillary electrophoresis determination of trace metals. Due to the dependence on the ionic strength of the sample matrix, samples

should ideally be in low ionic strength matrices to achieve the greatest sensitivity. One of the major reasons for the high sensitivity of the methyl mercury method is due to the solvent extraction of the methyl mercury. This effectively removes other ionic constituents from the sample and leaves the methyl mercury in a very low ionic strength matrix, which is ideal for analysis by capillary electrophoresis. The dependence on the ionic strength of the sample matrix does not make capillary electrophoresis the ideal method for the routine determination of metal ions in all environmental samples. However, the technique has proved very useful in a few niche areas of analysis, such as the analysis of mercury in biological samples.

Further investigation is required into the direct detection of trace metals using different chelating agents for specific tasks. This will probably involve sample pre-treatment methods to extract the analytes from complex matrices. Such techniques can then leave the sample in low ionic strength matrices.

Further investigation into the post-capillary reactor in the pressure driven mode is needed, particularly should a different membrane, such as PTFE become available.
A limited number of dyes were investigated in the voltage driven post-capillary reaction system, other reagents could prove interesting. Dithizone, although insoluble at lower pH values can be dissolved in an aqueous electrolyte with the aid of a surfactant such as polyoxyethylene tert-octylphenol (Triton X-100) [253]. The advantages of this reagent are that it forms coloured complexes with a wide range of metals. At low pH, it does not contribute to the ionic strength of the electrolyte and would not migrate electrophoretically across the membrane in the pressure driven mode. The insolubility of the metal-dithizone complexes should not be a problem

since these should also partition into the micelle. With this method, all the complexes should pass the detector window with uniform velocity, which would be purely attributable to the electroosmotic flow.

A further step in the development of the post-capillary reactor could make use of chemiluminescence. A simple reactor based on a coaxial flow system, such as the insertion of a 375μm OD capillary into a short section of 500μm ID gas chromatography megabore capillary. This should provide a reasonable compromise between the free solution reactor [234, 254] and the more complex coaxial system developed by Nickerson and Jorgensen [235].

In such a system, the flow of reagent into the reaction capillary can be achieved by a small 'T' bonded to the separation and reaction capillaries, with a low volume flow of reagent pumped into the reaction capillary through the 'T'. The lower flow resistance of the reaction capillary, due to its larger internal diameter, should ensure that the reagent flow is directed away from the separation capillary. The flow of reagent should ensure a constantly replenished supply of reagent at the separation capillary exit and the turbulence caused by the blunt separation capillary tip should aid mixing of the solute and reagent. Many chemiluminescent reactions are very fast and will take place at or close to the separation capillary exit. Therefore mixing is an important factor to ensure a high proportion of the analyte reacts with the reagent during its passage past the detector window.

Chemiluminescent detection on the CES 1 can be achieved either using the fluorescence photomultiplier supplied with the instrument, or alternatively, the photodiodes of the UV/Vis absorption detector can be used as these will still function with the light sources switched off.

Grounding of the electrode prior to the reaction capillary can be accomplished using a PTFE joint as described by Oshea *et al.* [255]. Grounding the electrode prior to the reaction capillary overcomes several obstacles. Since electrophoresis does not take place in the reaction capillary, the migration of the analytes and reagent is no longer of concern. As a result, the charge and mobility of the reagent should not matter. In addition, there is no requirement to match the conductivities of the separation electrolyte and the chemiluminescent reagent to maintain a constant electroosmotic flow. The pH and ionic strength of the reagent are independent of the separation electrolyte allowing the separation and reaction to take place under ideal conditions.

The post-capillary chemiluminescence system could be applied to a luminol/H_2O_2 system for the detection of transition metals. The mixing of the luminol and H_2O_2 can be simply accomplished via a 'T' connection in the reagent delivery line, close to the point of entry to the reaction capillary. Alternatively, the system could be applied to a ruthenium (II) tris(2,2′-bipyridine) system. The chemiluminescent reaction is produced by the reduction of the $Ru(bpy)_3^{3+}$ ion to $Ru(bpy)_3^{2+}$. Although the $Ru(bpy)_3^{3+}$ ion is unstable in aqueous solution it can be generated in-line by the oxidation of the stable $Ru(bpy)_3^{2+}$ion, by the insertion of a column packed with PbO_2 into the reagent delivery line.

A ruthenium (II) tris(2,2′-bipyridine) system could be applied to the detection of morphine analogues separated by capillary electrophoresis [256].

REFERENCES.

1. L. Michaelis, *Biochem.Z.*, 16 (1909) 81.

2. A.T. Andrews, *Electrophoresis: Theory, Techniques and Biochemical and Clinical Applications.* Clarendon Press, (1981).

3. A. Chambach, *The Practice of Quantitative Gel Electrophoresis*, VCH, 1985.

4. S. Hjerten, *Chromatogr.Rev.*, 9 (1967) 122.

5. F.E.P. Mikkers, F.M. Everaerts and T.P.E.M. Verheggen, *J. Chromatogr.*, 169 (1979) 11.

6. J.W. Jorgenson and K.D. Lukacs, *Anal. Chem.*, 53 (1981) 1298.

7. R.J. Hunter, in *Zeta Potential in Colloidal Sciences*, Academic Press, (1981), p. 11.

8. T.L. Huang, *Chromatographia*, 35 (1993) 395.

9. W.J. Lambert and D.L. Middleton, *Anal. Chem.*, 62 (1990) 1585.

10. F.E.P. Mikkers, F.M. Everaerts and T.P.E.M. Verheggen, *J. Chromatogr.*, 169 (1979) 1.

11. O.V. Krokhin, H. Hoshino, O.A. Shpigun and T. Yotsuyanagi, *Poster presented at IICS96*, (1996)

12. O.V. Krokhin, H. Hoshino, O.A. Shpigun and T. Yotsuyanagi, *J. Chromatogr. A*, 776 (1997) 329.

13. O.V. Krokhin, H. Hoshino, O.A. Shpigun and T. Yotsuyanagi, *J. Chromatogr. A*, 772 (1997) 339.

14. W. Buchberger and P.R. Haddad, *J. Chromatogr.*, 608 (1992) 59.

15. N. Iki, H. Hoshino and T. Yotsuyanagi, *Chem. Lett.*, (1993) 701.

16. S.V. Ermakov, M.Y. Zhukov, L. Capelli and P.G. Righetti, *J. Chromatogr. A*, 699 (1995) 297.

17. M. Chiari, M. Nesi and P.G. Righetti, *Capillary Electrophoresis in Analytical Biotechnology*, CRC Press, Boca Raton. FL, 1996.

18. K. Salomon, D.S. Burgi and J.C. Helmer, *J. Chromatogr.*, 559 (1991) 69.

19. A.M. Dougherty, N. Cooke and P. Shieh, in J.P. Landers (Editor), *Handbook of Capillary Electrophoresis*, CRC Press, Inc., (1997), p. 675.

20. A. Fridstrom, K.E. Markides and M.L. Lee, *Chromatographia*, 41 (1995) 295.

21. P.Z. Liu, A. Malik, M.C.J. Kuchar, W.P. Vorkink and M.L. Lee, *J. Microcol. Sep.*, 5 (1993) 245.

22. X.L. Ren, P.Z. Liu, A. Malik and M.L. Lee, *J. Microcol. Sep.*, 8 (1996) 535.

23. M. Thorsteinsdottir, R. Isaksson and D. Westerlund, *Electrophoresis*, 16 (1995) 557.

24. M. Macka, P. Nesterenko, P. Andersson and P.R. Haddad, *J. Chromatogr. A*, 803 (1998) 279.

25. J.K. Towns and F.E. Regnier, *Anal. Chem.*, 63 (1991) 1126.

26. R.W. Chiu, J.C. Jimenez and C.A. Monnig, *Anal. Chim. Acta*, 307 (1995) 193.

27. E. Cordova, J.M. Gao and G.M. Whitesides, *Anal. Chem.*, 69 (1997) 1370.

28. N. Cohen and E. Grushka, *J. Chromatogr. A*, 678 (1994) 167.

29. D. Corradini, G. Cannarsa, E. Fabbri and C. Corradini, *J. Chromatogr. A*, 709 (1995) 127.

30. S. Hjerten, *J. Chromatogr.*, 347 (1985) 191.

31. K.A. Cobb, V. Dolnik and M. Novotny, *Anal. Chem.*, 62 (1990) 2478.

32. J. Kohr and H. Engelhardt, *J. Microcol. Sep.*, 3 (1991) 491.

33. D. Schmalzing, C.A. Piggee, F. Foret, E. Carrilho and B.L. Karger, *J. Chromatogr. A*, 652 (1993) 149.

34. M.X. Huang, W.P. Vorkink and M.L. Lee, *J. Microcol. Sep.*, 4 (1992) 233.

35. M.X. Huang, E. Dubrovcakovaschneiderman and M.V. Novotny, *J. Microcol. Sep.*, 6 (1994) 571.

36. A. Cifuentes, M. Defrutos, J.M. Santos and J.C. Diezmasa, *J. Chromatogr. A*, 655 (1993) 63.

37. M. Chen and R.M. Cassidy, *J. Chromatogr.*, 602 (1992) 227.

38. M. Chiari, M. Nesi, J.E. Sandoval and J.J. Pesek, *J. Chromatogr. A*, 717 (1995) 1.

39. S. Hjerten and K. Kubo, *Electrophoresis*, 14 (1993) 390.

40. J.L. Liao, J. Abramson and S. Hjerten, *J. Cap. Elect.*, 2 (1995) 191.

41. M.X. Huang, J. Plocek and M.V. Novotny, *Electrophoresis*, 16 (1995) 396.

42. G.J.M. Bruin, R. Huisden, J.C. Kraak and H. Poppe, *J. Chromatogr.*, 480 (1989) 339.

43. M. Chiari, N. Dellorto and A. Gelain, *Anal. Chem.*, 68 (1996) 2731.

44. J.T. Smith and Z. Elrassi, *Electrophoresis*, 14 (1993) 396.

45. D.M. Whynot, R.A. Hartwick and S. Bane, *J. Chromatogr. A*, 767 (1997) 231.

46. Y. Mechref and Z. Elrassi, *Electrophoresis*, 16 (1995) 617.

47. P. Sun, A. Landman, G.E. Barker and R.A. Hartwick, *J. Chromatogr. A*, 685 (1994) 303.

48. C.L. Ng, H.K. Lee and S.F.Y. Li, *J. Chromatogr. A*, 659 (1994) 427.

49. N. Iki and E.S. Yeung, *J. Chromatogr. A*, 731 (1996) 273.

50. J.K. Towns, J.M. Bao and F.E. Regnier, *J. Chromatogr.*, 599 (1992) 227.

51. G.J.M. Bruin, J.P. Chang, R.H. Kuhlman, K. Zegers, J.C. Kraak and H. Poppe, *J. Chromatogr.*, 471 (1989) 429.

52. M.X. Huang, W.P. Vorkink and M.L. Lee, *J. Microcol. Sep.*, 4 (1992) 135.

53. Z.X. Zhao, A. Malik and M.L. Lee, *J. Microcol. Sep.*, 4 (1992) 411.

54. Z.X. Zhao, A. Malik and M.L. Lee, *Anal. Chem.*, 65 (1993) 2747.

55. X.L. Ren, Y.F. Shen and M.L. Lee, *J. Chromatogr. A*, 741 (1996) 115.

56. W. Nashabeh and Z. Elrassi, *J. Chromatogr.*, 559 (1991) 367.

57. M. Gilges, M.H. Kleemiss and G. Schomburg, *Anal. Chem.*, 66 (1994) 2038.

58. J.K. Towns and F.E. Regnier, *J. Chromatogr.*, 516 (1990) 69.

59. F.B. Erim, A. Cifuentes, H. Poppe and J.C. Kraak, *J. Chromatogr. A*, 708 (1995) 356.

60. Q.C. Liu, F.M. Lin and R.A. Hartwick, J. Liq. Chromatogr., 20 (1997) 707.

61. Q.C. Liu, F.M. Lin and R.A. Hartwick, *J. Chromatogr. Sci.*, 35 (1997) 126.

62. M.X. Huang, G.L. Yi, J.S. Bradshaw and M.L. Lee, *J. Microcol. Sep.*, 5 (1993) 199.

63. C.S. Chiou and J.S. Shih, *Analyst*, 121 (1996) 1107.

64. P. Sun, A. Landman and R.A. Hartwick, *J. Microcol. Sep.*, 6 (1994) 403.

65. K.Z. Cheng, Z.X. Zhao, R. Garrick, F.R. Nordmeyer, M.L. Lee and J.D. Lamb, *J. Chromatogr. A*, 706 (1995) 517.

66. J.T. Smith and Z. Elrassi, *J. High Res. Chromatogr.*, 15 (1992) 573.

67. Y. Guo, G.A. Imahori and L.A. Colon, *J. Chromatogr. A*, 744 (1996) 17.

68. P.Z. Liu, A. Malik, M.C.J. Kuchar and M.L.Lee, *J. Microcol. Sep.*, 6 (1994) 581.

69. X.L. Ren, P.Z. Liu and M.L. Lee, *J. Microcol. Sep.*, 8 (1996) 529.

70. H. Bayer and H. Engelhardt, *J. Microcol. Sep.*, 8 (1996) 479.

71. H.W. Zhang, X.G. Chen and Z.D. Hu, *J. Chromatogr. A*, 677 (1994) 159.

72. E.N. Fung and E.S. Yeung, *Anal. Chem.*, 67 (1995) 1913.

73. D.S. Burgi and R.L. Chien, *J. Microcol. Sep.*, 3 (1991) 199.

74. D.S. Burgi and R.L. Chien, *Anal. Chem.*, 63 (1991) 2042.

75. D.S. Burgi and R.L. Chien, *Anal. Biochem.*, 202 (1992) 306.

76. R.L. Chien and D.S. Burgi, *J. Chromatogr.*, 559 (1991) 153.

77. R.L. Chien and D.S. Burgi, *J. Chromatogr.*, 559 (1991) 141.

78. R.L. Chien and D.S. Burgi, *Anal. Chem.*, 64 (1992) 1046.

79. F.B. Regan, M.P. Meaney and S.M. Lunte, *J. Chromatogr. B*, 657 (1994) 409.

80. T. Saitoh, H. Hoshino and T. Yotsuyanagi, *J. Chromatogr.*, 469 (1989) 175.

81. D.F. Swaile and M.J. Sepaniak, *Anal. Chem.*, 63 (1991) 179.

82. S. Motomizu, M. Oshima, M. Kuwabara and Y. Obata, *Analyst*, 119 (1994) 1787.

83. M. Macka, B. Paull, P. Andersson and P.R. Haddad, *J. Chromatogr. A*, 767 (1997) 303.

84. K. Terabe, K. Otsuka, K. Ichikawa, A. Tsuchiya and T. Ando, *Anal. Chem.*, 56 (1984) 111.

85. S. Hjerten and M. Zhu, *J. Chromatogr.*, 346 (1985) 265.

86. S.M. Chen and J.E. Wiktorowicz, *Anal. Biochem.*, 206 (1992) 84.

87. S. Hjerten, J.L. Liao and K. Yao, *J. Chromatogr.*, 387 (1987) 127.

88. V. Pretorius, B.J. Hopkins and J.D. Schieke, *J. Chromatogr.*, 99 (1974) 23.

89. J.H. Knox and I.H. Grant, *Chromatographia*, 32 (1991) 317.

90. R.J. Boughtflower, T. Underwood and C.J. Paterson, *Chromatographia*, 40 (1995) 329.

91. C. Fujimoto, Y. Fujise and E. Matsuzawa, *Anal. Chem.*, 68 (1996) 2753.

92. G. Ross, M. Dittmann, F. Bek and G. Rozing, *American Laboratory*, March (1996) 34.

93. M.M. Dittmann, K. Wienand, F. Bek and G.P. Rozing, *LC-GC*, 13 (1995) 800.

94. R.G. Pearson, The HSAB Principle, Ch.1in *Chemical Hardness*, Wiley-VCH, Weinheim, (1997), p. 1-27

95. R.G. Pearson, in *Chemical Hardness*, Wiley-VCH, Weinheim, (1997), p. 3.

96. R.G. Pearson, in *Chemical Hardness*, Wiley-VCH, Weinheim, (1997), p. 4.

97. A. Ringbom, *Complexation in Analytical Chemistry*, John Wiley & Sons, (1963), p. 24.

98. A. Ringbom, *Complexation in Analytical Chemistry*, John Wiley & Sons, (1963), p. 35

99. A. Ringbom, *Chemical Analysis*, Clarendon Press, Oxford, (1977).

100. F. Foret, S. Fanali, A. Nardi and P. Bocek, *Electrophoresis*, 11 (1990) 780.

101. P. Jandik and W.R. Jones, *J. Chromatogr.*, 546 (1991) 431.

102. Y.C. Shi and J.S. Fritz, *J. Chromatogr. A*, 671 (1994) 429.

103. J.M. Riviello and M.P. Harrold, *J. Chromatogr. A*, 652 (1993) 385.

104. Q. Yang, M. Jimidar, T.P. Hamoir, J. Smeyersverbeke and D.L. Massart, *J. Chromatogr. A*, 673 (1994) 275.

105. E. Simunicova, D. Kaniansky and K. Loksikova, *J. Chromatogr. A*, 665 (1994) 203.

106. W.R. Barger, R.L. Mowery and J.R. Wyatt, *J. Chromatogr. A*, 680 (1994) 659.

107. M. Chen and R.M. Cassidy, *J. Chromatogr.*, 640 (1993) 425.

108. W. Beck and H. Engelhardt, *Fres. J. Anal. Chem.*, 346 (1993) 618.

109. C. Vogt and G. Werner, *J. Chromatogr. A*, 686 (1994) 325.

110. L. Gross and E.S. Yeung, *Anal. Chem.*, 62 (1990) 427.

111. K. Bachmann, J. Boden and I. Haumann, *J. Chromatogr.*, 626 (1992) 259.

112. P.L. Desbene, C.J. Morin, A.M.D. Monvernay and R.S. Groult, *J. Chromatogr. A*, 689 (1995) 135.

113. T. Saitoh, H. Hoshino and T. Yotsuyanagi, *Anal. Sci.*, 7 (1991) 495.

114. Y. Chen, J.V. Holtje and U. Schwarz, *J. Chromatogr. A*, 680 (1994) 63.

115. A.R. Timerbaev, W. Buchberger, O.P. Semenova and G.K. Bonn, *J. Chromatogr.*, 630 (1993) 379.

116. K. Saitoh, C. Kiyohara and N. Suzuki, *J. High Res. Chromatogr.*, 14 (1991) 245.

117. K. Saitoh, C. Kiyohara and N. Suzuki, *Anal. Sci.*, 7 (1997) 269.

118. A.R. Timerbaev, O.P. Semenova, G.K. Bonn and J.S. Fritz, *Anal. Chim. Acta*, 296 (1994) 119.

119. A.R. Timerbaev, O.P. Semenova and G.K. Bonn, *Analyst*, 119 (1994) 2795.

120. A.R. Timerbaev, O.P. Semenova, P. Jandik and G.K. Bonn, *J. Chromatogr. A*, 671 (1994) 419.

121. N. Iki, H. Hoshino and T. Yotsuyanagi, *J. Chromatogr. A*, 652 (1993) 539.

122. M. Aguilar, X.H. Huang and R.N. Zare, *J. Chromatogr.*, 480 (1989) 427.

123. W. Buchberger, O.P. Semenova and A.R. Timerbaev, *J. High Res. Chromatogr.*, 16 (1993) 153.

124. I. Medina, E. Rubi, M.C. Mejuto and R. Cela, *Talanta*, 40 (1993) 1631.

125. W. H. Schroeder, *Trends Anal. Chem.*, 8 (1989) 339.

126. E. Merian, *Metals and Their Compounds in the Environment*, VCH Verlagsgellschaft, Weinheim, (1991).

127. O. F. X. Donard and P. Quevauviller, *Mikrochim. Acta.*, 109 (1992) 1-3

128. W.F. Fitzgerald and R.P. Mason, in A. Sigel and H. Sigel (Editors), *Mercury and its Effects on Environment and Biology*, Marcel Dekker, Inc., New York, (1997), p. 52.

129. J.A. Dean, *Lange's Handbook of Chemistry*, McGraw-Hill, Inc., New York, (1992).

130. J.E. Huheey, in *Inorganic Chemistry: Principles of Structure and Reactivity*, Harper Collins, (1983), p. 286.

131. F. Baldi, in A. Sigel and H. Sigel (Editors), *Mercury and its Effects on Environment and Biology*, Marcel Dekker, Inc., New York, (1997), p. 213.

132. R.P. Mason and W.F. Fitzgerald, *Deep-sea Res.*, 40 (1993) 1897.

133. G. Compeau and R. Bartha, *Appl. Environ. Microbiol.*, 50 (1985) 498.

134. S.C. Choi and R. Bartha, *Appl. Environ. Microbiol.*, 59 (1993) 290.

135. M.R. Winfrey and J.W.M. Rudd, *Environ. Toxicol. Chem.*, 9 (1990) 853.

136. L. Xun, N.E.R. Campbell and J.W.M. Rudd, *Can. J. Fish Aquat. Sci.*, 44 (1987) 750.

137. A. Furantani and J.W.M. Rudd, *Appl. Environ. Microbiol.*, 40 (1980) 770.

138. D.W. Schindler, R.H. Hesslein, R. Wagemann and W.S. Broecker, *Can. J. Fish Aquat. Sci.*, 37 (1980) 373.

139. P.S. Ramlal, J.W.M. Rudd, A. Furantani and L. Xun, *Can. J. Fish Aquat. Sci.*, 42 (1985) 685.

140. S.M. Callister and M.R. Winfrey, *Water, Soil, Air, Pollut.*, 29 (1986) 453.

141. H. Nagase, Y. Ose, T. Sato and T. Ishikawa, *Sci. Tot. Env.*, 32 (1984) 147.

142. Y.H. Lee, H. Hultberg and I. Anderson, *Water, Soil, Air, Pollut.*, 25 (1985) 391.

143. N.S. Bloom and C.J. Watras, *Sci. Tot. Env.*, 87/88 (1989) 199.

144. V.L. St.Louis, J.W.M. Rudd, C.A. Kelly and L. Barrie, *Water, Soil, Air, Pollut.*, 80 (1995) 405.

145. N.S. Bloom, *Can. J. Fish Aquat. Sci.*, 49 (1992) 1010.

146. A. Boudou and F. Ribeyre, in A. Sigel and H. Sigel (Editors), *Mercury and its Effects on Environment and Biology*, Marcel Dekker, Inc., New York, (1997), p. 289.

147. J.J. Gutkneckt, *Membrane Biol.* , 61 (1981) 61.

148. R.P. Mason, J.R. Reinfelder and F.M.M. Morel, *Water, Soil, Air, Pollut.*, 80 (1995) 915.

149. Inspection Branch, Dept. of Fisheries and Forestry, Ottawa (1971).

150. R. Puk and J. H. Weber, *Appl. Organomet. Chem.*, 8 (1994) 303.

151. L. Magos, *Analyst (London)*, 96 1971) 847.

152. W. Baeyens and M. Leermakers, *J. Anal. At. Spectrom.*, 4 (1989) 635.

153. M. Horvat, V. Lupsina and B. Pihlar, *Anal. Chim. Acta.*, 243 (1991) 71.

154. E. Temmerman, C. Vandecasteele, G. Vermeir, R. Leyman and R. Dams, *Anal. Chim. Acta.*, 236 (1990) 371.

155. C. E. Oda and J. D. Ingle jr., *Anal. Chem.*, 53 (1981) 2305.

156. M. R. Rendez, R. C. Comp and A. J. Curtius, *J. Anal. Atom. Spectrom.*, 8 (1993) 247.

157. G. Westöö, *Acta. Chem. Scand.*, 20 (1966) 2131.

158. G. Westöö, *Acta. Chem. Scand.*, 21 (1967) 1790.

159. E. Bulska, D. C. Baxter and W. Frech, *Anal. Chim. Acta.*, 249 (1991) 545.

160. J. E. O'Reilly, *J. Chromatogr.*, 238 (1982) 433.

161. E. Rubí, R. A. Lorenzo, C. Casais, A. M. Carro and R. Cela, *J. Chromatogr.*, 605 (1992) 69.

162. O. Evans and G. D. McKee, *Analyst (London)*, 113 (1988) 243.

163. C. W. Huang and S. J. Jiang, *J. Anal. At. Spectrom.*, 8 (1993) 681.

164. C. Schicking and J. A. C. Broekaert, *Appl. Organomet. Chem.*, 9 (1995) 29.

165. J. Bettmer, K. Cammann and M. Robecke, *J. Chromatogr. A*, 654 (1993) 177.

166. D. Fabbri, M. Lombardo, C. Trombini and I Vassura, *Appl. Organomet. Chem.*, 9 (1995) 713.

167. E.P.C. Lai and E. Dabekzlotorzynska, *Am. Environ. Lab.*, 6 (1996) 5.

168. A.M. Carro-Díaz, R.A. Lorenzo-Ferreira and R. Cela-Torrijos, *J.Chromatogr. A*, 730 (1996) 345.

169. A.M. Carro-Díaz, R.A. Lorenzo-Ferreira and R. Cela-Torrijos, *Mikrochim. Acta*, 123 (1996) 73.

170. P. Jones and G. Nickless, *Analyst (London)*, 103 (1978) 1121.

171. H. Tanaka, M. Chikuma, M. Harada and T. Ueda, *Talanta*, 23 (1976) 489.

172. W.R. Jones and P. Jandik, *J. Chromatogr.*, 546 (1991) 445.

173. M.P. Harrold, M.J. Wojtusik, J. Riviello and P. Henson, *J. Chromatogr.*, 640 (1993) 463.

174. H. Wätzig, *J. Chromatogr. A*, 700 (1995) 1.

175. World Health Authority, *Methylmercury*, Environmental Health Criteria 101, WHO, Geneva, (1990).

176. C.T. Driscoll, C. Yan, C.L. Scofield, R. Munsen and J. Holsapple, *Environ. Sci. Technol.*, (1994), 28, 136A.

177. I. Drabaek and V.Carlsen *Int. J. Environ. Anal. Chem.*, (1984), 17, 231.

178. S. E. Long, *Uranium and Human Diet: a Literature Review*. United Kingdom Atomic Energy Authority, Harwell, (1987).

179. D. Ayres and D. Hellier, *Dictionary of Environmentally Important Chemicals*, Blackie Academic and Professional, London, (1988).

180. Technical Reports Series, 284, *Geochemical Exploration of Uranium*, International Atomic Energy Agency, Vienna, (1988)

181. J.D. Lee, *Concise Inorganic Chemistry*, Chapman and Hall, London, Fifth Edition, (1996) p891.

182. R. W. Fairbridge, *Encyclopedia Of Oceanography*, Van Nostrand Reinhold, New York, (1996), p732.

183. B.M.R. Green, L. Brown, K.D. Cliff, C.M.H. Driscoll, J.C.H. Miles and A.D. Wrixon, *Sci. Tot. Env.*, 15 (1985) 459.

184. E.I. Hamilton, *Health.Phys.*, 22 (1972) 149.

185. A.W.H. Aten, J.W. Dalenberg and W.C.M. Bakkum, *Health.Phys.*, 5 (1961) 225.

186. G.A. Welford and R. Baird, *Health.Phys.*, 13 (1967) 1321.

187. P. Henderson, *Inorganic Geochemistry*, Pergamon Press Ltd., Oxford, UK, First Edition, (1982).

188. A. G. Sharpe, Inorganic Chemistry, Longman Group Ltd., Essex, UK, Third Edition, (1991) p672.

189. T. Yoshino, H. Imada, S. Murakami and M. Kagawa, *Talanta*, **21**, (1974), 211.

190. A. Bermejobarrera, M.C. Yebrabiurrun and L.M. Fragatrillo, *Anal. Chim. Acta*, 239 (1990) 321.

191. G.M. Ritcey, *Sep. Sci. Technol.*, 18 (1983) 1617.

192. M. Rehkamper, *Chem. Geol.*, 119 (1995) 1.

193. J.A. Perez-Bustamante and J.A. Delgado, *Analyst*, 96 (1971) 407.

194. P. Pakalns and B.R. Mcallister, *Anal. Chim. Acta*, 62 (1972) 207.

195. O. Hiroshi and S. Kiichi, *Talanta*, 19 (1972) 273.

196. M.P. Harrold, A. Siriraks and J. Riviello, *J. Chromatogr.*, 602 (1992) 119.

197. T. Yamamuto and Y. Kanchiku, *Fres. J. Anal. Chem.*, 294 (1979) 284.

198. F.W.E. Stretlow and T.N. Van der Waly, *SA-Afr.J.Chemistry*, 32 (1979) 169.

199. J.Y. Sun, X.G. Chen and Z.D. Hu, *Anal. Lett.*, 27 (1994) 1989.

200. V.M. Aleksandruk and N.I. Pushlenkova, *Ind. Lab.*, 46 (1980) 309.

201. I. Mori, K. Taguchi, Y. Fujita and T. Matsuo, *Fres. J. Anal. Chem.*, 353 (1995) 174.

202. F.P. Hao, P.R. Haddad, P.E. Jackson and J. Carnevale, *J. Chromatogr.*, 640 (1993) 187.

203. D.J. Barkley, M. Blanchette, R.M. Cassidy and S. Elchuk, *Anal. Chem.*, 58 (1986) 2222.

204. J.P. Pavon, B.M. Cordero, E.R. Garcia and J.H. Mendez, *Anal. Chim. Acta*, 230 (1990) 217.

205. A.G. Adriaens, J.D. Fassett, W.R. Kelly, D.S. Simons and F.C. Adams, *Anal. Chem.*, 64 (1992) 2945.

206. P. Robinson, N.C. Higgins and G.A. Jenner, *Chem. Geol.*, 55 (1986) 121.

207. Y. Igarashi, C.K. Kim, Y. Takaku, K. Shiraishi, M. Yamamoto and N. Ikeda, *Anal. Sci.*, 6 (1990) 157.

208. D. Zamzow, D. Baldwin, S. Weeks, S. Bajic and A. D'Silva, *Environ. Sci. Technol.*, 28 (1994) 352.

209. B.A. Colburn, M.J. Sepaniak and E.R. Hinton, *J. Liq. Chromatogr.*, 18 (1995) 3699.

210. R.L. Chien and D.S. Burgi, *Anal. Chem.*, 64 (1992) A 489.

211. B.F. Liu, L.B. Liu and J.K. Cheng, *Anal. Chim. Acta*, 358 (1998) 157.

212. S.B. Savvin, *Talanta*, 8 (1961) 673.

213. S.B. Savvin, *Talanta*, 11 (1964) 7.

214. H. Rohwer, N. Collier and E. Hosten, *Anal. Chim. Acta*, 314 (1995) 219.

215. H. Rohwer and E. Hosten, *Anal. Chim. Acta*, 339 (1997) 271.

216. H. Rohwer, N. Rheeder and E. Hosten, *Anal. Chim. Acta*, 341 (1997) 263.

217. B. Budesinsky, *Coll.Czech.Chem.Commun.*, 28 (1963) 2902.

218. B. Budesinsky, *Z.Anal.Chem.*, 207 (1965) 247.

219. B. Budesinsky, *Talanta*, 16 (1969) 1277.

220. P.N. Palei, N.I. Udaltsova and A.A. Nemodruk, *Zh.Anal.Khim.*, 22 (1967) 1797.

221. P.K. Spitsyn and V.S. Shvarev, *Zh.Anal.Khim.*, 25 (1970) 1503.

222. I. Nemcova, B. Metal and J. Podlaha, *Talanta*, 33 (1986) 841.

223. W.R. Jones and P. Jandik, *J. Chromatogr.*, 546 (1991) 445.

224. A. Emmer, A. Jansson and J. Roeraade, *J. Chromatogr.*, 547 (1991) 544.

225. J.E. Wiktorowicz and J.C. Colburn, *Electrophoresis*, 11 (1990) 769.

226. H. Engelhardt and M.A. Cunatwalter, *J. Chromatogr. A*, 716 (1995) 27.

227. M. Nakatani, A. Shibukawa and T. Nakagawa, *Electrophoresis*, 16 (1995) 1451.

228. X.H. Huang, M.J. Gordon and R.N. Zare, *Anal. Chem.*, 60 (1988) 375.

229. F.D.Snell, *Photometric and Fluorimetric Methods of Analysis*, Metals Part 1, John Wiley and Sons New York (1978).

230. E.B. Sandell and H. Onishi, *Photometric Determination of Trace Metals: General Aspects*, Chemical Analysis, Vol. 3 Part 1, John Wiley and Sons, New York, (1987).

231. R. M. Cassidy and B. D. Karcher, *Post-Column Reaction Detection of Inorganic Species*, in I. S. Krull (Editor), Chromatographic Science, Vol. 34: Reaction Detection in Liquid Chromatography, Marcel Dekker, NewYork, (1986), p130.

232. W. Buchberger and P.R. Haddad, *J. Chromatogr. A*, 687 (1994) 343.

233. W.F. Smyth, G.B. Harland, S. Mcclean, G. McGrath and D. Oxspring, *J. Chromatogr. A*, 772 (1997) 161.

234. D.J. Rose, J. Chromatogr., 540 (1991) 343.

235. B. Nickerson and J.W. Jorgenson, *J. Chromatogr.*, 480 (1989) 157.

236. D.J. Rose and J.W. Jorgenson, *J. Chromatogr.*, 447 (1988) 117.

237. T. Tsuda, Y. Kobayashi, A. Hori, T. Matsumoto and O. Suzuki, *J. Chromatogr.*, 456 (1988) 375.

238. S.L. Pentoney, X.H. Huang, D.S. Burgi and R.N. Zare, *Anal. Chem.*, 60 (1988) 2625.

239. M. Albin, R. Weinberger, E. Sapp and S. Moring, *Anal. Chem.*, 63 (1991) 417.

240. R.M. Cassidy, W.Z. Lu and V.P. Tse, *Anal. Chem.*, 66 (1994) 2578.

241. R. Zhu and W.T. Kok, *J. Chromatogr. A*, 716 (1995) 123.

242. W.G. Kuhr, L. Licklider and L. Amankwa, *Anal. Chem.*, 65 (1993) 277.

243. Riviello, J. and Pohl, C. Dionex Technical Note, (1983).

244. Shibata.S, in A.Flaschka and A.J.Barnard (Editors), *Chelates in Analytical Chemistry*, HMarcel Dekker Inc., New York, (1972) p.117.

245. M.B. Gholivand, F. Bamdad and J. Ghasemi, *Talanta*, 46 (1998) 875.

246. M. Yamada, *Bunseki Kagaku*, 25 (1976) 850.

247. B. Budesinsky, in H.A. Flaschka and A.J. Barnard (Editors), *Chelates in Analytical Chemistry*, Marcel Dekker, New York, (1967), p. 15.

248. A.E. Martell, *Critical Stability Constants*, Vol. 6, Plenum Press, London, (1989).

249. A.E. Martell, *Critical Stability Constants*, Vol. 1, Plenum Press, London, (1974).

250. A.E. Martell, *Critical Stability Constants*, Vol. 3, Plenum Press, London, (1977).

251. A. Ringbom, *Complexation in Analytical Chemistry*, John Wiley & Sons, (1963), p.324.

252. A. Ringbom, *Complexation in Analytical Chemistry*, John Wiley & Sons, (1963), p.297.

253. R.P. Paradkar and R.R. Williams, *Analytical Chemistry*, 66 (1994) 2752.

254. N.W. Barnett, B.J. Hindson, S.W. Lewis and S.D. Purcell, *Anal. Comm.*, 35 (1998) 321.

255. T.J. Oshea, R.D. Greenhagen, S.M. Lunte, C.E. Lunte, M.R. Smyth, D.M. Radzik and N. Watanabe, *J. Chromatogr.*, 593 (1992) 305.

256. D. Visky, M. Kraszni, S. Hosztafi and B. Noszal, *Chromatographia*, 51 (2000) 294.